SLIDING MODE GUIDANCE OF AN AIR-TO-AIR MISSILE

A THESIS SUBMITTED TO
THE GRADUATE SCHOOL OF NATURAL AND APPLIED SCIENCES
OF
MIDDLE EAST TECHNICAL UNIVERSITY

MUHARREM ULU

IN PARTIAL FULFILLMENT OF THE REQUIREMENTS
FOR
THE DEGREE OF MASTER OF SCIENCE
IN
ELECTRICAL AND ELECTRONICS ENGINEERING

SEPTEMBER 2013

Approval of the thesis:

SLIDING MODE GUIDANCE OF AN AIR-TO-AIR MISSILE

submitted by **MUHARREM ULU** in partial fulfillment of the requirements for the degree of **Master of Science in Electrical and Electronics Engineering Department, Middle East Technical University** by,

Prof. Dr. Canan Özgen
Dean, Graduate School of **Natural and Applied Sciences** _____

Prof. Dr. Gönül Turhan Sayan
Head of Department, **Electrical and Electronics Engineering** _____

Prof. Dr. M. Kemal Leblebicioğlu
Supervisor, **Electrical and Electronics Engineering Dept., METU** _____

Examining Committee Members:

Prof. Dr. M. Kemal Özgören
Mechanical Engineering Department, METU _____

Prof. Dr. M. Kemal Leblebicioğlu
Electrical and Electronics Engineering Department, METU _____

Prof. Dr. Mustafa Kuzuoğlu
Electrical and Electronics Engineering Department, METU _____

Assist. Prof. Dr. Umut Orguner
Electrical and Electronics Engineering Department, METU _____

Çağdaş Evcimen, M.Sc.
Chief Research Engineer, TÜBİTAK SAGE _____

Date: 03.09.2013

I hereby declare that all information in this document has been obtained and presented in accordance with academic rules and ethical conduct. I also declare that, as required by these rules and conduct, I have fully cited and referenced all material and results that are not original to this work.

Name, Last Name: MUHARREM ULU

Signature :

ABSTRACT

SLIDING MODE GUIDANCE OF AN AIR-TO-AIR MISSILE

Ulu, Muharrem

M.S., Department of Electrical and Electronics Engineering

Supervisor : Prof. Dr. M. Kemal Leblebicioğlu

September 2013, 153 pages

Pursuit of a highly maneuverable aircraft by an air-to-air missile requires a solution to a challenging guidance and control problem. Precision is the most important need for these missiles. Appropriate guidance commands that are generated by the guidance method and an autopilot that can fulfil the agility needs of such a missile are the keys of minimizing the distance between the missile and the target and a successful interception. In this thesis, autopilot and guidance method design of an air-to-air missile (AAM) that has maximum 100 seconds time of flight is studied. As the first step, nonlinear 6 degrees-of-freedom (6DOF) mathematical model of the missile is derived by using the equations of motion with aerodynamic coefficients found by Missile Datcom program. Mathematical model is linearized around chosen flight conditions to design an autopilot. In this thesis, the guidance problem is handled by using first and second order sliding mode control and these guidance rules are compared for different interception scenarios.

Keywords: Mathematical Modelling of Missile, Autopilot, Guidance, Sliding Mode Control, Super Twisting Algorithm.

ÖZ

BİR HAVADAN HAVAYA FÜZENİN KAYAN KİPLİ GÜDÜMÜ

Ulu, Muharrem
Yüksek Lisans, Elektrik ve Elektronik Mühendisliği Bölümü
Tez Yöneticisi : Prof. Dr. M. Kemal Leblebicioğlu

Eylül 2013 , 153 sayfa

Yüksek manevra kabiliyetli bir hava aracının bir havadan havaya füze tarafından takibi zorlayıcı bir güdüm ve kontrol problemine çözüm gerektirir. İsabet kabiliyeti bir hava-hava füzesi için en önemli ihtiyaçtır. Güdüm yöntemi ile uygun güdüm komutlarının üretilmesi ve bu tip çevik bir füze için ihtiyacı karşılayacak bir otopilot, füze ile hedef arasındaki mesafeyi kısaltmanın ve başarılı bir vuruş sağlamanın anahtarıdır. Bu tezde uçuş süresi azami 100 saniye olan bir havadan havaya füzenin otopilot ve güdüm yöntemi tasarımı üzerine çalışılmıştır. İlk aşamada füzenin doğrusal olmayan 6 serbestlik dereceli matematiksel modeli, hareket denklemlerinde Missile Datcom programı ile bulunan aerodinamik katsayılar kullanılarak elde edilmiştir. Matematiksel model otopilot tasarımı için seçilen uçuş koşulları etrafında doğrusallaştırılmıştır. Bu tezde güdüm problemi, birinci ve ikinci dereceden kayan kipli kontrol yöntemi kullanılarak ele alınmıştır ve bu güdüm kuralları farklı angajman senaryoları için karşılaştırılmıştır.

Anahtar Kelimeler: Füzenin Matematiksel Modellemesi, Otopilot, Güdüm, Kayan Kipli Kontrol, Üstün Burulma Algoritması.

To my family

ACKNOWLEDGMENTS

I would like to express my sincere appreciation to my supervisor, Prof. Dr. M. Kemal Leblebicioğlu for his guidance, valuable comments, helpful suggestions and continuous support throughout this study.

This thesis has been supported by TUBITAK SAGE and TUBITAK SAGE is greatly acknowledged for providing the necessary substructure of this research.

Additionally, I also thank to all of my colleagues in TUBITAK SAGE for their support and motivation.

I would like to extend my appreciation to my dear friend Fırat Yılmaz Cevher for his invaluable support and encouragement.

I would like to express my deepest gratitude to my dearest one for her endless support, patience and love.

Finally, I am thankful to my family for their trust, encouragement and patience. None of this would have been even possible without their support.

TABLE OF CONTENTS

ABSTRACT v

ÖZ vi

ACKNOWLEDGMENTS viii

TABLE OF CONTENTS ix

LIST OF TABLES xiv

LIST OF FIGURES xvi

LIST OF ABBREVIATIONS xxviii

CHAPTERS

1 INTRODUCTION 1

1.1 Introduction 1

1.2 Literature Survey 3

1.3 Contribution 4

1.4 Thesis Organization 5

2 MATHEMATICAL MODELLING 7

2.1 Introduction 7

2.2 Coordinate Frames 7

2.2.1 Inertial Frame 8

2.2.2 Earth Centered Earth Fixed Frame (ECEF) 8

2.2.3 Navigation Frame 9
2.2.4 Local Cartesian Frame 9
2.2.5 Body Frame 10
2.2.6 Transformation Matrices 10
2.3 Aerodynamic Model 13
2.3.1 Flight Parameters 13
2.3.2 Aerodynamic Data 14
2.3.3 Aerodynamic Forces and Moments 22
2.4 Equations of Motion 23
2.4.1 Nonlinear Equations of Motion 23
2.4.1.1 Kinematical Equations of Motion 25
Translational Kinematics 25
Rotational Kinematics 25
2.4.1.2 Dynamical Equations of Motion 26
Translational Dynamics 26
Rotational Dynamics 28
2.4.2 Linear Equations of Motion 29
2.4.2.1 Linearization of Differential Equations . . 29
2.4.2.2 Linearization of Aerodynamic Model . . . 31
2.4.2.3 Linearization of Equations of Motion . . . 32
2.5 Control Surface Deflection Angles 35
2.6 Control Actuation System Model 36
2.7 Linear Missile Model 37

2.7.1 Pitch Plane State Space Model 37
2.7.2 Roll-Yaw Plane State Space Model 37
2.8 Conclusion 37
3 AUTOPILOT DESIGN 39
3.1 Introduction 39
3.2 Linear Quadratic Regulator 41
3.3 Linear Quadratic Tracker 42
3.3.1 Optimal Linear Quadratic Tracker (OLQT) 42
3.3.2 Practical Suboptimal Tracker (PST) 44
3.4 Quadratic Weight Selection 45
3.5 Linear Quadratic Autopilot Design 47
3.5.1 Pitch Plane Autopilot Design 47
3.5.2 Yaw Plane Autopilot Design 55
3.5.3 Roll Autopilot Design 62
3.6 Nonlinear Simulation Results 70
3.7 Conclusion 73
4 GUIDANCE DESIGN 75
4.1 Introduction 75
4.2 First Order Sliding Mode Guidance 75
4.2.1 LOS Rate Surface 76
4.2.1.1 Equivalent Control 78
4.2.1.2 Switching Control 78
4.2.2 Proportinal-Integral (PI) Surface 79

4.2.2.1 Equivalent Control 80
4.2.2.2 Switching Control 80
4.2.2.3 Optimization with Genetic Algorithm . . 81
4.3 Second Order Sliding Mode Guidance 83
4.4 Conclusion 86
5 SIMULATION STUDIES 87
5.1 Introduction 87
5.2 First Order versus Second Order Sliding Mode Guidance . . . 88
5.2.1 Scenario - 1 88
5.2.2 Scenario - 2 93
5.3 Static versus Adaptive Gain Super Twisting Guidance 99
5.3.1 Scenario - 1 99
5.3.2 Scenario - 2 104
5.4 Engagement Scenarios of PI, ST and PNG Methods Comparison 107
5.4.1 Scenario - 1 107
5.4.2 Scenario - 2 112
5.4.3 Scenario - 3 117
5.4.4 Scenario - 4 121
5.4.5 Scenario - 5 124
5.4.6 Scenario - 6 127
5.4.7 Scenario - 7 131
5.4.8 Scenario - 8 134
5.4.9 Scenario - 9 138

5.4.10 Scenario - 10 141

5.5 Conclusion 144

6 CONCLUSION AND FUTURE WORK 147

6.1 Summary 147

6.2 Results and Future Work 148

REFERENCES 151

LIST OF TABLES

TABLES

Table 2.1 For an inherently stable missile, uncoupled terms of aerodynamic stability, control and dynamic derivatives 16

Table 2.2 Related parameters of missile 23

Table 3.1 Initial conditions of Scenario – 1 70

Table 4.1 Initial conditions of refecence scenario – 1 81

Table 4.2 Initial conditions of refecence scenario – 2 82

Table 5.1 Initial conditions of Scenario – 1 88

Table 5.2 Initial conditions of Scenario – 2 94

Table 5.3 Initial conditions of Scenario – 2 104

Table 5.4 Initial conditions of Scenario – 1 108

Table 5.5 Initial conditions of Scenario – 2 113

Table 5.6 Initial conditions of Scenario – 3 118

Table 5.7 Initial conditions of Scenario – 4 122

Table 5.8 Initial conditions of Scenario – 5 125

Table 5.9 Initial conditions of Scenario – 6 128

Table 5.10 Initial conditions of Scenario – 7 131

Table 5.11 Initial conditions of Scenario – 8 134

Table 5.12 Initial conditions of Scenario – 9 138

Table 5.13 Initial conditions of Scenario – 10 141

LIST OF FIGURES

FIGURES

Figure 1.1 AIM-9L short range missile 2

Figure 1.2 AIM-9X short range missile 2

Figure 1.3 AIM-120 AMRAAM 2

Figure 1.4 Meteor missile 2

Figure 1.5 Missile guidance and control scheme 3

Figure 2.1 Inertial reference coordinate system [29] 8

Figure 2.2 Earth Centered Earth Fixed coordinate system [29] 9

Figure 2.3 Inertial, Earth and NED coordinate system representation 9

Figure 2.4 Local Cartesian coordinate system definition 10

Figure 2.5 Body coordinate system at the center of gravity of missile 10

Figure 2.6 Euler angles 11

Figure 2.7 Rotation about Z axis 11

Figure 2.8 Rotation about Y axis 11

Figure 2.9 Rotation about X axis 12

Figure 2.10 Angle of attack descripton 13

Figure 2.11 Angle of sideslip description 13

Figure 2.12 Baseline geometry 14
Figure 2.13 Axisymmetric body geometry variables [30] 15
Figure 2.14 Wing and fin geometry variables [30] 15
Figure 2.15 Wing and fin orders [30] 15
Figure 2.16 Nose geometry and HEX airfoil variables [30] 15
Figure 2.17 Lift coefficient change with alpha 16
Figure 2.18 Drag coefficient change with alpha 17
Figure 2.19 Side force coefficient change with beta 17
Figure 2.20 Side force control derivative change with beta 17
Figure 2.21 Side force dynamic derivative change with alpha 18
Figure 2.22 Normal force coefficient change with alpha 18
Figure 2.23 Normal force control derivative change with alpha 18
Figure 2.24 Normal force dynamic derivative change with alpha 19
Figure 2.25 Rolling moment control derivative change with beta 19
Figure 2.26 Rolling moment dynamic derivative change with alpha 19
Figure 2.27 Rolling stability derivative change with alpha 20
Figure 2.28 Pitching moment coefficient change with alpha 20
Figure 2.29 Pitching moment control derivative change with alpha 20
Figure 2.30 Pitching moment dynamic derivative change with alpha 21
Figure 2.31 Yawing moment coefficient change with beta 21
Figure 2.32 Yawing moment control derivative change with beta 21
Figure 2.33 Yawing moment dynamic derivative change with alpha 22

Figure 2.34 Translational and rotational definitions 23

Figure 2.35 components of the gravitational force 24

Figure 2.36 'X' configuration for the control surfaces 35

Figure 2.37 Block diagram of the CAS 36

Figure 3.1 Block diagram represenatation of PST [32] 44

Figure 3.2 Flowchart of the q search algorithm 46

Figure 3.3 Pitch autopilot structure 48

Figure 3.4 Penalty term for design points 49

Figure 3.5 K_α gain for design points 49

Figure 3.6 K_q gain for design points 49

Figure 3.7 K_{δ_e} gain for design points 50

Figure 3.8 $K_{\dot{\delta}_e}$ gain for design points 50

Figure 3.9 K_e gain for design points 50

Figure 3.10 Gain margin for design points 51

Figure 3.11 Phase margin for design points 51

Figure 3.12 Settling time for design points 51

Figure 3.13 Deflection rate for design points 52

Figure 3.14 Rate loop bandwidth over natural frequency of system for design points 52

Figure 3.15 Acceleration loop gain margin for design points 52

Figure 3.16 Acceleration phase margin for design points 53

Figure 3.17 Acceleration loop settling time for design points 53

Figure 3.18 Acceleration loop settling value for design points 53

Figure 3.19 Acceleration loop rise time for design points 54

Figure 3.20 Acceleration loop integral gain for design points 54

Figure 3.21 Acceleration loop proportional gain for design points 54

Figure 3.22 Yaw autopilot structure 56

Figure 3.23 Penalty term for design points 56

Figure 3.24 K_β gain for design points 57

Figure 3.25 K_r gain for design points 57

Figure 3.26 K_{δ_r} gain for design points 57

Figure 3.27 $K_{\dot{\delta}_r}$ gain for design points 58

Figure 3.28 K_e gain for design points 58

Figure 3.29 Gain margin for design points 58

Figure 3.30 Phase margin for design points 59

Figure 3.31 Settling time for design points 59

Figure 3.32 Deflection rate for design points 59

Figure 3.33 Rate loop bandwidth over natural frequency of system for design points 60

Figure 3.34 Acceleration loop gain margin for design points 60

Figure 3.35 Acceleration phase margin for design points 60

Figure 3.36 Acceleration loop settling time for design points 61

Figure 3.37 Acceleration loop settling value for design points 61

Figure 3.38 Acceleration loop rise time for design points 61

Figure 3.39 Acceleration loop integral gain for design points 62

Figure 3.40 Acceleration loop proportional gain for design points 62

Figure 3.41 Roll autopilot structure 63

Figure 3.42 Penalty term for design points 64

Figure 3.43 K_p gain for design points 64

Figure 3.44 K_{δ_a} gain for design points 64

Figure 3.45 $K_{\dot{\delta}_a}$ gain for design points 65

Figure 3.46 K_e gain for design points 65

Figure 3.47 Gain margin for design points 65

Figure 3.48 Phase margin for design points 66

Figure 3.49 Settling time for design points 66

Figure 3.50 Deflection rate for design points 66

Figure 3.51 Roll rate loop bandwidth over pitch rate bandwidth for design points 67

Figure 3.52 Phi loop gain margin for design points 67

Figure 3.53 Phi loop phase margin for design points 67

Figure 3.54 Phi loop proportional gain for design points 68

Figure 3.55 Phi loop settling time for design points 68

Figure 3.56 Phi loop settling value for design points 68

Figure 3.57 Pitch acceleration loop step responses 69

Figure 3.58 Yaw acceleration loop step responses 69

Figure 3.59 Phi loop step responses 70

Figure 3.60 Body pitch rate autopilot response 70

Figure 3.61 Body pitch rate autopilot response 71

Figure 3.62 Body yaw rate autopilot response 71

Figure 3.63 Body roll rate autopilot response 71

Figure 3.64 Longitudinal acceleration autopilot response 72

Figure 3.65 Lateral acceleration autopilot response 72

Figure 3.66 Roll autopilot response 72

Figure 4.1 Geometry of planar engagement of parallel guidance [37] 76

Figure 4.2 Missile-target engagement geometry 77

Figure 4.3 Missile and target trajectories 81

Figure 4.4 Missile and target trajectories 82

Figure 5.1 6DOF model blocks and signal flow 87

Figure 5.2 Missile and target trajectories 88

Figure 5.3 Longitudinal acceleration command 89

Figure 5.4 Longitudinal sliding surface 89

Figure 5.5 Longitudinal sliding surface (zoomed) 89

Figure 5.6 Longitudinal sliding surface (zoomed) 90

Figure 5.7 Derivative of longitudinal sliding variable 90

Figure 5.8 Derivative of longitudinal sliding variable (zoomed) 90

Figure 5.9 Derivative of longitudinal sliding variable (zoomed) 91

Figure 5.10 Lateral acceleration command 91

Figure 5.11 Lateral sliding surface 91

Figure 5.12 Lateral sliding surface (zoomed) 92

Figure 5.13 Lateral sliding surface (zoomed) 92

Figure 5.14 Derivative of lateral sliding variable 92

Figure 5.15 Derivative of lateral sliding variable (zoomed) 93

Figure 5.16 Derivative of lateral sliding variable (zoomed) 93

Figure 5.17 Missile and target trajectories 94

Figure 5.18 Longitudinal acceleration command 94

Figure 5.19 Longitudinal sliding surface 95

Figure 5.20 Longitudinal sliding surface (zoomed) 95

Figure 5.21 Longitudinal sliding surface (zoomed) 95

Figure 5.22 Derivative of longitudinal sliding variable 96

Figure 5.23 Derivative of longitudinal sliding variable (zoomed) 96

Figure 5.24 Derivative of longitudinal sliding variable (zoomed) 96

Figure 5.25 Lateral acceleration command 97

Figure 5.26 Lateral sliding surface 97

Figure 5.27 Lateral sliding surface (zoomed) 97

Figure 5.28 Lateral sliding surface (zoomed) 98

Figure 5.29 Derivative of lateral sliding variable 98

Figure 5.30 Derivative of lateral sliding variable (zoomed) 98

Figure 5.31 Derivative of lateral sliding variable (zoomed) 99

Figure 5.32 Missile and target trajectories 99

Figure 5.33 Longitudinal acceleration command 100

Figure 5.34 Longitudinal sliding surface 100

Figure 5.35 Longitudinal sliding surface (zoomed) 100

Figure 5.36 Derivative of longitudinal sliding variable 101

Figure 5.37 Derivative of longitudinal sliding variable (zoomed) 101

Figure 5.38 Derivative of longitudinal sliding variable (zoomed) 101

Figure 5.39 Lateral acceleration command 102

Figure 5.40 Lateral sliding surface 102

Figure 5.41 Lateral sliding surface (zoomed) 102

Figure 5.42 Derivative of lateral sliding variable 103

Figure 5.43 Derivative of lateral sliding variable (zoomed) 103

Figure 5.44 Derivative of lateral sliding variable (zoomed) 103

Figure 5.45 Missile and target trajectories 104

Figure 5.46 Longitudinal acceleration command 105

Figure 5.47 Longitudinal sliding surface 105

Figure 5.48 Derivative of longitudinal sliding variable 105

Figure 5.49 Derivative of longitudinal sliding variable (zoomed) 106

Figure 5.50 Lateral acceleration command 106

Figure 5.51 Lateral sliding surface 106

Figure 5.52 Derivative of lateral sliding variable 107

Figure 5.53 Derivative of lateral sliding variable (zoomed) 107

Figure 5.54 Missile and target trajectories 108

Figure 5.55 Longitudinal acceleration command 108

Figure 5.56 Longitudinal sliding surface 109

Figure 5.57 Longitudinal sliding surface (zoomed) 109

Figure 5.58 Derivative of longitudinal sliding variable 109

Figure 5.59 Derivative of longitudinal sliding variable (zoomed) 110

Figure 5.60 Derivative of longitudinal sliding variable (zoomed) 110

Figure 5.61 Lateral acceleration command 110

Figure 5.62 Lateral sliding surface 111

Figure 5.63 Lateral sliding surface (zoomed) 111

Figure 5.64 Derivative of lateral sliding variable 111

Figure 5.65 Derivative of lateral sliding variable (zoomed) 112

Figure 5.66 Derivative of lateral sliding variable (zoomed) 112

Figure 5.67 Missile and target trajectories 113

Figure 5.68 Longitudinal acceleration command 113

Figure 5.69 Longitudinal sliding surface 114

Figure 5.70 Longitudinal sliding surface (zoomed) 114

Figure 5.71 Derivative of longitudinal sliding variable 114

Figure 5.72 Derivative of longitudinal sliding variable (zoomed) 115

Figure 5.73 Derivative of longitudinal sliding variable (zoomed) 115

Figure 5.74 Lateral acceleration command 115

Figure 5.75 Lateral sliding surface 116

Figure 5.76 Lateral sliding surface (zoomed) 116

Figure 5.77 Derivative of lateral sliding variable 116

Figure 5.78 Derivative of lateral sliding variable (zoomed) 117

Figure 5.79 Derivative of lateral sliding variable (zoomed) 117

Figure 5.80 Missile and target trajectories 118

Figure 5.81 Longitudinal acceleration command 118

Figure 5.82 Longitudinal sliding surface 119

Figure 5.83 Derivative of longitudinal sliding variable 119

Figure 5.84 Derivative of longitudinal sliding variable (zoomed) 119

Figure 5.85 Derivative of longitudinal sliding variable (zoomed) 120

Figure 5.86 Lateral acceleration command 120

Figure 5.87 Lateral sliding surface 120

Figure 5.88 Derivative of lateral sliding variable 121

Figure 5.89 Derivative of lateral sliding variable (zoomed) 121

Figure 5.90 Missile and target trajectories 122

Figure 5.91 Longitudinal acceleration command 122

Figure 5.92 Longitudinal sliding surface 123

Figure 5.93 Derivative of longitudinal sliding variable 123

Figure 5.94 Lateral acceleration command 123

Figure 5.95 Lateral sliding surface 124

Figure 5.96 Derivative of lateral sliding variable 124

Figure 5.97 Missile and target trajectories 125

Figure 5.98 Longitudinal acceleration command 125

Figure 5.99 Longitudinal sliding surface 126

Figure 5.100 Derivative of longitudinal sliding variable 126

Figure 5.101 Lateral acceleration command 126

Figure 5.102 Lateral sliding surface 127

Figure 5.103 Derivative of lateral sliding variable 127

Figure 5.104 Missile and target trajectories 128

Figure 5.105 Longitudinal acceleration command 128

Figure 5.106 Longitudinal sliding surface 129

Figure 5.107 Derivative of longitudinal sliding variable 129

Figure 5.108 Derivative of longitudinal sliding variable (zoomed) 129

Figure 5.109 Lateral acceleration command 130

Figure 5.110 Lateral sliding surface 130

Figure 5.111 Derivative of lateral sliding variable 130

Figure 5.112 Derivative of lateral sliding variable (zoomed) 131

Figure 5.113 Missile and target trajectories 132

Figure 5.114 Longitudinal acceleration command 132

Figure 5.115 Longitudinal sliding surface 132

Figure 5.116 Derivative of longitudinal sliding variable 133

Figure 5.117 Lateral acceleration command 133

Figure 5.118 Lateral sliding surface 133

Figure 5.119 Derivative of lateral sliding variable 134

Figure 5.120 Missile and target trajectories 135

Figure 5.121 Longitudinal acceleration command 135

Figure 5.122 Longitudinal sliding surface 135

Figure 5.123 Derivative of longitudinal sliding variable 136

Figure 5.124 Derivative of longitudinal sliding variable (zoomed) 136

Figure 5.125 Lateral acceleration command 136

Figure 5.126 Lateral sliding surface 137

Figure 5.127 Derivative of lateral sliding variable 137

Figure 5.128 Derivative of lateral sliding variable (zoomed) 137

Figure 5.129 Missile and target trajectories 138

Figure 5.130 Longitudinal acceleration command 139

Figure 5.131 Longitudinal sliding surface 139

Figure 5.132 Derivative of longitudinal sliding variable 139

Figure 5.133 Lateral acceleration command 140

Figure 5.134 Lateral sliding surface 140

Figure 5.135 Derivative of lateral sliding variable 140

Figure 5.136 Missile and target trajectories 141

Figure 5.137 Longitudinal acceleration command 142

Figure 5.138 Longitudinal sliding surface 142

Figure 5.139 Derivative of longitudinal sliding variable 142

Figure 5.140 Derivative of longitudinal sliding variable (zoomed) 143

Figure 5.141 Lateral acceleration command 143

Figure 5.142 Lateral sliding surface 143

Figure 5.143 Derivative of lateral sliding variable 144

Figure 5.144 Derivative of lateral sliding variable (zoomed) 144

LIST OF ABBREVIATIONS

DOF	Degree of Freedom
AAM	Air-to-Air Missile
AIM	Air Intercept Missile
UAV	Unmanned Aerial Vehicle
BVR	Beyond Visual Range
WVR	Within Visual Range
TVC	Thrust Vector Control
IMU	Inertial Measurement Unit
LQR	Linear Quadratic Regulator
LQT	Linear Quadratic Tracker
PI	Proportional-Integral
NED	North-East-Down
ECEF	Earth Centered Earth Fixed Frame
DCM	Direction Cosine Matrix
LTI	Linear Time Invariant
AOA	Angle of Attack
AOS	Angle of Sideslip
CAS	Control Actutation System
HOT	Higher Order Terms
SMC	Sliding Mode Control
LOS	Line-of-Sight
FOV	Field of View
PNG	Proportional Navigation Guidance
ST	Super Twisting
GA	Genetic Algorithm

CHAPTER 1

INTRODUCTION

1.1 Introduction

An air-to-air missile (AAM) is a weapon that is fired from an aerial platform to another aerial platform to destroy or make it ineffective. These aerial platforms may be a fighter aircraft, a helicopter or a UAV (Unmanned Aerial Vehicle). From the first operational guided AAM developed in 1946, known as AIM-4 Falcon, tactical AAM guidance in pursuit of a maneuverable aircraft is possibly the most challenging guidance and control problem in missile guidance. The problem consists of generation of guidance commands and construction of an autopilot structure to steer the missile towards target interception by following the commands generated by a guidance rule. Nonlinear, multivariable and time varying coupled nature of the AAM make them highly complex integrated systems. An AAM flies at supersonic speeds for most of the time until intercept to a target and operates in extremely adverse operational environments and has to be agile to defeat the target which is mostly a very maneuverable fighter aircraft. This high speed and agile flight requires fast response to guidance commands and a precise control to steer the missile to enemy aircraft which has to end up with a successful interception. AAMs can be categorized with within visual range (WVR) and beyond visual range (BVR) missiles. WVR missiles are designed to engage opposing aircraft at ranges of less than 30 km. They can be called 'dogfight' missiles because they emphasize agility rather than range. WVR missile are generally heat-seeking missiles and the old ones mostly have IR(Infra-Red) seekers such as AIM-9 P/L/M (USA) and Vympel R-73 (Russia). Relatively new ones have IIR (Imaging Infra-Red) seekers to see and track the target, such as AIM-9X (USA), IRIS-T (NATO countries) and Python 5 (Israel). IIR seekers use electro-optical imaging to scan designated area to find target aircraft's heat signature. WVR missiles are expected to be highly maneuverable (> 35g) and have high off-boresight capability ($> 90^\circ$). This abilities are generally provided by thrust vector control (TVC).

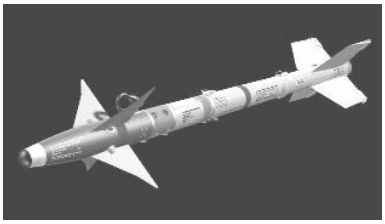

Figure 1.1: AIM-9L short range missile

Figure 1.2: AIM-9X short range missile

BVR missiles generally have active radar seekers that contain radar transceiver and electronics necessary to find and track a target autonomously. There is a datalink between the launching platform and the missile. With this datalink, shooter aircraft sends target position updates that comes from its radar to the missile until the missile 'goes active', that means the active radar seeker detects and tracks the target by itself. After the missile goes active, there is no need to aid the missile with target updates through datalink. This capability is called 'fire and forget', because the attacking aircraft is free to pursue other targets or escape the area after launching the missile. AIM-120 AMRAAM (USA), Vympel R-77 (Russia), Meteor(Europa) are some of the examples of BVR AAMs.

Figure 1.3: AIM-120 AMRAAM

Figure 1.4: Meteor missile

In this thesis, a BVR missile that can fly 100 seconds is considered. It is assumed that it has an active radar seeker and supported by data link so that target position is known during the flight. Also it is assumed that body acceleration and rate infor-

mation are provided by an inertial measurement unit (IMU). Maximum speed is taken as approximately 3.5 Mach and it has thrust throughout the flight. This missile is controlled by tail fins and it has no TVC ability but its aerodynamic features allow up to 40 g acceleration capability. Simply a typical missile guidance and control system can be represented in Figure 1.5.

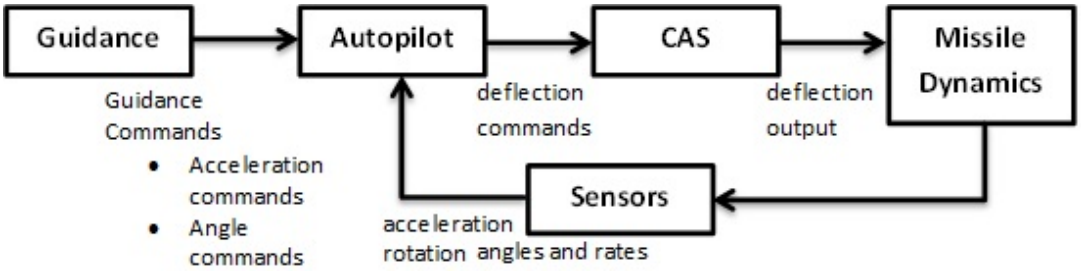

Figure 1.5: Missile guidance and control scheme

1.2 Literature Survey

Guidance of an AAM is possibly the most challenging guidance problem. Agility and long range capabilities are the main necessities when the subject comes to that kind of missiles. A pilot always wants to lock on target aircraft first, because this is the key for survival against the enemy [1]. Consider a head-on BVR engagement scenario that two fighter aircrafts are flying towards each other. The fighter which has a longer range missile shoots first and this is a very important chance to damage the opponent fighter or force it to maneuver back and fly away. Also consider another scenario that a dogfight between two fighter and each of them tries to lock on each other with many complex maneuvers one after the other to catch a clear sight and keep the target in suitable geometry for launch. In this scenario, when today's highly maneuverable fighters are considered, if you do not have such a maneuverable fighter, you have to have a highly maneuverable missile that possibly has a high off-boresight capability. When BVR AAM's are considered, long range capability need is ahead of agility. Also the propellant needs to go further make BVR missiles longer and a little thicker than WVR missiles and that generally limits the g capability of the missile. When WVR missiles are considered, their g capabilities may reach 70g's according to open sources. Real g capabilities of such missiles are classified information, but according to the general rule of thumb, the missile is required to have five times the g capability of the target to accomplish a successful intercept [1]. When the sustained g capabilities of fighters are considered, the enemy fighter is assumed to be able to pull a sustained 8g maneuver, so a missile that has 40g acceleration capability is considered in this study and the geometry of the missile is chosen according to this aerodynamic load factor need. Guidance is the process for guiding the path of an object towards a given point, which in general may be moving [2]. Many guidance laws based on Proportional Navigation Guidance (PNG) and its variants with several

modifications are stated in open literature [3, 4, 5, 6]. The aim of the PNG law is to zeroize the Line-of-Sight (LOS) rate against the targets and performs reasonably well in a wide range of engagement geometries. The main disadvantage of these variants is the requirement of the knowledge of target acceleration. From the implementation point of view, estimation of target acceleration with suitable analytical methods are required. A large number of target acceleration estimation methods available in the literature are generally based on Kalman filter and the extended Kalman filter structures [7, 8]. With that approaches, some assumptions have to be made about the target acceleration dynamics. When these assumptions are violated, they may result in poor estimates of the target acceleration or divergence of the estimation process [12].

Sliding mode control (SMC) is the main mode of operation of Variable Structure Control (VSC) that is recognized as an efficient tool to design controllers which are robust with respect to uncertainty such as uncertain plant parameters and perturbations [9]. In SMC method, the purpose is to drive the nonlinear plant's state trajectory onto a user-chosen surface in the state space and to maintain the plant's state trajectory on this surface for all subsequent time [10]. This surface is called *switching surface* or *sliding surface*. Imagine that the gains in feedback path switch between two values according to a rule dependent to system state, in this context, the rule is sliding surface and when the plant state trajectory is above the surface one gain is applied to the system and a different gain if the trajectory is below the surface. This provides to drive the state trajectory to the surface and keeps it move along surface, that is, sliding mode occurs. SMC methodology is addressed in many papers including guidance law derivation for guided missiles against maneuvering targets [11, 12, 13]. Most of them are derived as first order sliding mode guidance laws. In order to attenuate the chattering affect, higher order, mostly second order, sliding mode control is introduced [14, 15, 16]. One of the second order sliding mode control methods, called super twisting algorithm, is defined as better than the other second order methods and applied to many control applications [14, 17, 18, 19]. In spite of the control applications of super twisting control method, the number of missile guidance applications are very limited [20, 21].

1.3 Contribution

In this thesis, sliding mode guidance of an AAM is studied. As a first order sliding mode guidance method, PI surface that is generally used in actuator control applications is applied to the missile guidance problem. As a second study, super twisting method of second order sliding mode control, is applied to the guidance problem with a proposed adaptive rule to determine the parameters of the method. The comparison of these two methods are incorporated in a paper and has received an acceptance to be presented at TOK 2013 [24]. The studies on a journal article are in progress.

1.4 Thesis Organization

This thesis consists of a mathematical modelling of an AAM, autopilot and guidance design, and also comparison of derived guidance rules with some interception scenarios. As a summary;

- Chapter 1 states basic definitions about AAMs and well-known examples from different nations, includes literature survey and scope of this thesis.
- Chapter 2 starts with definition of coordinate systems then, it continues with aerodynamic model of a generic AAM, 6 DOF nonlinear and linear equations of motion with kinematical and dynamical parts, control surface deflection definitions and control actuation system model. Finally, pitch plane and roll-yaw plane state space models are obtained.
- Chapter 3 obtains linear quadratic regulator (LQR) theory, linear quadratic tracker (LQT) and then LQT design of pitch, yaw and roll rate autopilot as known as stability augmentation loop. As outer of these loops pitch and yaw acceleration autopilots are designed with PI controller structure. Roll autopilot is designed as the outer loop of the roll rate autopilot. Design requirements stated, results are obtained and stated with figures.
- Chapter 4 defines the guidance rules which are derived by using sliding mode control theory. In the beginning, first order sliding mode guidance rule is constructed with PI sliding surface. As the second step, second order sliding mode guidance rule is derived by using super twisting algorithm.
- Chapter 5 includes the simulation studies which the performance comparison of guidance methods is made with different interception scenarios from easy to hard difficulty levels.

CHAPTER 2

MATHEMATICAL MODELLING

2.1 Introduction

Mathematical modelling of the missile incorporates different definitions such as coordinate systems, aerodynamic model, equations of motion, control surface deflection and control actuation system (CAS). Equations of motion that are required to define a missile motion contains six kinematical and six dynamical equations. Both of the kinematical and dynamical equations can be divided into two parts as translational and rotational equations of motion. Euler angles are used to define the conversion between coordinate systems and also makes connection between these rotational kinematics and rotational dynamics. Dynamical equations are basically defined by using Newton's second law of motion that relates the translational accelerations to forces and the rotational accelerations to moments. In this chapter, coordinate systems are presented to define the relative motion of the missile. Nonlinear mathematical model is derived by using equations of motion that includes aerodynamic model that generates aerodynamic forces and moments. These equations are simplified and linearized around trim conditions and these steps converge to state space models and transfer functions that are needed for autopilot design.

2.2 Coordinate Frames

There are five basic coordinate frames to describe the position and motion of an aerospace vehicle:

1. Inertial frame,
2. Earth centered Earth fixed frame,
3. Navigation(North-East-Down(NED)) frame,
4. Cartesian frame,
5. Body frame.

2.2.1 Inertial Frame

The inertial frame is fixed with its origin at the center of the earth and has no acceleration and rotation relative to stars as seen in Figure 2.1.

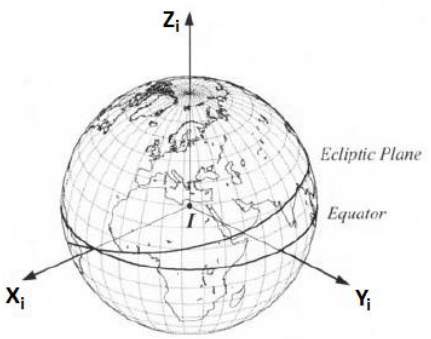

Figure 2.1: Inertial reference coordinate system [29]

X_i direction is defined as the vector from the center of the Earth pointed to the Sun and passes through the intersection of the ecliptic plane and the equator in spring. Inertial sensors that are used in inertial navigation systems measures acceleration and rates with respect to inertial coordinate system.

Origin : Center of the Earth,
X_i axis: Direction of vernal equinox,
Y_i axis: Orthogonal to the X_i and Z_i direction according to the right hand rule,
Z_i axis: Directed to the North pole.

2.2.2 Earth Centered Earth Fixed Frame (ECEF)

The origin of the Earth centered Earth fixed frame is attached to the center on the Earth and its axes are X_e,Y_e,Z_e as stated in Figure 2.2. The vector starts from the center of the Earth to the intersection of the prime meridian that traces through the Royal Observatory at Greenwich with equator represents the direction of X_e. ECEF coordinate system rotates with $\vec{\omega} = 7.2921151467\text{x}10^{-5}$ about Z_e axis with respect to inertial frame.

Origin : Center of the Earth,
X_e axis : Directed to the intersection of Greenwich meridian and the equator,
Y_e axis : Orthogonal to the X_i and Z_i direction according to the right hand rule,
Z_e axis : Directed to the North pole.

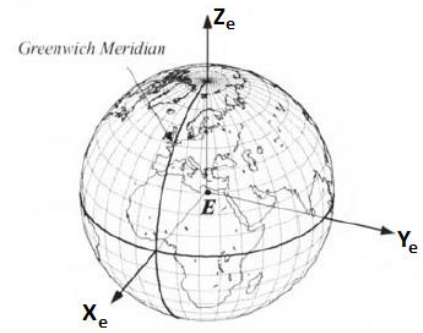

Figure 2.2: Earth Centered Earth Fixed coordinate system [29]

2.2.3 Navigation Frame

This reference frame, is also called North-East-Down (NED) frame , is defined at the center of the inertial navigation system of missile and translates with missile but not rotates.

Origin : Center of the inertial navigation system of missile,
X_n : Directed to ellipsoid north,
Y_n : Directed to ellipsoid east,
Z_n : Directed to ellipsoid down.

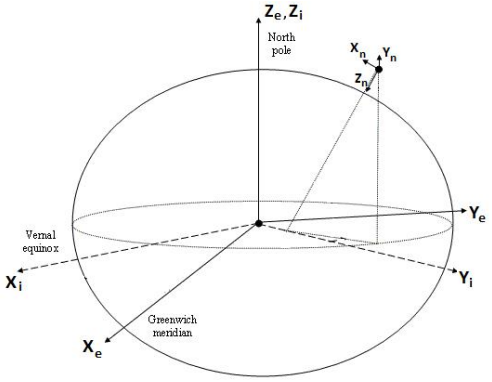

Figure 2.3: Inertial, Earth and NED coordinate system representation

2.2.4 Local Cartesian Frame

To represent the relative distances between missile and target and also the trajectory that missile follows, there is a need to define a coordinate system. In addition, guidance algorithms also needs the relative Cartesian locations between missile and target. Local Cartesian coordinate system is defined to supply these needs.

Origin : Projection of where motion of missile starts on zero altitude,

X_c : Directed to ellipsoid north,
Y_c : Directed to ellipsoid east,
Z_c : Directed to ellipsoid down.

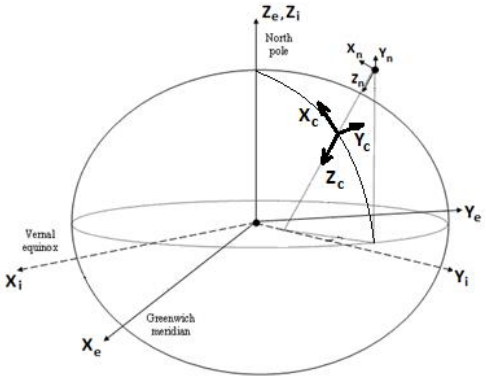

Figure 2.4: Local Cartesian coordinate system definition

2.2.5 Body Frame

The origin of the body coordinate system is linked to the missile body and the center of mass. Its axes are X_b, Y_b, Z_b. The x-axis, called the roll axis, points towards the nose of missile; the y-axis, called the pitch axis is directed to right when the missile viewed from rear and orthogonal to X_b. The z-axis is directed according to the right hand rule.

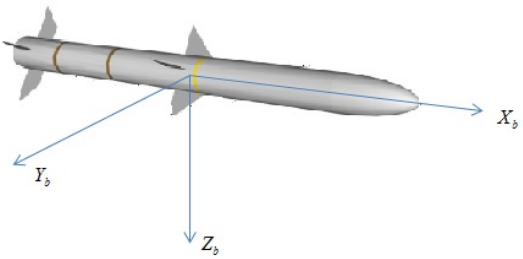

Figure 2.5: Body coordinate system at the center of gravity of missile

Origin : Center of gravity of missile,
X_b : Directed from center of the coordinate system the nose of missile,
Y_b : When viewed from rear directed to right. Orthogonal to X_b,
Z_b : Orthogonal to the X_b and Y_b direction according to the right hand rule.

2.2.6 Transformation Matrices

A vector defined in one coordinate system can be redefined in another coordinates system. This is achieved by axis transformations. Any set of axes definition of a

vector can be obtained from any other set by a sequence of three rotations. For each rotation, a transformation matrix is applied to the vectorial quantities. The final transformation matrix is simply the product of the three matrices, multiplied in the order of the rotations. Common law of the aeronautics states that firstly rotate the system by ψ (yaw angle) about Z axis, then by θ (pitch angle) about new Y axis, and by ϕ (roll angle) about the latest X axis which are called *Euler Angles*.

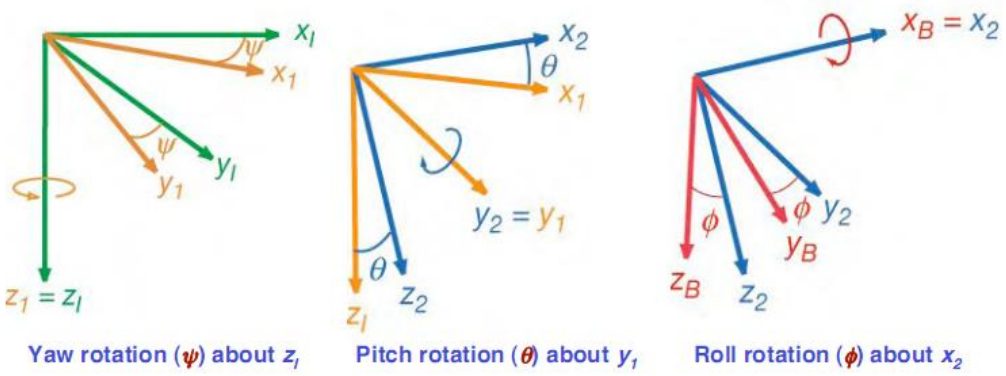

Figure 2.6: Euler angles

The transformation matrices are defined with order of rotation about Z, Y and X axis.

The first rotation about Z axis (ψ angle)

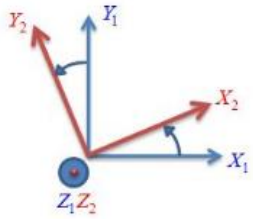

$$\begin{bmatrix} X_2 \\ Y_2 \\ Z_2 \end{bmatrix} = C_\psi \begin{bmatrix} X_1 \\ Y_1 \\ Z_1 \end{bmatrix} = \begin{bmatrix} cos(\psi) & sin(\psi) & 0 \\ -sin(\psi) & cos(\psi) & 0 \\ 0 & 0 & 1 \end{bmatrix} \begin{bmatrix} X_1 \\ Y_1 \\ Z_1 \end{bmatrix}$$

Figure 2.7: Rotation about Z axis

the second rotation about Y axis (θ angle)

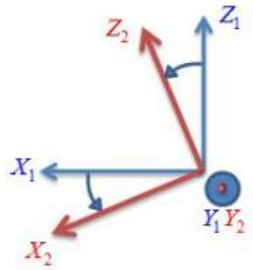

$$\begin{bmatrix} X_2 \\ Y_2 \\ Z_2 \end{bmatrix} = C_\theta \begin{bmatrix} X_1 \\ Y_1 \\ Z_1 \end{bmatrix} = \begin{bmatrix} cos(\theta) & 0 & -sin(\theta) \\ 0 & 1 & 0 \\ sin(\theta) & 0 & cos(\theta) \end{bmatrix} \begin{bmatrix} X_1 \\ Y_1 \\ Z_1 \end{bmatrix}$$

Figure 2.8: Rotation about Y axis

and the third rotation about X axis (ϕ angle) is stated as follows.

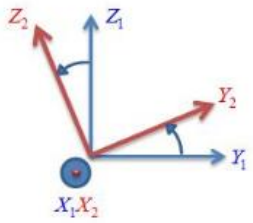

$$\begin{bmatrix} X_2 \\ Y_2 \\ Z_2 \end{bmatrix} = C_\phi \begin{bmatrix} X_1 \\ Y_1 \\ Z_1 \end{bmatrix} = \begin{bmatrix} 1 & 0 & 0 \\ 0 & cos(\phi) & sin(\phi) \\ 0 & -sin(\phi) & cos(\phi) \end{bmatrix} \begin{bmatrix} X_1 \\ Y_1 \\ Z_1 \end{bmatrix}$$

Figure 2.9: Rotation about X axis

This sequential rotations defines a transformation matrix called 'Direction Cosine Matrix' (DCM) that will define a transformation of a motion from Earth coordinate system to body coordinate system as follows.

$$\begin{bmatrix} X_b \\ Y_b \\ Z_b \end{bmatrix} = C_\phi C_\theta C_\psi \begin{bmatrix} X_e \\ Y_e \\ Z_e \end{bmatrix}$$

$$= \begin{bmatrix} 1 & 0 & 0 \\ 0 & cos(\phi) & sin(\phi) \\ 0 & -sin(\phi) & cos(\phi) \end{bmatrix} \begin{bmatrix} cos(\theta) & 0 & -sin(\theta) \\ 0 & 1 & 0 \\ sin(\theta) & 0 & cos(\theta) \end{bmatrix} \begin{bmatrix} cos(\psi) & sin(\psi) & 0 \\ -sin(\psi) & cos(\psi) & 0 \\ 0 & 0 & 1 \end{bmatrix} \begin{bmatrix} X_e \\ Y_e \\ Z_e \end{bmatrix}$$

$$= \begin{bmatrix} cos(\theta)cos(\psi) & cos(\theta)sin(\psi) & -sin(\theta) \\ -cos(\phi)sin(\psi) + sin(\phi)sin(\theta)cos(\psi) & cos(\phi)cos(\psi) + sin(\phi)sin(\theta)sin(\psi) & sin(\phi)cos(\theta) \\ sin(\phi)sin(\psi) + cos(\phi)sin(\theta)cos(\psi) & -sin(\phi)cos(\psi) + cos(\phi)sin(\theta)sin(\psi) & cos(\phi)cos(\theta) \end{bmatrix}$$

$$\begin{bmatrix} X_b \\ Y_b \\ Z_b \end{bmatrix} = C^{(b,e)} \begin{bmatrix} X_e \\ Y_e \\ Z_e \end{bmatrix} \tag{2.1}$$

This representation stands for the transformation from the Earth axis to the body axis system.

$$\left[C^{(b,e)}\right]^{-1} = \left[C^{(b,e)}\right]^T = C^{(e,b)} \Rightarrow \begin{bmatrix} X_e \\ Y_e \\ Z_e \end{bmatrix} = C^{(e,b)} \begin{bmatrix} X_b \\ Y_b \\ Z_b \end{bmatrix} \tag{2.2}$$

represents the transformation from body axis to Earth axis.

2.3 Aerodynamic Model

2.3.1 Flight Parameters

Before defining aerodynamic forces and moments, it is required to define some flight parameters and dynamic pressure.

Angle of Attack : The angle between the projection of velocity vector of missile on $X_b - Z_b$ plane and X_b axis of missile in longitudinal plane. It is positive when the missile velocity component along z-axis is positive. It is shown by α

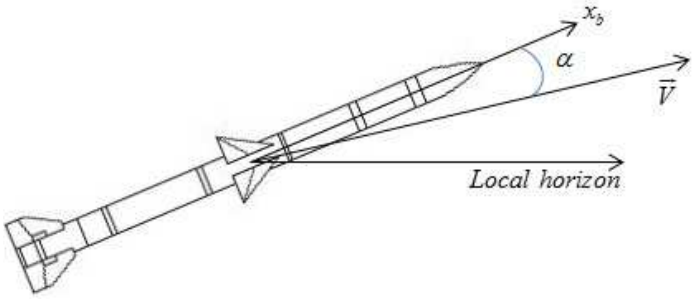

Figure 2.10: Angle of attack descripton

$$\alpha = \arctan\left(\frac{w}{u}\right) \tag{2.3}$$

Angle of Sideslip : The angle between the projection of velocity vector of missile on $X_b - Y_b$ plane and X_b axis of missile in lateral plane. It is positive when the missile velocity component along y-axis is positive. It is shown by β.

$$\beta = \arcsin\left(\frac{v}{V}\right) \tag{2.4}$$

where V is the magnitude of total velocity defined as

$$V = \sqrt{u^2 + v^2 + w^2} \tag{2.5}$$

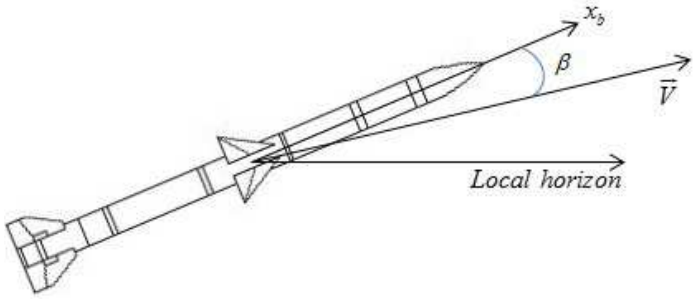

Figure 2.11: Angle of sideslip description

Mach number : In fluid mechanics, it represents the ratio of speed of an object moving through a fluid and the local speed of sound. C represents the speed of the sound, then Mach number can be expressed as

$$M = \frac{V}{C} \tag{2.6}$$

C can be stated as $C = \gamma RT$ where γ is the specific heat ratio of the air which is taken to be equal to 1.4, and R is the universal air gas constant which is equal to $287 J/kgK$. T is the ambient temperature which changes with altitude, and can be expressed as

$$T = \left\{ \begin{array}{ll} T_0 \left(1 - 0.00002256h\right) & for \;\; h \leq 10000m \\ 0.7744 T_0 & for \;\; h > 10000m \end{array} \right\} \tag{2.7}$$

Dynamic Pressure : It is defined as

$$Q = \frac{1}{2}\rho V^2 \tag{2.8}$$

The term ρ is the air density and calculated as follows

$$\rho = \left\{ \begin{array}{ll} \rho_0 \left(1 - 0.00002256h\right)^{4.256} & for \;\; h \leq 10000m \\ 0.412 e^{-0.000151(h-10000)} & for \;\; h > 10000m \end{array} \right\} \tag{2.9}$$

where ρ_0 is the air density at sea level $1.223 kg/m^3$ and h is the altitude.

2.3.2 Aerodynamic Data

To construct a mathematical model, there has to be physical meaning of the plant. In missile case, mathematical model requires aerodynamic data that emphasizes the aerodynamic force and moment coefficients stating agility of the missile airframe. Missile Datcom is a program that provides estimation of aerodynamics of a wide variety of missile configuration designs quickly. It has predictive accuracy for suitable preliminary design. To get aerodynamic data, firstly the physical features of the missile are required. The modelled missile has $140''$ length and $7''$ diameter. It has non-moving four wings in the middle that placed with 90° angle difference and four movable fins(control surfaces) at back to give direction to the missile. Approximate geometry is represented in Figure 2.12.

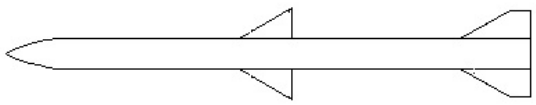

Figure 2.12: Baseline geometry

Missile Datcom has some parameters to express the physical features of the missile. They can be shown in Figure 2.13-2.16.

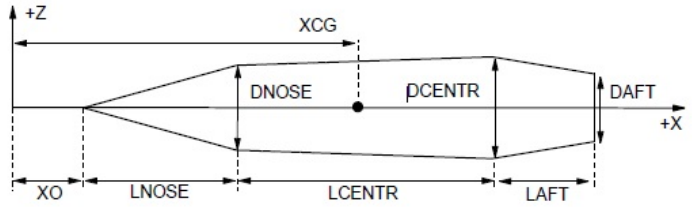

Figure 2.13: Axisymmetric body geometry variables [30]

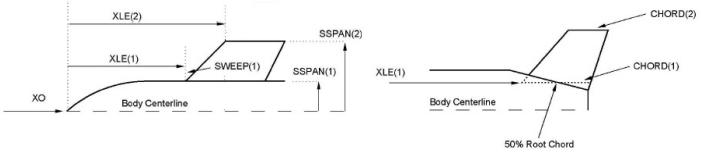

Figure 2.14: Wing and fin geometry variables [30]

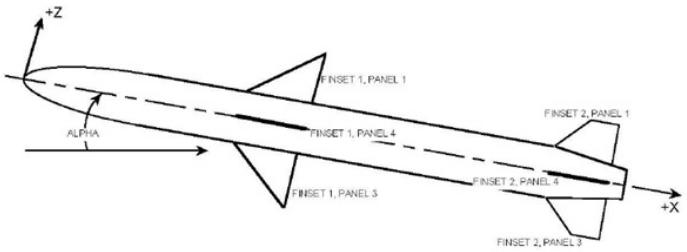

Figure 2.15: Wing and fin orders [30]

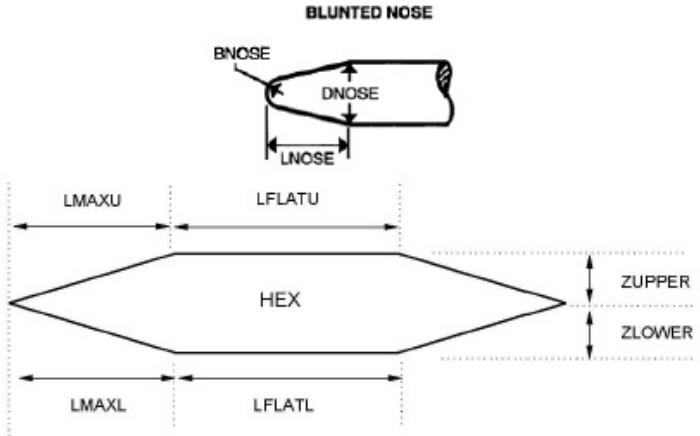

Figure 2.16: Nose geometry and HEX airfoil variables [30]

With the values assigned to these variables, missile geometry is defined for the Missile Datcom input file. Details about the program and the input file are stated in [30]. The missile is assumed to fly at X configuration, so the aerodynamic data is obtained

for the wings and fins are located at 45°, 135°, 225° and 315° angles. Flight regime area is defined to Missile Datcom with the flight parameters as

$\alpha \quad = \{-20, -18, -16, ..., 16, 18, 20\}$
$\beta \quad = \{-20, -18, -16, ..., 16, 18, 20\}$
Mach $= \{0.4, 0.8, 1.2, 1.6, 2.0, 2.4, 2.8, 3.2, 3.6, 4.0\}$

The obtained aerodynamic data is used for 6DOF simulation model and autopilot design. When the subject comes to control, a missile that is inherently stable in most of the flight parameter region is preferred in many cases. For a completely stable missile, stability, control and dynamic derivatives of aerodynamic coefficients must have appropriate signs. This is summarized in Table 2.1. If the case is an AAM, agility is the most critical requirement for effectiveness and the agility requires instability in some flight region. Some of the aerodynamic coefficients of the missile are plotted to figures as follows to understand the parallel and contradictive parts to the Table 2.1.

Table2.1: For an inherently stable missile, uncoupled terms of aerodynamic stability, control and dynamic derivatives

Stability	Sign	Control	Sign	Dynamic	Sign
C_{Y_β}	$-$	$C_{Y_{\delta_r}}$	$-$	C_{Y_r}	$+$
C_{N_α}	$+$	$C_{N_{\delta_e}}$	$-$	C_{N_q}	$+$
C_{l_β}	$+$	$C_{l_{\delta_a}}$	$+$	C_{l_p}	$-$
C_{m_α}	$-$	$C_{m_{\delta_e}}$	$+$	C_{m_q}	$-$
C_{n_β}	$-$	$C_{n_{\delta_r}}$	$+$	C_{n_r}	$-$

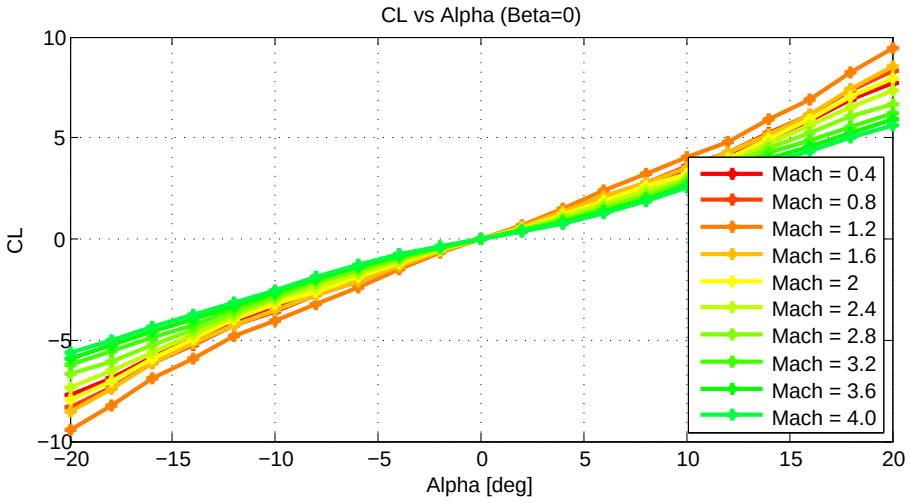

Figure 2.17: Lift coefficient change with alpha

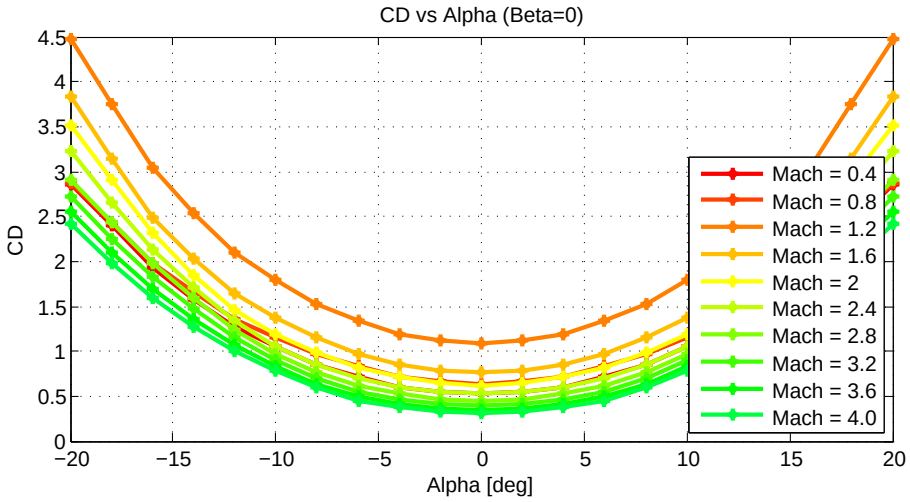

Figure 2.18: Drag coefficient change with alpha

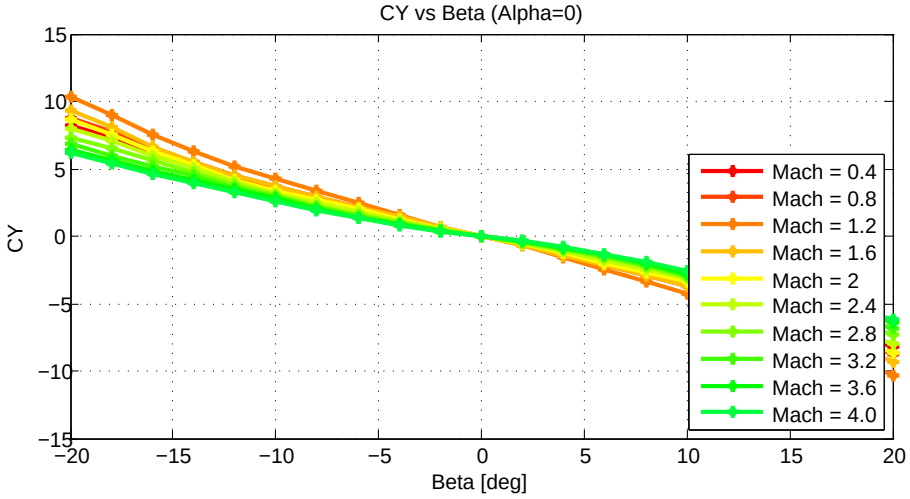

Figure 2.19: Side force coefficient change with beta

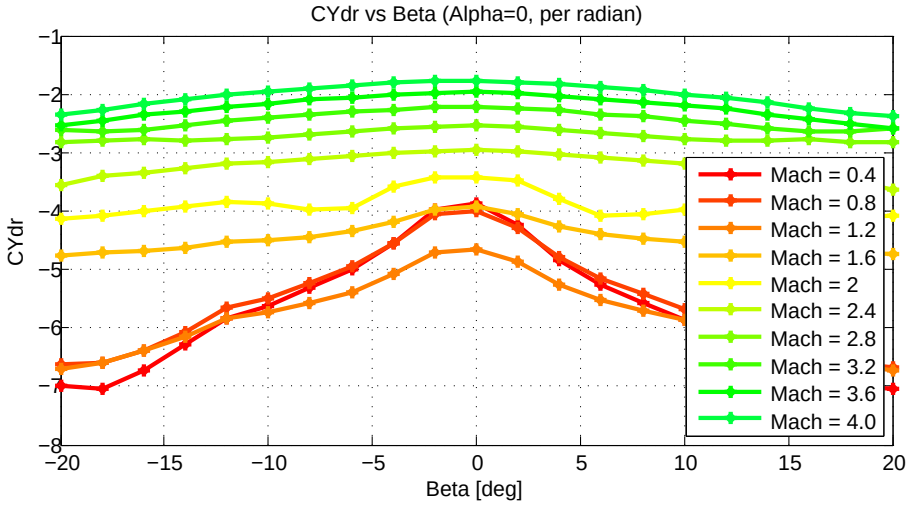

Figure 2.20: Side force control derivative change with beta

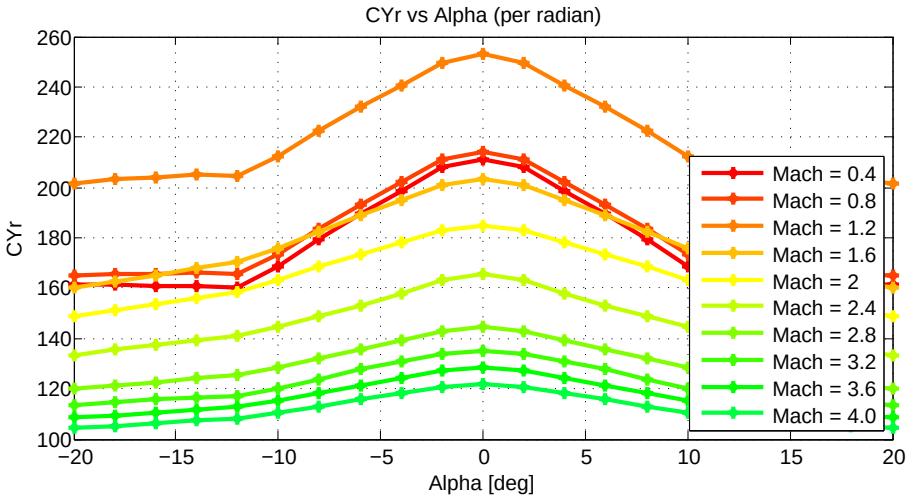

Figure 2.21: Side force dynamic derivative change with alpha

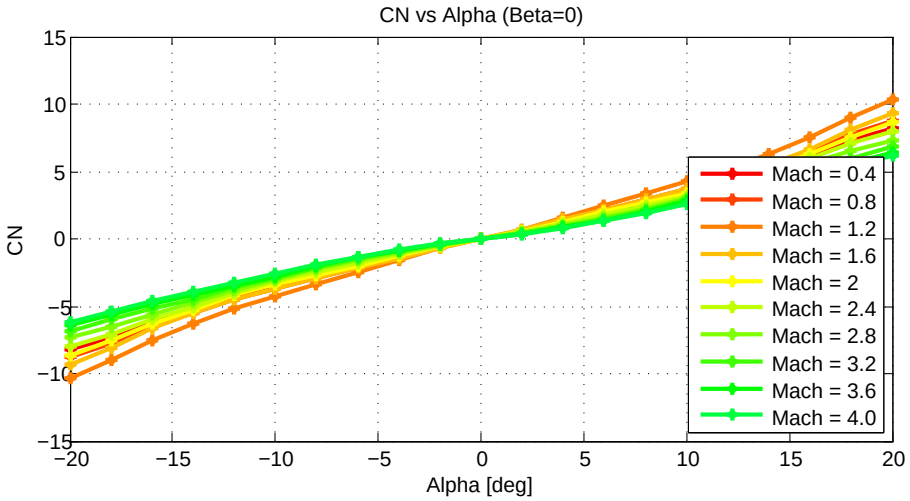

Figure 2.22: Normal force coefficient change with alpha

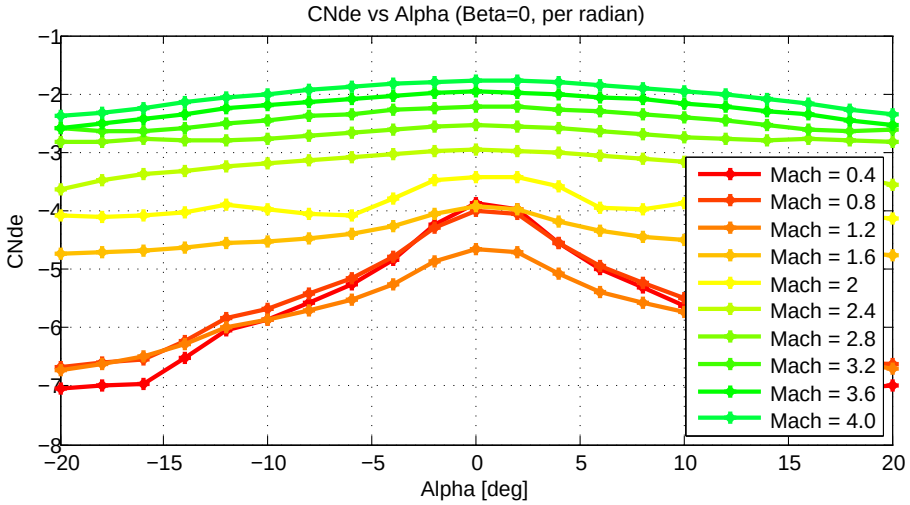

Figure 2.23: Normal force control derivative change with alpha

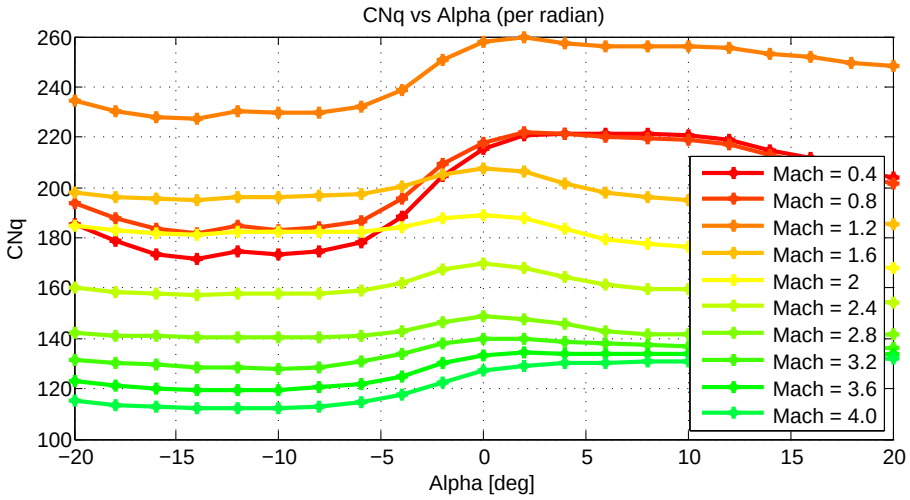

Figure 2.24: Normal force dynamic derivative change with alpha

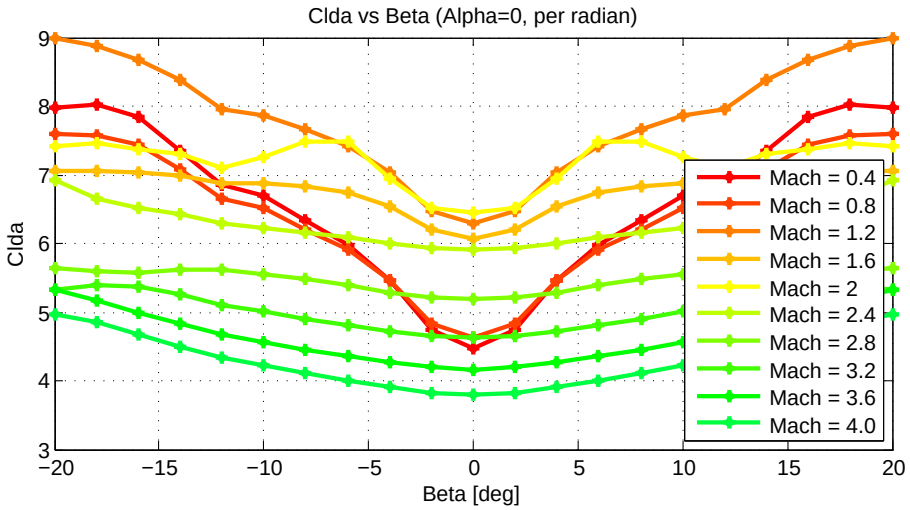

Figure 2.25: Rolling moment control derivative change with beta

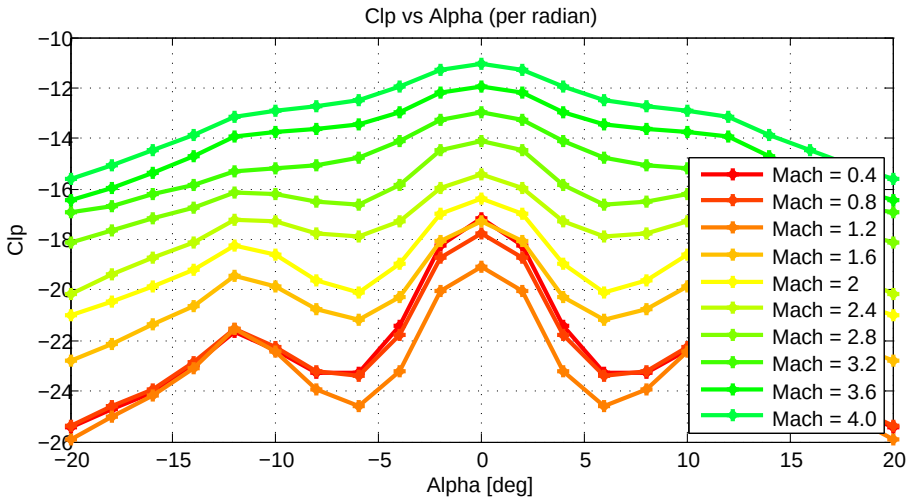

Figure 2.26: Rolling moment dynamic derivative change with alpha

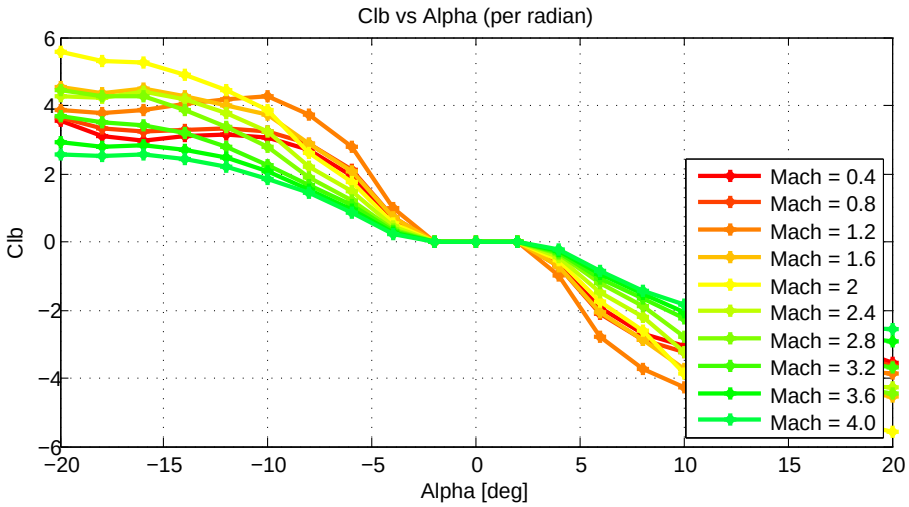

Figure 2.27: Rolling stability derivative change with alpha

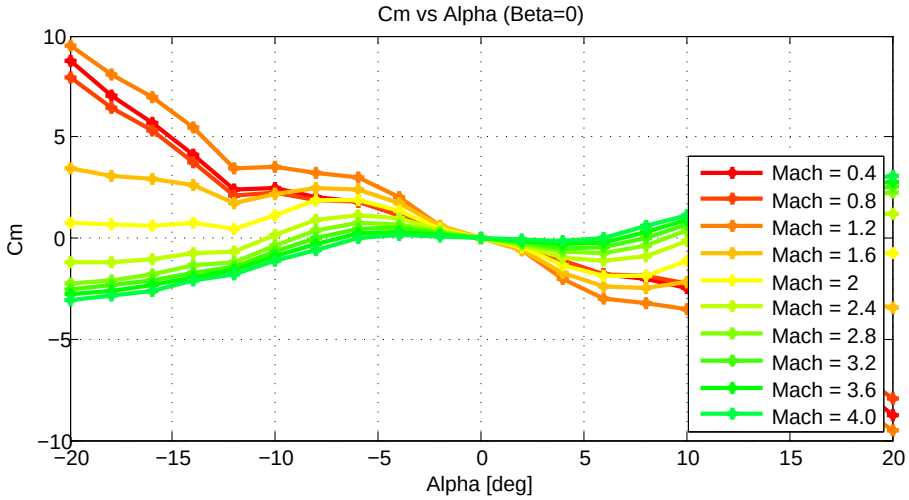

Figure 2.28: Pitching moment coefficient change with alpha

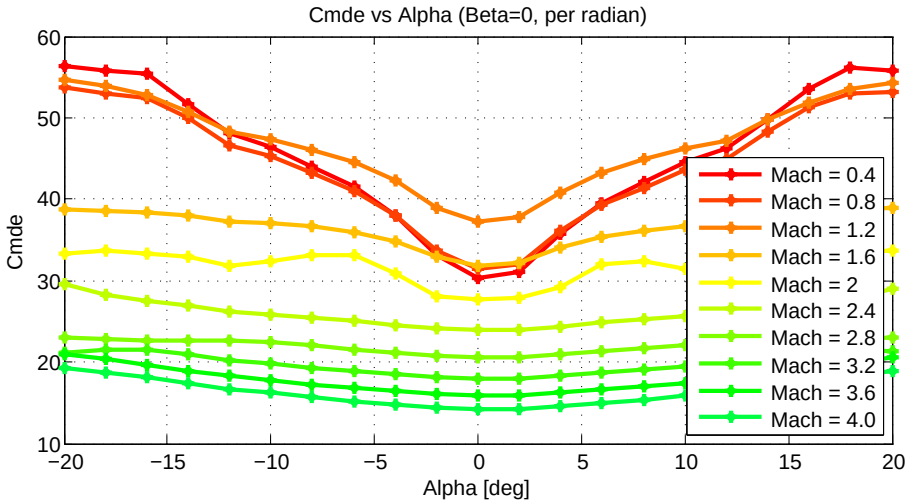

Figure 2.29: Pitching moment control derivative change with alpha

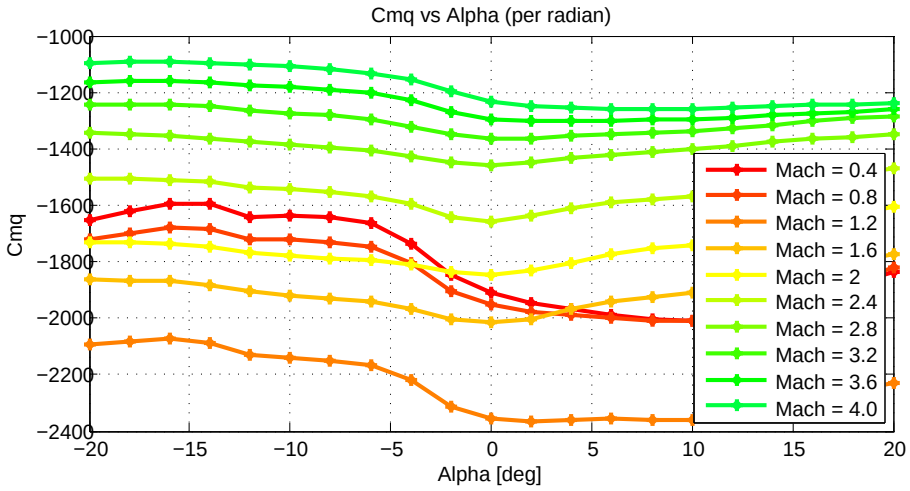

Figure 2.30: Pitching moment dynamic derivative change with alpha

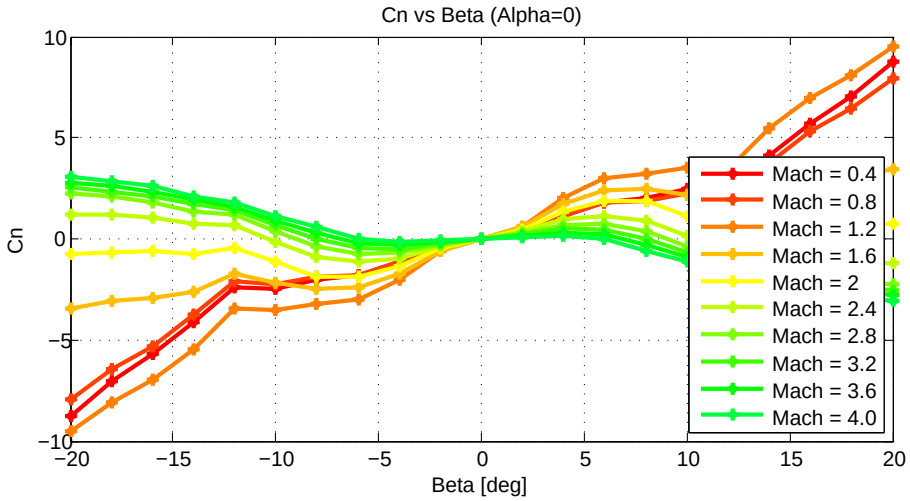

Figure 2.31: Yawing moment coefficient change with beta

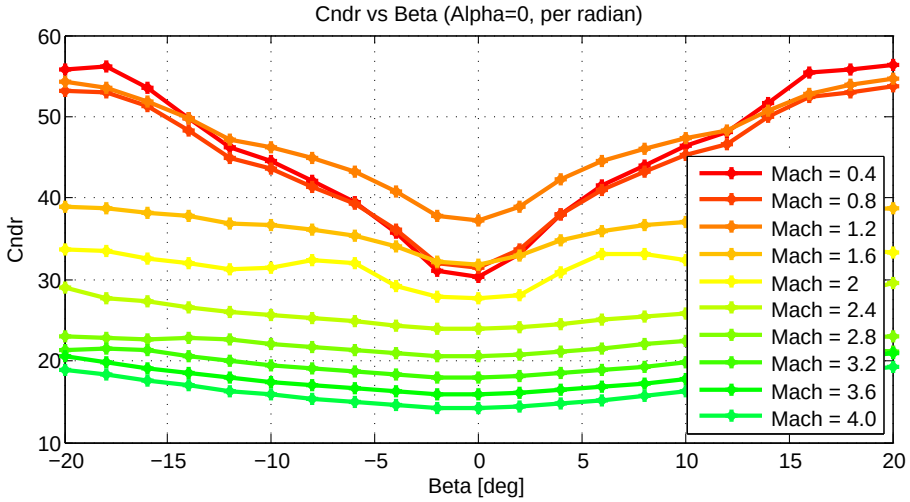

Figure 2.32: Yawing moment control derivative change with beta

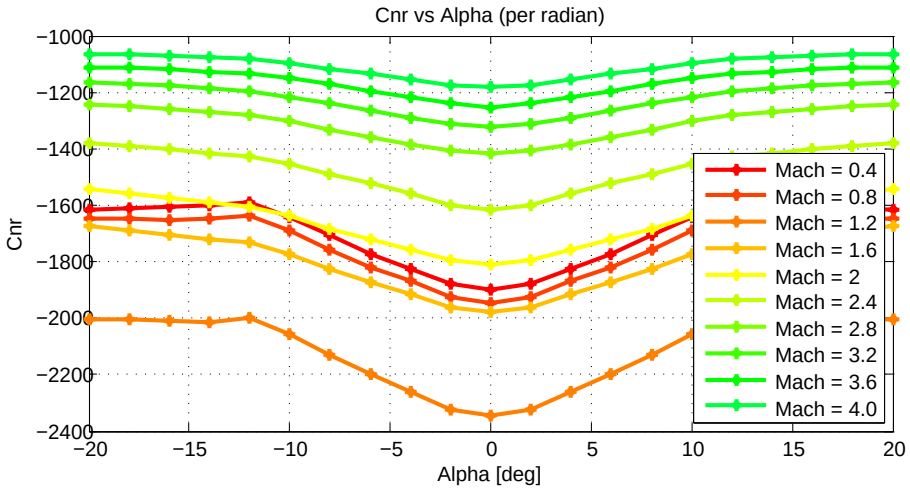

Figure 2.33: Yawing moment dynamic derivative change with alpha

2.3.3 Aerodynamic Forces and Moments

Aerodynamic forces and moments can be represented with their coefficients. If reference area is A, reference length is d, dynamic pressure is Q and C_X, C_Y and C_Z are aerodynamic coefficients for forces respectively, then the aerodynamics forces can be stated as follows

$$\begin{bmatrix} F_{ax} \\ F_{ay} \\ F_{az} \end{bmatrix} = QA \begin{bmatrix} C_X \\ C_Y \\ C_Z \end{bmatrix} \tag{2.10}$$

For C_l, C_m, and C_n are moment coefficients, aerodynamic moments can be stated as

$$\begin{bmatrix} L \\ M \\ N \end{bmatrix} = QAd \begin{bmatrix} C_l \\ C_m \\ C_n \end{bmatrix} \tag{2.11}$$

where

C_X : Axial force coefficient,
C_Y : Side force coefficient,
C_Z : Normal force coefficient,
C_l : Rolling moment coefficient,
C_m : Pitching moment coefficient,
C_n : Yawing moment coefficient.

Aerodynamic coefficients can be stated to be a function of several flight variables as

$$C_i = C_i\left(M, \alpha, \beta, \delta_a, \delta_e, \delta_r, p, q, r, \dot{\alpha}, \dot{\beta}\right)$$

In real world, these coefficients are functions of much more flight parameters and higher order terms. Force and moment coefficients can be found from look up tables that are created from Mach number, angle of attack, angle of sideslip, elevator fin deflection (δ_e), aileron fin deflection(δ_a), and rudder fin deflection (δ_r). These table variables can be decreased to simplify the table, but this decreases the level of fidelity. For 6DOF simulations and linear autopilot design, linearized forms of these aerodynamic coefficients are derived in Section 2.4.2.2.

2.4 Equations of Motion

2.4.1 Nonlinear Equations of Motion

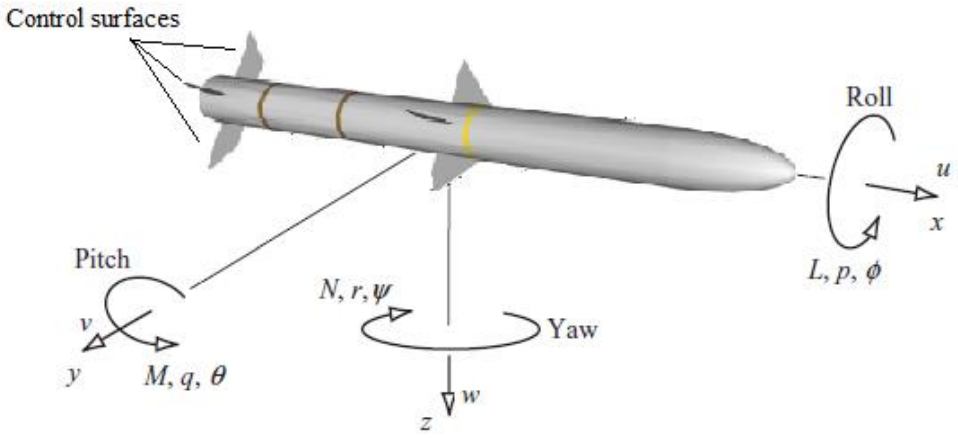

Figure 2.34: Translational and rotational definitions

The parameters related to the missile are defined in Table 2.2 below.

Table2.2: Related parameters of missile

	x	y	z
Angle	Φ (roll)	Θ (pitch)	Ψ (yaw)
Velocity	u	v	w
Position	x_B	y_B	z_B
Angular Rate	p	q	r
Force	F_x	F_y	F_z
Moment	L	M	N
Inertia	I_{xx}	I_{yy}	I_{zz}
Product of Inertia	I_{yz}	I_{xz}	I_{xy}

Two assumptions are made before starting the derivation:

- mass of the missile remains constant,
- missile is a rigid body.

The forces and moments acting on a missile are given as F_x, F_y, F_z and M_x, M_y, M_z. Actually, these forces and moments are total of some distinct forces and moments. Aerodynamic forces, thrust forces and the gravitational effects have to be taken into consideration while talking about these forces and moments. In fact, these forces and moments can be written as

$$\begin{bmatrix} F_X \\ F_Y \\ F_Z \end{bmatrix} = \begin{bmatrix} F_{ax} + mg_x + T_x \\ F_{ay} + mg_y + T_y \\ F_{az} + mg_z + T_z \end{bmatrix} \tag{2.12}$$

$$\begin{bmatrix} M_X \\ M_Y \\ M_Z \end{bmatrix} = \begin{bmatrix} L + L_T \\ M + M_T \\ N + N_T \end{bmatrix} \tag{2.13}$$

In the above equations, F_{ax}, F_{ay}, F_{az}, F_{ay}, L, M and N are the forces and moments which only occurs due to aerodynamics effects on the missile flight. g_x, g_y, and g_z are the body frame components of the gravitational acceleration which is assumed to be oriented directly towards the Earth center. T_x, T_y, T_z, L_T, M_T, N_T, are thrust force and thrust moment components.

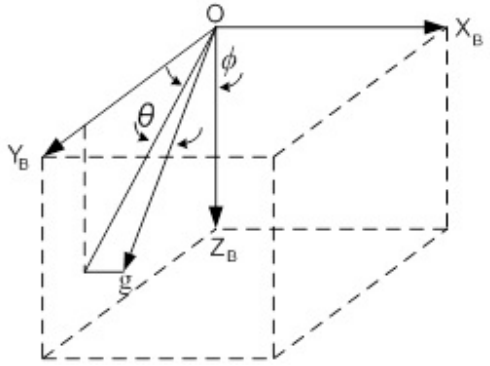

Figure 2.35: components of the gravitational force

According to the Figure 2.35, body coordinate system components of the gravitational acceleration can be expressed as follows

$$\begin{bmatrix} g_x \\ g_y \\ g_z \end{bmatrix} = \begin{bmatrix} -g\sin(\theta) \\ g\sin(\phi)cos(\theta) \\ g\cos(\phi)cos(\theta) \end{bmatrix} \tag{2.14}$$

2.4.1.1 Kinematical Equations of Motion

Translational Kinematics

Velocity expressed in the body coordinate system can be transformed to the Earth coordinate system by using the transpose of DCM that is calculated before.

$$\begin{bmatrix} V_X \\ V_Y \\ V_Z \end{bmatrix} = C^{(e,b)} \begin{bmatrix} u \\ v \\ w \end{bmatrix} \tag{2.15}$$

and if the calculation is extended, the following equations are obtained.

$$V_X = (\cos(\theta)\cos(\psi))\, u + (\sin(\phi)\sin(\theta)\cos(\psi) - \cos(\phi)\sin(\psi))\, v + (\cos(\phi)\sin(\theta)\cos(\psi) + \sin(\phi)\sin(\psi))\, w \tag{2.16}$$

$$V_Y = (\cos(\theta)\sin(\psi))\, u + (\sin(\phi)\sin(\theta)\sin(\psi) + \cos(\phi)\cos(\psi))\, v + (\cos(\phi)\sin(\theta)\sin(\psi) - \sin(\phi)\cos(\psi))\, w \tag{2.17}$$

$$V_Z = (-\sin(\theta))\, u + (\sin(\phi)\cos(\theta))\, v + (\cos(\phi)\cos(\theta))\, w \tag{2.18}$$

where V_X,V_Y and V_Z are the velocity components of the body with respect to the Earth fixed frame stated in Earth fixed frame and u, v, w are the velocities with respect to Earth fixed frame stated in body frame.

Rotational Kinematics

The rotational kinematic equations relates the time rate of change of the Euler angles(orientation of missile with respect to the reference coordinate frame) to the angular rates of missile body. Using the identity feature

$$\left[C^{(e,b)}\right]^T C^{(e,b)} = I \tag{2.19}$$

it is known that derivative of a constant is zero.

$$\frac{d}{dx}\left(\left[C^{(e,b)}\right]^T C^{(e,b)}\right) = \frac{d}{dx}(I) \tag{2.20}$$

$$\left[C^{(e,b)}\right]^T \dot{C}^{(e,b)} = \left[-\dot{C}^{(e,b)}\right]^T C^{(e,b)} \tag{2.21}$$

$$\left[C^{(e,b)}\right]^T \dot{C}^{(e,b)} = -\left(\left[C^{(e,b)}\right]^T \dot{C}^{(e,b)}\right) \tag{2.22}$$

The above equation indicates that $\left[C^{(e,b)}\right]^T \dot{C}^{(e,b)}$ is a skew symmetric matrix and so there exists a skew symmetric $\tilde{\omega}$ generated from a column $\vec{w}$ such that $\tilde{\omega} = \left[C^{(e,b)}\right]^T \dot{C}^{(e,b)} \vec{w}_{ang}$ is composed of the components of the angular velocity of the body frame with respect to the Earth frame stated in body frame.

More explicitly,

$$\vec{w}_{ang} = \begin{bmatrix} p \\ q \\ r \end{bmatrix} \tag{2.23}$$

thus the corresponding skew symmetric matrix is

$$\tilde{\omega} = \begin{bmatrix} 0 & -r & q \\ r & 0 & -p \\ -q & p & 0 \end{bmatrix} \tag{2.24}$$

Solving $\left[C^{(e,b)}\right]^T \dot{C}^{(e,b)} = \tilde{\omega}$ for the Euler angle rates, the rotational kinematical equations are found as

$$\dot{\phi} = p + (qsin(\phi) + rcos(\phi))\, tan(\theta) \tag{2.25}$$

$$\dot{\theta} = qcos(\phi) - rsin(\phi) \tag{2.26}$$

$$\dot{\psi} = \frac{qsin(\phi) + rcos(\phi)}{cos(\theta)} \tag{2.27}$$

2.4.1.2 Dynamical Equations of Motion

Translational Dynamics

For derivation of translational dynamics, force equation of the Newton's Second Law is used as follows. If the Earth rotation with respect to the inertial frame is neglected, the Earth frame can be declared as the inertial frame then equations can be derived as if translational and angular velocities are defined in the Earth frame.

$$\vec{F} = \frac{d}{dt}\left(m\vec{V}\right)|_E = m\frac{d}{dt}\left(\vec{V}\right)|_E \tag{2.28}$$

$$\vec{F} = \vec{F}_{aero} + \vec{F}_{thrust} + \vec{F}_{gravity} \tag{2.29}$$

where F is the sum of all externally applied forces acting on the missile including aerodynamic forces, thrust forces and gravity forces, m is the mass of missile, V is the velocity of center of mass with respect to the Earth frame. $|_E$ indicates that the differentiation of the related terms are done in the Earth frame. In the body frame, Equation 2.28 can be written as

$$\vec{F} = m\{\frac{d}{dt}\vec{V}|_B\} + \vec{w}_{ang} \times \vec{V} \tag{2.30}$$

where $|_B$ indicates that the differentiation is done in the body frame. $\vec{F}$ vector is represented as

$$\vec{F} = \begin{bmatrix} F_X \\ F_Y \\ F_Z \end{bmatrix} \tag{2.31}$$

and the linear velocity vector $\vec{V}$ is stated as

$$\vec{V} = \begin{bmatrix} u \\ v \\ w \end{bmatrix} \tag{2.32}$$

and the angular velocity vector is

$$\vec{w}_{ang} = \begin{bmatrix} p \\ q \\ r \end{bmatrix} \tag{2.33}$$

Then Equation 2.30 is written as

$$\begin{bmatrix} F_X \\ F_Y \\ F_Z \end{bmatrix} = m \left\{ \begin{bmatrix} \dot{u} \\ \dot{v} \\ \dot{w} \end{bmatrix} + \begin{bmatrix} p \\ q \\ r \end{bmatrix} \times \begin{bmatrix} u \\ v \\ w \end{bmatrix} \right\} \tag{2.34}$$

leave acceleration terms at one side.

$$\begin{bmatrix} \dot{u} \\ \dot{v} \\ \dot{w} \end{bmatrix} = \begin{bmatrix} \frac{F_X}{m} \\ \frac{F_Y}{m} \\ \frac{F_Z}{m} \end{bmatrix} - \begin{bmatrix} p \\ q \\ r \end{bmatrix} \times \begin{bmatrix} u \\ v \\ w \end{bmatrix} \tag{2.35}$$

after calculation of cross product

$$\begin{bmatrix} \dot{u} \\ \dot{v} \\ \dot{w} \end{bmatrix} = \begin{bmatrix} \frac{F_X}{m} \\ \frac{F_Y}{m} \\ \frac{F_Z}{m} \end{bmatrix} - \begin{bmatrix} qw - rv \\ ru - pw \\ pv - qu \end{bmatrix} \tag{2.36}$$

and finally translational equations are derived as

$$\dot{u} = \frac{F_X}{m} - qw + rv \tag{2.37}$$

$$\dot{v} = \frac{F_Y}{m} - ru + pw \tag{2.38}$$

$$\dot{w} = \frac{F_Z}{m} - pv + qu \tag{2.39}$$

Rotational Dynamics

For the derivation of rotational dynamic equations, following equality will be used.

$$\vec{M} = \frac{d}{dt}\left(\vec{H}\right)|_E \tag{2.40}$$

$\vec{M}$ represents the sum of all externally applied torques to missile. $\vec{H} = \hat{J}\vec{w}_{ang}$ is the angular momentum of the missile, $\hat{J}$ is the inertia dyadic. In the body coordinate system Equation 2.40 can be written as

$$\vec{M} = \hat{J}\left\{\frac{d}{dt}\left(\vec{H}\right)|_B\right\} + \vec{w}_{ang} \times \hat{J}\vec{w}_{ang} \tag{2.41}$$

The inertia dyadic can be expressed in the body frame by the following matrix

$$\hat{J} = \begin{bmatrix} I_{xx} & -I_{xy} & -I_{xz} \\ -I_{xy} & I_{yy} & -I_{yz} \\ -I_{xz} & -I_{yz} & I_{zz} \end{bmatrix} \tag{2.42}$$

The body axis of the missile is taken to be coincident with the principle axis of inertia. Hence product of cross inertia terms I_{xy}, I_{xz} and I_{yz} vanish. Due to the symmetric structure of the missile used in this study, $I_{yy} = I_{zz}$ equality will be used. Thus the inertia matrix can be simplified for a symmetric missile as

$$\hat{J} = \begin{bmatrix} I_{xx} & 0 & 0 \\ 0 & I_{yy} & 0 \\ 0 & 0 & I_{zz} \end{bmatrix} \tag{2.43}$$

The column vector representation of total moment is

$$\vec{M} = \begin{bmatrix} M_X \\ M_Y \\ M_Z \end{bmatrix} \tag{2.44}$$

if Equation 2.40 is constructed

$$\begin{bmatrix} M_X \\ M_Y \\ M_Z \end{bmatrix} = \begin{bmatrix} I_{xx} & 0 & 0 \\ 0 & I_{yy} & 0 \\ 0 & 0 & I_{zz} \end{bmatrix} \begin{bmatrix} \dot{p} \\ \dot{q} \\ \dot{r} \end{bmatrix} + \begin{bmatrix} p \\ q \\ r \end{bmatrix} \times \begin{bmatrix} I_{xx} & 0 & 0 \\ 0 & I_{yy} & 0 \\ 0 & 0 & I_{zz} \end{bmatrix} \begin{bmatrix} p \\ q \\ r \end{bmatrix} \tag{2.45}$$

After dot product calculation

$$\begin{bmatrix} M_X \\ M_Y \\ M_Z \end{bmatrix} = \begin{bmatrix} I_{xx}\dot{p} \\ I_{yy}\dot{q} \\ I_{zz}\dot{r} \end{bmatrix} + \begin{bmatrix} p \\ q \\ r \end{bmatrix} \times \begin{bmatrix} I_{xx}p \\ I_{yy}q \\ I_{zz}r \end{bmatrix} \tag{2.46}$$

with calculation of cross product

$$\begin{bmatrix} M_X \\ M_Y \\ M_Z \end{bmatrix} = \begin{bmatrix} I_{xx}\dot{p} \\ I_{yy}\dot{q} \\ I_{zz}\dot{r} \end{bmatrix} + \begin{bmatrix} I_{zz}qr - I_{yy}qr \\ -I_{zz}pr + I_{xx}pr \\ I_{yy}pq - I_{xx}pq \end{bmatrix} \tag{2.47}$$

and finally rotational dynamic equations are obtained as

$$\dot{p} = \frac{M_X - qr\left(I_{zz} - I_{yy}\right)}{I_{xx}} \tag{2.48}$$

$$\dot{q} = \frac{M_Y - rp\left(I_{xx} - I_{zz}\right)}{I_{yy}} \tag{2.49}$$

$$\dot{r} = \frac{M_Z + pq\left(I_{yy} - I_{xx}\right)}{I_{zz}} \tag{2.50}$$

2.4.2 Linear Equations of Motion

2.4.2.1 Linearization of Differential Equations

Linearization refers to finding the linear approximation to a function at a given point. In dynamical systems, linearization is a method for assessing the local stability of

an equilibrium point of a system of nonlinear differential equations. Suppose that a nonlinear system model can be represented as in the following most general notation.

$$\dot{x} = f(x,u) \qquad where \qquad x \in \Re^n \quad and \quad u \in \Re^m \tag{2.51}$$

Let $u_e = [u_{1e}, u_{2e}, ..., u_{me}]^T$ be a constant input that forces the system above to settle into a constant equilibrium state $x_e = [x_{1e}, x_{2e}, ..., x_{ne}]^T$, that is, u_e and x_e satisfy

$$f(x_e, u_e) = 0 \tag{2.52}$$

Let us now perturb the equilibrium input vector by allowing

$$u = u_e + \Delta u \Rightarrow x = x_e + \Delta x \tag{2.53}$$

Taylor's expansions yields

$$\dot{x} = f(x_e+\Delta x, u_e+\Delta u) = f(x_e,u_e)+\frac{\partial f}{\partial x}(x_e,u_e)\Delta x+\frac{\partial f}{\partial u}(x_e,u_e)\Delta u+HOT = A\Delta x+B\Delta u \tag{2.54}$$

In this equation, Jacobian matrices of f with respect to x and u, evaluated at (x_e, u_e), called autopilot design conditions in this study, are equal to the following matrices

$$\frac{\partial f}{\partial x}(x_e,u_e) = \begin{bmatrix} \frac{\partial f_1}{\partial x_1} & \cdots & \frac{\partial f_1}{\partial x_n} \\ \vdots & \ddots & \vdots \\ \frac{\partial f_n}{\partial x_1} & \cdots & \frac{\partial f_n}{\partial x_n} \end{bmatrix}_{x=x_e, u=u_e} \tag{2.55}$$

$$\frac{\partial f}{\partial u}(x_e,u_e) = \begin{bmatrix} \frac{\partial f_1}{\partial u_1} & \cdots & \frac{\partial f_1}{\partial u_n} \\ \vdots & \ddots & \vdots \\ \frac{\partial f_n}{\partial u_1} & \cdots & \frac{\partial f_n}{\partial u_n} \end{bmatrix}_{x=x_e, u=u_e} \tag{2.56}$$

Similarly, if the nonlinear system model are of the form $y = h(x,u)$, its linear form can be derived as the rules explained above and resultant model is

$$y = y_e + \Delta y \quad , \quad \Delta y = C\Delta x + D\Delta u \quad , \quad C = \frac{\partial h}{\partial x}(x_e,u_e) \quad , \quad D = \frac{\partial h}{\partial u}(x_e,u_e) \tag{2.57}$$

2.4.2.2 Linearization of Aerodynamic Model

For the missile model to be used in simulations, the aerodynamic coefficients are taken to be nonlinear functions of flight parameters. However, in order to use in the autopilot studies, they can be linearized by using the Taylor series expansion around the trim values of the flight parameters as follows.

$$C_i = C_i\left(M,\alpha,\beta,\delta_a,\delta_e,\delta_r,p,q,r,\dot{\alpha},\dot{\beta}\right) = C_{i0}(\beta,M,\alpha)+C_{i\alpha}(\beta,M,\alpha)\alpha+C_{i\beta}(\beta,M,\alpha)\beta + C_{i\delta_a}(\beta,M,\alpha)\delta_a+C_{i\delta_e}(\beta,M,\alpha)\delta_e+C_{i\delta_r}(\beta,M,\alpha)\delta_r + C_{ip}(\beta,M,\alpha)p\frac{d}{2V}+C_{iq}(\beta,M,\alpha)q\frac{d}{2V}+C_{ir}(\beta,M,\alpha)r\frac{d}{2V}+H.O.T.$$

$$i = X,Y,Z,l,m,n \tag{2.58}$$

In the above equation, $H.O.T$ stands for the higher order terms in the Taylor series expansion and will be neglected. $\frac{d}{2V}$ term is included as a multiplier to the dynamic aerodynamic derivatives to make the final product dimensionless. Following notation can be used for aerodynamic derivatives.

$$C_{ij} = \frac{\partial C_i}{\partial j}|_{j=j_0} \qquad j = \alpha,\beta,\delta_a,\delta_e,\delta_r,p,q,r \tag{2.59}$$

Aerodynamic derivatives may not only be a function of Mach number but also angle of attack and sideslip angles can be input parameters to these functions. According to Missile Datcom program, most of the derivatives are function of Mach number, angle of attack, angle of sideslip and deflection. They are basically tables that have dimension of the number of input parameters stated.

The derivation of non-dimensional form of aerodynamic forces and moment coefficients can be found as follows.

$$C_X = -C_a(\beta,M,\alpha) \tag{2.60}$$

$$C_Y = C_{Y\beta}\beta + C_{Y\delta_a}\delta_a + C_{Y\delta_r}\delta_r + C_{Yp}p\frac{d}{2V} + C_{Yr}r\frac{d}{2V} \tag{2.61}$$

$$C_Z = C_{Z\alpha}\alpha + C_{Z\delta_e}\delta_e + C_{Zq}q\frac{d}{2V} \tag{2.62}$$

$$C_l = C_{l\beta}\beta + C_{l\delta_a}\delta_a + C_{l\delta_r}\delta_r + C_{lp}p\frac{d}{2V} + C_{lr}r\frac{d}{2V} \tag{2.63}$$

$$C_m = C_{m\alpha}\alpha + C_{m\delta_e}\delta_e + C_{mq}q\frac{d}{2V} \tag{2.64}$$

$$C_n = C_{n\beta}\beta + C_{n\delta_a}\delta_a + C_{n\delta_r}\delta_r + C_{np}p\frac{d}{2V} + C_{nr}r\frac{d}{2V} \tag{2.65}$$

2.4.2.3 Linearization of Equations of Motion

For designing a linear controller, one firstly needs a linear system model. Linearization of the aerodynamic model is performed in previous section. Equation of motion should also be linearized around equilibrium (trim) flight points. In this study, steady state flight condition of the missile is taken as the equilibrium point where the linearization wil be performed. Besides, some logical assumptions should be made in order to simplify the nonlinear equations during the linearization process by considering the flight configuration of missile that focused on. The missile considered is a skid-to-turn missile so no roll action is needed to turn the missile and this gives the chance to decouple the longitudinal and lateral motion. That means, when longitudinal motion is considered no roll and yaw angles and angular rates occur. Assumptions can be summarized as follows:

- Rolling motion is constant and very small ($\phi \approx 0°, \quad p \approx 0°/s$).
- If q is available, $r = 0$.
- If r is available, $q = 0$.
- Taking into account the equations above and remembering $V = \sqrt{u^2 + v^2 + w^2}$, it can be assumed that total velocity of the missile V is constant and $V \approx u$.

By the help of these assumptions, rate equations simplifies to equations below.

For $q = 0$ Equation 2.48 becomes

$$\dot{p} = \frac{M_X}{I_{xx}} = \frac{QAd\left(C_{l\beta}\beta + C_{l\delta_a}\delta_a + C_{l\delta_r}\delta_r + C_{lp}p\frac{d}{2V} + C_{lr}r\frac{d}{2V}\right)}{I_{xx}} \tag{2.66}$$

For $p = 0$ Equation 2.49 becomes

$$\dot{q} = \frac{M_Y}{I_{yy}} = \frac{QAd\left(C_{m\alpha}\alpha + C_{m\delta_e}\delta_e + C_{mq}q\frac{d}{2V}\right)}{I_{yy}} \tag{2.67}$$

For $q = 0$ Equation 2.50 becomes

$$\dot{r} = \frac{M_Z}{I_{zz}} = \frac{QAd\left(C_{n\beta}\beta + C_{n\delta_a}\delta_a + C_{n\delta_r}\delta_r + C_{np}p\frac{d}{2V} + C_{nr}r\frac{d}{2V}\right)}{I_{zz}} \tag{2.68}$$

To simplify the demonstration, equations above can be stated as

$$\dot{p} = L_\beta \beta + L_{\delta_a} \delta_a + L_{\delta_r} \delta_r + L_p p + L_r r \tag{2.69}$$

$$\dot{q} = M_\alpha \alpha + M_{\delta_e} \delta_e + M_q q \tag{2.70}$$

$$\dot{r} = N_\beta \beta + N_{\delta_a} \delta_a + N_{\delta_r} \delta_r + N_p p + N_r r \tag{2.71}$$

where

$$L_\beta = \frac{QAd}{I_{xx}} C_{l\beta} \quad L_p = \frac{QAd}{I_{xx}} \frac{d}{2V} C_{lp} \quad L_r = \frac{QAd}{I_{xx}} \frac{d}{2V} C_{lr} \quad L_{\delta_a} = \frac{QAd}{I_{xx}} C_{l\delta_a} \tag{2.72}$$

$$L_{\delta_r} = \frac{QAd}{I_{xx}} C_{l\delta_r} \quad M_\alpha = \frac{QAd}{I_{yy}} C_{m\alpha} \quad M_q = \frac{QAd}{I_{yy}} \frac{d}{2V} C_{mq} \quad M_{\delta_e} = \frac{QAd}{I_{yy}} C_{m\delta_e} \tag{2.73}$$

$$N_\beta = \frac{QAd}{I_{zz}} C_{n\beta} \quad N_p = \frac{QAd}{I_{zz}} \frac{d}{2V} C_{np} \quad N_r = \frac{QAd}{I_{zz}} \frac{d}{2V} C_{nr} \quad N_{\delta_a} = \frac{QAd}{I_{zz}} C_{n\delta_a} \tag{2.74}$$

$$N_{\delta_r} = \frac{QAd}{I_{zz}} C_{n\delta_r} \tag{2.75}$$

By assuming that angle of attack and angle of sideslip are small, small angle approximation can be applied as follows.

$$\alpha = \arctan\left(\frac{w}{u}\right) \approx \frac{w}{u} \tag{2.76}$$

$$\beta = \arcsin\left(\frac{v}{V}\right) \approx \frac{v}{V} \tag{2.77}$$

In addition to this, axial velocity can be approximately constant at every linearization point and much more larger than other velocity components.

$$v, w \ll u \approx V \tag{2.78}$$

By using these approximations, derivative of angle of attack and sideslip angle equations are simplified as

$$\dot{\alpha} \approx \frac{\dot{w}}{V} = \frac{\frac{F_Z}{m} - pv + qu}{V} \tag{2.79}$$

$$\dot{\beta} \approx \frac{\dot{v}}{V} = \frac{\frac{F_Y}{m} - ru + pw}{V} \tag{2.80}$$

Taking roll rate approximately zero as before and using linearized forms of aerodynamic coefficients

$$\dot{\alpha} = \frac{QA}{mV}\left(C_{Z\alpha}\alpha + C_{Z\delta_e}\delta_e + C_{Zq}q\frac{d}{2V}\right) + q \tag{2.81}$$

$$\dot{\beta} = \frac{QA}{mV}\left(C_{Y\beta}\beta + C_{Y\delta_a}\delta_a + C_{Y\delta_r}\delta_r + C_{Yp}p\frac{d}{2V} + C_{Yr}r\frac{d}{2V}\right) - r \tag{2.82}$$

To simplify the demonstration,

$$\dot{\alpha} = Z_\alpha\alpha + (Z_q + 1)\, q + Z_{\delta_e}\delta_e \tag{2.83}$$

$$\dot{\beta} = Y_\beta\beta + Y_p p + (Y_r - 1)\, r + Y_{\delta_a}\delta_a + Y_{\delta_r}\delta_r \tag{2.84}$$

where

$$Z_\alpha = \frac{QA}{mV}C_{Z\alpha} \quad Z_q = \frac{QA}{mV}\frac{d}{2V}C_{Zq} \quad Z_{\delta_e} = \frac{QA}{mV}C_{Z\delta_e} \quad Y_\beta = \frac{QA}{mV}C_{Y\beta} \tag{2.85}$$

$$Y_p = \frac{QA}{mV}\frac{d}{2V}C_{Yp} \quad Y_r = \frac{QA}{mV}\frac{d}{2V}C_{Yr} \quad Y_{\delta_r} = \frac{QA}{mV}C_{Y\delta_r} \quad Y_{\delta_a} = \frac{QA}{mV}C_{Y\delta_a} \tag{2.86}$$

Translational kinematic equations are only for transforming body axes velocities to the Earth fixed frame so they are not included in linear state space model and there is no need to linearize these equations. As the final step, rotational kinematic equations are simplified by considering steady state and uncoupled flight conditions of missile that small roll and pitch angles occurrence. For $\theta \approx 0$, Equation 2.25 becomes

$$\dot{\phi} = p \tag{2.87}$$

For $\theta \approx 0$, Equation 2.26 becomes

$$\dot{\theta} = q \tag{2.88}$$

For $\theta \approx 0$, Equation 2.27 becomes

$$\dot{\psi} = r \tag{2.89}$$

2.5 Control Surface Deflection Angles

The missile considered in this study is a tail controlled missile and flies in X configuration as seen in Figure 2.36. Direction of the arrows show the positive deflection rotation of fins that gives positive roll angle when looked from rear.

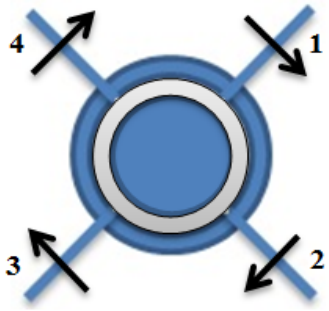

Figure 2.36: 'X' configuration for the control surfaces

When looking from back, the deflection angles which result in positive roll motion states the positive deflection angles that are expressed with arrows. To **roll** the missile to the right or left, all four control surfaces deflects with the same angle. **Pitch** is to make the missile descend or climb. If 1 and 2 have '+', 3 and 4 have '-' deflections then the missile shows pitch-up maneuver. If the opposite sign deflections occur the the missile shows pitch-down maneuver. **Yaw** is the turning of the missile. If 1 and 4 have '-', 2 and 3 have '+' deflections then the missile steers to right when looked from back. If the opposite sign deflections occur the missile steers to left.

Fin deflections are named according to the fin number stated as δ_1,δ_2,δ_3,δ_4. These four fins cause three rotation motion on each body axis cumulatively called

$\delta_a = aileron\ deflection\ (cause\ roll\ motion)$
$\delta_e = elevator\ deflection\ (cause\ pitch\ motion)$
$\delta_r = rudder\ deflection\ (cause\ yaw\ motion)$

These deflections are calculated from four fin deflections as follows

$$\delta_a = \frac{\delta_1 + \delta_2 + \delta_3 + \delta_4}{4} \tag{2.90}$$

$$\delta_e = \frac{\delta_1 + \delta_2 - \delta_3 - \delta_4}{4} \tag{2.91}$$

$$\delta_r = \frac{\delta_1 - \delta_2 - \delta_3 + \delta_4}{4} \tag{2.92}$$

2.6 Control Actuation System Model

Control actuation system is basically a motor system that actuates fins. It has its own closed loop control mechanism which takes autopilot fin commands as input and reacts on the system with its output according to its command tracking performance. Its dynamics can be stated as a second order linear system shown below.

$$\frac{\delta(s)}{\delta_c(s)} = \frac{\omega_n^2}{s^2 + 2\zeta\omega_n s + \omega_n^2} \tag{2.93}$$

where

$\omega_n = natural\ frequency\ (rad/s)$
$\zeta = damping\ ratio$

Practically these systems have a rotation rate limit and also another limit comes from missile fin deflection angle limit. Where the lifting performance starts to decrease, i.e., control effectiveness, determines this deflection limit. As the limit of the deflections rate $\pm 200^\circ/s$ is appropriate. CAS parameters can be selected as

$\omega_n = 75\ rad/s$
$\zeta = 0.707$
$\delta_{max} = 20^\circ$
$\dot{\delta}_{max} = 200^\circ/s$

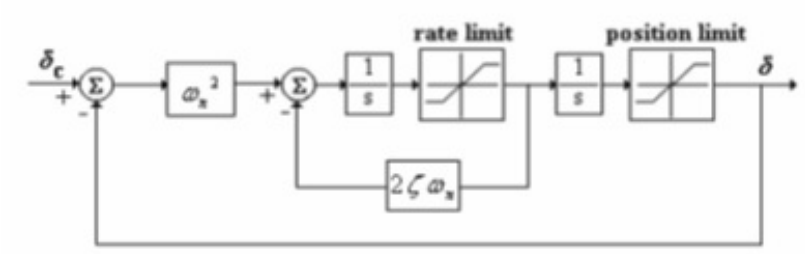

Figure 2.37: Block diagram of the CAS

Fin motor model or generally called CAS (control actuation system) model is shown as follows.

$$\frac{d}{dt}\begin{bmatrix}\delta(t)\\ \dot{\delta}(t)\end{bmatrix} = \begin{bmatrix}0 & 1\\ -\omega_n^2 & -2\zeta\omega_n^2\end{bmatrix}\begin{bmatrix}\delta(t)\\ \dot{\delta}(t)\end{bmatrix} + \begin{bmatrix}0\\ \omega_n^2\end{bmatrix}\delta_c(t) \tag{2.94}$$

2.7 Linear Missile Model

2.7.1 Pitch Plane State Space Model

All pitch plane equations derived in previous sections are used to build the pitch plane state space model. By using Equation 2.70, 2.83, 2.88 and 2.94, following state space model is obtained.

$$\begin{bmatrix} \dot{\alpha} \\ \dot{\theta} \\ \dot{q} \\ \dot{\delta}_e \\ \ddot{\delta}_e \end{bmatrix} = \begin{bmatrix} Z_\alpha & 0 & Z_q + 1 & Z_{\delta_e} & 0 \\ 0 & 0 & 1 & 0 & 0 \\ M_\alpha & 0 & M_q & M_{\delta_e} & 0 \\ 0 & 0 & 0 & 0 & 1 \\ 0 & 0 & 0 & -\omega_n^2 & -2\zeta\omega_n \end{bmatrix} \begin{bmatrix} \alpha \\ \theta \\ q \\ \delta_e \\ \dot{\delta}_e \end{bmatrix} + \begin{bmatrix} 0 \\ 0 \\ 0 \\ 0 \\ \omega_n^2 \end{bmatrix} \delta_{ec} \tag{2.95}$$

2.7.2 Roll-Yaw Plane State Space Model

By using Equation 2.69, 2.71, 2.84, 2.87, 2.89 and 2.94, following state space model is obtained.

$$\begin{bmatrix} \dot{\beta} \\ \dot{\phi} \\ \dot{\psi} \\ \dot{p} \\ \dot{r} \\ \dot{\delta}_a \\ \ddot{\delta}_a \\ \dot{\delta}_r \\ \ddot{\delta}_r \end{bmatrix} = \begin{bmatrix} Y_\beta & 0 & 0 & Y_p & Y_r - 1 & Y_{\delta_a} & 0 & Y_{\delta_r} & 0 \\ 0 & 0 & 0 & 1 & 0 & 0 & 0 & 0 & 0 \\ 0 & 0 & 0 & 0 & 1 & 0 & 0 & 0 & 0 \\ L_\beta & 0 & 0 & L_p & L_r & L_{\delta_a} & 0 & L_{\delta_r} & 0 \\ N_\beta & 0 & 0 & N_p & N_r & N_{\delta_a} & 0 & N_{\delta_r} & 0 \\ 0 & 0 & 0 & 0 & 0 & 0 & 1 & 0 & 0 \\ 0 & 0 & 0 & 0 & 0 & -\omega_n^2 & -2\zeta\omega_n & 0 & 0 \\ 0 & 0 & 0 & 0 & 0 & 0 & 0 & 0 & 1 \\ 0 & 0 & 0 & 0 & 0 & 0 & 0 & -\omega_n^2 & -2\zeta\omega_n \end{bmatrix} \begin{bmatrix} \beta \\ \phi \\ \psi \\ p \\ r \\ \delta_a \\ \dot{\delta}_a \\ \delta_r \\ \dot{\delta}_r \end{bmatrix} + \begin{bmatrix} 0 & 0 \\ 0 & 0 \\ 0 & 0 \\ 0 & 0 \\ 0 & 0 \\ 0 & 0 \\ 0 & 0 \\ \omega_n^2 & 0 \\ 0 & 0 \\ 0 & \omega_n^2 \end{bmatrix} \begin{bmatrix} \delta_{ac} \\ \delta_{rc} \end{bmatrix} \tag{2.96}$$

2.8 Conclusion

Basic definitions about missile dynamics are stated and the coordinate frame definitions and transformation matrices are mentioned. With dynamical and kinematical equations of motion, 6DOF dynamics of a missile is presented.

As a result of linearization process, two state space models are derived to give a basis for the autopilot design. For state space structure of longitudinal, lateral and

roll dynamics, LQR controller can be designed. By adding error state for angular rate loops to state space model, a controller structure that has no steady state error for rate dynamics can be constructed.

To close the acceleration loops for both longitudinal, lateral motion and roll autopilot loop, proportional and also proportional-integral called PI autopilot structure can be constructed as the next step.

CHAPTER 3

AUTOPILOT DESIGN

3.1 Introduction

Unlike the cruise missiles, AAMs are generally symmetric skid-to-turn missiles and in this case it is possible to decouple the longitudinal and lateral dynamics by implementing a roll autopilot that keeps roll angle zero. In this study, pitch, yaw and roll autopilots are designed with uncoupled models and the design process is mentioned with this order in three headings. Linear state space models that are obtained in previous chapter are used for design process. Only difference is roll and yaw channels are decoupled from each other and separated designs are handled. Autopilots are the controllers that try to follow the guidance commands comes from a guidance rule. If the controller is fast enough, then the response delays are decreased and this affects directly the interception success. According to the needs, autopilot structures that follow angles such as angle of attack or pitch angle can be implemented or as other option acceleration autopilots are designed to follow the acceleration commands directly.

Design specifications of all autopilots are stated as follows.

- Pitch rate autopilot:
  gain margin $>$ 10dB,
  phase margin $> 40°$,
  bandwidth of rate loop / natural frequency > 1,
  elevator deflection rate $< 200°/s$,
  settling time (%2) $<$ 2s.

- Pitch acceleration autopilot:
  gain margin $>$ 10dB,
  phase margin $> 40°$,
  bandwidth of rate loop / bandwidth of acceleration loop > 1,
  settling time (%2) $<$ 2s.

- Yaw rate autopilot:
  gain margin $>$ 10dB,
  phase margin $>$ 40°,
  bandwidth of rate loop / natural frequency $>$ 1,
  rudder deflection rate $<$ 200°/s,
  settling time (%2) $<$ 2s.

- Yaw acceleration autopilot:
  gain margin $>$ 10dB,
  phase margin $>$ 40°,
  bandwidth of rate loop / bandwidth acceleration loop $>$ 1,
  settling time (%2) $<$ 2s.

- Roll rate autopilot:
  gain margin $>$ 10dB,
  phase margin $>$ 40°,
  bandwidth of rate loop / bandwidth of pitch rate loop $>$ 1,
  aileron deflection rate $<$ 200°/s,
  settling time (%2) $<$ 1s.

- Roll angle autopilot:
  gain margin $>$ 10dB,
  phase margin $>$ 40°,
  1 $<$ bandwidth of rate loop / bandwidth of phi loop $<$ 8,
  bandwidth of phi loop / bandwidth of pitch acceleration loop $>$ 1,
  settling time (%2) $<$ 1.5s.

Autopilot design points are
Mach design points = [0.8, 1.2, 1.6, 2.0, 2.4, 2.8, 3.2, 3.6, 4.0]
α design points [deg] = [-20, -6, 0, 6, 20]
β design points [deg] = [-20, -6, 0, 6, 20]
Altitude design points [m] = [0, 3000, 6000, 9000, 12000, 15000]

In addition to these needs, there are other requirements about FAS stated in Section 2.6 that must be satisfied. So while designing inner loop autopilots, to be able to consider the FAS specifications, state space design method called linear quadratic tracker (LQT) method based on LQR design is considered. By adding the FAS states that are limited to the state vector as addition to the states that are aimed to control, it is faster to check the FAS states after each design without doing any other additional work that can make the design process slower. The stability and robustness features of the LQR such

that infinite gain margin and phase margin over 60° also make this choice beneficial for the inner rate loops and also simple to apply an automatized design procedure. As the next step after rate loops design, outer loops are considered as acceleration loops for longitudinal and lateral channels and a roll autopilot to decouple the these channels that is for to keep the roll angle zero during the flight. Acceleration commands that are generated from guidance rule must be followed as close as possible for a successful intercept. Because of this need, acceleration loops are closed with a PI controller as a classical control method. For the roll autopilot, and integrator already located in open loop that is required for roll rate to obtain roll angle. Since this integrator, P controller design is adequate and is a good choice to get fast results when considered the total computational costs.

3.2 Linear Quadratic Regulator

The linear quadratic regulator (LQR) is a well-known optimal controller design technique that provides practical feedback gains to operate a dynamic system at minimum cost. The 'L' part of LQR comes from linear differential equations that defines the linear dynamics of the system. This can be defined as

$$\dot{x} = Ax + Bu \tag{3.1}$$

where $x \in R^n$ is state vector and $u \in R^m$ is a control vector. Here, $A \in R^{n \times n}$ and $B \in R^{n \times m}$ are constant matrices for a LTI system.

The Q part comes from the quadratic functional that defines the cost function for optimality calculations.$Q \in R^{n \times n}$ is a positive semi-definite matrix and called as quadratic weight, and $R \in R^{m \times m}$ is a positive definite matrix in Equation 3.2. Since the integration interval is infinite, this is called infinite horizon performance index, that is, the performance objectives are referred to an infinite control interval $[0, \infty)$. Since the control horizon is infinite, Riccati equation may reach a steady state solution [31]

$$J = \frac{1}{2} \int_0^\infty \left(x^T Q x + u^T R u \right) dt \tag{3.2}$$

The 'R' comes from the aim to find an u(t) for Equation 3.1 that will regulate the system at '0'. Thus, LQR defines an optimal control problem that the state equation used is linear, the cost function is quadratic and the entire state is measured. For

$$u = -K_{LQR} x \tag{3.3}$$

in Equation 3.1

$$\dot{x} = (A - BK_{LQR})\, x = A_c x \tag{3.4}$$

In order to guarantee stability of the closed-loop system in Equation 3.4 and a unique positive-definite limiting solution to Ricatti equation, observability of $\left(\sqrt{Q}, A\right)$ pair and controllability of (A, B) pair are needed. As long as these requirements are satisfied, steady state LQR yields gains that stabilize the system. The performance index in Equation 3.2 can be considered as energy functional, so making it small keeps the total energy of the closed loop system small. If J is small, then neither $x(t)$ nor $u(t)$ can be too large. If J is minimized, it is certainly finite. That means $x(t)$ goes to zero as t goes the infinity since it is an infinite integral and that guarantees that the closed loop system stability.

3.3 Linear Quadratic Tracker

3.3.1 Optimal Linear Quadratic Tracker (OLQT)

In this approach, cost function includes tracking error instead of states stated in LQR since the aim is to keep error small for satisfactory tracking performance. The cost function that is used for tracking purpose is as follows.

$$J = \frac{1}{2} \int_0^\infty \left(e^T Q e + u^T R u\right) dt \tag{3.5}$$

Tracking error and performance output are

$$e = r - y \tag{3.6}$$

$$y = Cx \tag{3.7}$$

where r refers the the reference signal. In derivation procedure, the reference signal is assumed constant. OLQT can be derived by using the well-known Hamiltonian approach. Hamiltonian matrix becomes

$$H = \frac{1}{2} \left(e^T Q e + u^T R u\right) + p^T \left(Ax + Bu\right) \tag{3.8}$$

and with use of Equation 3.6 and 3.7

$$H = \frac{1}{2}\left(r^T Q r - 2x^T C^T Q r + x^T C^T Q C x + u^T R u\right) + p^T\left(Ax + Bu\right) \tag{3.9}$$

The co-state equation is

$$\dot{p} = -\frac{\partial H}{\partial x} = C^T Q r - C^T Q C x - A^T p \tag{3.10}$$

and the stationary condition is

$$0 = \frac{\partial H}{\partial u} = Ru + B^T p \tag{3.11}$$

Let us assume here that co-state is dependent on the state vector by the equation

$$p = Kx - S \tag{3.12}$$

Then with Equation 3.11 and 3.12, the control input is found as

$$u = -R^{-1}B^T K x + R^{-1}B^T S \tag{3.13}$$

Equation 3.1 and 3.10 becomes

$$\dot{x} = Ax - BR^{-1}B^T K x + BR^{-1}B^T S = \left(A - BR^{-1}B^T K\right)x + BR^{-1}B^T S \tag{3.14}$$

$$\dot{p} = K\dot{x} = C^T Q r - C^T Q C x - A^T K x + A^T S \tag{3.15}$$

By using Equation 3.14 and 3.15

$$\left(KA + A^T K - KBR^{-1}B^T K + C^T Q C\right)x = \left(A^T - KBR^{-1}B^T\right)S + C^T Q r \tag{3.16}$$

According to the Equation 3.16, an algorithm can be stated systematically by making the assumption that left and right hand sides are exactly zero. The steps are stated as follows:

- Solve the algebraic Riccati equation first and find K.

$$KA + A^T K - KBR^{-1}B^T K + C^T Q C = 0 \tag{3.17}$$

- Next, solve for S.

$$S = -\left(A^T - KBR^{-1}B^T\right)^{-1} C^T Qr \tag{3.18}$$

- Take Equation 3.18 and use it in Equation 3.13.

$$u = -R^{-1}B^T Kx - R^{-1}B^T \left(A^T - KBR^{-1}B^T\right)^{-1} C^T Qr \tag{3.19}$$

To simplify the cumulative state equation, the following definitions are used.

$$K_T = R^{-1}B^T K \tag{3.20}$$

$$G_r = R^{-1}B^T \left(A^T - KBR^{-1}B^T\right)^{-1} C^T Q \tag{3.21}$$

$$G_T = BG_r \tag{3.22}$$

Finally, the closed loop state equation can be written as follows.

$$\dot{x} = (A - BK_T)\, x + G_T r \tag{3.23}$$

3.3.2 Practical Suboptimal Tracker (PST)

In this section, the pitch, yaw and roll rate autopilot structures are stated. The block diagram can be seen in Figure 3.1.

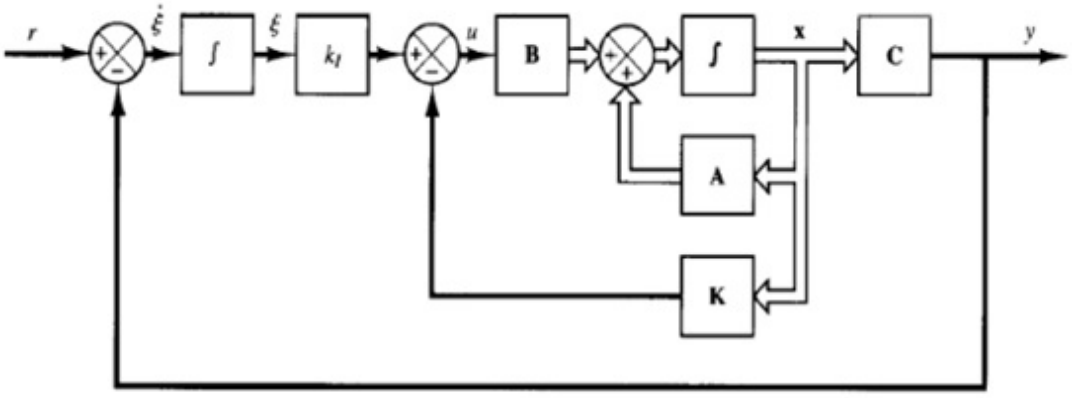

Figure 3.1: Block diagram represenatation of PST [32]

In this block diagram state space Equation 3.1 and full state feedback assumptions are valid.

Let us take ξ as integral of error and as a state variable. New state space form can be represented as follows.

$$\begin{bmatrix} \dot{x} \\ \dot{\xi} \end{bmatrix} = \begin{bmatrix} A & 0 \\ -C & 0 \end{bmatrix} \begin{bmatrix} x \\ \xi \end{bmatrix} + \begin{bmatrix} B \\ 0 \end{bmatrix} u + \begin{bmatrix} 0 \\ I \end{bmatrix} r$$

$$y = Cx \tag{3.24}$$

$$u = -Kx + k_I \xi, \quad K_T = \begin{bmatrix} K & = k_I \end{bmatrix}$$

With this new form, new state vector is

$$\hat{x} = \begin{bmatrix} x & \xi \end{bmatrix}^T \tag{3.25}$$

and the stata space model defined below can be represented as

$$\frac{d}{dt} = \bar{A}\hat{x} + \bar{B}u + \bar{G}r \tag{3.26}$$

$$u = -K_T \hat{x} \tag{3.27}$$

K_T can be found with classical LQR design and as explained in Section 3.2, LQR design make the states converge to zero and this method makes the integral of error zero, that is, tracking error converges to zero. Then the closed loop system is

$$\frac{d}{dt} = \left(\bar{A} - \bar{B}K_T\right)\hat{x} + \bar{G}r \tag{3.28}$$

To design controllers with satisfactory tracking capabilities and robustness, this method is used to design all rate loops.

3.4 Quadratic Weight Selection

Determination of weighting matrices Q and R is up to the controller design requirements since how these parameters are selected, closed loop system shows different responses. If Q is largely selected, that means the designer wants to keep the $x(t)$ is small to minimize J and this results in being further left of closed loop poles in s-plane, so the states decay faster to zero. If R is largely selected, the aim is to keep $u(t)$ small to minimize J and that means less control effort is used. That results in moving the closed loop poles to right that slow the system response and also larger values of the

state vector $x(t)$.

In general, selection of Q and R matrices is an iterative procedure. Basically, while defining Q matrix, the states in state vector $x(t)$ are considered to determine which diagonal component of Q must be weighted much to keep the referring state small. In this application, there are many design points that must satisfy the selected design requirements. So an automatic design procedure is considered to handle a Q matrix search. R matrix is selected as unity matrix. For the sake of simplicity, diagonal component of Q which refers to the integral of error, which is stated in Section 3.3, is weighted only and one appropriate parameter is searched. The logic of the procedure is basically to search a parameter q roughly that makes the system stable and then a fine search to find a solution that satisfies the design requirements and choosing one design parameter q that gives the fastest response. A simple flowchart of the procedure is shown in Figure 3.2.

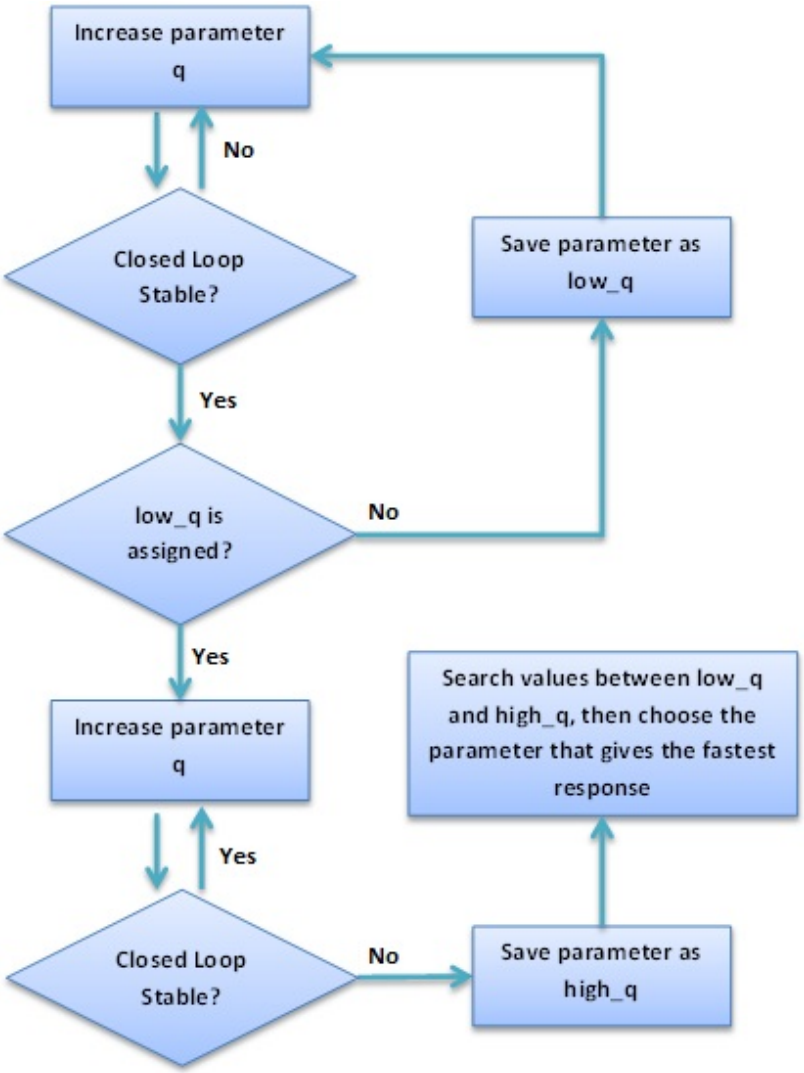

Figure 3.2: Flowchart of the q search algorithm

3.5 Linear Quadratic Autopilot Design

3.5.1 Pitch Plane Autopilot Design

Pitch autopilot design process is handled in two steps:

- inner pitch rate loop autopilot,
- outer acceleration loop autopilot.

For the rate loop autopilot, suboptimal tracker solution with LQR design is considered and state space model is constructed as follows.

$$\begin{bmatrix} \dot{\alpha} \\ \dot{q} \\ \dot{\delta}_e \\ \ddot{\delta}_e \\ e_q \end{bmatrix} = \begin{bmatrix} Z_\alpha & Z_q + 1 & Z_{\delta_e} & 0 & 0 \\ M_\alpha & M_q & M_{\delta_e} & 0 & 0 \\ 0 & 0 & 0 & 1 & 0 \\ 0 & 0 & -\omega_n^2 & -2\zeta\omega_n & 0 \\ 0 & -1 & 0 & 0 & 0 \end{bmatrix} \begin{bmatrix} \alpha \\ q \\ \delta_e \\ \dot{\delta}_e \\ \int e_q \end{bmatrix} + \begin{bmatrix} 0 \\ 0 \\ 0 \\ \omega_n^2 \\ 0 \end{bmatrix} \delta_{ec} + \begin{bmatrix} 0 \\ 0 \\ 0 \\ 0 \\ 1 \end{bmatrix} q_c \tag{3.29}$$

$$y = \begin{bmatrix} 0 & 1 & 0 & 0 & 0 \end{bmatrix} \begin{bmatrix} \alpha \\ q \\ \delta_e \\ \dot{\delta}_e \\ \int e_q \end{bmatrix} \tag{3.30}$$

$$e_q = q_c - q \tag{3.31}$$

Deflection states are included in order to keep deflection rates under control and consider fin actuation system (FAS) limitations while designing. FAS parameters are given in Section 2.6 LQR design ensures an asymptotically stable closed loop system with guaranteed levels of stability robustness. The controller obtained as the result is a linear, unique, optimal and a full state feedback controller. LQR is a regulator so its aim is to regulate the state vector $x(t)$ of an initially deviated system to its equilibrium position as quickly as possible. The restrictive part of LQR design is that it requires measurement about all states and in this design process it is assumed that all states are known.

Q, weight matrix of states and R, weight matrix of input are selected as

$$Q = \begin{bmatrix} 0 & 0 & 0 & 0 & 0 \\ 0 & 0 & 0 & 0 & 0 \\ 0 & 0 & 0 & 0 & 0 \\ 0 & 0 & 0 & 0 & 0 \\ 0 & 0 & 0 & 0 & q \end{bmatrix} \tag{3.32}$$

and

$$R = 1 \tag{3.33}$$

Where q is the weight coefficient of integral of the pitch rate error and this coefficient determines characteristics of the pitch rate tracking such as settling time, overshoot, rise time and also the deflection rate response of the system. Determination of q value is handled by a search process with sequential iterations stated in Section 3.4. After the suitable q values that provides design requirements are collected, the one that gives the fastest response is selected as the q value of that design point. For the acceleration loop, PI controller is designed to have zero steady state error and fast transient response. Pitch autopilot structure is shown in Figure 3.3.

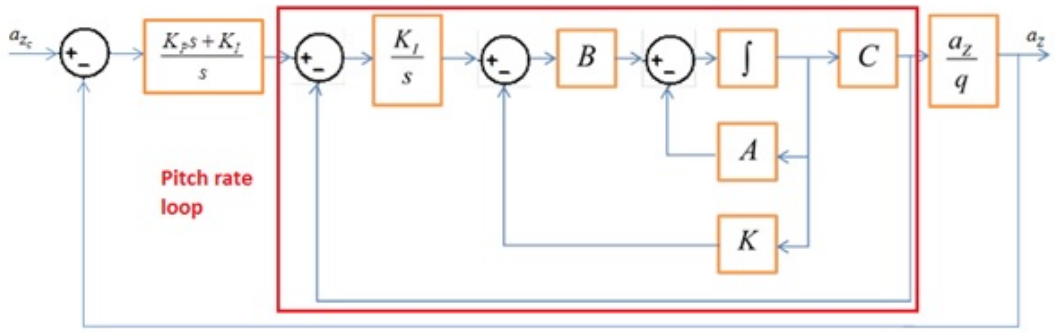

Figure 3.3: Pitch autopilot structure

The transfer function between longitudinal acceleration and pitch angular rate is stated as

$$\frac{a_z(s)}{q(s)} = V\left(\frac{Z_{\delta_e}s^2 + (Z_q M_{\delta_e} - M_q Z_{\delta_e})\,s + Z_\alpha M_{\delta_e} - M_\alpha Z_{\delta_e}}{M_{\delta_e}s + M_\alpha Z_{\delta_e} - Z_\alpha M_{\delta_e}}\right) \tag{3.34}$$

The terms in Equation 3.34 are stated in Section 2.4.2.3. By using Equation 3.34 and closed loop transfer function of pitch rate loop, a new open loop system is obtained to design PI controllers for acceleration loop for all design points to close the loop. In Figure 3.4 - 3.21, design results of pitch rate and acceleration autopilots are represented.

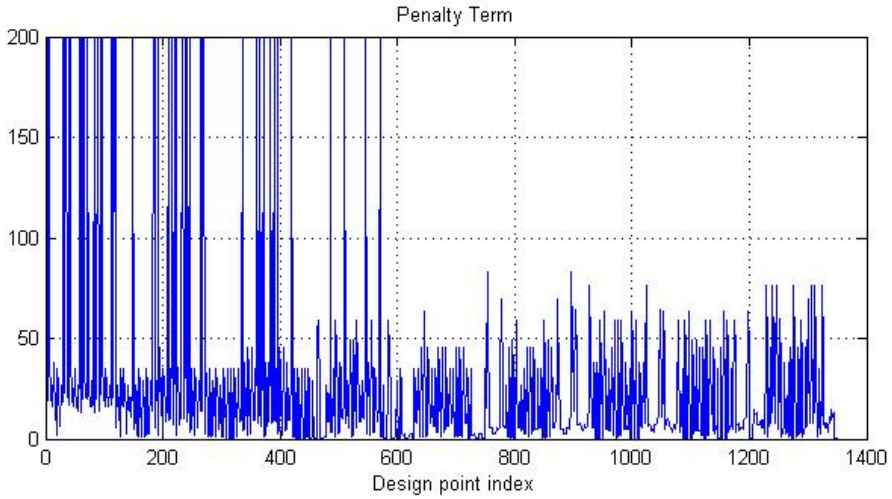

Figure 3.4: Penalty term for design points

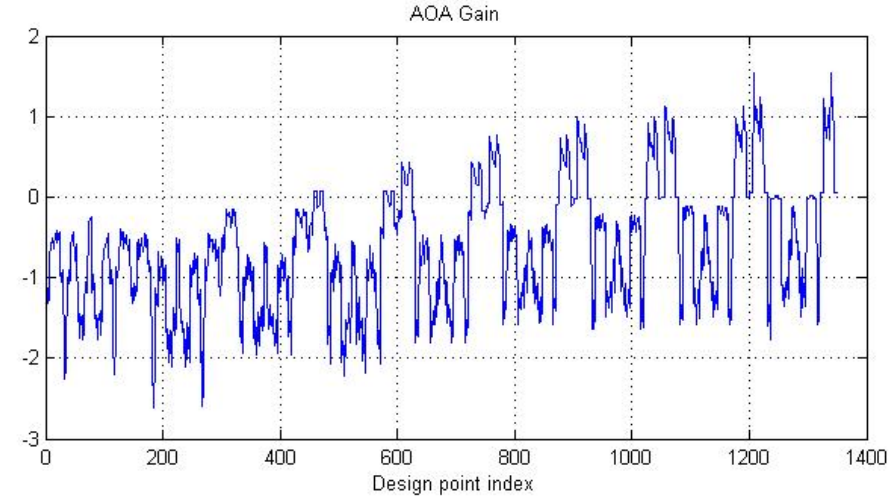

Figure 3.5: K_α gain for design points

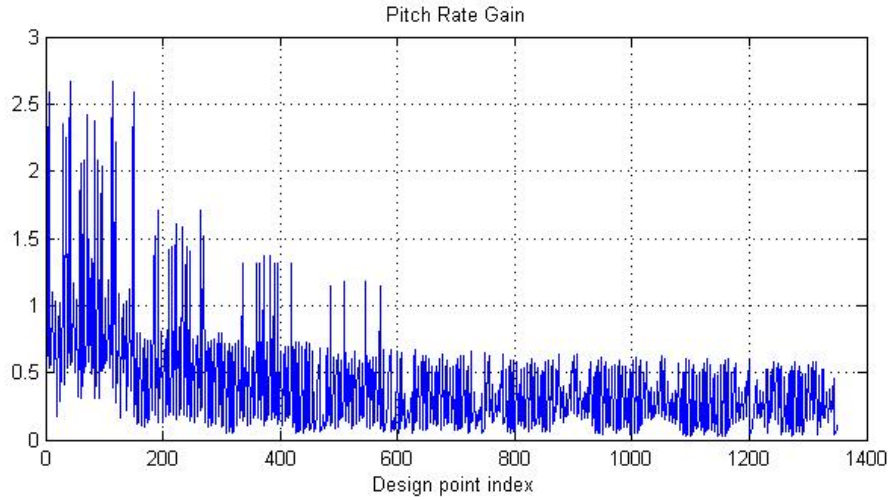

Figure 3.6: K_q gain for design points

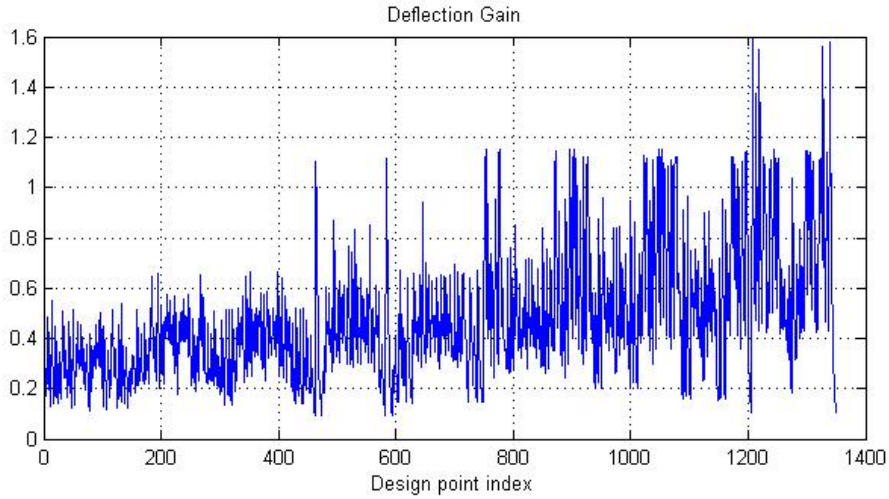

Figure 3.7: K_{δ_e} gain for design points

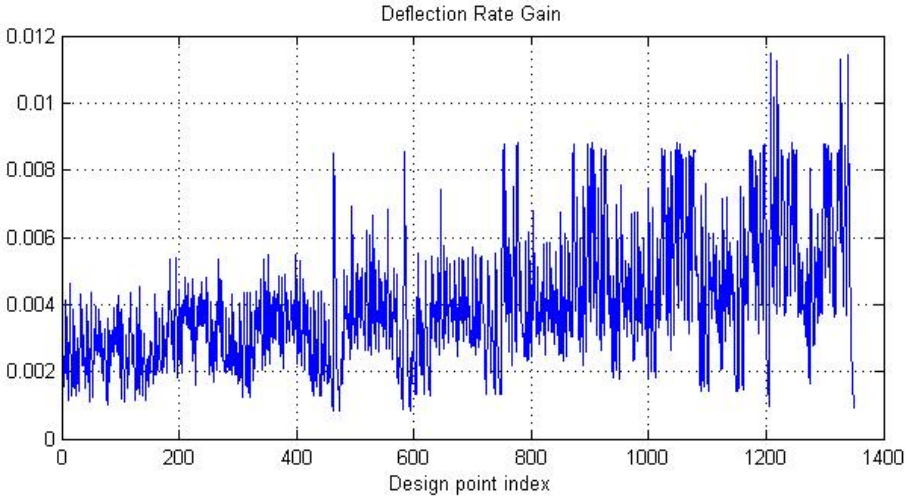

Figure 3.8: $K_{\dot{\delta}_e}$ gain for design points

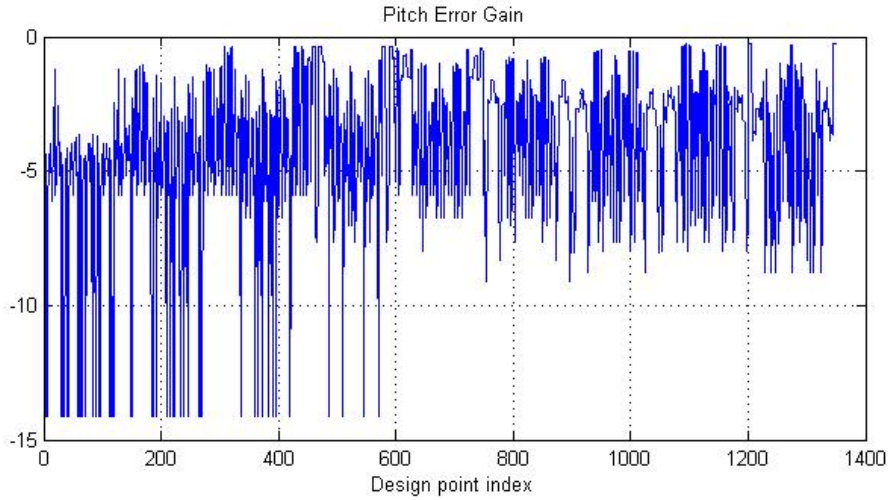

Figure 3.9: K_e gain for design points

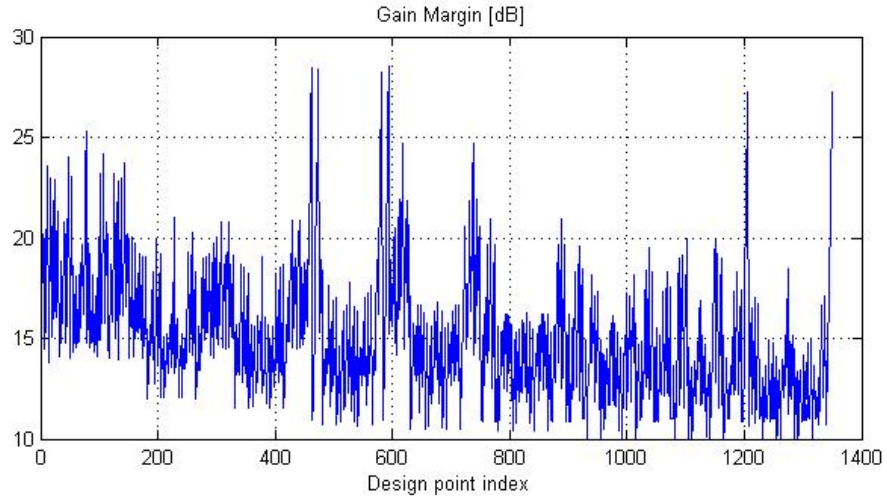

Figure 3.10: Gain margin for design points

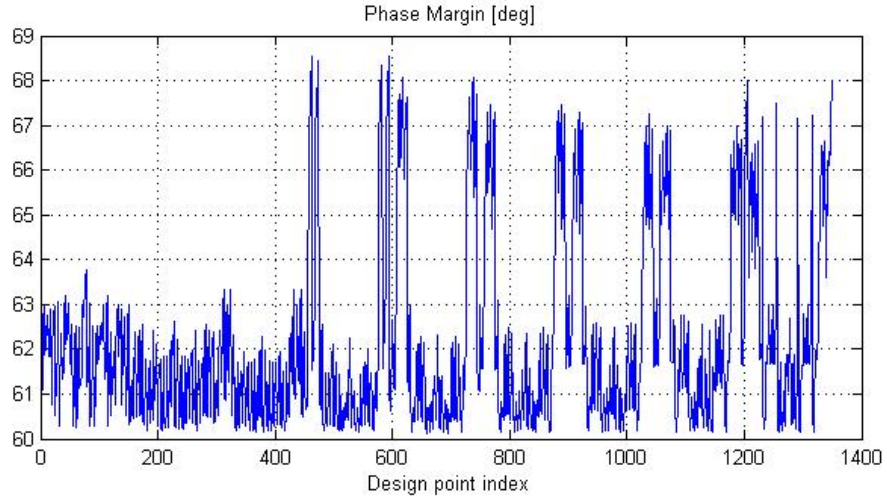

Figure 3.11: Phase margin for design points

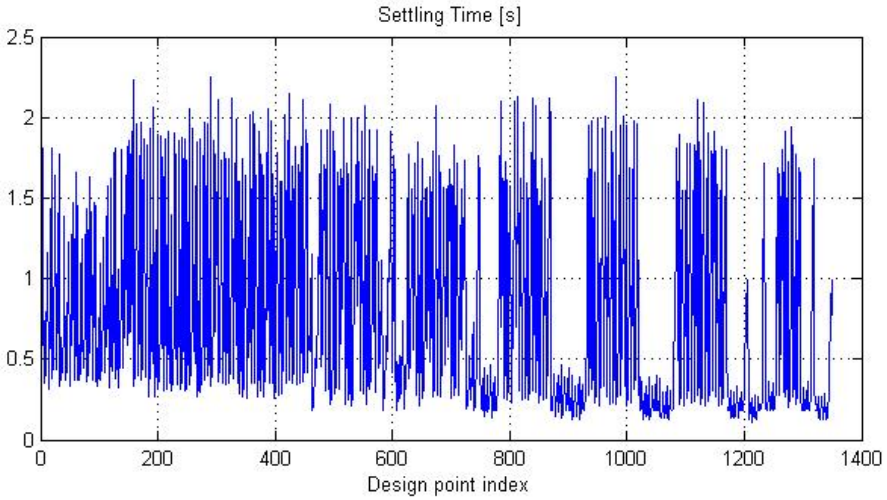

Figure 3.12: Settling time for design points

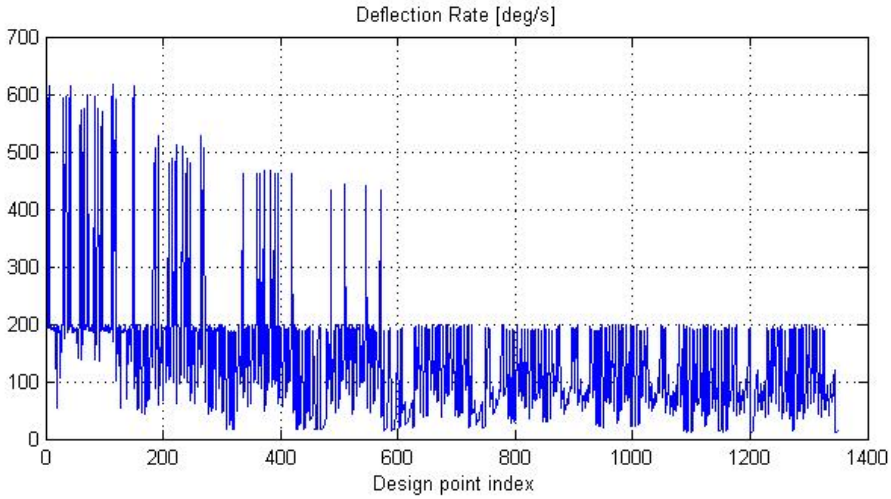

Figure 3.13: Deflection rate for design points

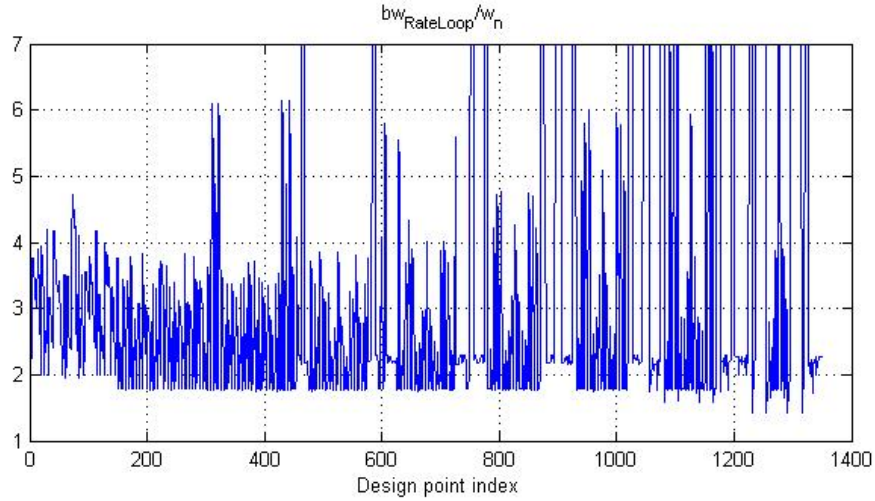

Figure 3.14: Rate loop bandwidth over natural frequency of system for design points

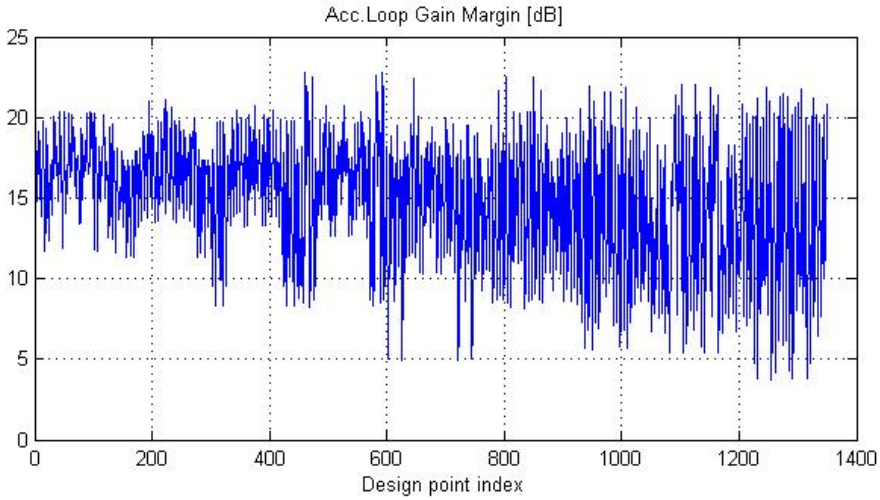

Figure 3.15: Acceleration loop gain margin for design points

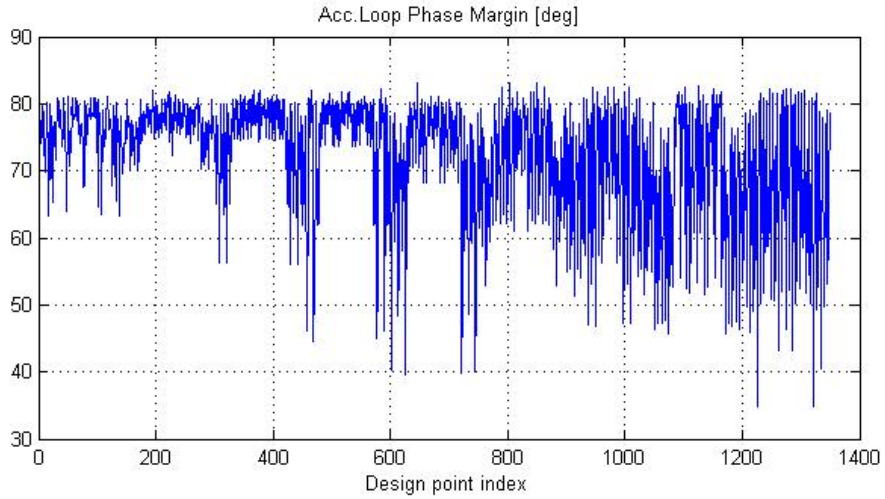

Figure 3.16: Acceleration phase margin for design points

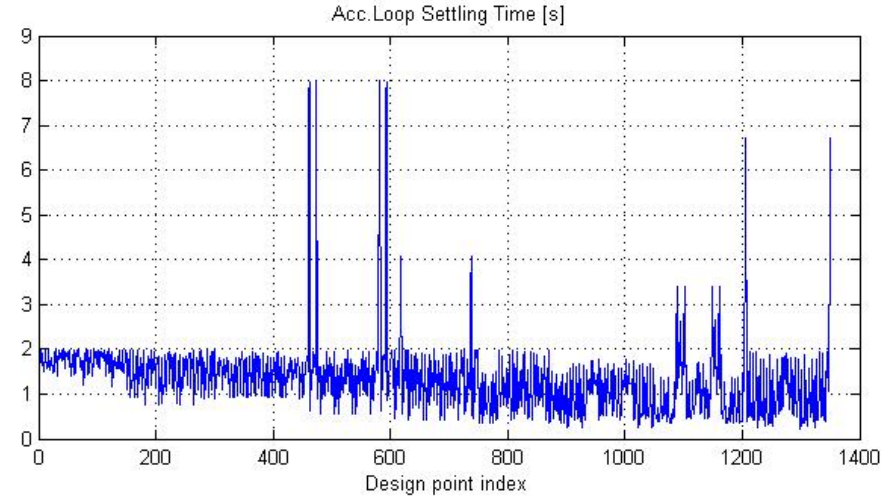

Figure 3.17: Acceleration loop settling time for design points

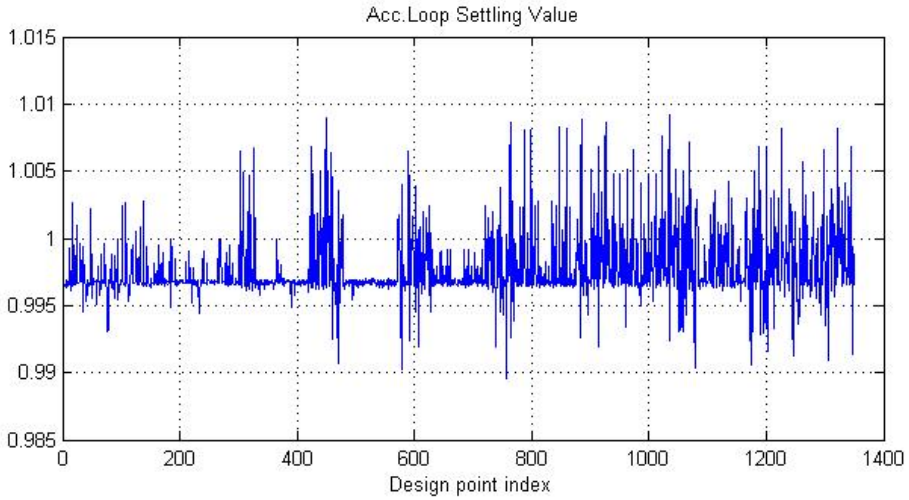

Figure 3.18: Acceleration loop settling value for design points

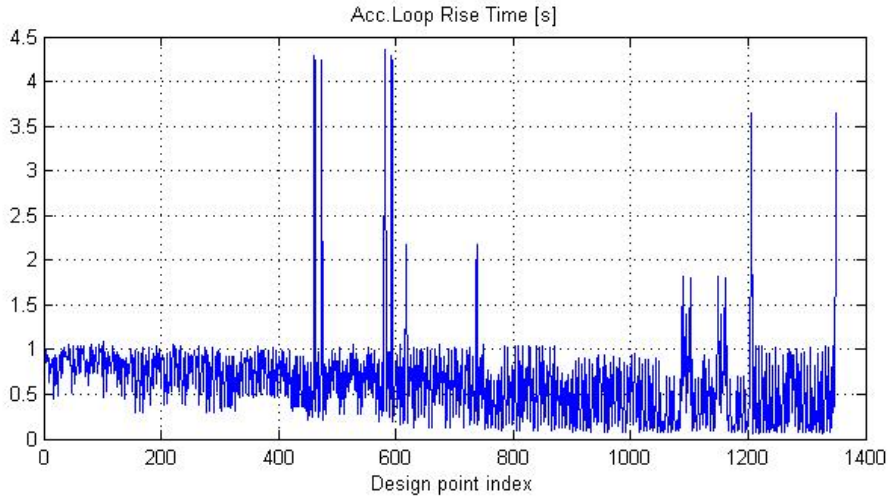

Figure 3.19: Acceleration loop rise time for design points

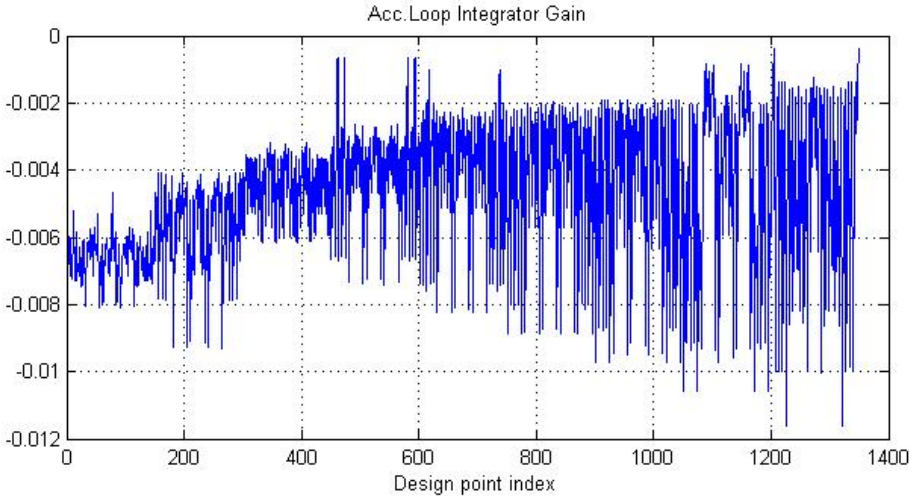

Figure 3.20: Acceleration loop integral gain for design points

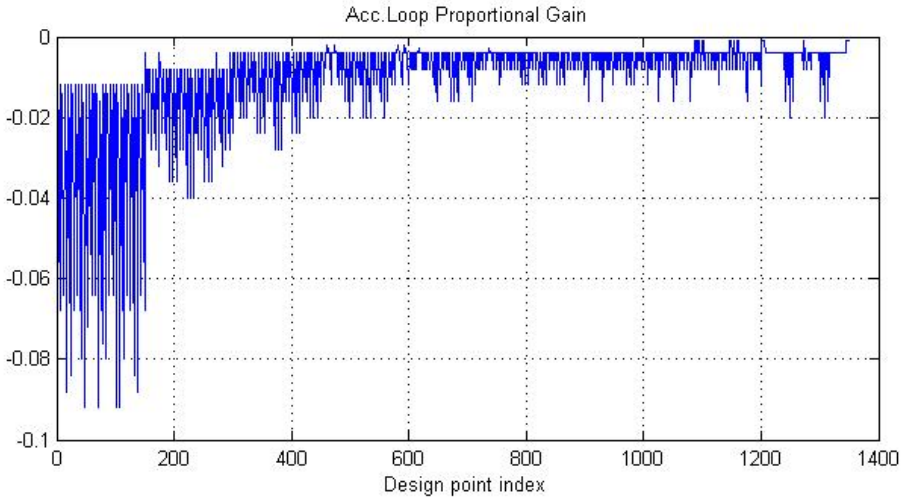

Figure 3.21: Acceleration loop proportional gain for design points

For the rate and acceleration loops, gain margin is greater than 10 dB, phase margin is greater than 60 degrees and settling time of step responses are lower than 2 seconds for most of the design points. Existence of integrator for both inner and outer loops results in negligible steady state errors.

3.5.2 Yaw Plane Autopilot Design

Yaw autopilot design process is handled in two steps:

- inner yaw rate loop autopilot,
- outer acceleration loop autopilot.

For the rate loop autopilot, suboptimal tracker solution with LQR design is considered and state space model is constructed as follows.

$$\begin{bmatrix} \dot{\beta} \\ \dot{r} \\ \dot{\delta}_r \\ \ddot{\delta}_r \\ e_r \end{bmatrix} = \begin{bmatrix} Y_\beta & Y_r - 1 & Y_{\delta_r} & 0 & 0 \\ N_\beta & N_r & N_{\delta_r} & 0 & 0 \\ 0 & 0 & 0 & 1 & 0 \\ 0 & 0 & -\omega_n^2 & -2\zeta\omega_n & 0 \\ 0 & -1 & 0 & 0 & 0 \end{bmatrix} \begin{bmatrix} \beta \\ r \\ \delta_r \\ \dot{\delta}_r \\ \int e_r \end{bmatrix} + \begin{bmatrix} 0 \\ 0 \\ 0 \\ \omega_n^2 \\ 0 \end{bmatrix} \delta_{rc} + \begin{bmatrix} 0 \\ 0 \\ 0 \\ 0 \\ 1 \end{bmatrix} r_c \tag{3.35}$$

$$y = \begin{bmatrix} 0 & 1 & 0 & 0 & 0 \end{bmatrix} \begin{bmatrix} \beta \\ r \\ \delta_r \\ \dot{\delta}_r \\ \int e_r \end{bmatrix} \tag{3.36}$$

$$e_r = r_c - r \tag{3.37}$$

Q, weight matrix of states and R, weight matrix of inputs are selected as in pitch rate autopilot design.

For the acceleration loop, PI controller is designed as in pitch rate design. Yaw autopilot structure is shown in Figure 3.22.

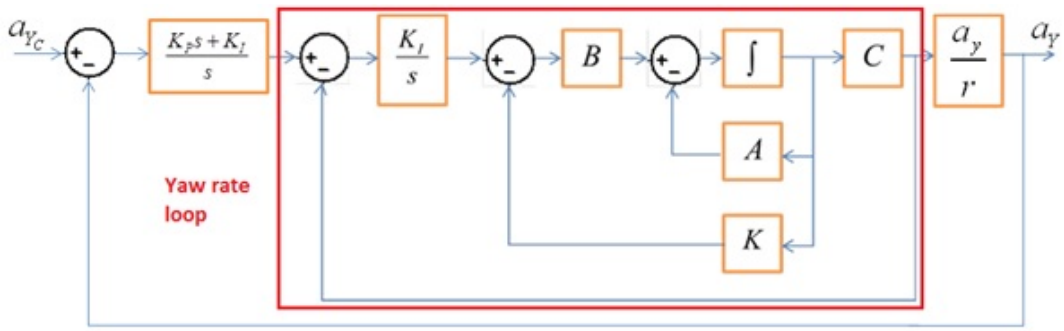

Figure 3.22: Yaw autopilot structure

The transfer function between longitudinal acceleration and yaw angular rate is stated as

$$\frac{a_y(s)}{r(s)} = V\left(\frac{Y_{\delta_r}s^2 + (Y_r N_{\delta_r} - N_r Y_{\delta_r})\,s + Y_\beta N_{\delta_r} - N_\beta Y_{\delta_r}}{N_{\delta_r}s + N_\beta Y_{\delta_r} - Y_\alpha N_{\delta_r}}\right) \tag{3.38}$$

The terms in Equation 3.38 are stated in Section 2.4.2.3.
By using Equation 3.38 and closed loop transfer function of yaw rate loop, a new open loop system is obtained to design PI controllers for acceleration loop for all design points. In Figure 3.23 - 3.40, design results of yaw rate and acceleration autopilots are represented.

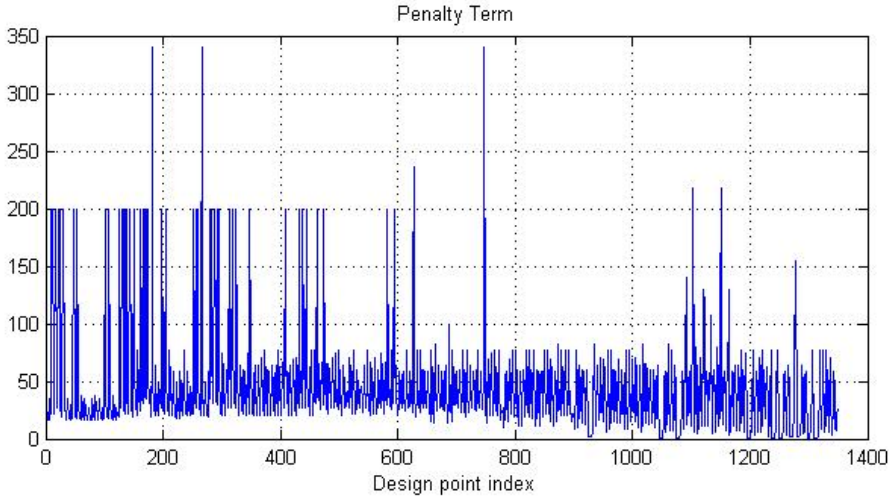

Figure 3.23: Penalty term for design points

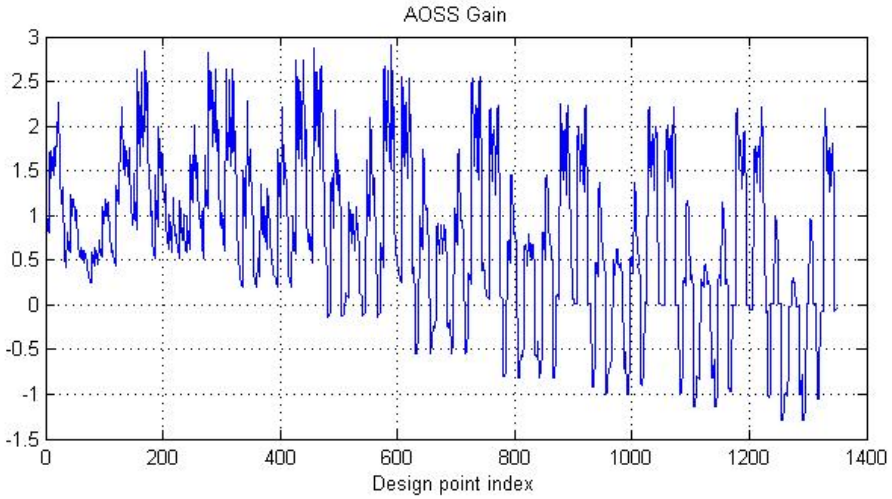

Figure 3.24: K_β gain for design points

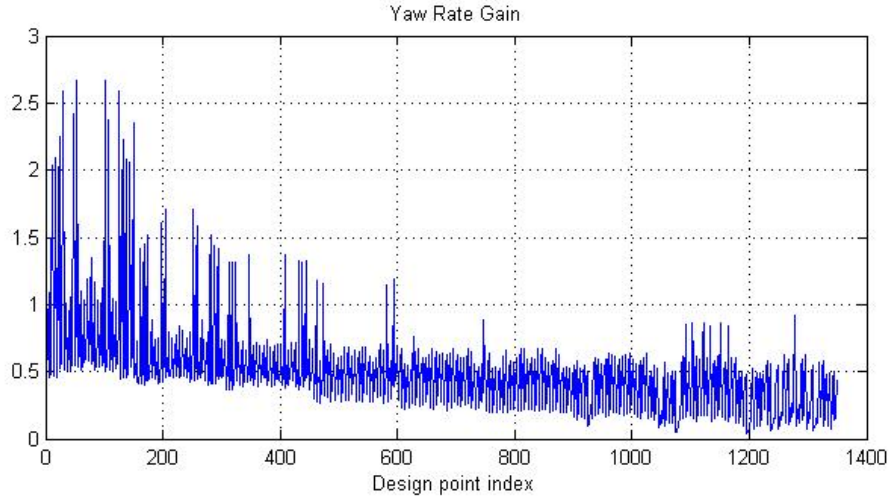

Figure 3.25: K_r gain for design points

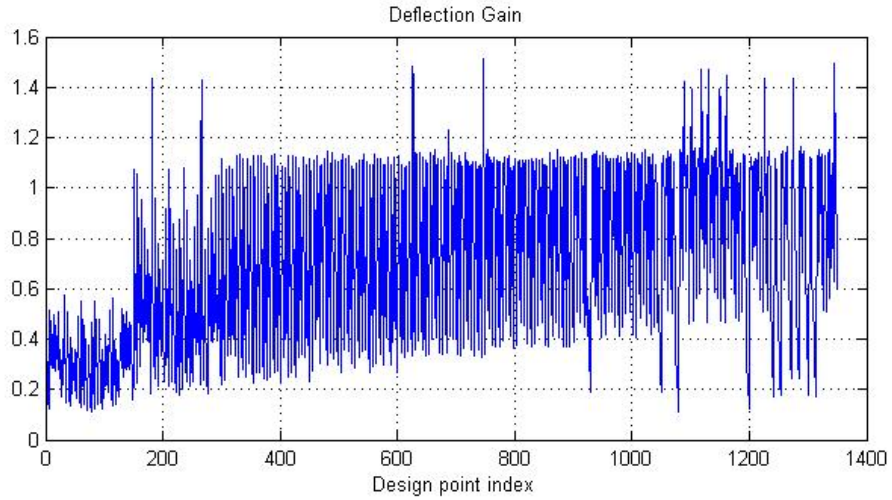

Figure 3.26: K_{δ_r} gain for design points

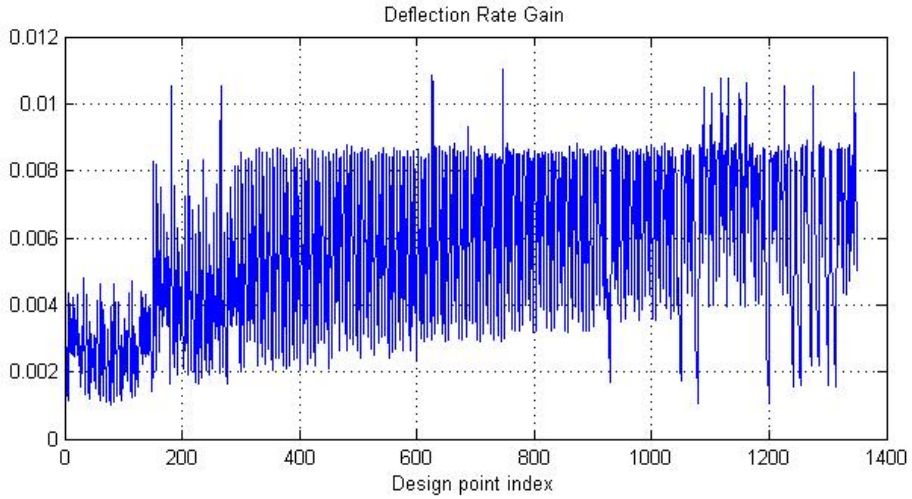

Figure 3.27: $K_{\dot{\delta}_r}$ gain for design points

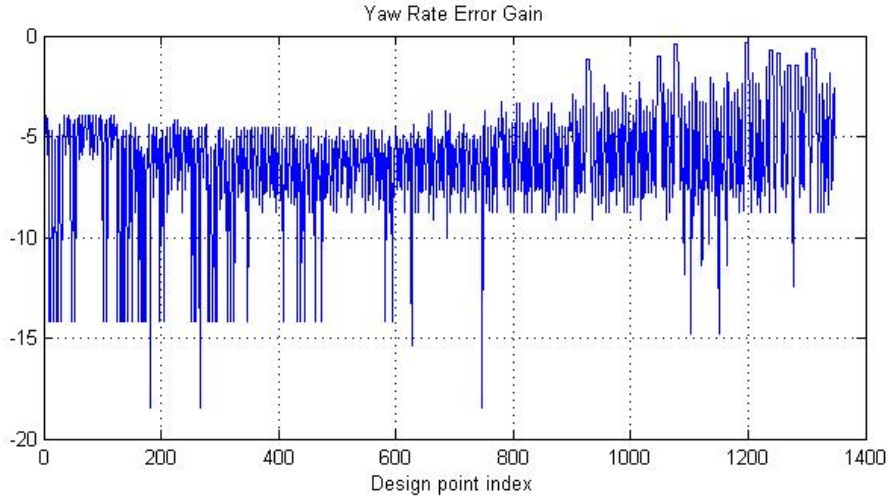

Figure 3.28: K_e gain for design points

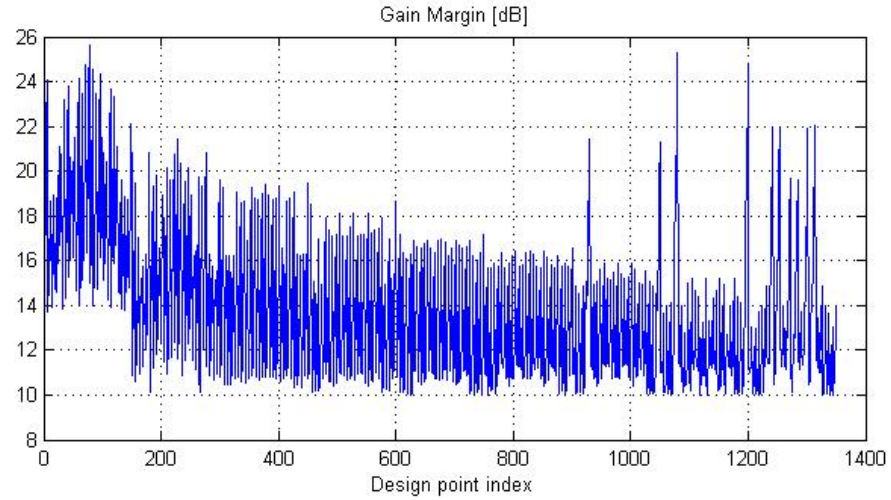

Figure 3.29: Gain margin for design points

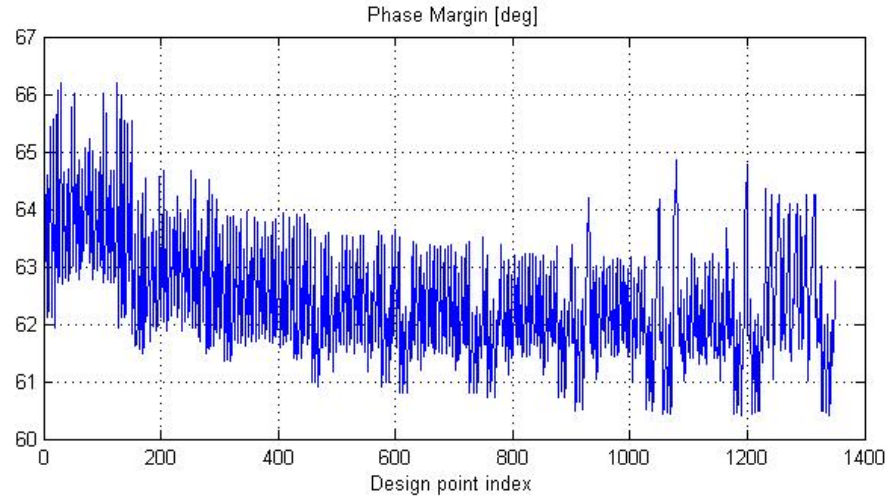

Figure 3.30: Phase margin for design points

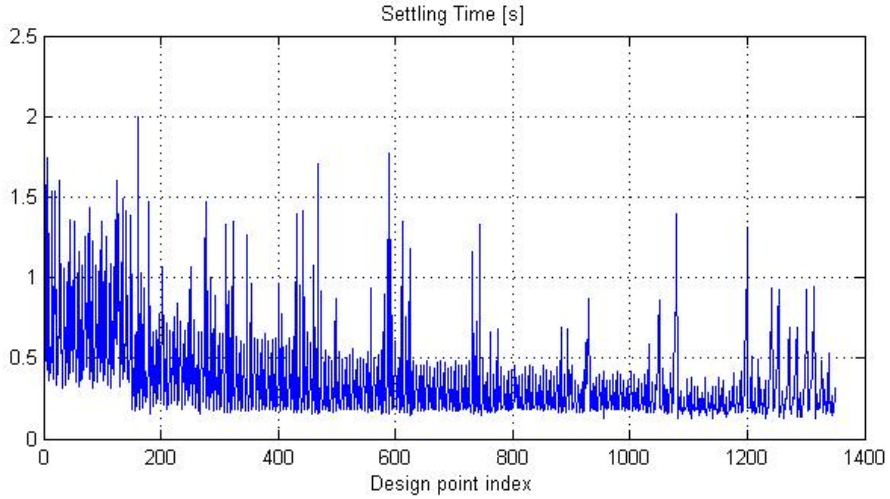

Figure 3.31: Settling time for design points

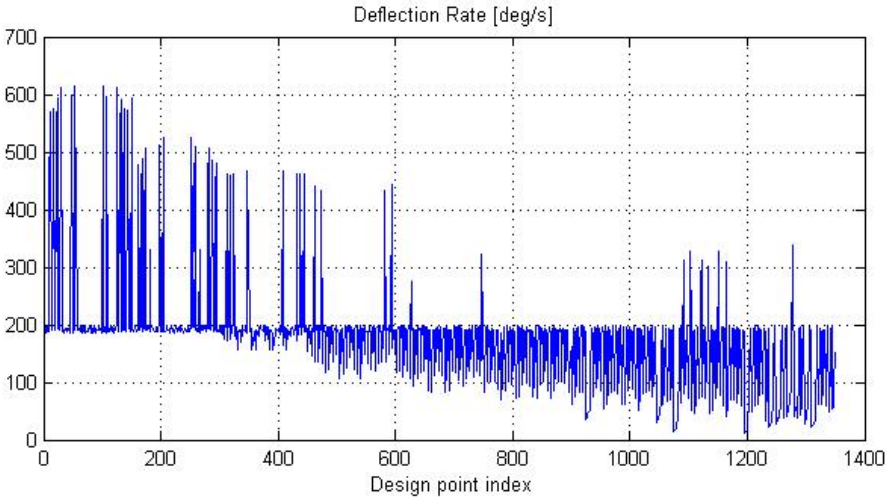

Figure 3.32: Deflection rate for design points

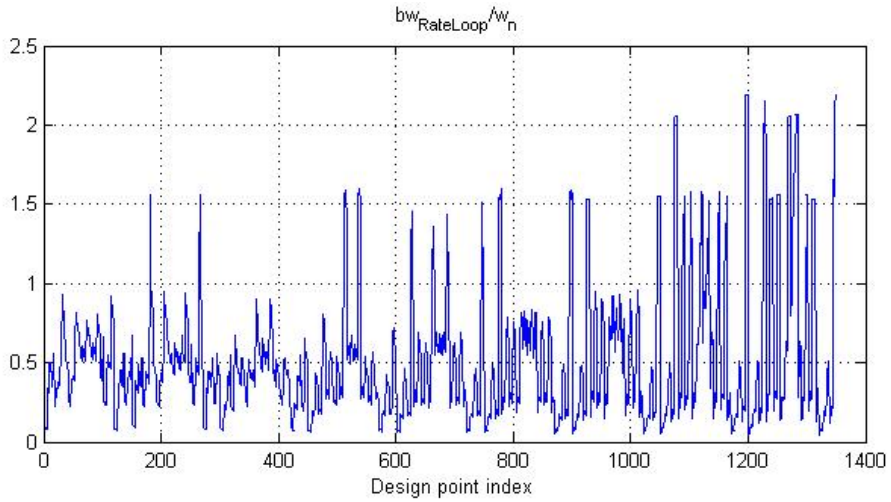

Figure 3.33: Rate loop bandwidth over natural frequency of system for design points

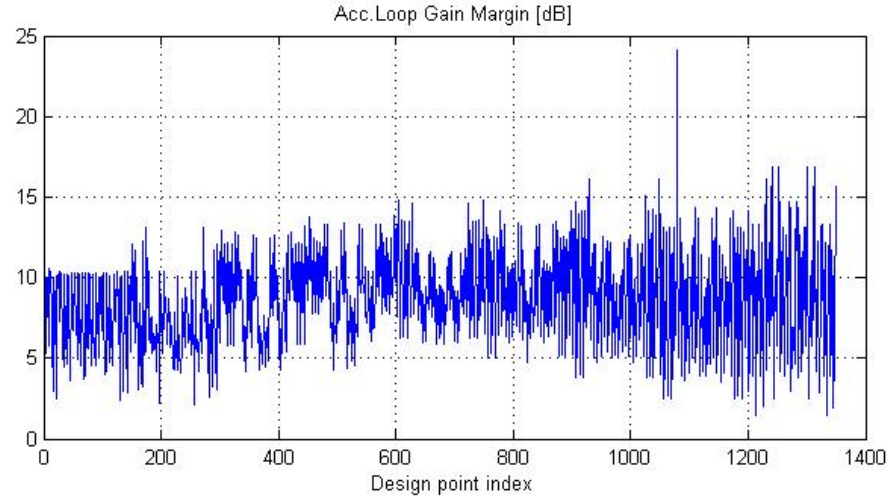

Figure 3.34: Acceleration loop gain margin for design points

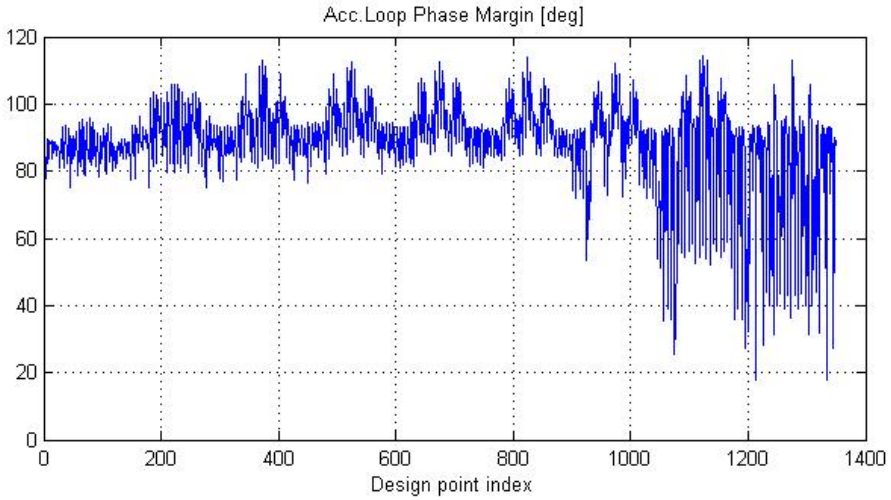

Figure 3.35: Acceleration phase margin for design points

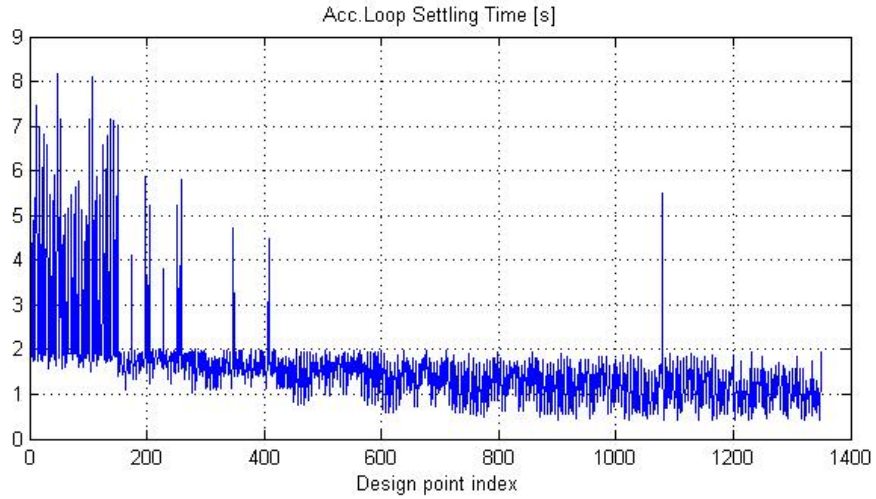

Figure 3.36: Acceleration loop settling time for design points

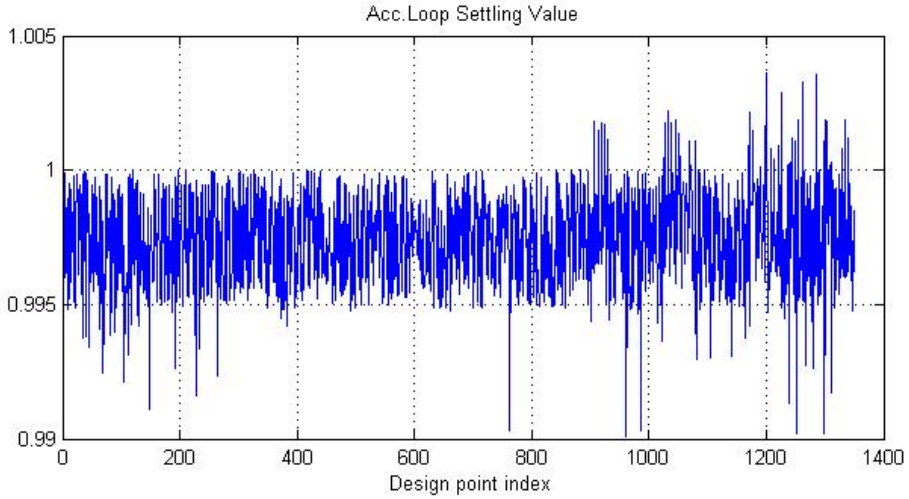

Figure 3.37: Acceleration loop settling value for design points

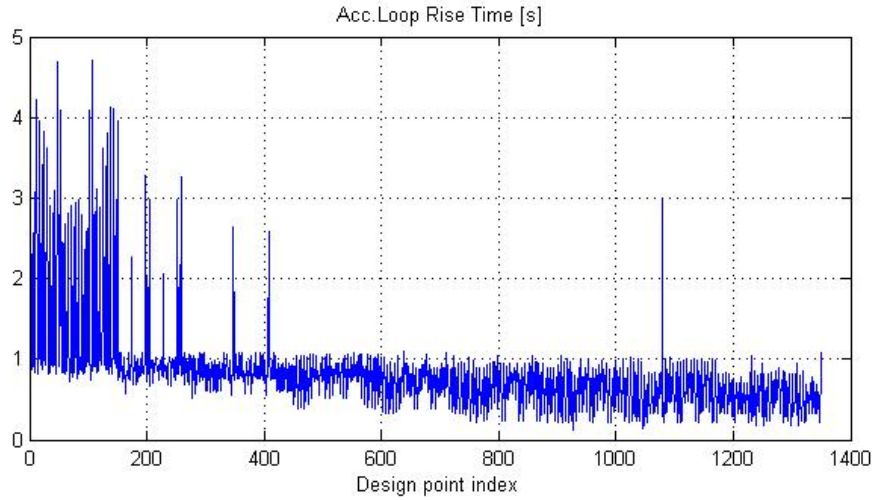

Figure 3.38: Acceleration loop rise time for design points

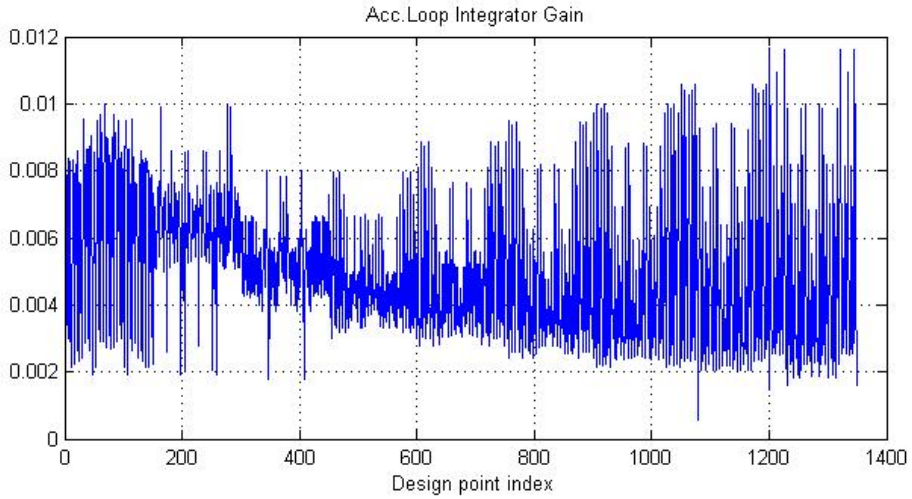

Figure 3.39: Acceleration loop integral gain for design points

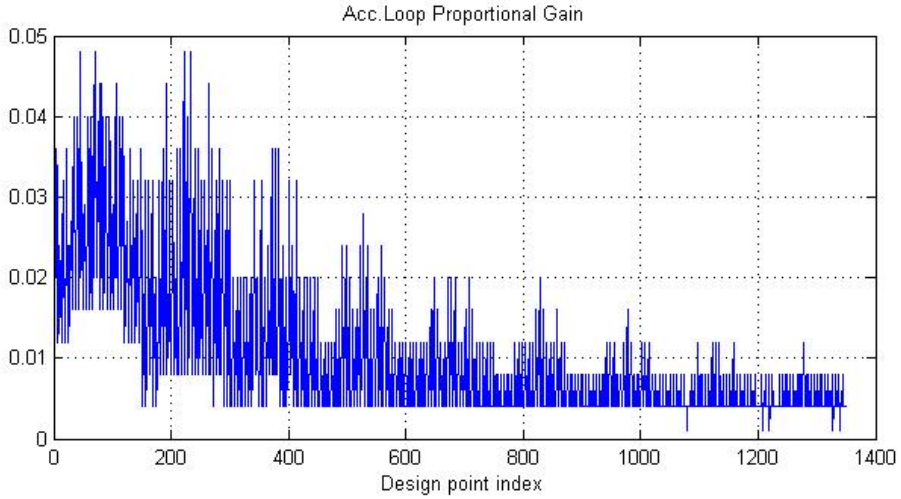

Figure 3.40: Acceleration loop proportional gain for design points

For the rate loop, gain margin is greater than 10 dB, phase margin is greater than 60 degrees and settling time of step responses are lower than 2 seconds for all design points. For the acceleration loop, gain margin is generally between 5 dB and 10 dB, phase margin is greater than 60 degrees and settling time is lower than 2 seconds for most of the cases. Existence of integrator for both inner and outer loops results in negligible steady state errors.

3.5.3 Roll Autopilot Design

Roll autopilot design process is handled in two steps:

- inner roll rate loop autopilot,
- outer phi loop autopilot.

For the rate loop autopilot, suboptimal tracker solution with LQR design is considered and state space model is constructed as follows.

$$\begin{bmatrix} \dot{p} \\ \dot{\delta}_a \\ \ddot{\delta}_a \\ e_p \end{bmatrix} = \begin{bmatrix} L_p & L_{\delta_a} & 0 & 0 \\ 0 & 0 & 1 & 0 \\ 0 & -\omega_n^2 & -2\zeta\omega_n & 0 \\ -1 & 0 & 0 & 0 \end{bmatrix} \begin{bmatrix} p \\ \delta_a \\ \dot{\delta}_p \\ \int e_p \end{bmatrix} + \begin{bmatrix} 0 \\ 0 \\ \omega_n^2 \\ 0 \end{bmatrix} \delta_{ac} + \begin{bmatrix} 0 \\ 0 \\ 0 \\ 1 \end{bmatrix} p_c \tag{3.39}$$

$$y = \begin{bmatrix} 0 & 1 & 0 & 0 & 0 \end{bmatrix} \begin{bmatrix} p \\ \delta_p \\ \dot{\delta}_p \\ \int e_p \end{bmatrix} \tag{3.40}$$

$$e_p = p_c - p \tag{3.41}$$

Q, weight matrix of states and R, weight matrix of inputs are selected as

$$Q = \begin{bmatrix} 0 & 0 & 0 & 0 \\ 0 & 0 & 0 & 0 \\ 0 & 0 & 0 & 0 \\ 0 & 0 & 0 & q \end{bmatrix} \tag{3.42}$$

and

$$R = 1 \tag{3.43}$$

For the phi loop, P controller is designed since there is an integrator in the loop already. Roll autopilot structure is shown in Figure 3.41.

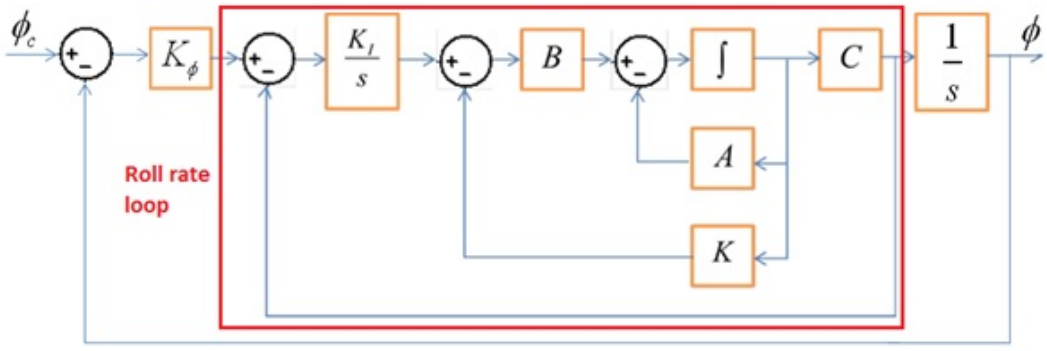

Figure 3.41: Roll autopilot structure

The terms in Equation 3.39 are stated in Section 2.4.2.3. By using the integrator in open loop and closed loop transfer function of roll rate loop, a new open loop system is obtained to design P controllers for roll angle loop for all design points. In Figure 3.42 - 3.56, design results of roll rate and roll angle autopilots are represented.

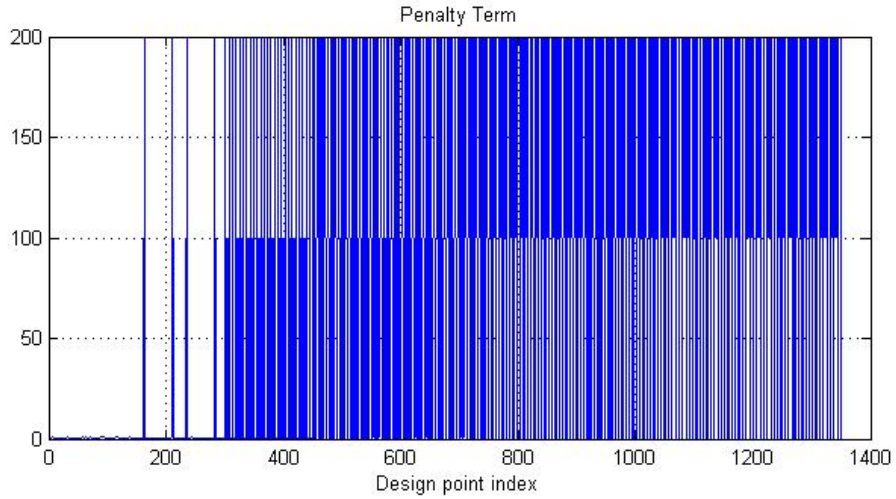

Figure 3.42: Penalty term for design points

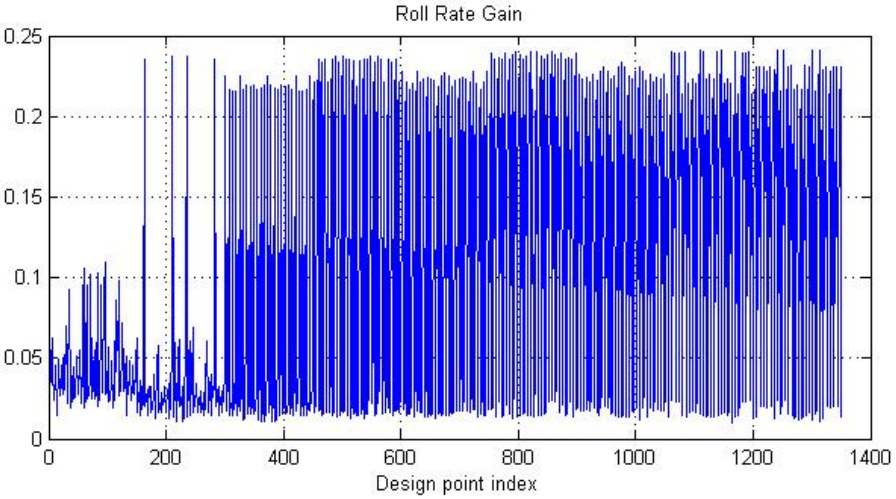

Figure 3.43: K_p gain for design points

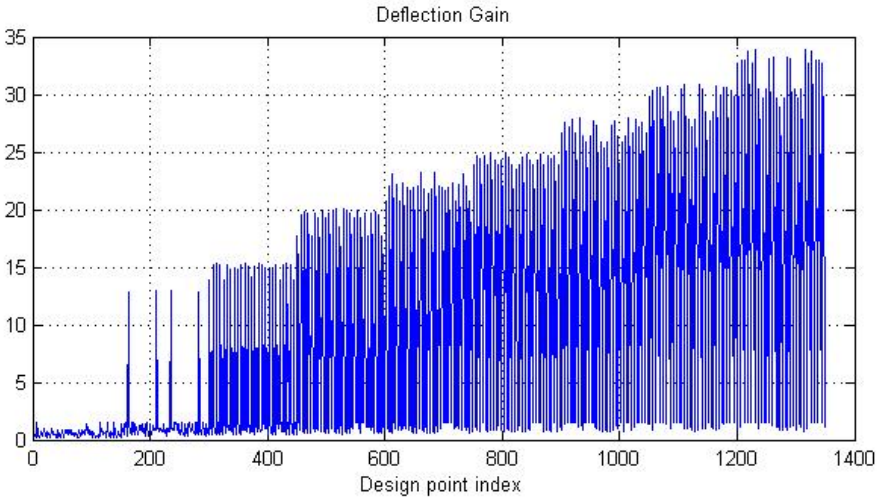

Figure 3.44: K_{δ_a} gain for design points

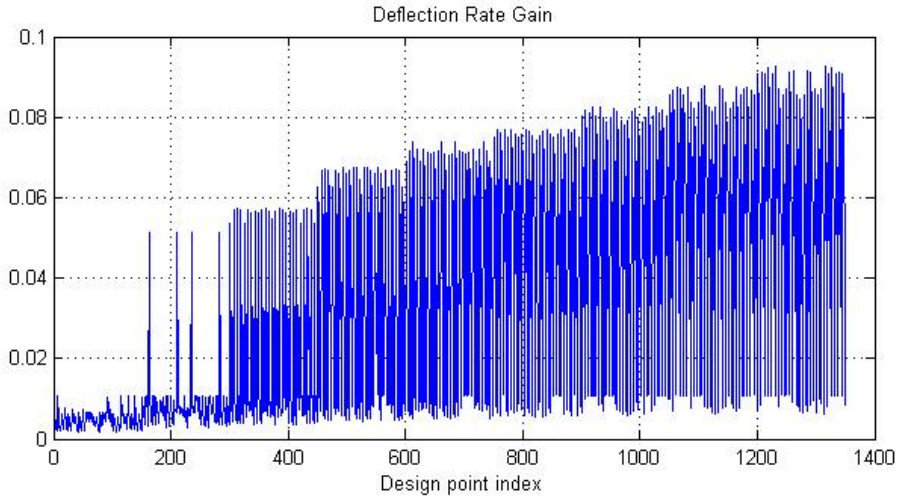

Figure 3.45: $K_{\dot{\delta}_a}$ gain for design points

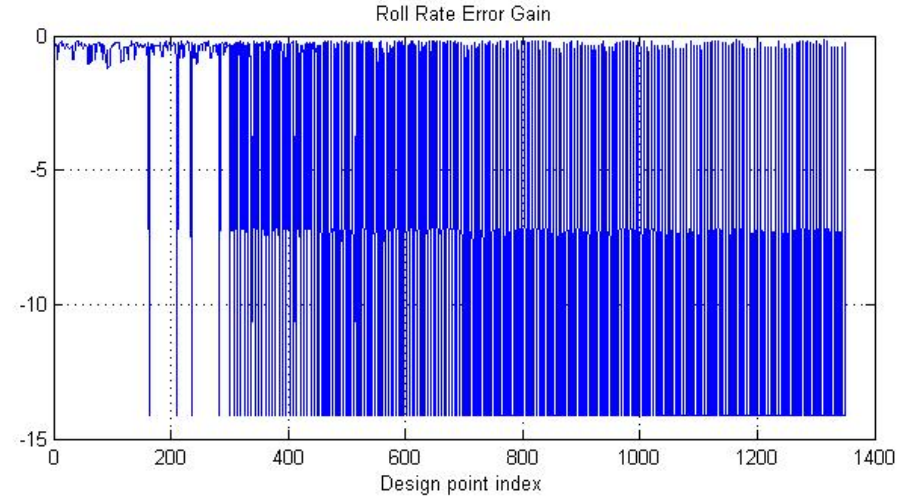

Figure 3.46: K_e gain for design points

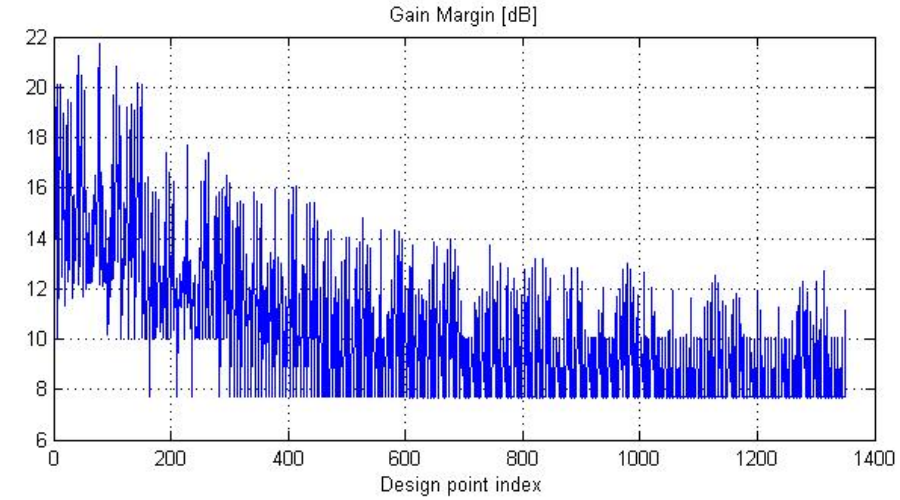

Figure 3.47: Gain margin for design points

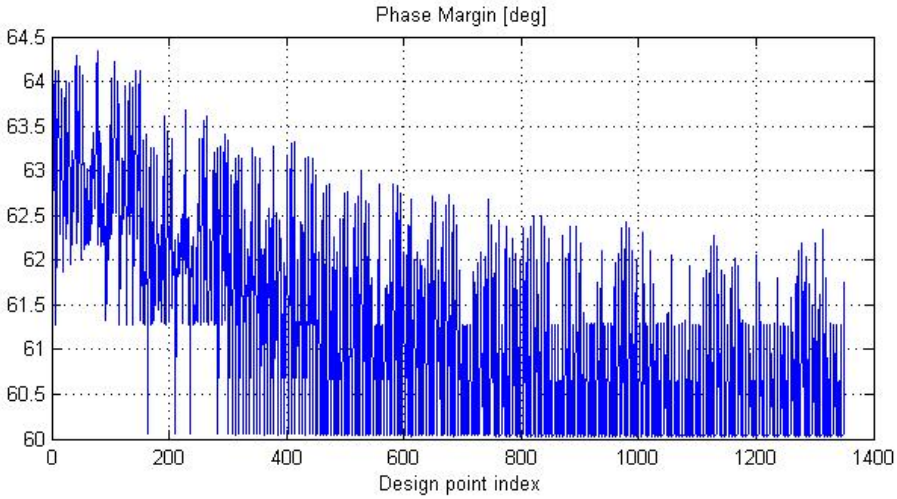

Figure 3.48: Phase margin for design points

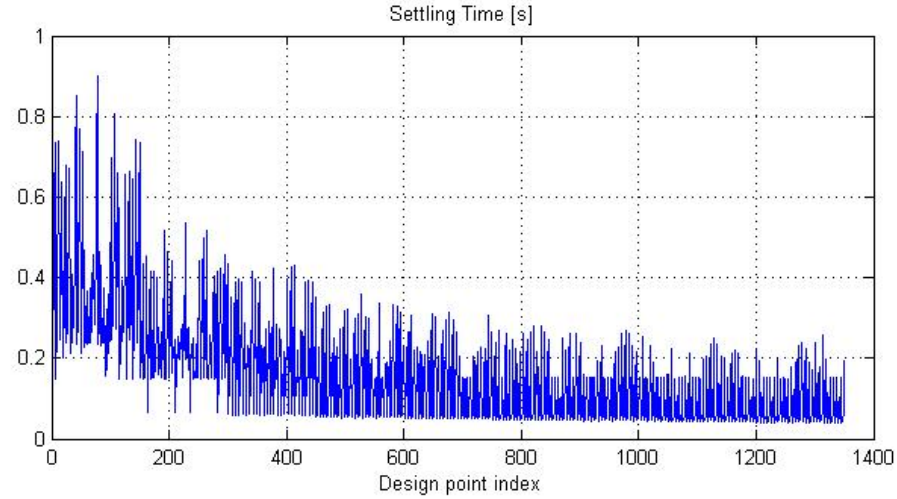

Figure 3.49: Settling time for design points

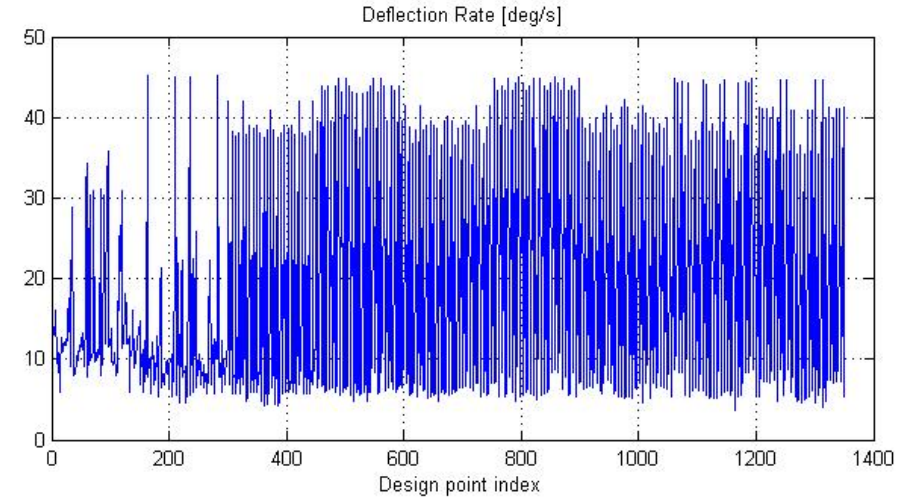

Figure 3.50: Deflection rate for design points

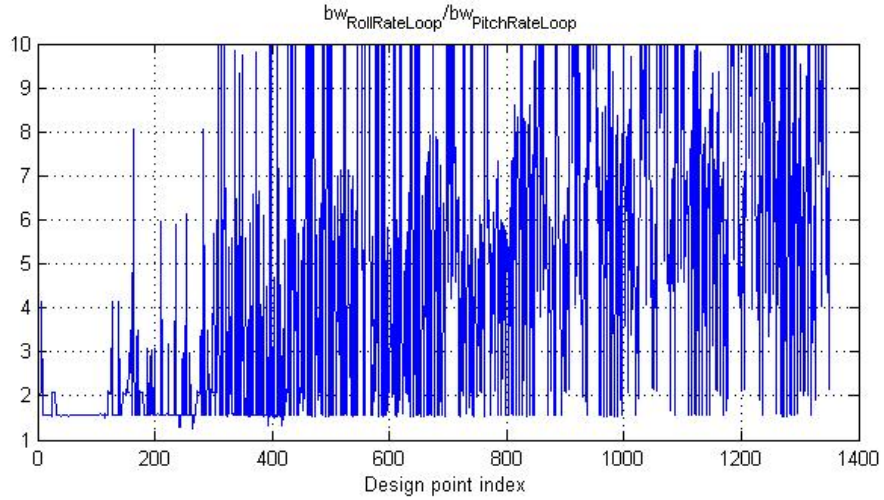

Figure 3.51: Roll rate loop bandwidth over pitch rate bandwidth for design points

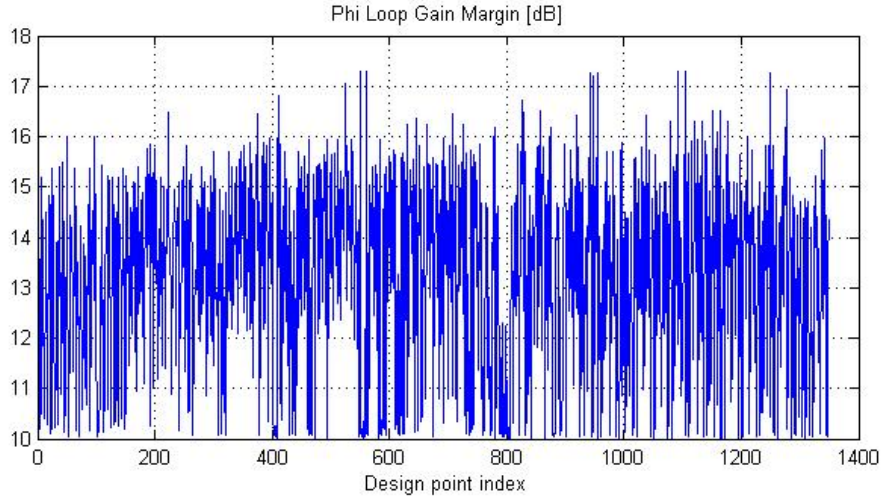

Figure 3.52: Phi loop gain margin for design points

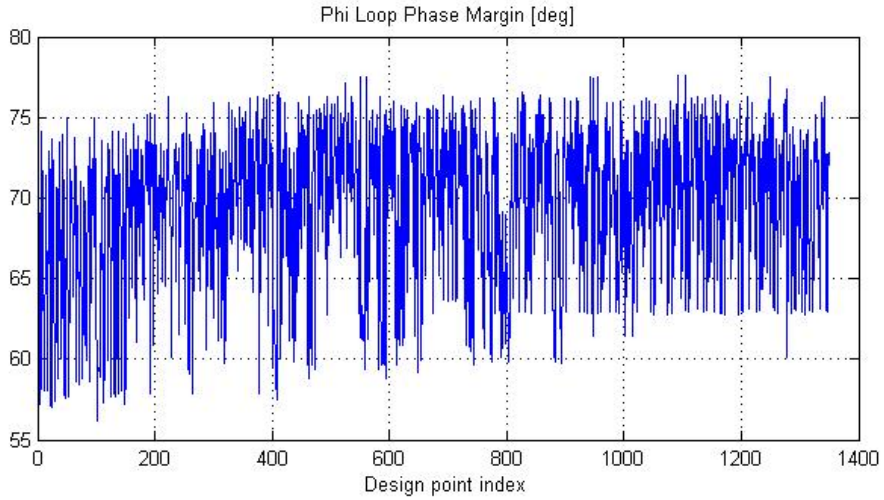

Figure 3.53: Phi loop phase margin for design points

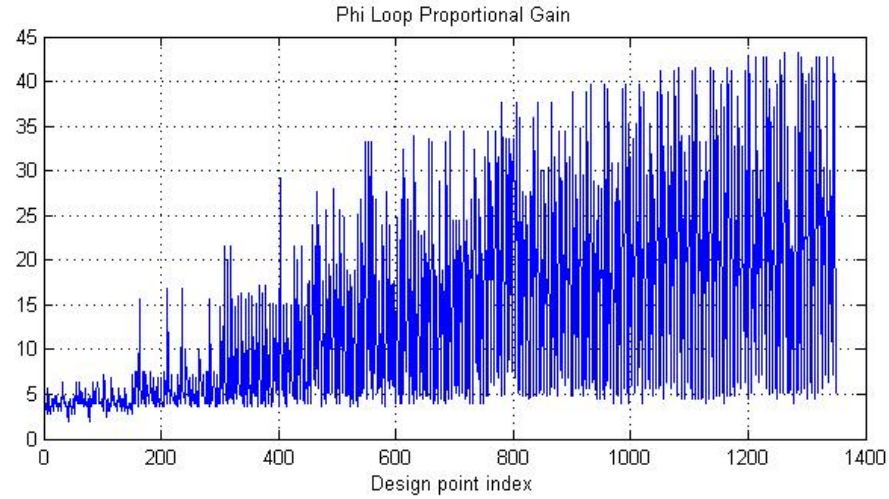

Figure 3.54: Phi loop proportional gain for design points

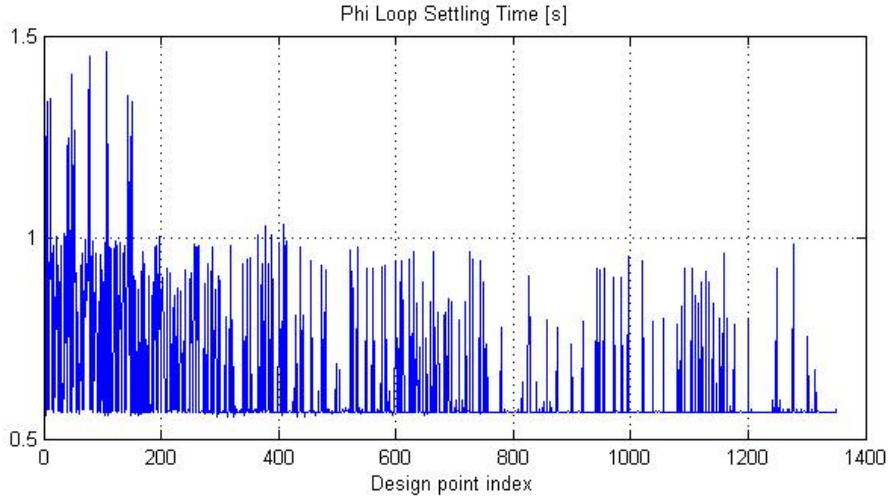

Figure 3.55: Phi loop settling time for design points

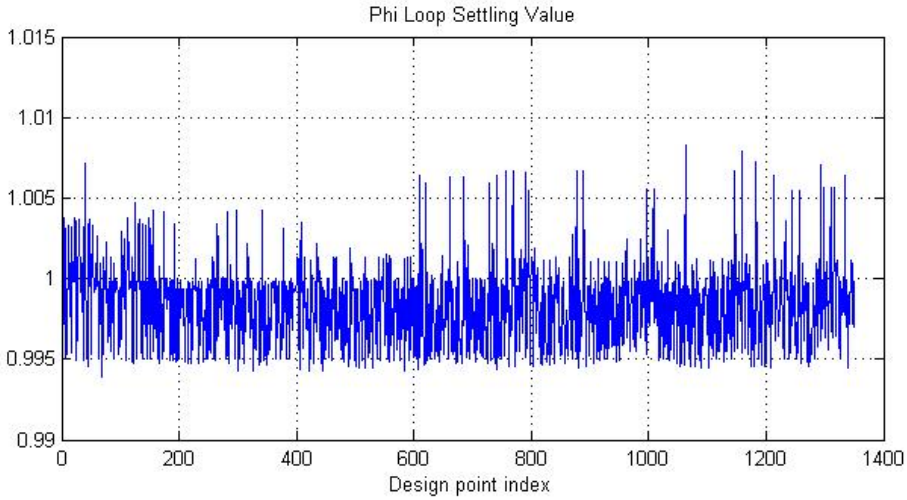

Figure 3.56: Phi loop settling value for design points

For the rate loop, gain margin is greater than 7 dB, phase margin is greater than 60 degrees and settling time of step responses are lower than 1 second for all design points. For the roll angle loop, gain margin is greater than 10 dB, phase margin is greater than 50 degrees and settling time is lower than 1 second for most of the cases. Existence of integrator for both inner and outer loops results in negligible steady state errors.

Step responses of outer loop LTI systems are represented as follows. Some of the responses are plotted to prevent figure complexity.

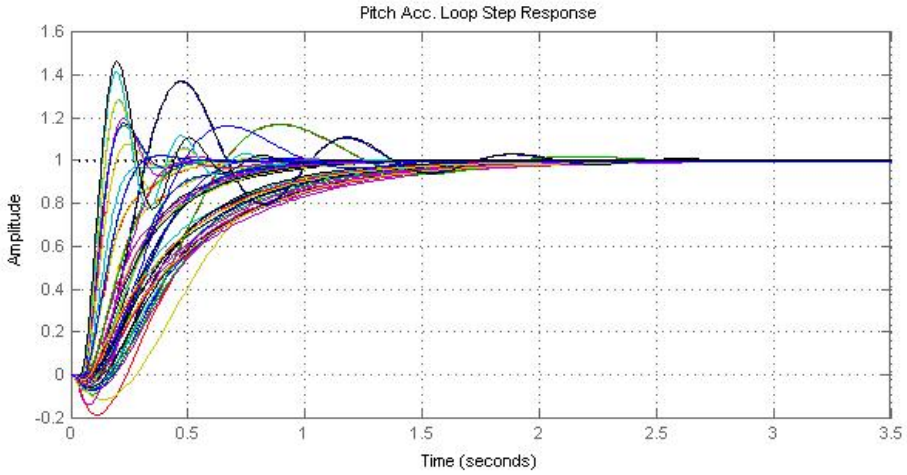

Figure 3.57: Pitch acceleration loop step responses

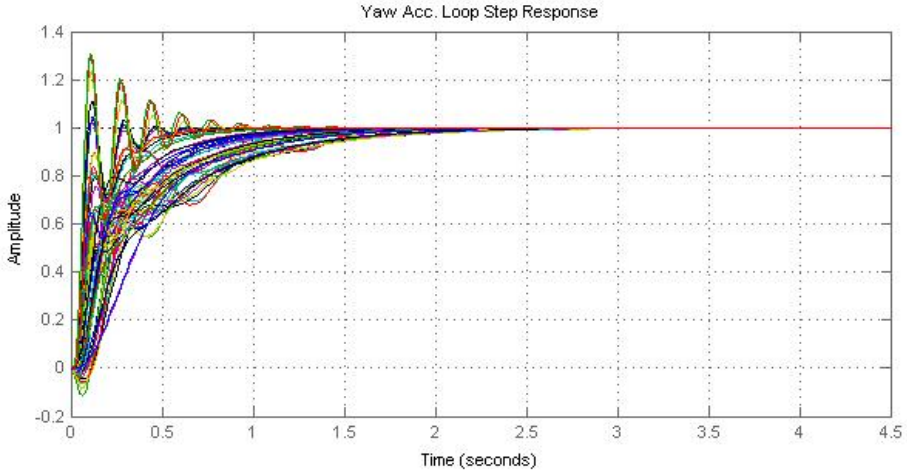

Figure 3.58: Yaw acceleration loop step responses

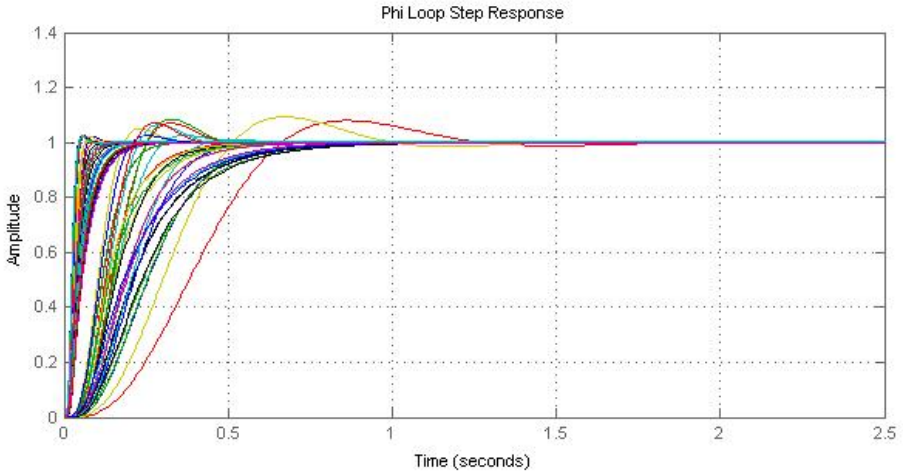

Figure 3.59: Phi loop step responses

3.6 Nonlinear Simulation Results

For an example scenario seen in Figure 3.60, nonlinear 6DOF simulation results of rate, acceleration and roll autopilots are given as follows.

Table3.1: Initial conditions of Scenario – 1

Scenario(t_0)	Missile	Target
$X[km]$	0	5
$Y[km]$	0	0
$Altitude[km]$	6	5
$Velocity[Mach]$	0.85	1
$Heading\ Angle[deg]$	0	90
$Target\ Maneuver$	10 g longitudinal	

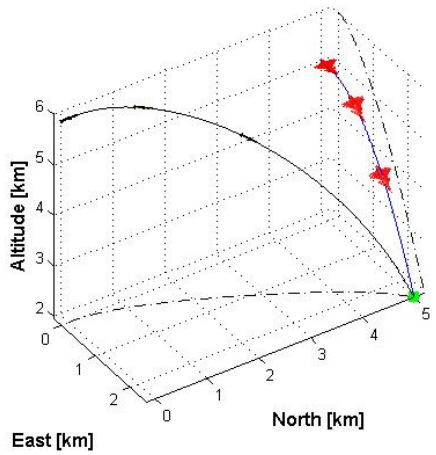

Figure 3.60: Body pitch rate autopilot response

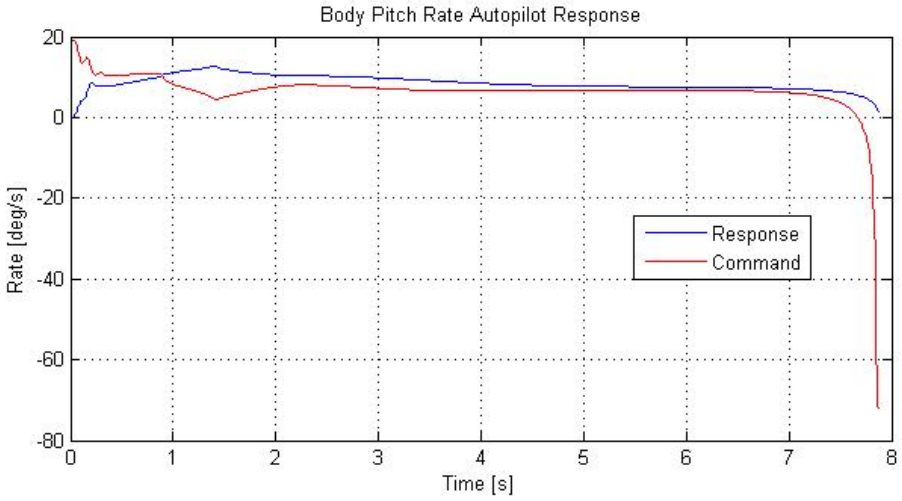

Figure 3.61: Body pitch rate autopilot response

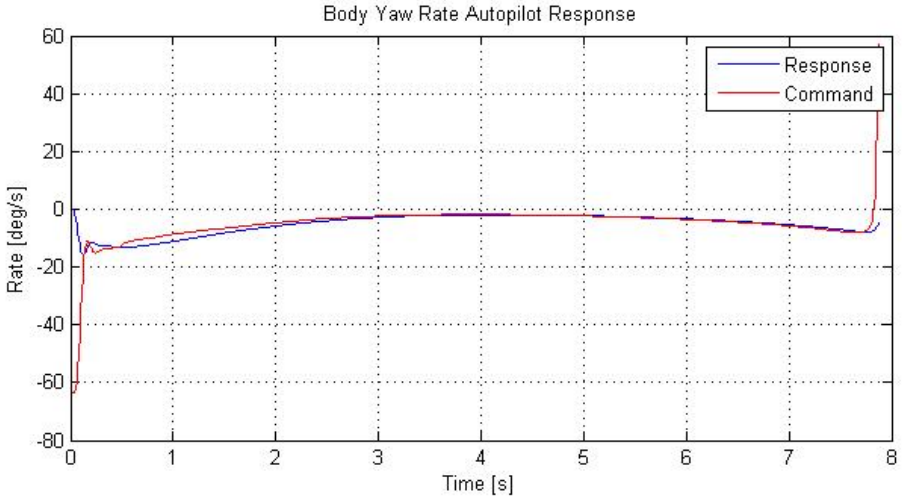

Figure 3.62: Body yaw rate autopilot response

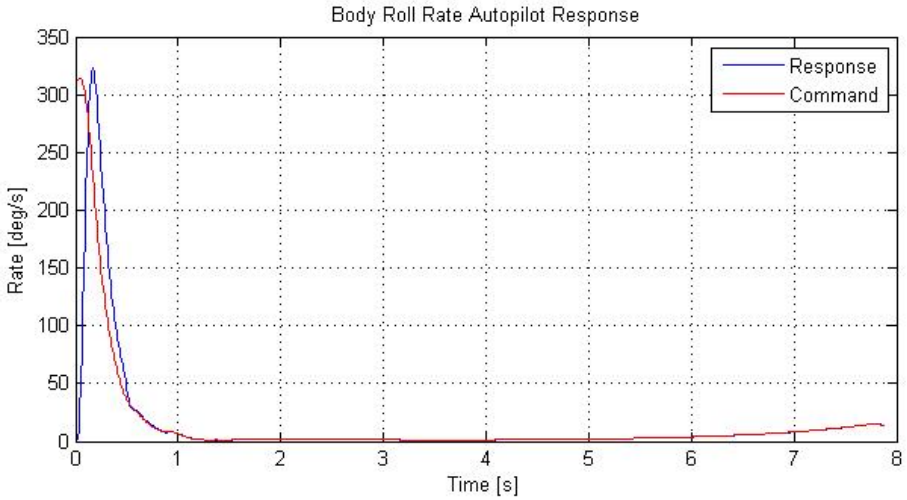

Figure 3.63: Body roll rate autopilot response

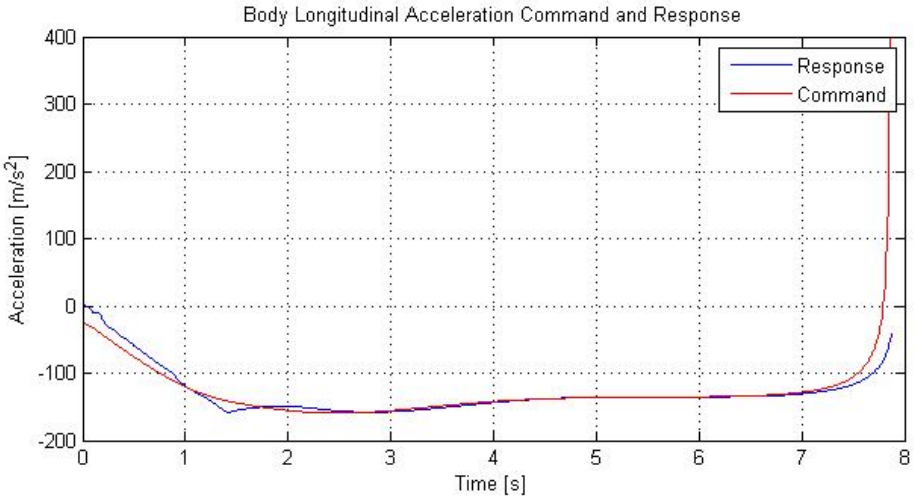

Figure 3.64: Longitudinal acceleration autopilot response

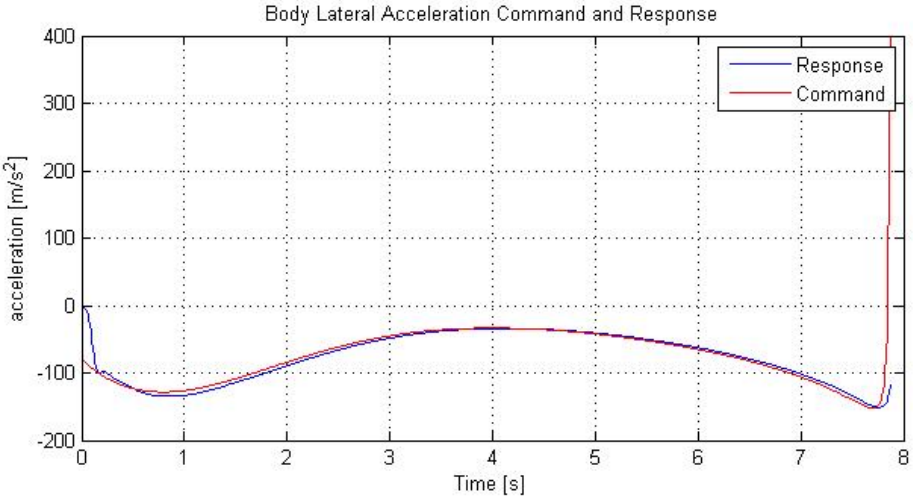

Figure 3.65: Lateral acceleration autopilot response

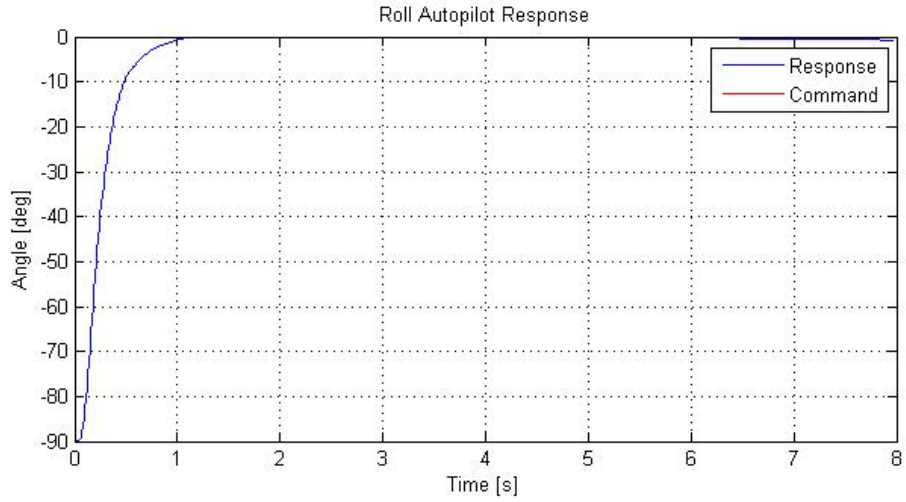

Figure 3.66: Roll autopilot response

3.7 Conclusion

In this chapter, autopilot design logic, procedure and results are stated. Aerodynamic characteristic of the missile become unstable as the agility increases and as a result, necessity of controller design for many design points for cumulative flight region is considered and handled with PST, PI and P controller designs and satisfactory results are obtained for all longitudinal and lateral autopilots. Firstly pitch, yaw and roll rate autopilots are designed with PST method and acceleration loops are closed with PI controllers for pitch and yaw channels. Then, to decouple the pitch and yaw channels roll autopilot is designed with P controllers. Gain margin, phase margin and settling time specifications are generally met. As seen from the step responses of LTI models in Figure 3.57, 3.58 and 3.59, no steady state error and fine settling characteristics are obtained with PI and P designs. In addition to this, nonlinear simulation results show that satisfactory command tracking performance is obtained until interception.

CHAPTER 4

GUIDANCE DESIGN

4.1 Introduction

Most of the SMC applications for missile guidance are first order sliding mode applications. r^{th} order sliding mode means up to $(r-1)^{th}$ order derivative of sliding variable is equal to zero. That is,

$$s = \dot{s} = \ddot{s} = ... = s^{r-1} = 0 \tag{4.1}$$

As seen from Equation 4.1, order of sliding mode also represents the smoothness of state trajectory on sliding surface and the higher order means smoother sliding on surface. As stated above, being state trajectory below and above of the surface results in a high frequency control signal changes. This action during the sliding mode is called *chattering* and this effect causes undesirable results such as triggering high frequency modes of the plant and instability, also may harm actuators that control the plant [14]. To decrease chattering, higher order sliding mode control is proposed and mostly the second order methods are commonly applied in literature and one of these methods is super twisting algorithm [16]. This method has applied to many areas such that diesel engine control [17], vehicle path following [18], pneumatic artificial muscle control [19] and aircraft pitch control [14]. According to the proposed guidance laws that are stated in the following sections, there is no need for the target acceleration to be known accurately.

4.2 First Order Sliding Mode Guidance

In this heading, two different first order sliding mode guidance rules are derived. At first, Line-of-Sight (LOS) rate is considered as a sliding surface. This surface choice comes from the idea of zero LOS rate finals with interception in most cases, and this is the general choice of sliding surface in sliding mode guidance design applications [11, 12, 13]. This guidance rule is derived for comparison with the second order sliding

mode guidance rule which is derived in Section 4.3 that uses same surface. Secondly, a proportional-integral (PI) sliding surface is proposed to provide a better interception performance than the guidance law that uses LOS rate sliding surface. Since making LOS rate equal to zero in engagement not always means interception and oppositely may mean flying away from the target in some cases, additional term of LOS angle is added to LOS rate with a gain.

4.2.1 LOS Rate Surface

For missile guidance technics, aim is generally not to let LOS angular rate increase and make as close as to zero to hold the target in field of view (FOV) and result with an interception in most cases. As stated in [3] and [37], aim of the proportional navigation guidance (PNG) which is the most widely used guidance law in practice, is to nullify the LOS rate between target and interceptor. According to the parallel guidance in Figure 4.1 which is the idea of PNG, LOS rate must be equal to zero. In reality, it differs from zero, so that guidance command which is proportional to the rate of the LOS change may decrease the absolute value of the LOS rate and it will tend to closer to zero.

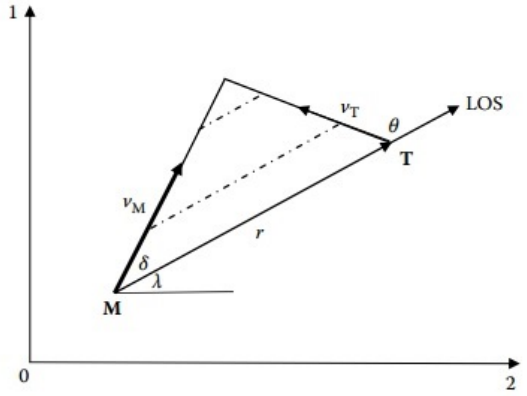

Figure 4.1: Geometry of planar engagement of parallel guidance [37]

This idea of nullification of LOS rate gives the inspiration to a solution to the guidance problem that uses sliding mode control method and leads to the general choice of sliding surface definition as LOS rate [11, 12, 13]. Then, as a sliding surface $s = \dot{\lambda}$ is applied for the first guidance rule derivation.

Firstly, basic engagement definitions of LOS angle and sigma angle are stated below with Figure 4.2 and the equations. These equations are used in the following guidance law derivations.

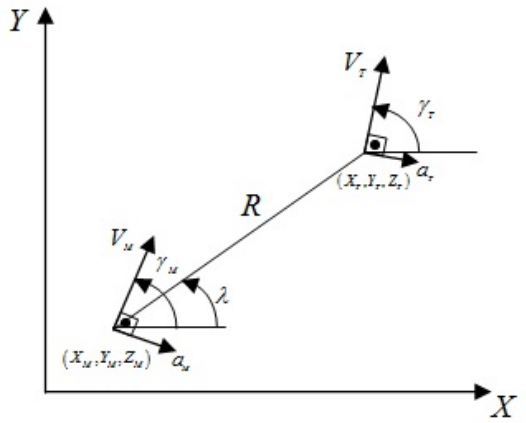

Figure 4.2: Missile-target engagement geometry

$$\lambda(t) = \arctan\left(\frac{Y_T - Y_M}{X_T - X_M}\right) \tag{4.2}$$

$$\dot{\lambda}(t) = \frac{\Delta V_Y \Delta X - \Delta V_X \Delta Y}{R^2(t)} \tag{4.3}$$

$$\ddot{\lambda}(t) = \frac{a_T(t)\cos(\sigma_T) - a_M(t)\cos(\sigma_M) - 2\dot{R}(t)\dot{\lambda}(t)}{R(t)} \tag{4.4}$$

where

$$\Delta X = X_T - X_M \tag{4.5}$$

$$\Delta Y = Y_T - Y_M \tag{4.6}$$

$$\Delta V_Y = V_{Y_T} - V_{Y_M} \tag{4.7}$$

$$\Delta V_X = V_{X_T} - V_{X_M} \tag{4.8}$$

$$\sigma_M(t) = \gamma_M - \lambda(t) \tag{4.9}$$

$$\sigma_T(t) = \gamma_T - \lambda(t) \tag{4.10}$$

Sliding mode guidance rule is constructed by calculating equivalent control and switching control rules. Sum of the equivalent control and switching control defines the control law that is applied to missile. The aim of sliding control is to drive the nonlinear plant states to a predefined surface, which is called sliding surface that determines the behaviour of the states, with switching control law, and after reaching to the surface,

keep the states on the surface. The term 'switching' comes from the change of the control signal when the states are above or below the surface. That means when the plant state trajectory is above the surface, one feedback gain and a different gain if the trajectory drops below the surface.

4.2.1.1 Equivalent Control

Whenever the initial state is on the surface, the control law that keeps the states on the surface when exciting the system is called equivalent control. So the equivalent control component of the control law is obtained by equating the derivative of the sliding variable to zero [10]. While calculating equivalent control, target acceleration term is considered as uncertainty and ignored.

$$s = \dot{\lambda}(t) \tag{4.11}$$

$$\dot{s} = \ddot{\lambda}(t) = \frac{a_T(t)\cos(\sigma_T) - a_M(t)\cos(\sigma_M) - 2\dot{R}(t)\dot{\lambda}(t)}{R(t)} \tag{4.12}$$

If Equation 4.12 is equated to zero, then equivalent control component of the guidance law can be found as

$$a_{M_{eq}} = \frac{-2\dot{R}(t)\dot{\lambda}(t)}{\cos(\sigma_M(t))} \tag{4.13}$$

4.2.1.2 Switching Control

Switching control law, also defined as *reaching law*, is the component that provides the convergence of the state that is chosen as surface to zero. To guarantee the convergence, it is required to obtain an appropriate switching control. This component has a switching term(generally a signum function) as function of surface, it changes its value according to the state values is below or above of the surface. The switching control component is proposed as

$$a_{M_{sw}} = \frac{k_{sw} sgn(s)}{cos(\sigma_M(t))} \tag{4.14}$$

To check whether this rule provides convergence, firstly a Lyapunov function is determined as in [11, 12, 13].

$$V = \frac{1}{2}s^2 \tag{4.15}$$

This equation is a positive definite function for $s \neq 0$, so it is suitable to choose as a Lyapunov function. To check whether the reaching law is suitable, Lyapunov stability criteria is applied and according to this rule, derivative of the Lyapunov function must be a negative term [10].

$$\begin{aligned}\dot{V} &= s(t)\dot{s}(t) < 0 \\ &= s(t)\left(\frac{a_T(t)\cos(\sigma_T(t)) - \left(a_{M_{eq}}(t) + a_{M_{sw}}(t)\right)\cos(\sigma_M(t)) - 2\dot{R}(t)\dot{\lambda}(t)}{R(t)}\right) \\ &\leq \frac{s(t)}{R}\left(a_{T_{max}} - k_{sw}sgn(s)\right) < 0 \end{aligned} \tag{4.16}$$

$$if \quad s < 0 \Rightarrow (a_{T_{max}} + k_{sw}sgn(s)) > 0$$
$$if \quad s > 0 \Rightarrow (a_{T_{max}} - k_{sw}sgn(s)) < 0$$

That means, according to the Lyapunov stability criteria $k_{sw} > a_{T_{max}}$ is required. $a_{T_{max}}$ is the maximum acceleration capability of the target and taken as $10g(\approx 98.1m/s^2)$ and k_{sw} term is taken as $100m/s^2$. That is where the necessity of the knowledge of target acceleration during flight vanishes. Here, sliding mode control provides to derive a guidance rule with only assigning a maximum value of target acceleration to cope with this uncertainty. As a result, a guidance law in Equation 4.17 that is robust up to $10g$ target acceleration is obtained.

$$a_M = \frac{-2\dot{R}(t)\dot{\lambda}(t) + k_{sw}sgn(s)}{\cos(\sigma_M(t))} \tag{4.17}$$

4.2.2 Proportinal-Integral (PI) Surface

To hold LOS rate zero with PNG guidance may not mean intercept in some scenarios, there can be such scenarios that missile gets away from the target while LOS rate is zero, especially for high off-boresight shoots. In such situations, steering to the target immediately and keep it in field of view of the seeker become important. With an additional LOS angle term to LOS rate, a new sliding surface can be obtained. Many of PI and PID surface applications are stated in literature and some of them use these methods in controlling DC motor [25] and robotic manipulators [27, 28], and also for a torpedo control [26]. This logic is applied to the missile guidance problem.

$$s(t) = k_P e(t) + k_I \int_0^t e(\tau)d\tau \tag{4.18}$$

To apply this PI rule to the missile guidance problem, analogically LOS rate is applied

to the error term in Equation 4.18.

$$s(t) = k_P\dot{\lambda}(t) + k_I\lambda(t) \tag{4.19}$$

$$\dot{s}(t) = k_P\ddot{\lambda}(t) + k_I\dot{\lambda}(t) \tag{4.20}$$

4.2.2.1 Equivalent Control

As stated in Section 4.2.1.1, if the definitions in Equation 4.3 and 4.4 are used and the derivative of the sliding variable 4.20 is equated to zero, the equivalent control component is obtained as

$$a_{M_{eq}} = \left(k_I\dot{\lambda}(t) - k_P\frac{2\dot{R}(t)\dot{\lambda}(t)}{R(t)}\right)\frac{R}{k_P\cos(\sigma_M(t))} \tag{4.21}$$

4.2.2.2 Switching Control

By using the same switching control component in Equation 4.14

$$\begin{aligned}\dot{V} &= s(t)\dot{s}(t) < 0\\ &= s(t)\left(k_P\ddot{\lambda}(t) + k_I\dot{\lambda}(t)\right)\\ &= s(t)\left(k_I\dot{\lambda}(t) + k_P\left(\frac{a_T(t)\cos(\sigma_T(t)) - \left(a_{M_{eq}}(t) + a_{M_{sw}}(t)\right)\cos(\sigma_M(t)) - 2\dot{R}(t)\dot{\lambda}(t)}{R(t)}\right)\right)\\ &\leq \frac{s(t)k_P}{R}\left(a_{T_{max}} - k_{sw}sgn(s)\right) < 0\end{aligned} \tag{4.22}$$

$if \quad s < 0 \Rightarrow (a_{T_{max}} + k_{sw}sgn(s)) > 0$
$if \quad s > 0 \Rightarrow (a_{T_{max}} - k_{sw}sgn(s)) < 0$

According to the Lyapunov stability criteria $k_{sw} > a_{T_{max}}$ is required.

Finally, with summation of Equation 4.21 and the switching control component, total acceleration command is obtained as

$$a_M = \left(\frac{k_I\dot{\lambda}(t)R(t)}{k_P} - 2\dot{R}(t)\dot{\lambda}(t) + k_{sw}sgn(s)\right)\frac{1}{\cos(\sigma_M(t))} \tag{4.23}$$

4.2.2.3 Optimization with Genetic Algorithm

Genetic algorithm (GA) is an optimization method that imitates genetic science with its features that provides variation such as natural selection, crossover and mutation to find an optimal solution by creating optimal solution candidates in each generation. In this method, possible solution candidates are selected and used to create the next generation with crossover and mutation to obtain new members and populations.

To determined the k_P and k_I parameters, genetic algorithm is applied. Firstly, two scenarios are constructed which the first one has a non-maneuvering and the second one has a maneuvering target. Then, for these scenarios, optimization procedures are started and a gain set is obtained. Defined reference scenarios are as follows.

Table4.1: Initial conditions of refecence scenario – 1

Scenario(t_0)	Missile	Target
$X[km]$	0	20
$Y[km]$	0	-10
$Altitude[km]$	6	6
$Velocity[Mach]$	0.85	1.2
$Heading\ Angle[deg]$	0	225
$Target\ Maneuver$	0 g	

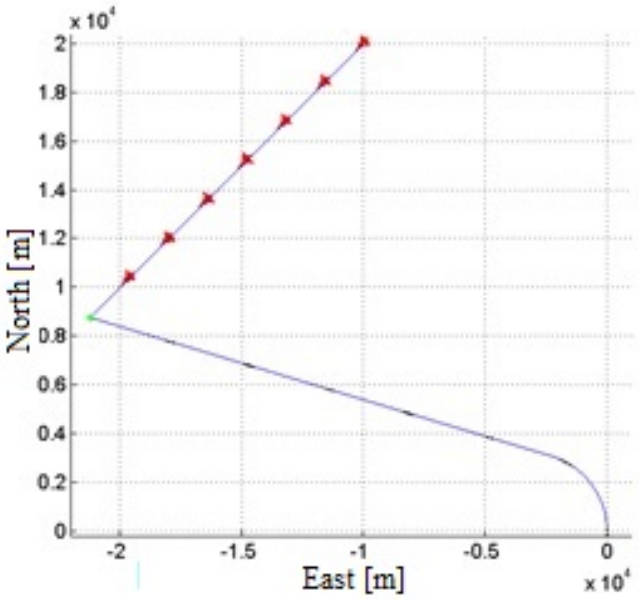

Figure 4.3: Missile and target trajectories

Table4.2: Initial conditions of refecence scenario – 2

Scenario(t_0)	Missile	Target
$X[km]$	0	20
$Y[km]$	0	0
$Altitude[km]$	6	6
$Velocity[Mach]$	0.85	1.4
$Heading\ Angle[deg]$	0	225
$Target\ Maneuver$	10 g lateral	

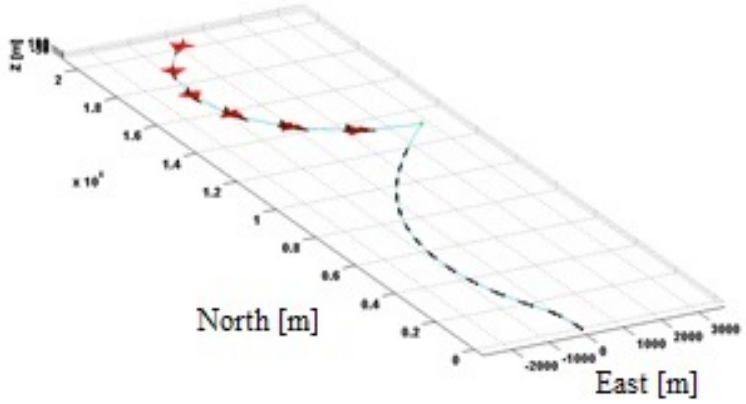

Figure 4.4: Missile and target trajectories

The cost function is selected as

$$J(x,t) = w_1k_1J_1(x,t) + w_2k_2J_2(x,t) + w_3k_3J_3(x,t) + w_4k_4J_4(x,t) + B.F. \quad (4.24)$$

where

$J_1(x,t)$: time integral of sliding surface,
$J_2(x,t)$: time integral of derivative of sliding variable,
$J_3(x,t)$: time integral of missile acceleration,
$J_4(x,t)$: missile-target interception time,
w_1, w_2, w_3, w_4 : cost weighting coefficients,
k_1, k_2, k_3, k_4 : cost scaling coefficients,
$B.F.$: barrier function.

Cost weighting coefficients are in the order of cost function pieces definition from larger to smaller. That is, time integral of sliding surface is weighted more than other cost pieces. As a result of optimization, following gains are obtained.

$$k_P = 13.2 \quad (4.25)$$

$$k_I = 0.1 \tag{4.26}$$

4.3 Second Order Sliding Mode Guidance

As stated earlier, the sliding order determines the smoothness degree related to the motion constraint on the sliding surface $s = 0$. In other words, it is the degree of keeping the system on the sliding manifold. r^{th} order sliding mode means $(r-1)^{th}$ and its previous derivatives of the sliding manifold is equal to zero when sliding mode occurs as represented in Equation 4.1.

Generally the sliding mode order implies the total number of time derivatives of the sliding variable that the control appears explicitly, that is, for second order sliding mode, u, control input appears in the second time derivative of the sliding variable. However, second order sliding mode control can be used also for the cases that control input appears in the first time derivative of the sliding variable for chattering attenuation.

In this study, one of the second order sliding mode methods, called *super twisting method* is applied to the missile guidance problem. This method is used for the cases that control input appears in the first time derivative of the sliding variable to attenuate chattering and obtained much smoother control signals when compared to first order sliding mode control.

Consider a system which the relative degree is 1, that is

$$\frac{\partial \dot{\sigma}}{\partial u} \neq 0 \tag{4.27}$$

The aim is to stabilize the following system.

$$y_1 = \sigma(t, x) \tag{4.28}$$

$$\dot{y}_1 = y_2 \tag{4.29}$$

$$\dot{y}_2 = \phi(.) + \gamma(t, x)\dot{u}(t) \tag{4.30}$$

where y_1 represent the actual sliding variable and its derivative y_2 is not available for measurement, and uncertain terms $\phi(.)$ and $\gamma(t, x)$ are bounded such that

$$|\phi(.)| \leq \Phi \tag{4.31}$$

$$0 < G_1 < \gamma(t,x) < G_2 \tag{4.32}$$

Control algorithm for the system above is defined as

$$u(t) = -K|y_1|^{\rho} sgn(y_1) + u_1 \tag{4.33}$$

$$\dot{u}_1 = -a.sgn(y_1) \tag{4.34}$$

where

$$a > \frac{\Phi}{G_1} \tag{4.35}$$

$$K^2 > \frac{4\Phi G_2\,(a+\Phi)}{G_1^3\,(a-\Phi)} \tag{4.36}$$

$$0 < \rho < 0.5 \tag{4.37}$$

in [16, 17, 18].

In our guidance problem, the system to stabilize is determined as

$$y_1 = \sigma(t,x) = \dot{\lambda}(t) \tag{4.38}$$

$$\dot{y}_1 = y_2 = \ddot{\lambda}(t) \tag{4.39}$$

$$\dot{y}_2 = \dddot{\lambda}(t) = \phi(.) + \gamma(t,x)\dot{u}(t) \tag{4.40}$$

LOS rate is stated with Equation 4.4, and its first time derivative is stated as

$$\begin{aligned}\dddot{\lambda}(t) = \frac{-2\ddot{R}\dot{\lambda}}{R} + \frac{6\dot{R}^2\dot{\lambda}}{R^2} + \frac{3\dot{R}\,(a_M\cos(\sigma_M) - a_T\cos(\sigma_T))}{R^2} + \frac{a_M\sin(\sigma_M)\dot{\sigma}_M}{R} - \\ \frac{a_T\sin(\sigma_T)\dot{\sigma}_T}{R} + \frac{\dot{a}_T\cos(\sigma_T)}{R} + \underbrace{\left(\frac{-\cos(\sigma_M)}{R}\right)}_{\gamma(t,x)}\dot{a}_M\end{aligned} \tag{4.41}$$

Uncertain terms $\phi(.)$ and $\gamma(t,x)$ are dependent on the missile-target interception scenarios. For some different scenarios, these values are noted and the controller gains are calculated and applied. However, the results show that this logic is not applicable to missile guidance application. In [14], it is stated that the most appropriate way to

find the suitable parameter values is to adjust them during simulation to get rid of the large values obtained with rough evaluation technique. This method is also applied but causes very large missile acceleration commands and saturates the commands during simulation and no satisfactory results are obtained. Finally, it is considered to obtain these K, a, and ρ parameters by optimization and GA is used to find them as applied for PI surface. The same scenarios in Section 4.2.2.3 are used. As a result, the following gains are found.

$$K = 292.66 \tag{4.42}$$

$$a = 30.5 \tag{4.43}$$

$$\rho = 0.146 \tag{4.44}$$

These gains are applied to many scenarios and satisfactory results are obtained. However, these scenarios have shown that the parameters that are found by GA can be determined according to a rule related to the sliding surface adaptively. As a result, an adaptive rule stated below is proposed to find these gains.

$$a = 300\dot{\lambda}(t) + 20 \tag{4.45}$$

$$K = 10a \tag{4.46}$$

$$\rho = 0.2 \tag{4.47}$$

This rule is generated by making connection between LOS rate and the parameter a. As a result of observation and analysis of many optimization results of scenarios, parameter a is required to stay between approximately 20 and 50. So, a linear relation is defined between LOS rate and a that is stated in Equation 4.45. Besides, in many cases, GA process is resulted with K parameter which is approximately ten times of parameter a. As stated in Equation 4.42 and 4.3. The parameter ρ is selected with a tuning around the static gain that GA gives. A comparison of static and adaptive gain ST method is examined in Section 5.3.

All methods derived with first and second order sliding modes are compared with different scenarios in the next chapter.

4.4 Conclusion

In this chapter, first order and second order sliding mode guidance rules are derived. First order guidance derivation results in two different rules that choose LOS rate as a surface and PI surface that get LOS rate and LOS angle as parameters. The need of first order rule that uses LOS rate surface is for a logical comparison with the second order guidance rule that uses the same surface, to see the improvement about chattering attenuation which is realized by first order time derivative of the sliding variable. Next, PI surface is proposed as a first order sliding mode guidance rule to eliminate the possible interception scenarios that result in failure with first order guidance law that uses LOS rate surface. The resulting guidance law is also used for performance comparison with the super twisting guidance rule. Finally, second order sliding mode guidance rule is constructed by using super twisting method. This method relies on the idea of getting the derivative of system input as the input that signum function, that cause chattering and discontinuity, appears. So, this indirect discontinuity affect helps to attenuate the chattering effect.

CHAPTER 5

SIMULATION STUDIES

5.1 Introduction

6DOF simulation model is constructed in MATLAB/Simulink. Model blocks and signal flow of the model is shown in Figure 5.1.

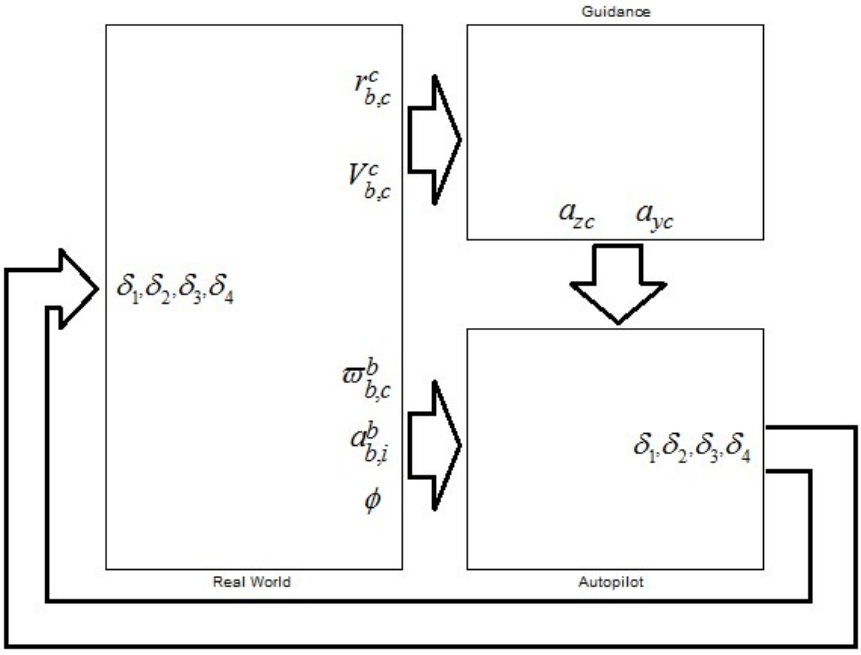

Figure 5.1: 6DOF model blocks and signal flow

In 'Real World' block, aerodynamic force and moments coefficients are stated with interpolation tables. According to the flight parameters that are angle of attack, angle of sideslip, Mach number, fin deflection angles and body angular velocities, aerodynamic force and moments are calculated. After adding thrust force and gravitational force components, total force and moments on missile body are handled to calculate body translational and angular velocities, translational acceleration and Euler angles according to the nonlinear equations of motion.

In 'Guidance' block, guidance rules that are stated in Chapter 4 and PNG law are constructed for comparison. All intercept geometry variables are calculated in this block to generate the appropriate guidance signals to feed the autopilot.

In 'Autopilot' block, rate, acceleration and roll autopilot structures are constructed. Rate, acceleration and roll angle feedbacks are fed from 'Real World' block and longitudinal and lateral acceleration commands are fed from 'Guidance' block.

5.2 First Order versus Second Order Sliding Mode Guidance

5.2.1 Scenario - 1

In this long range scenario, shooter and target are flying at opposite directions at approximately 20000ft. The shooter flies with heading to north and releases the missile at 0.85 Mach when the target flies with heading to south at 0.85 Mach. At the time of shoot, there is approximately 100 km distance between the shooter and target. In this scenario it is assumed that the target makes no evasion maneuver. Initial conditions are stated in Table 2 and the results are stated with figures as follows.

Table5.1: Initial conditions of Scenario – 1

Scenario(t_0)	Missile	Target
$X[km]$	0	70
$Y[km]$	0	70
$Altitude[km]$	6	6
$Velocity[Mach]$	0.85	0.85
$Heading\ Angle[deg]$	0	180
$Target\ Maneuver$	0	

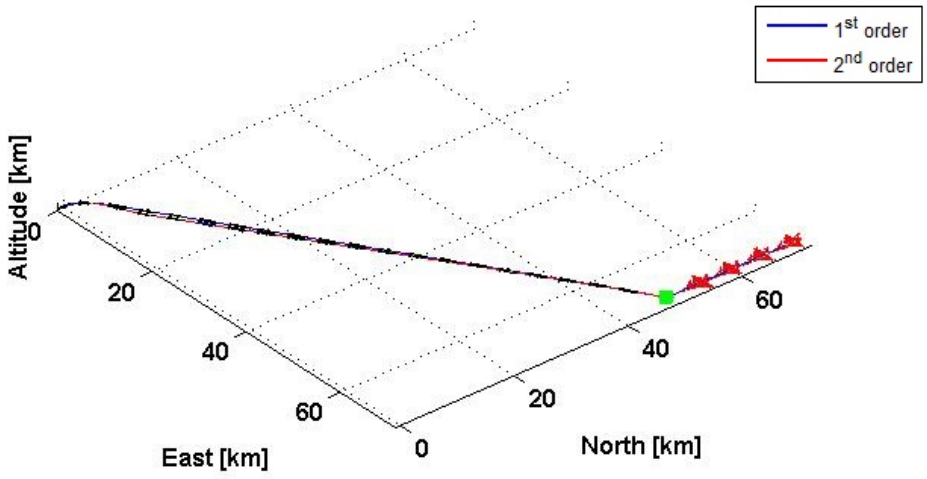

Figure 5.2: Missile and target trajectories

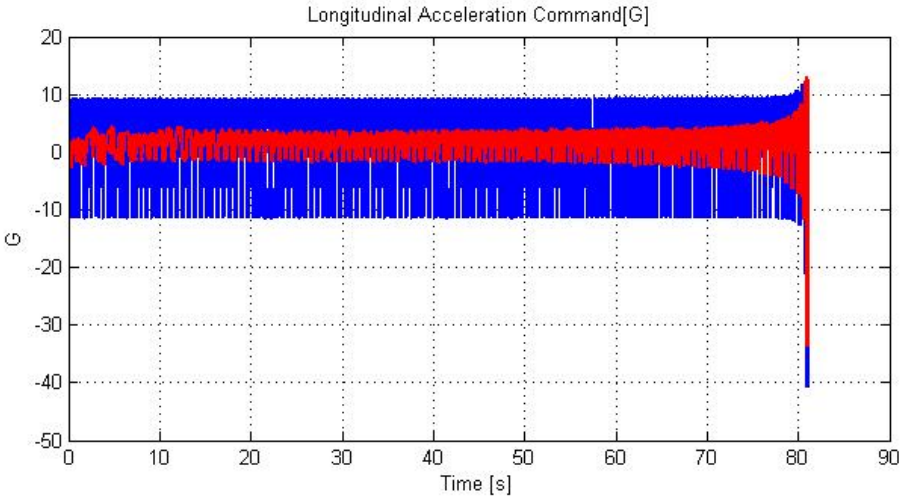

Figure 5.3: Longitudinal acceleration command

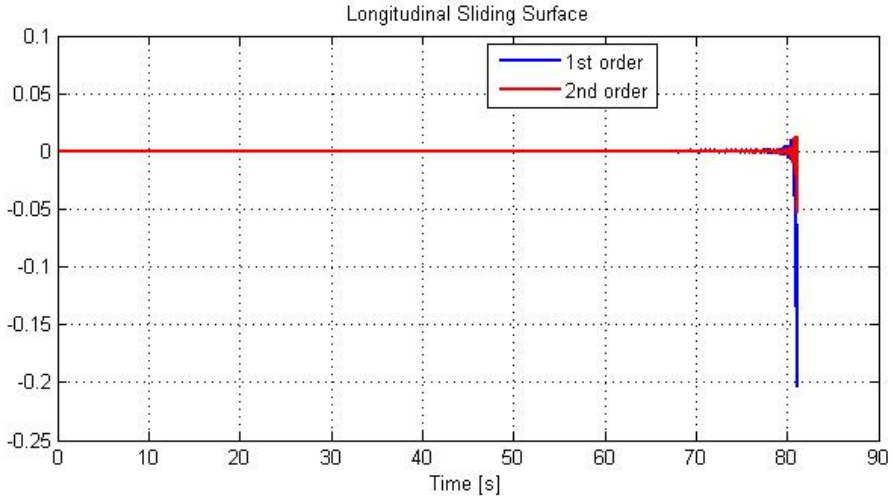

Figure 5.4: Longitudinal sliding surface

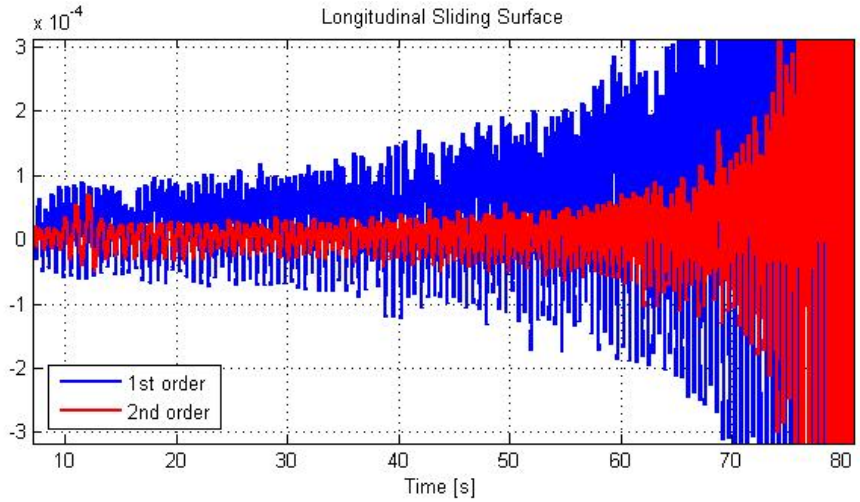

Figure 5.5: Longitudinal sliding surface (zoomed)

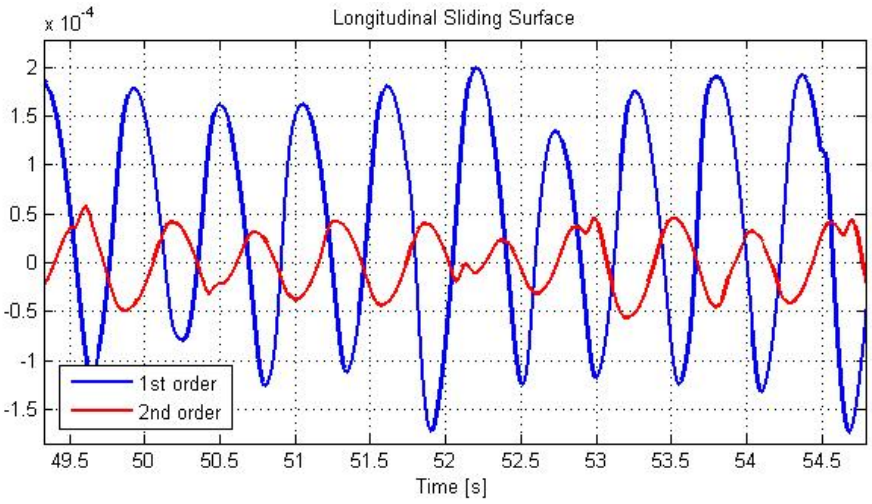

Figure 5.6: Longitudinal sliding surface (zoomed)

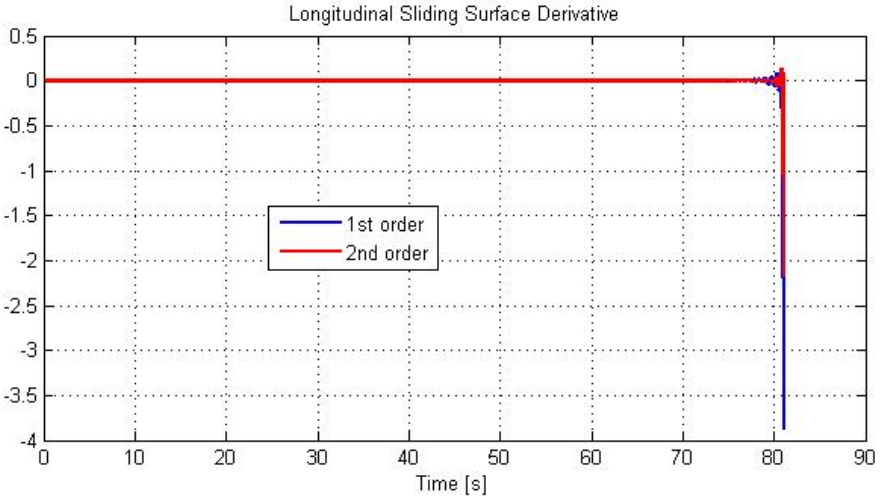

Figure 5.7: Derivative of longitudinal sliding variable

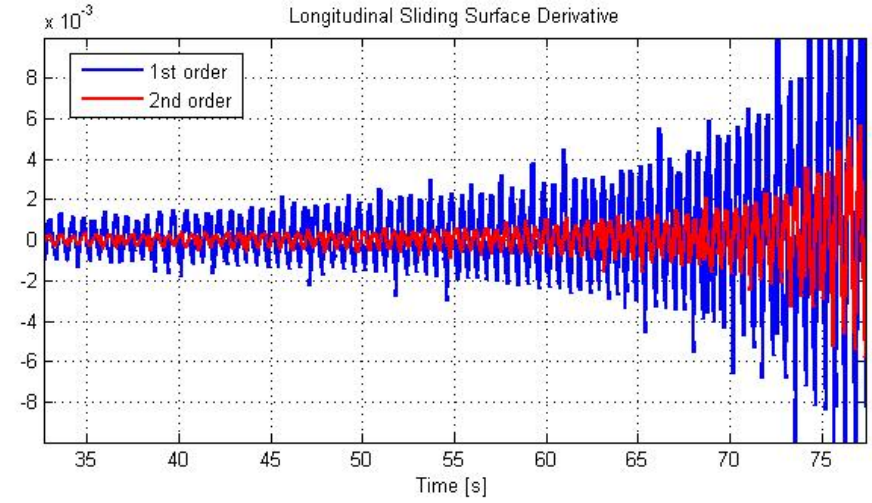

Figure 5.8: Derivative of longitudinal sliding variable (zoomed)

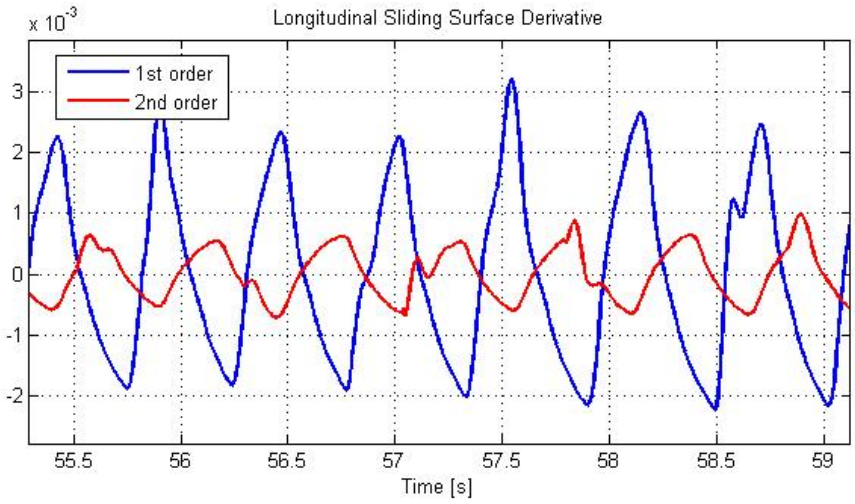

Figure 5.9: Derivative of longitudinal sliding variable (zoomed)

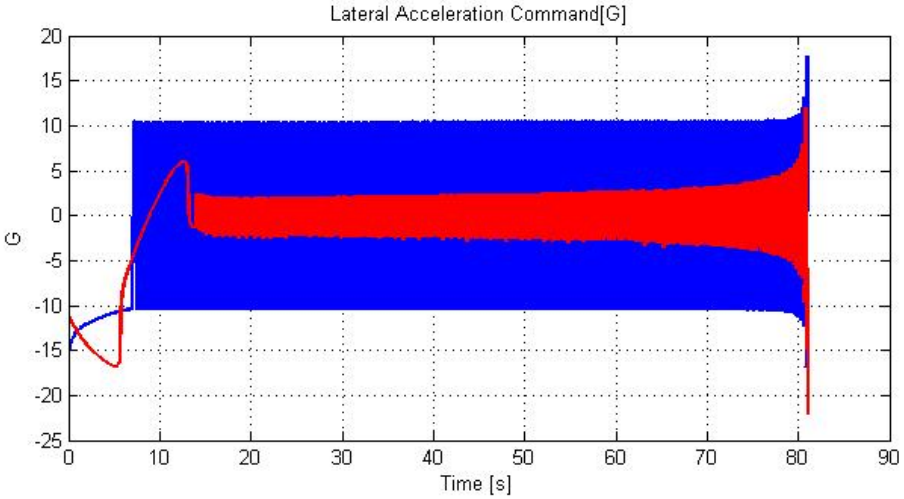

Figure 5.10: Lateral acceleration command

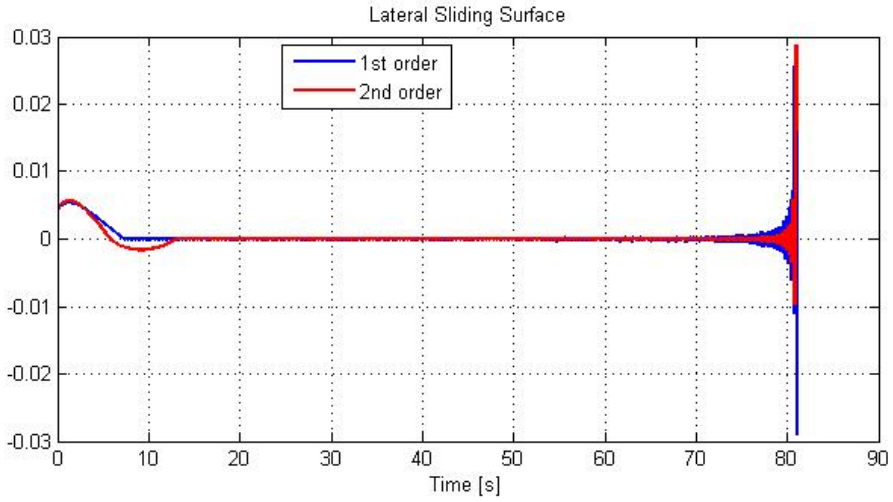

Figure 5.11: Lateral sliding surface

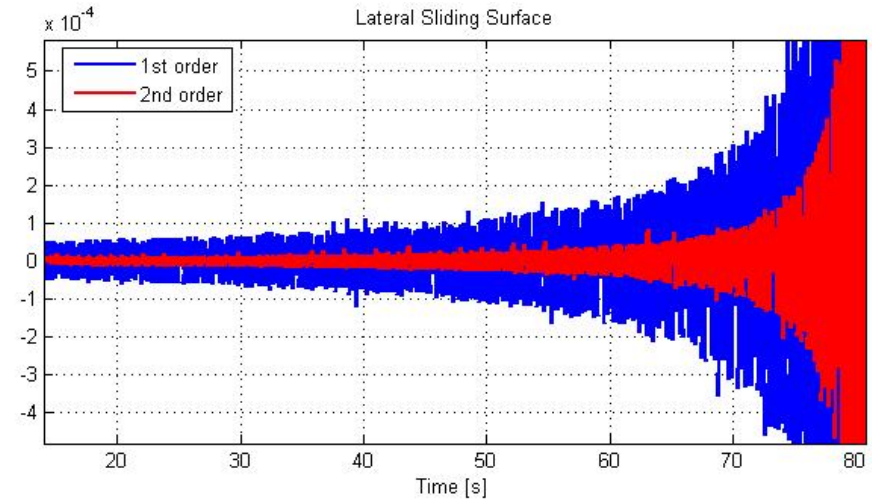

Figure 5.12: Lateral sliding surface (zoomed)

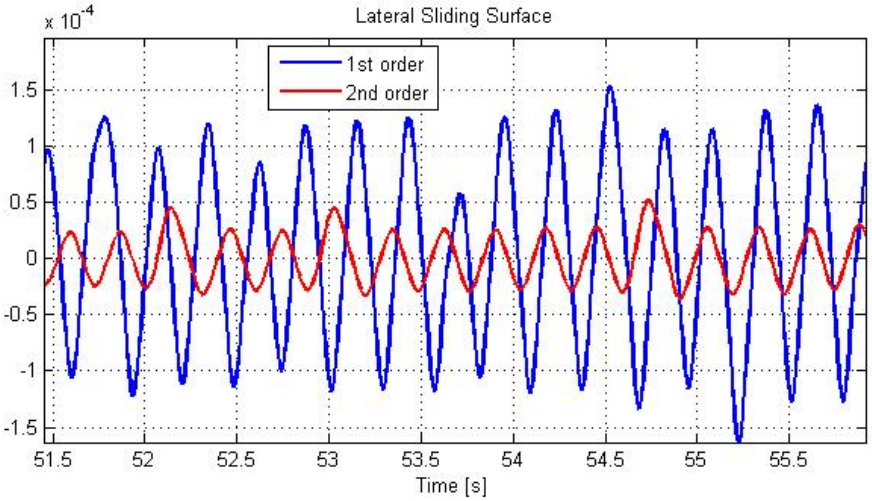

Figure 5.13: Lateral sliding surface (zoomed)

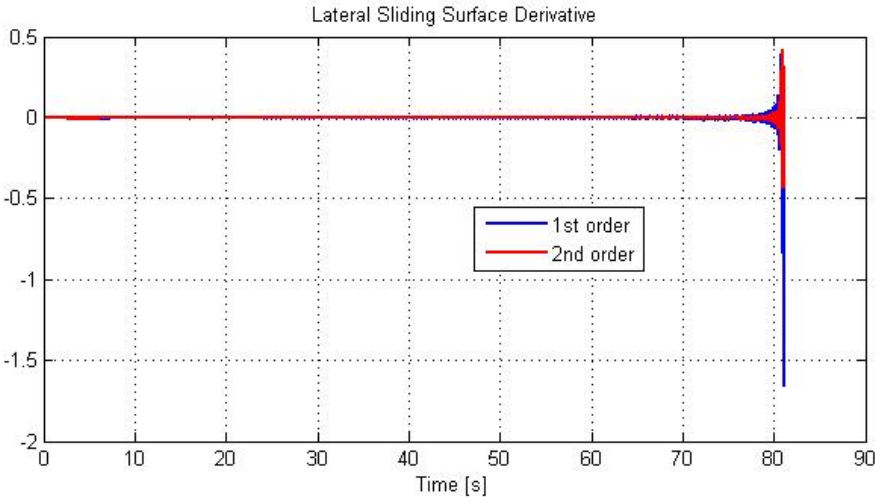

Figure 5.14: Derivative of lateral sliding variable

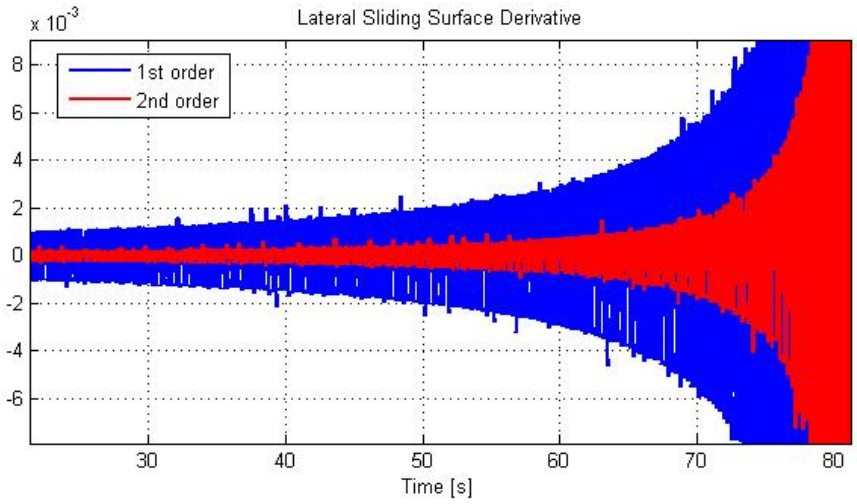

Figure 5.15: Derivative of lateral sliding variable (zoomed)

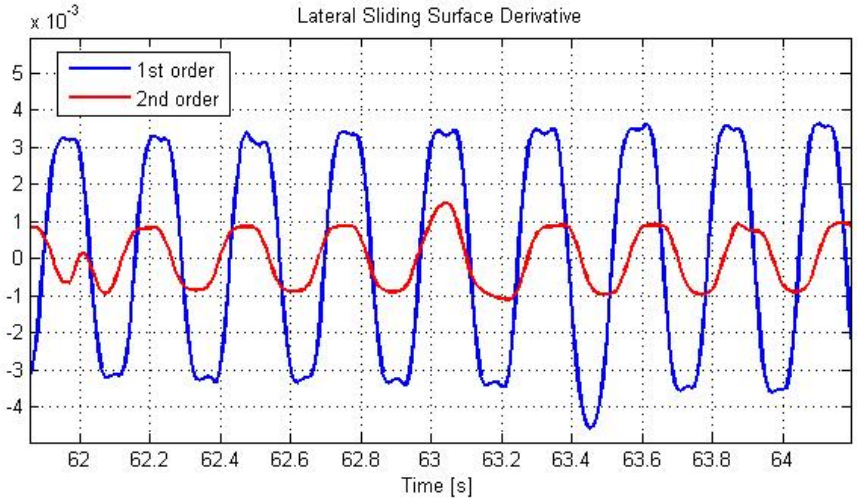

Figure 5.16: Derivative of lateral sliding variable (zoomed)

Guidance commands grow close to the intercept caused by LOS rate increase during the approach. This is a general result that can be seen in most of the guidance laws that use LOS rate. In Figure 5.8,5.9, 5.15 and 5.16, chattering attenuation can be seen clearly with derivative of sliding variable in both longitudinal and lateral channels. Also the magnitude of acceleration commands after sliding mode occurs is smaller than the first order method.

5.2.2 Scenario - 2

In this long range scenario, the shooter flies with heading to north and releases the missile at 0.85 Mach when the target flies with heading to south at 0.85 Mach. At the time of shoot, there is approximately 100 km distance between the shooter and target as before. In this scenario, the target starts an evasion maneuver when the distance to

missile is 10 km. Initial conditions are stated in Table 5.2 and the results are stated with figures as follows.

Table5.2: Initial conditions of Scenario – 2

Scenario(t_0)	Missile	Target
$X[km]$	0	70
$Y[km]$	0	70
$Altitude[km]$	6	6
$Velocity[Mach]$	0.85	0.85
$Heading\ Angle[deg]$	0	135
$Target\ Maneuver$	0 until 10km left between missile and target then 7 g lateral -2 g longitudinal	

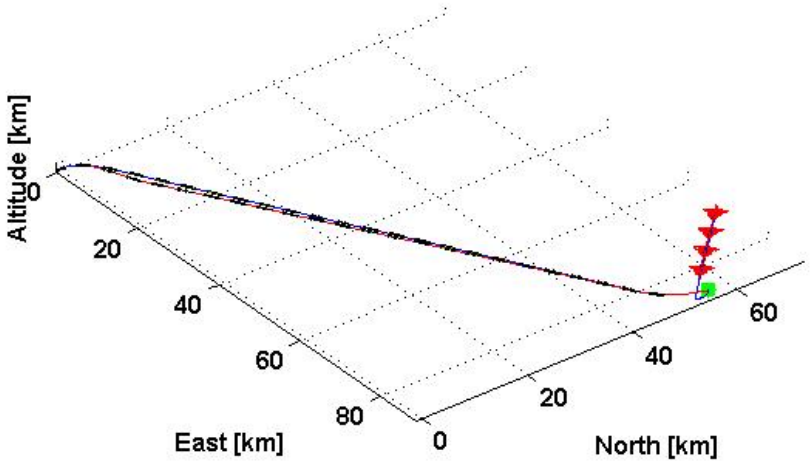

Figure 5.17: Missile and target trajectories

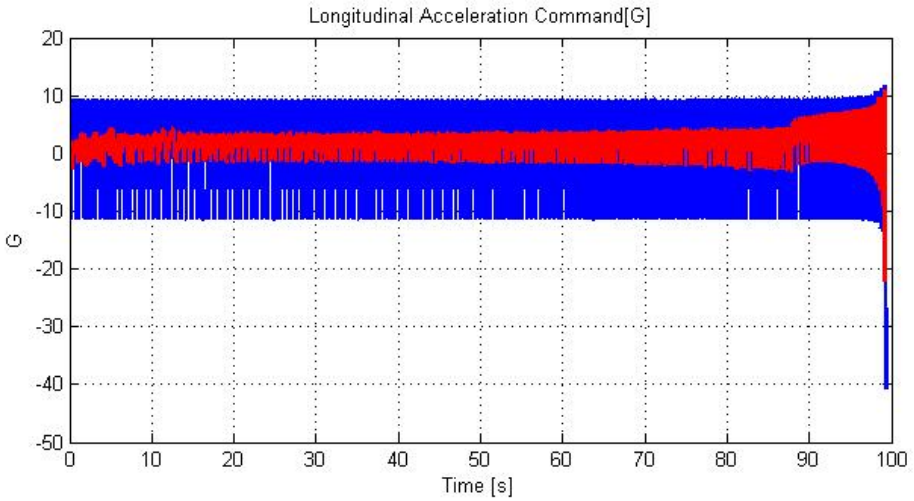

Figure 5.18: Longitudinal acceleration command

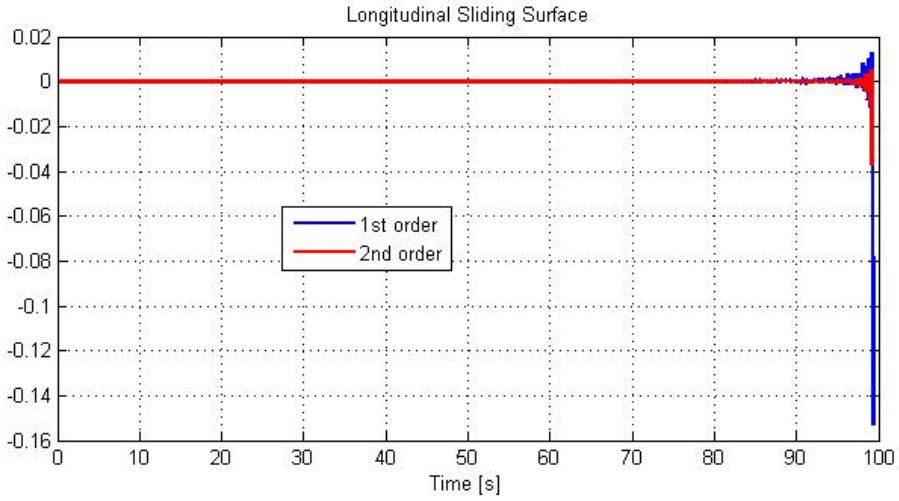

Figure 5.19: Longitudinal sliding surface

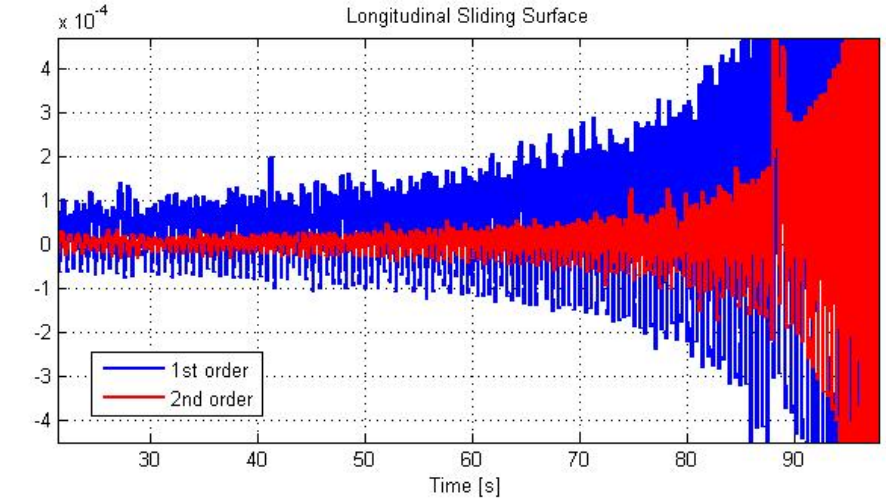

Figure 5.20: Longitudinal sliding surface (zoomed)

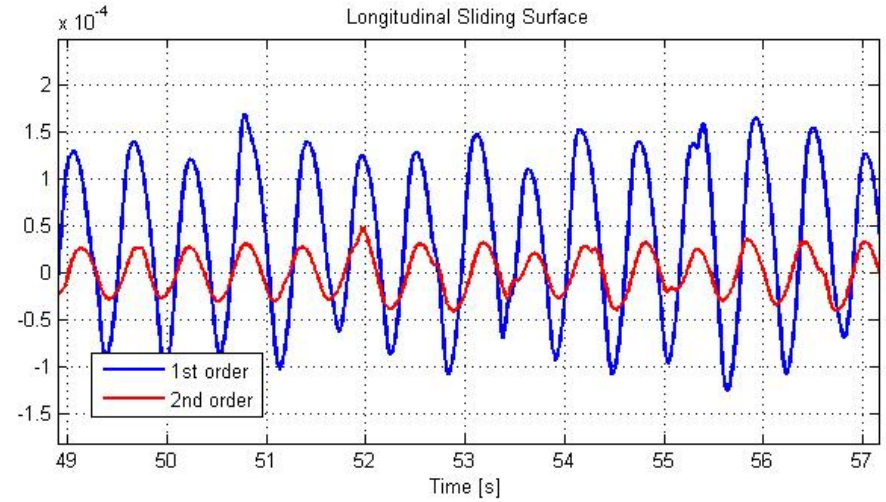

Figure 5.21: Longitudinal sliding surface (zoomed)

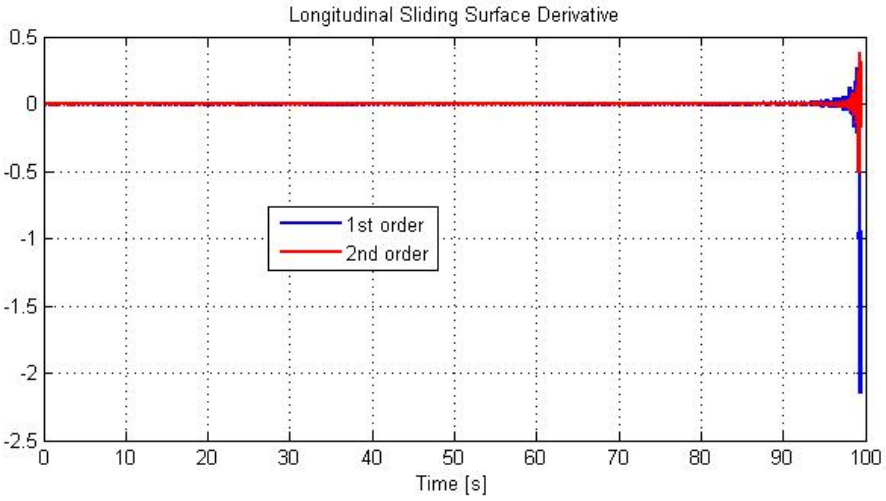

Figure 5.22: Derivative of longitudinal sliding variable

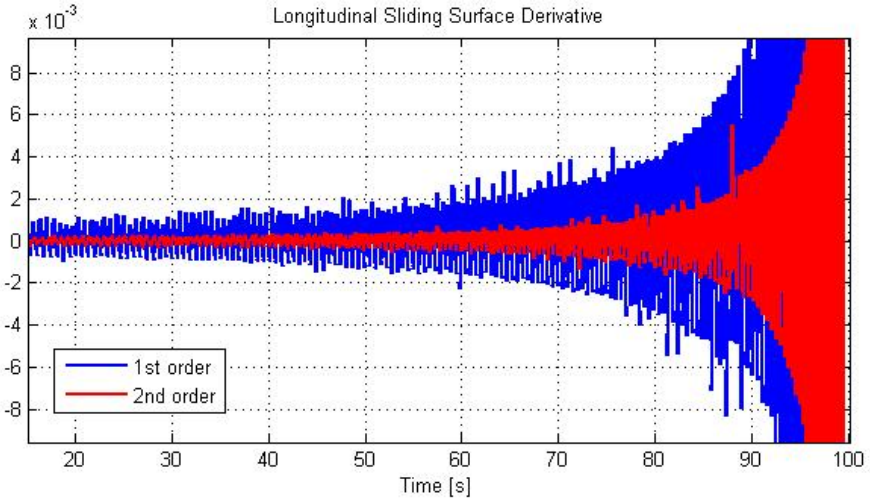

Figure 5.23: Derivative of longitudinal sliding variable (zoomed)

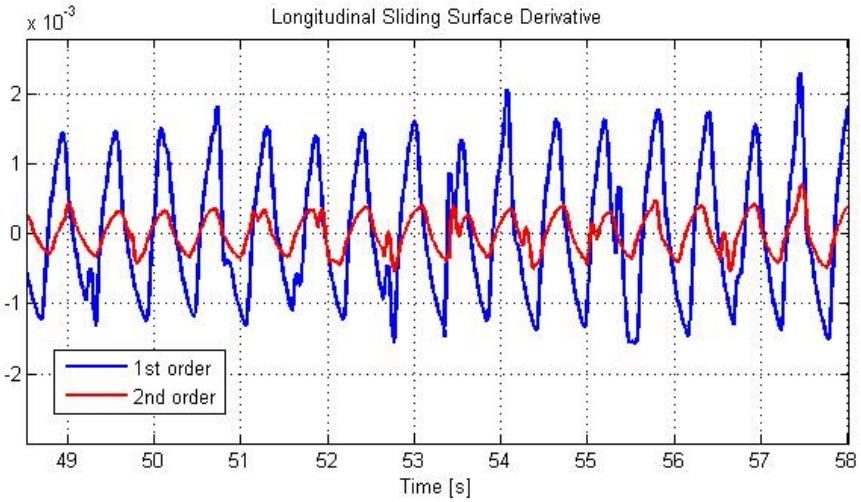

Figure 5.24: Derivative of longitudinal sliding variable (zoomed)

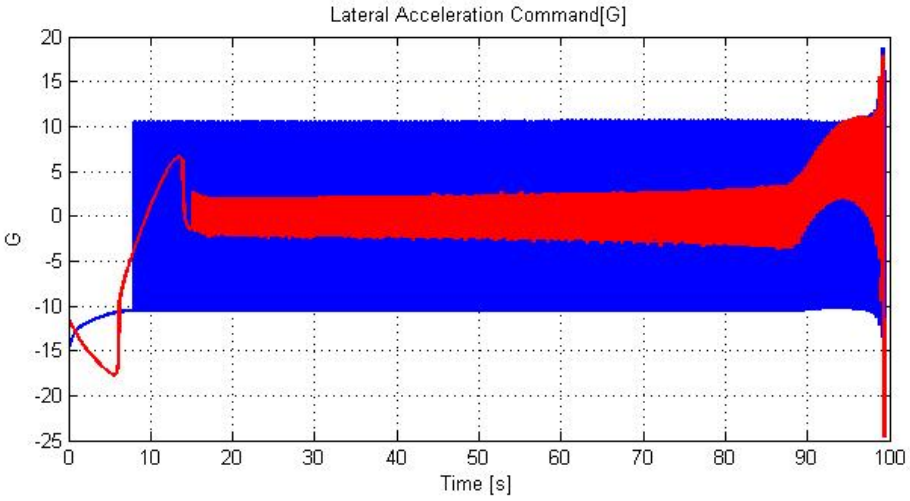

Figure 5.25: Lateral acceleration command

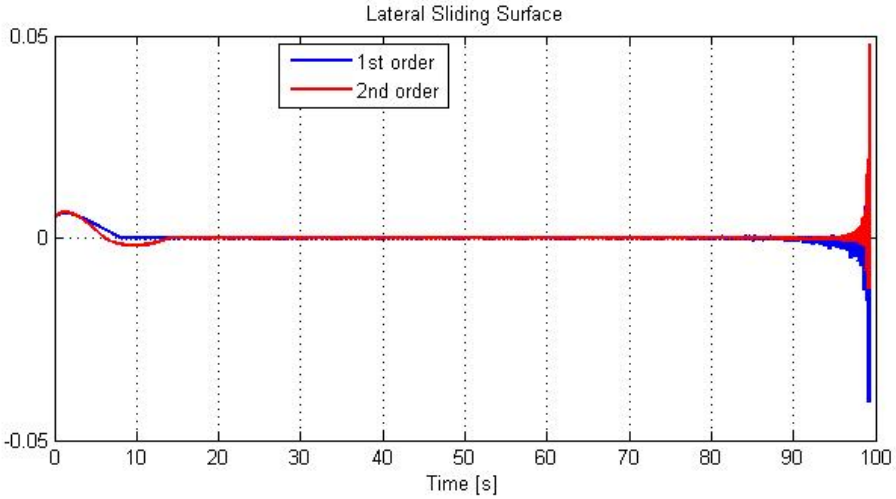

Figure 5.26: Lateral sliding surface

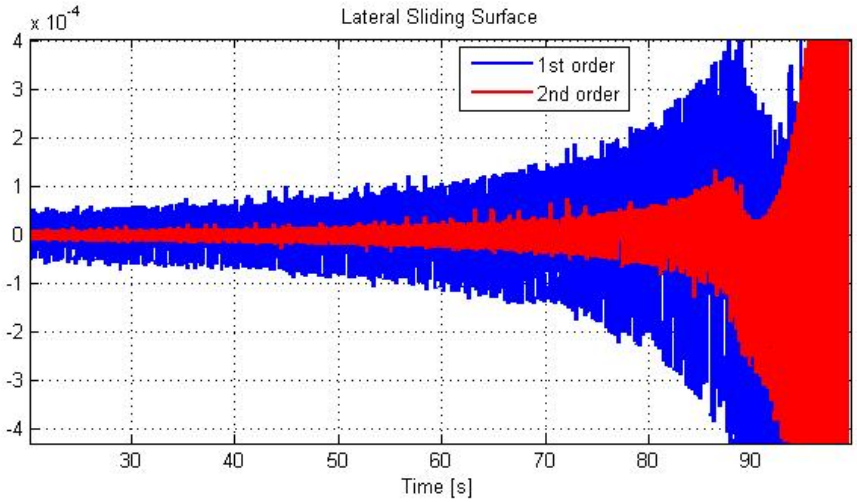

Figure 5.27: Lateral sliding surface (zoomed)

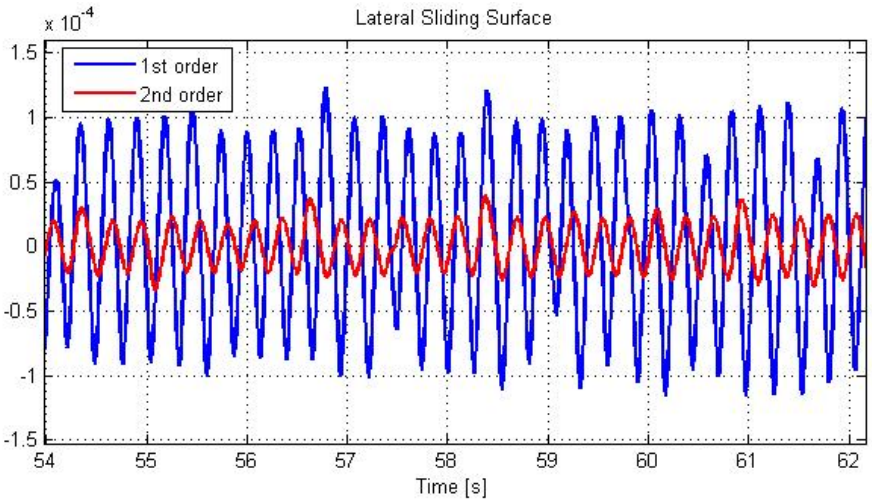

Figure 5.28: Lateral sliding surface (zoomed)

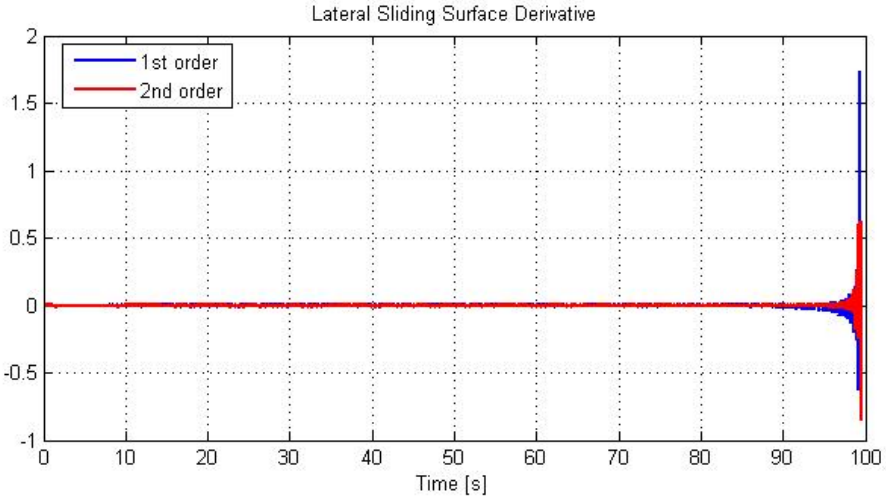

Figure 5.29: Derivative of lateral sliding variable

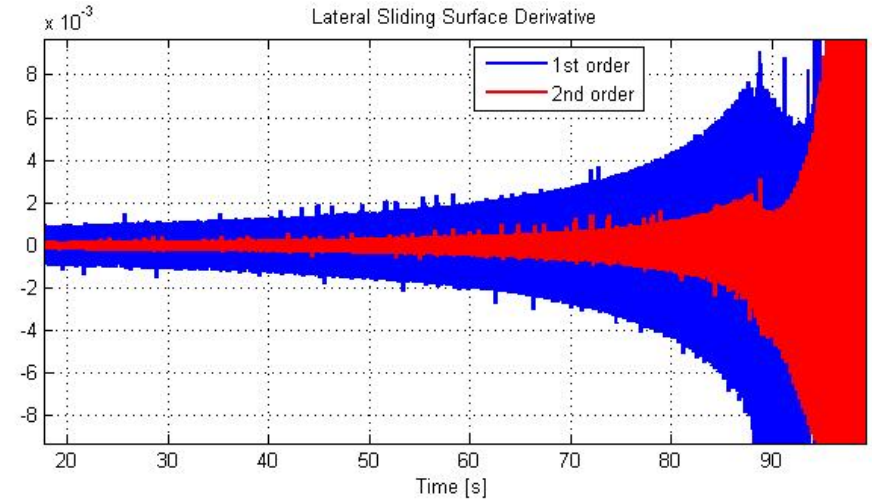

Figure 5.30: Derivative of lateral sliding variable (zoomed)

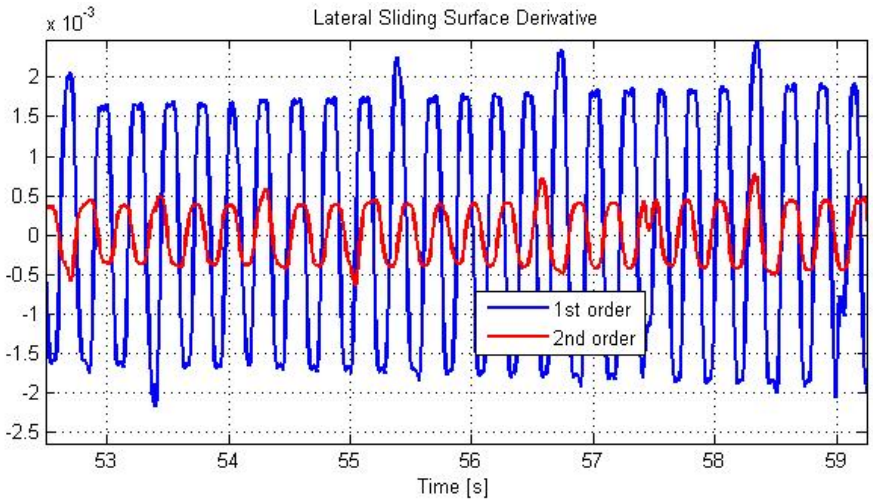

Figure 5.31: Derivative of lateral sliding variable (zoomed)

5.3 Static versus Adaptive Gain Super Twisting Guidance

5.3.1 Scenario - 1

This is the same scenario with Section 5.2.1.

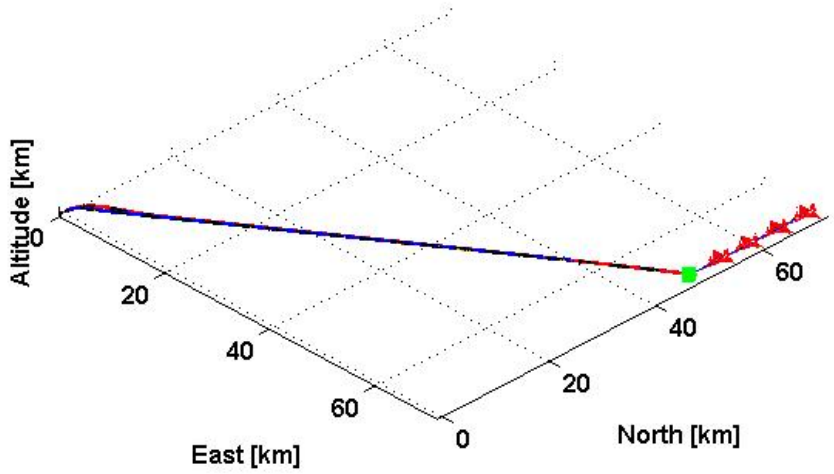

Figure 5.32: Missile and target trajectories

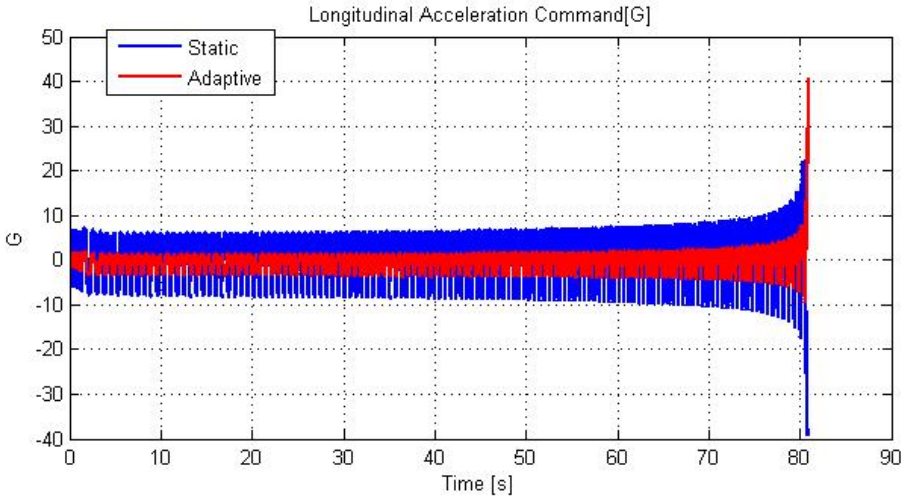

Figure 5.33: Longitudinal acceleration command

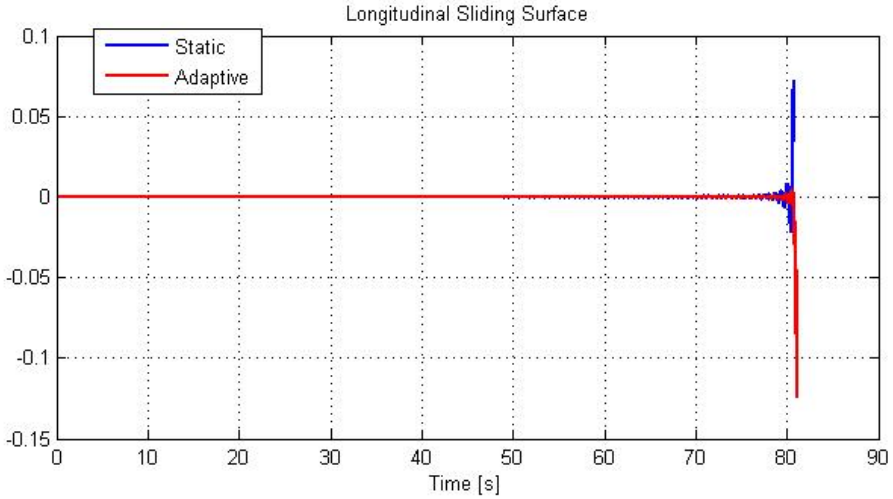

Figure 5.34: Longitudinal sliding surface

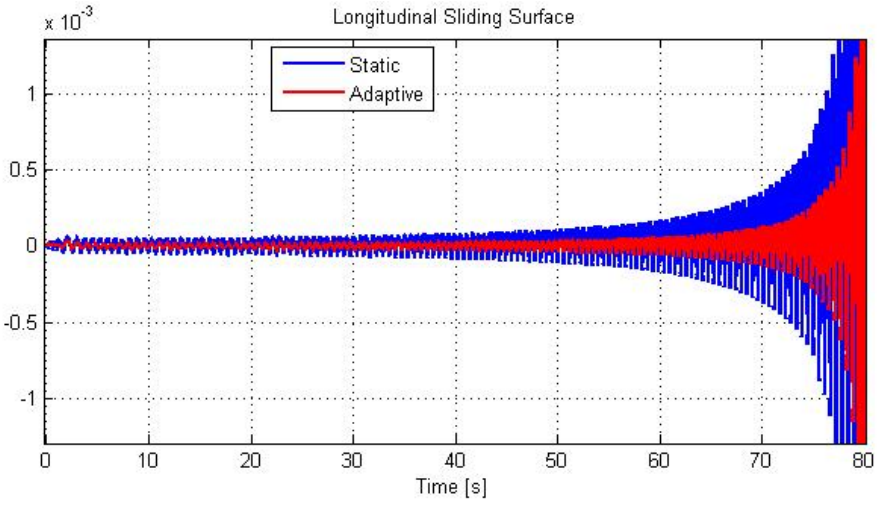

Figure 5.35: Longitudinal sliding surface (zoomed)

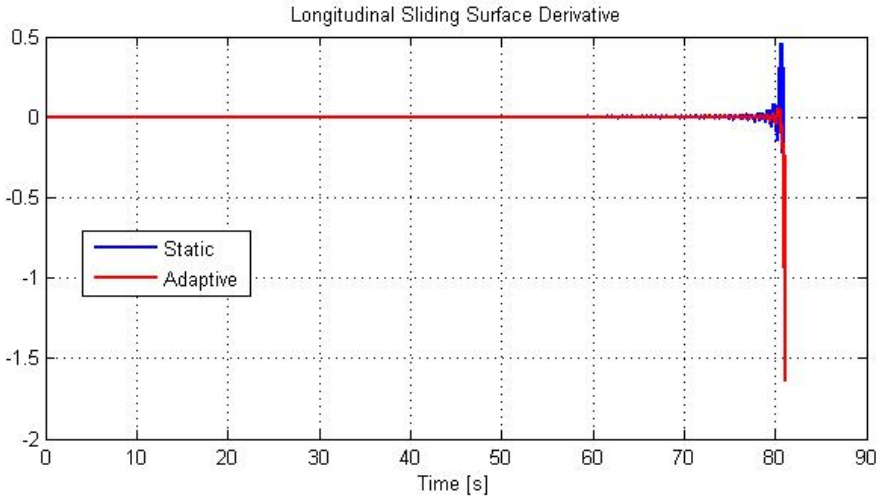

Figure 5.36: Derivative of longitudinal sliding variable

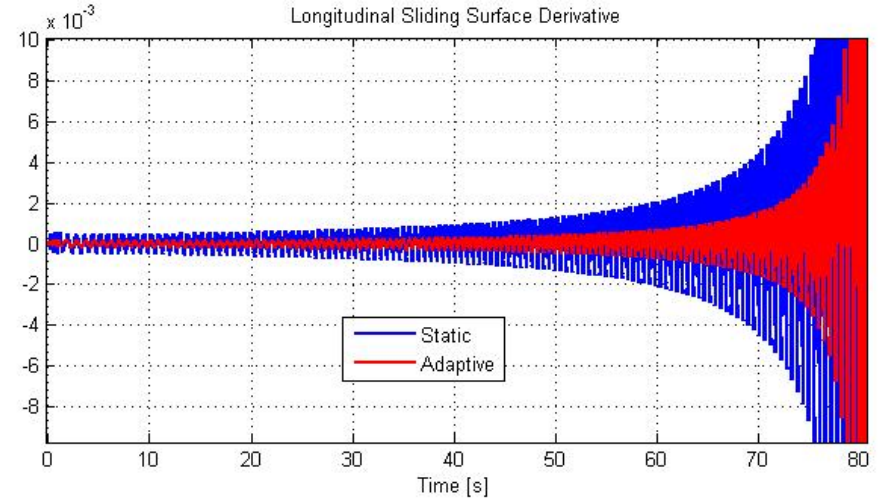

Figure 5.37: Derivative of longitudinal sliding variable (zoomed)

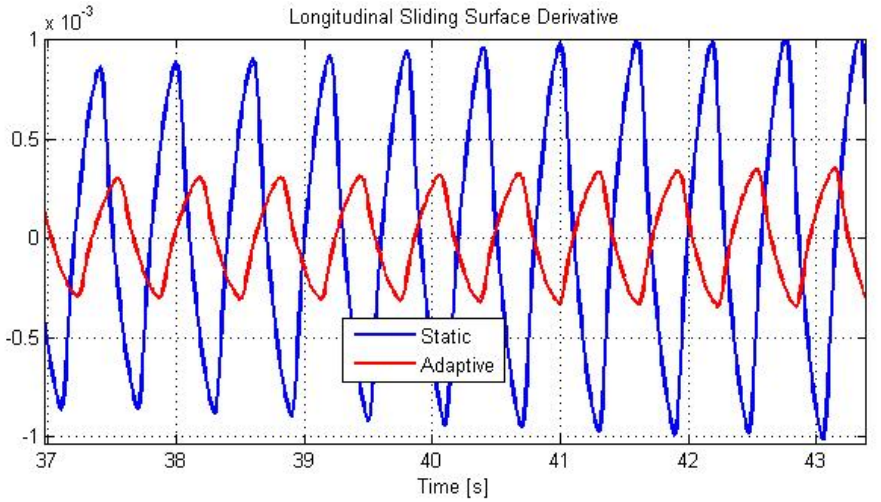

Figure 5.38: Derivative of longitudinal sliding variable (zoomed)

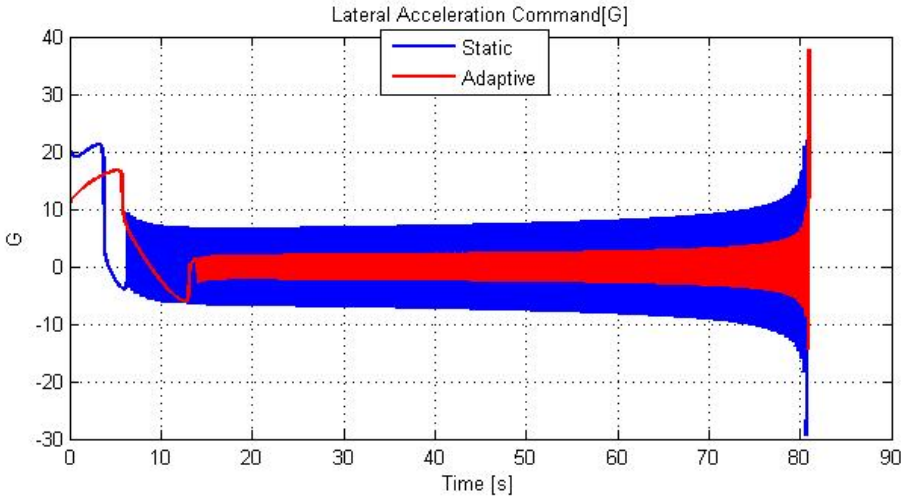

Figure 5.39: Lateral acceleration command

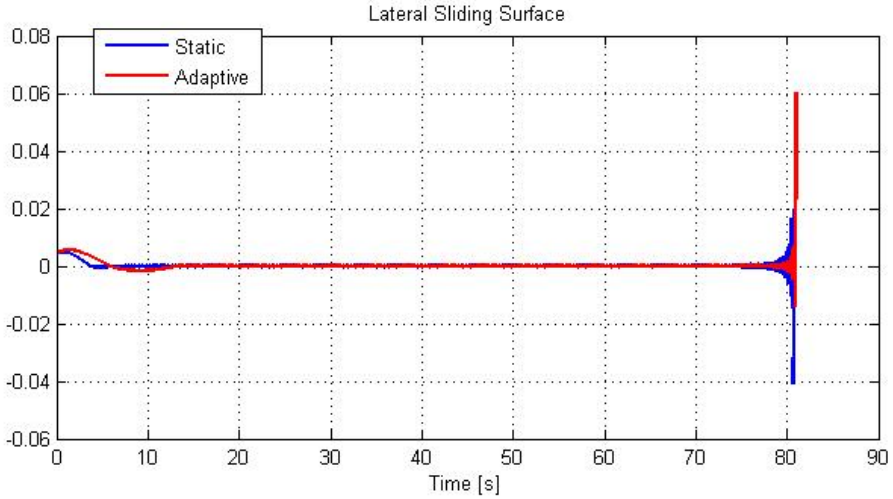

Figure 5.40: Lateral sliding surface

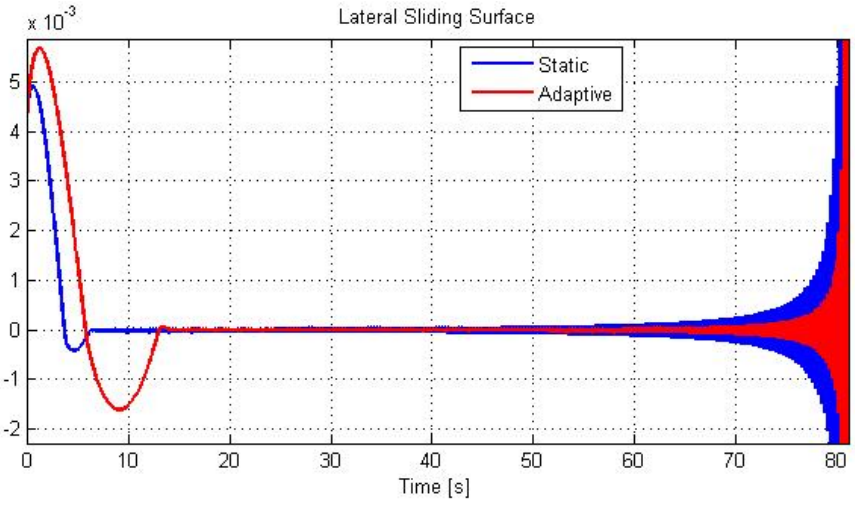

Figure 5.41: Lateral sliding surface (zoomed)

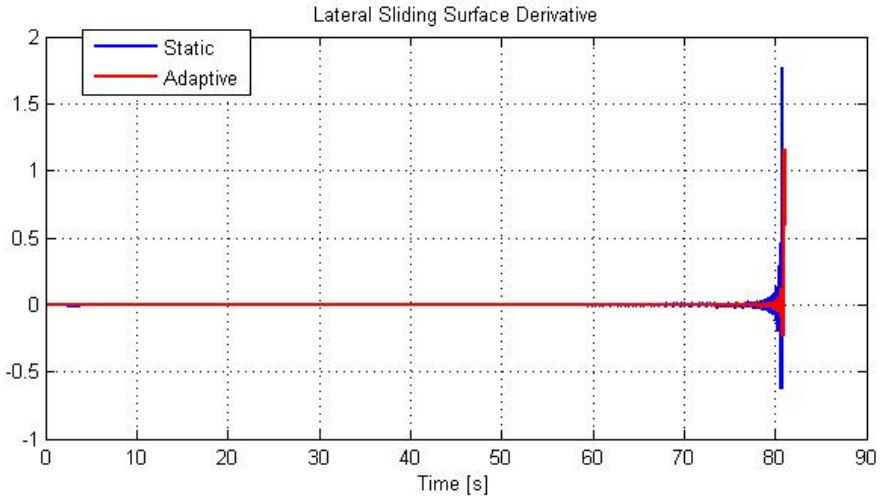

Figure 5.42: Derivative of lateral sliding variable

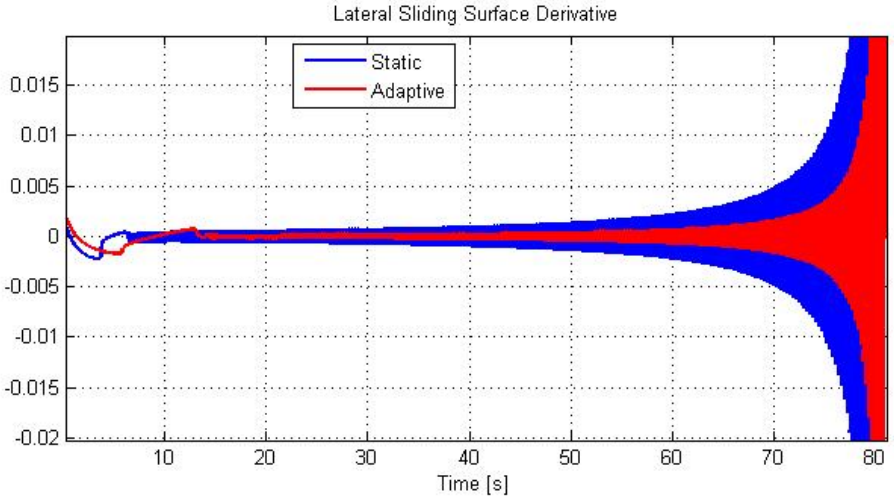

Figure 5.43: Derivative of lateral sliding variable (zoomed)

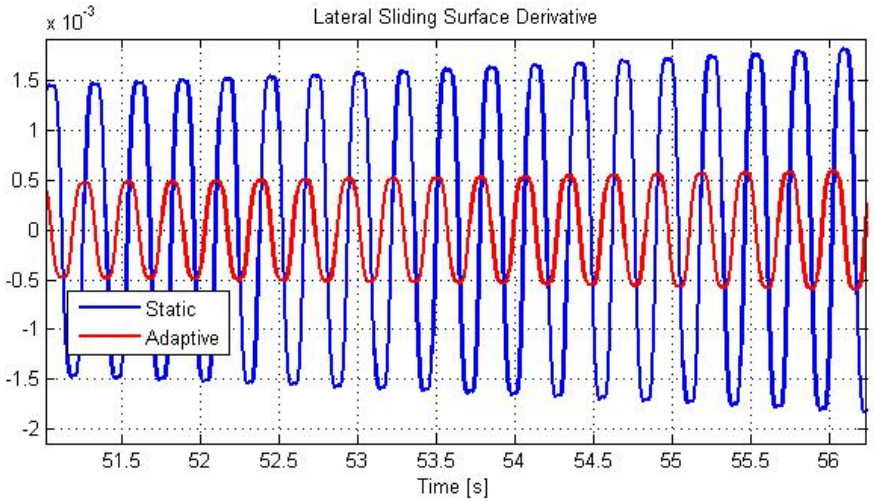

Figure 5.44: Derivative of lateral sliding variable (zoomed)

5.3.2 Scenario - 2

In this high off-boresight scenario, the shooter flies with $-45°$ heading and releases the missile at 0.85 Mach when the target flies with 135° heading at 0.85 Mach. At the time of shoot, there is approximately 11.2 km distance between the shooter and target. In this scenario it is assumed that the target makes no evasion maneuver. Initial conditions are stated in Table 5.3 and the results are stated with figures as follows.

Table5.3: Initial conditions of Scenario – 2

Scenario(t_0)	Missile	Target
$X[km]$	0	10
$Y[km]$	0	5
$Altitude[km]$	6	6
$Velocity[Mach]$	0.85	0.85
$Heading\ Angle[deg]$	-45	135
$Target\ Maneuver$	0	

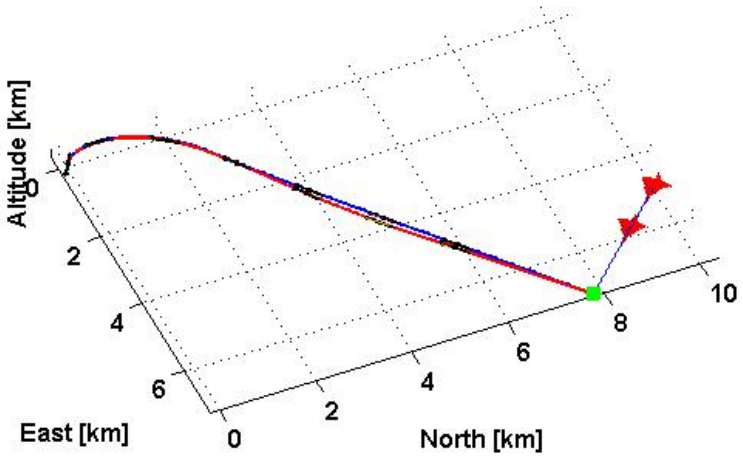

Figure 5.45: Missile and target trajectories

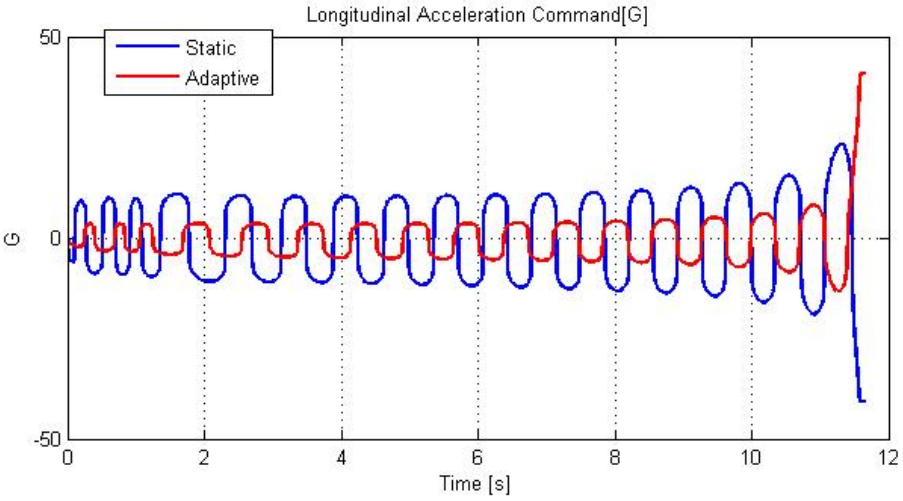

Figure 5.46: Longitudinal acceleration command

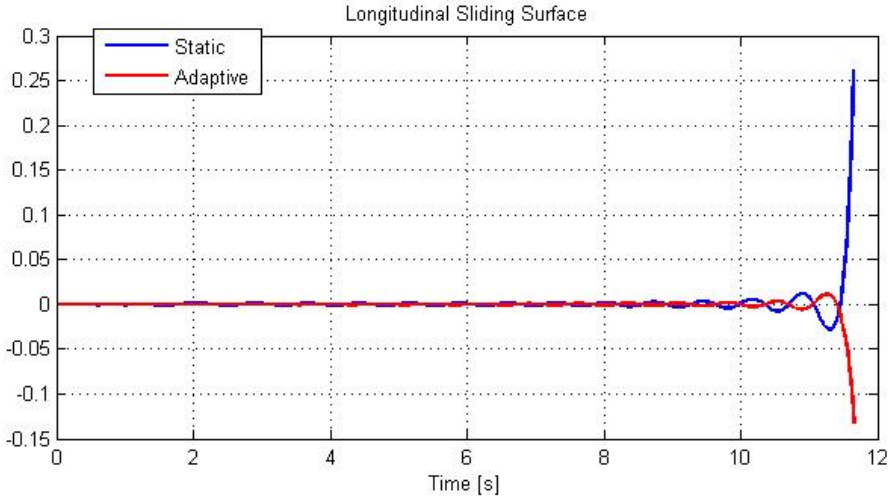

Figure 5.47: Longitudinal sliding surface

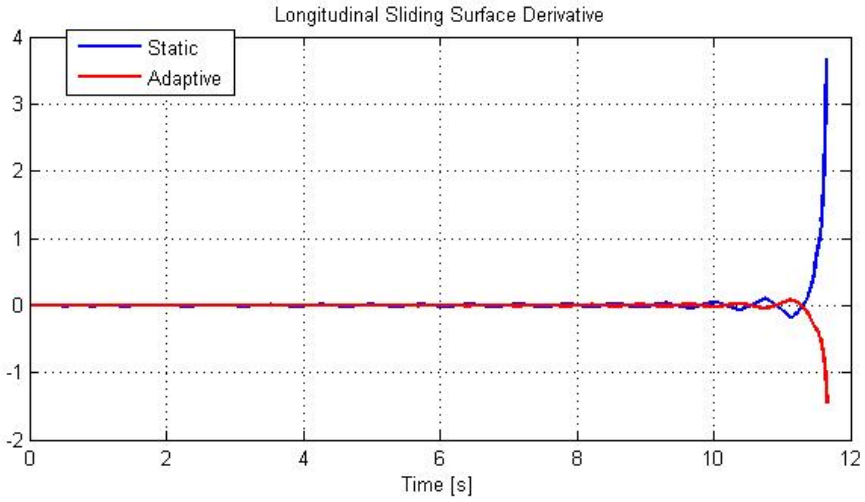

Figure 5.48: Derivative of longitudinal sliding variable

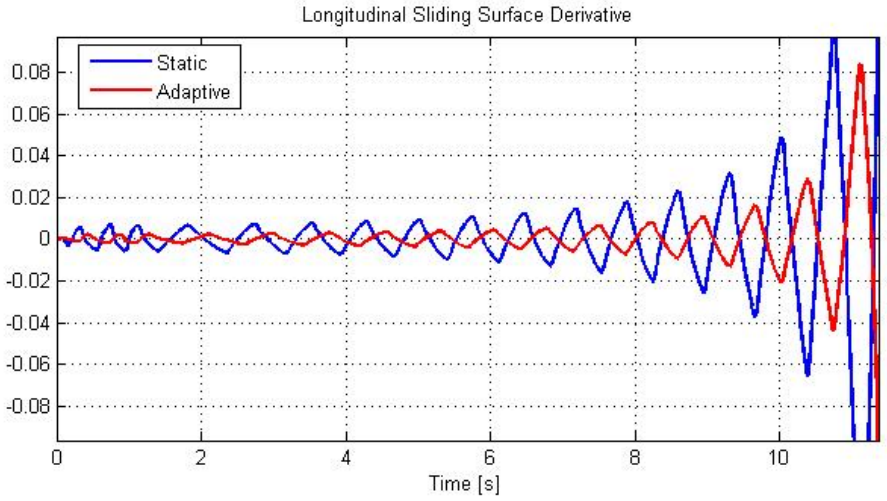

Figure 5.49: Derivative of longitudinal sliding variable (zoomed)

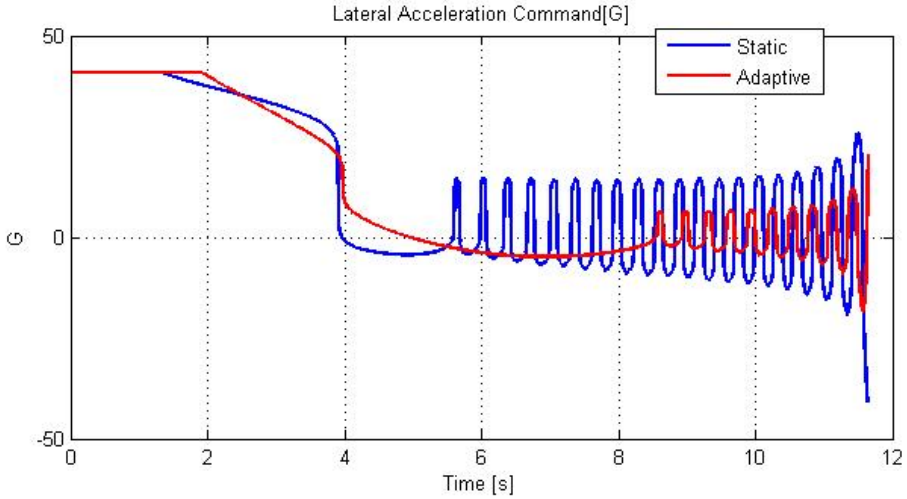

Figure 5.50: Lateral acceleration command

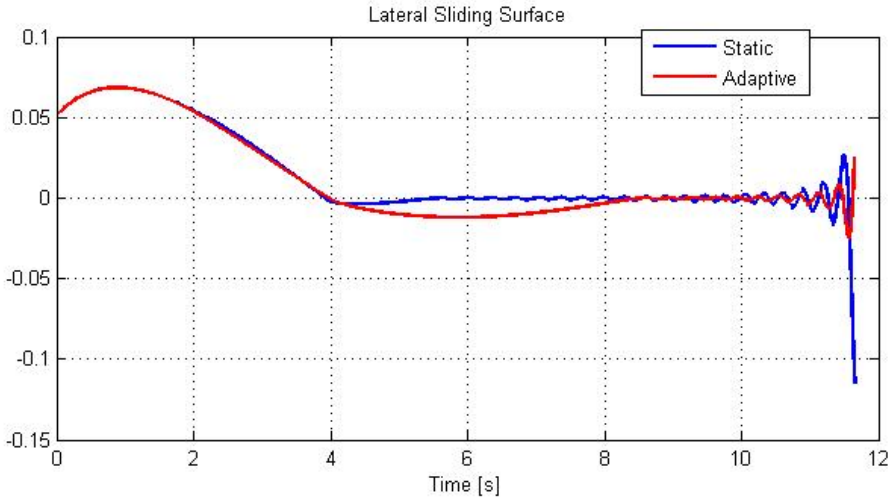

Figure 5.51: Lateral sliding surface

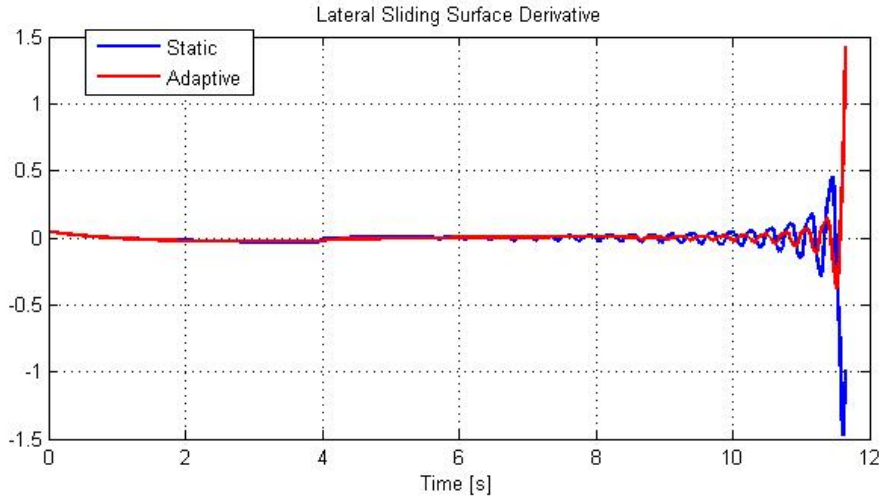

Figure 5.52: Derivative of lateral sliding variable

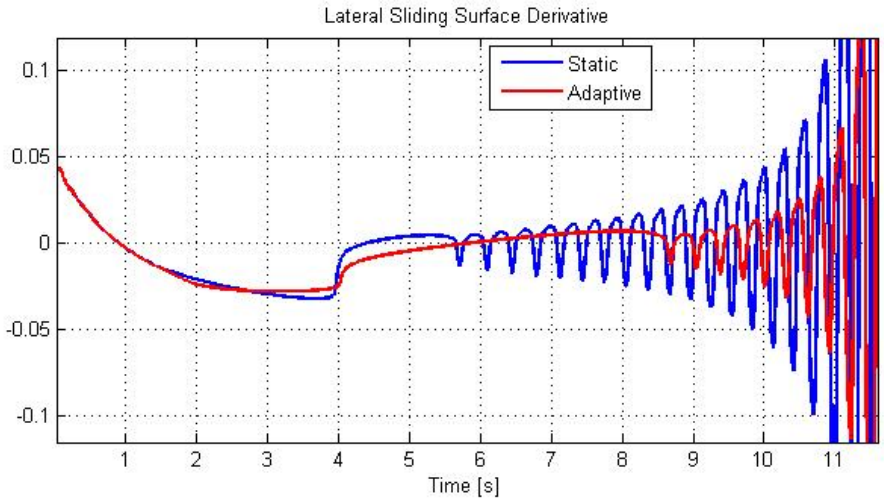

Figure 5.53: Derivative of lateral sliding variable (zoomed)

5.4 Engagement Scenarios of PI, ST and PNG Methods Comparison

5.4.1 Scenario - 1

In this scenario, the shooter flies with heading to north and releases the missile at 0.85 Mach when the target flies with heading to south at 0.85 Mach. At the time of shoot, there is approximately 100 km distance between the shooter and target. In this scenario it is assumed that the target makes no evasion maneuver. Initial conditions are stated in Table 5.4 and the results are stated with figures as follows.

Table5.4: Initial conditions of Scenario – 1

Scenario(t_0)	Missile	Target
$X[km]$	0	70
$Y[km]$	0	70
$Altitude[km]$	6	6
$Velocity[Mach]$	0.85	0.85
$Heading\ Angle[deg]$	0	180
$Target\ Maneuver$	0	

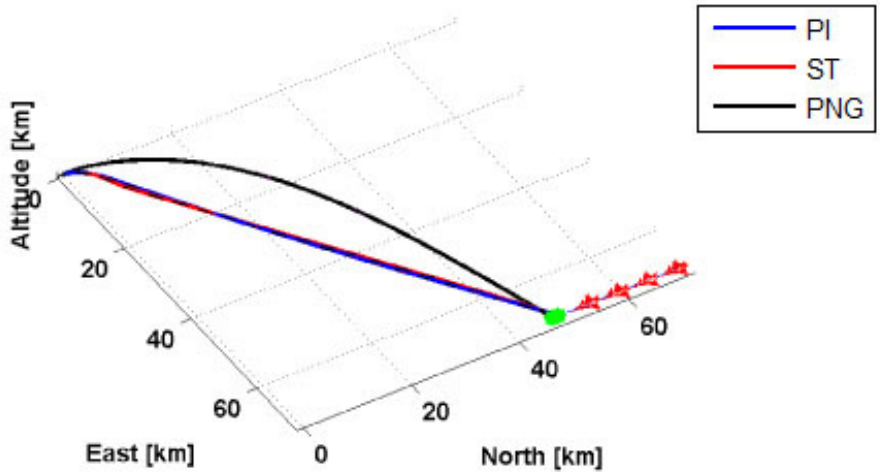

Figure 5.54: Missile and target trajectories

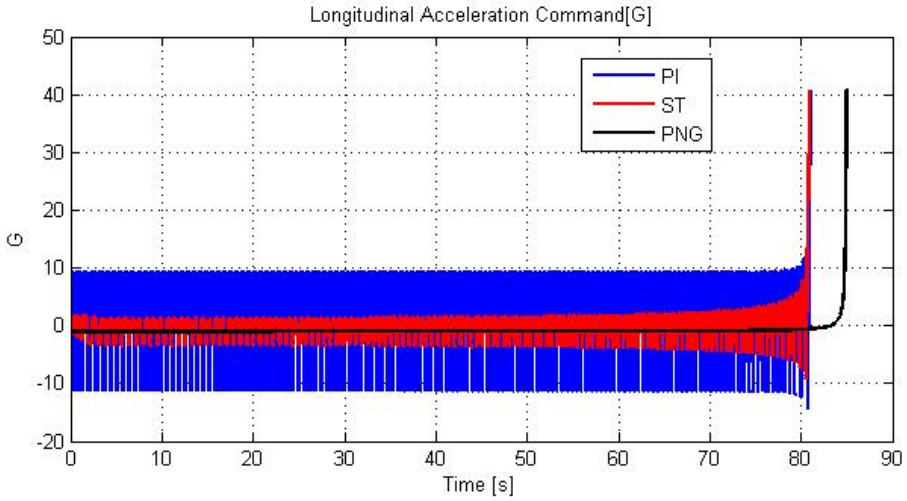

Figure 5.55: Longitudinal acceleration command

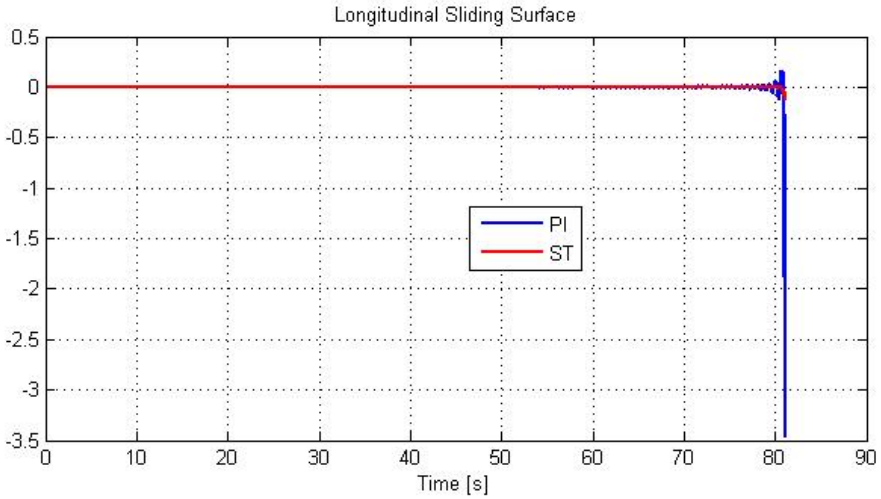

Figure 5.56: Longitudinal sliding surface

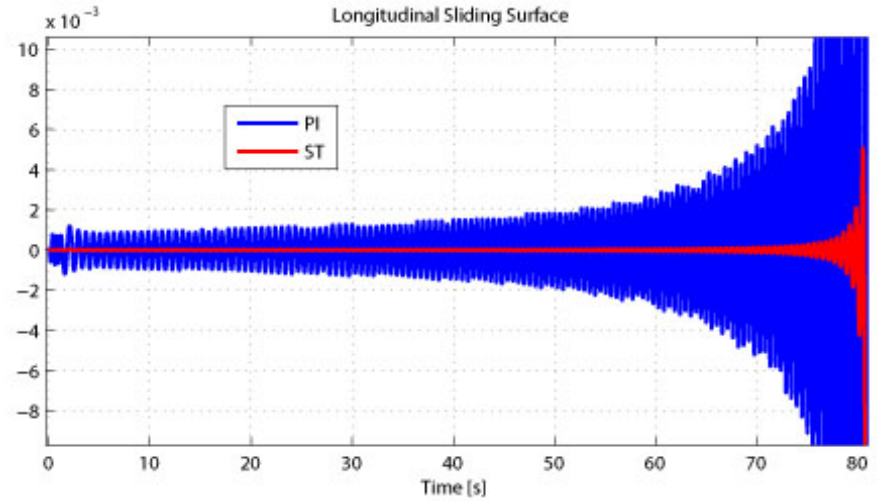

Figure 5.57: Longitudinal sliding surface (zoomed)

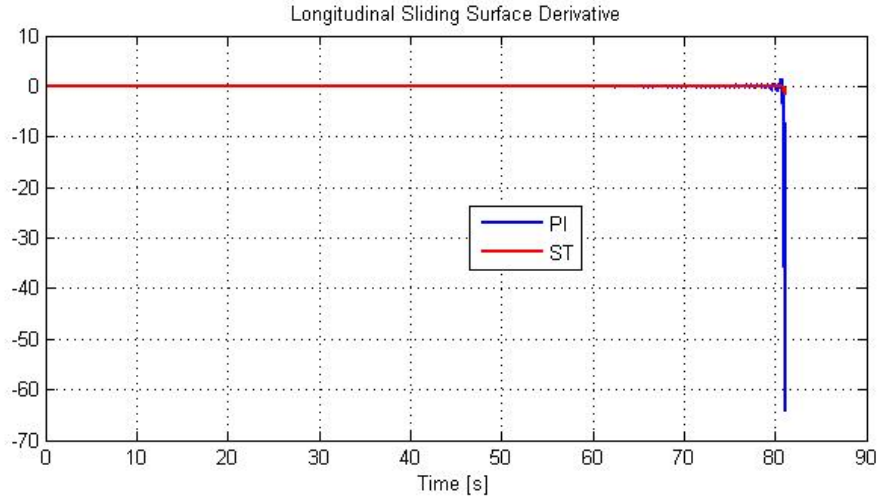

Figure 5.58: Derivative of longitudinal sliding variable

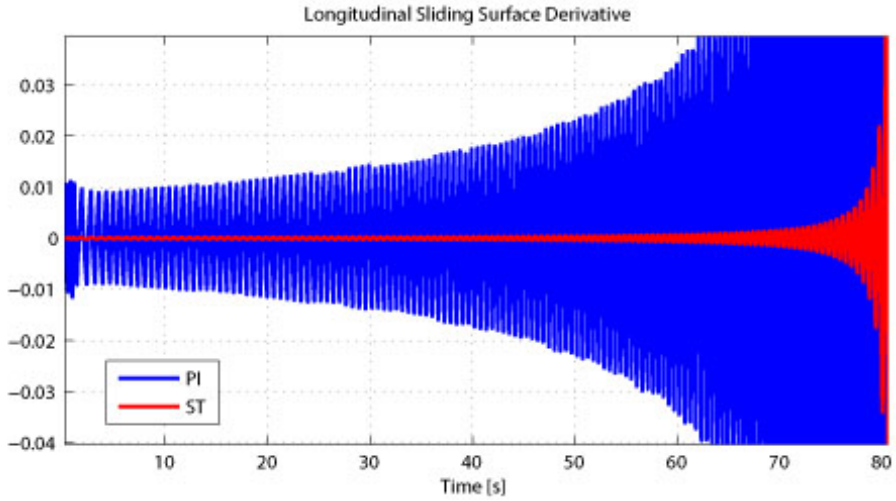

Figure 5.59: Derivative of longitudinal sliding variable (zoomed)

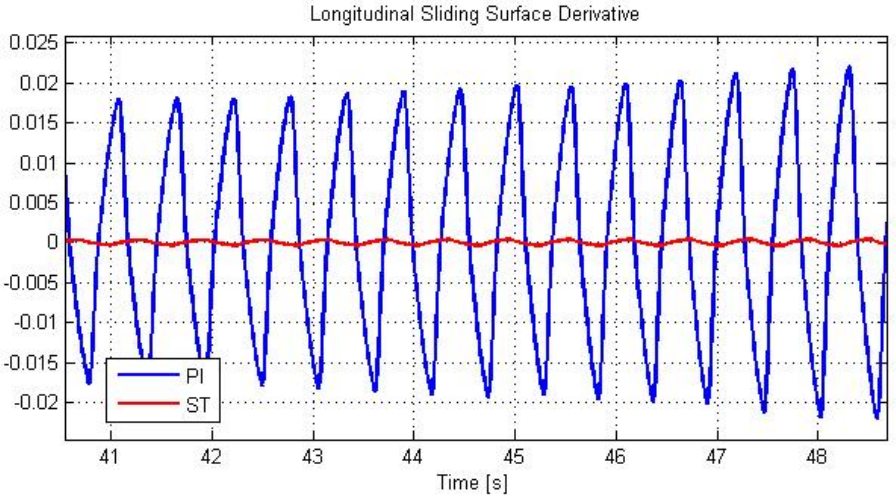

Figure 5.60: Derivative of longitudinal sliding variable (zoomed)

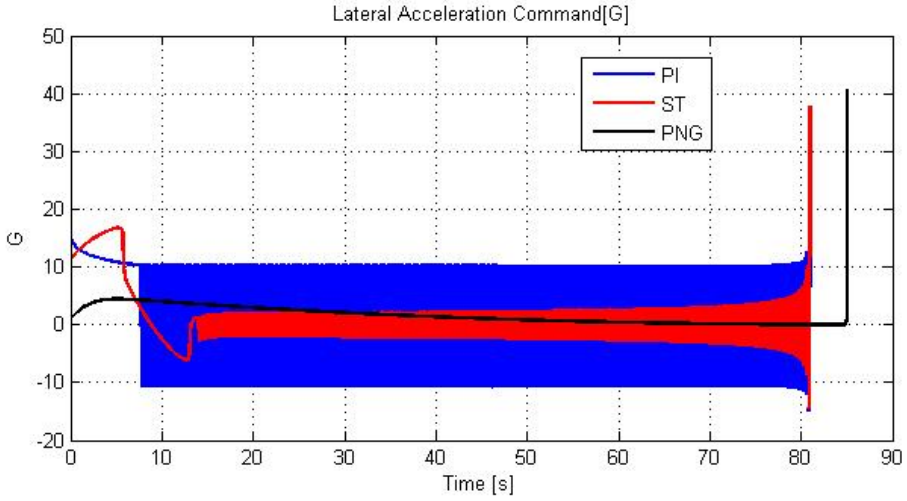

Figure 5.61: Lateral acceleration command

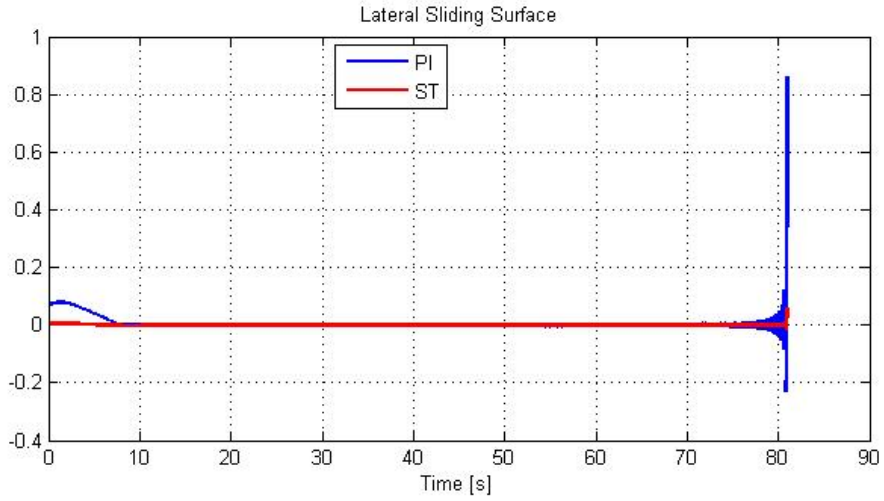

Figure 5.62: Lateral sliding surface

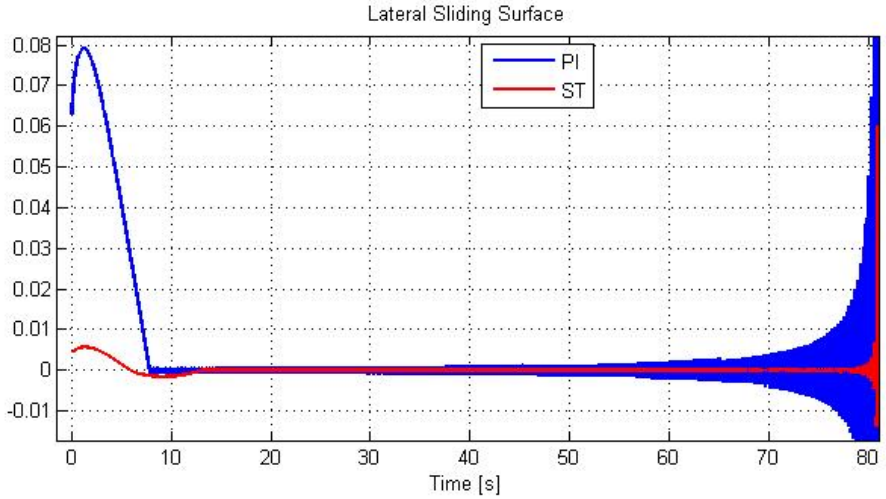

Figure 5.63: Lateral sliding surface (zoomed)

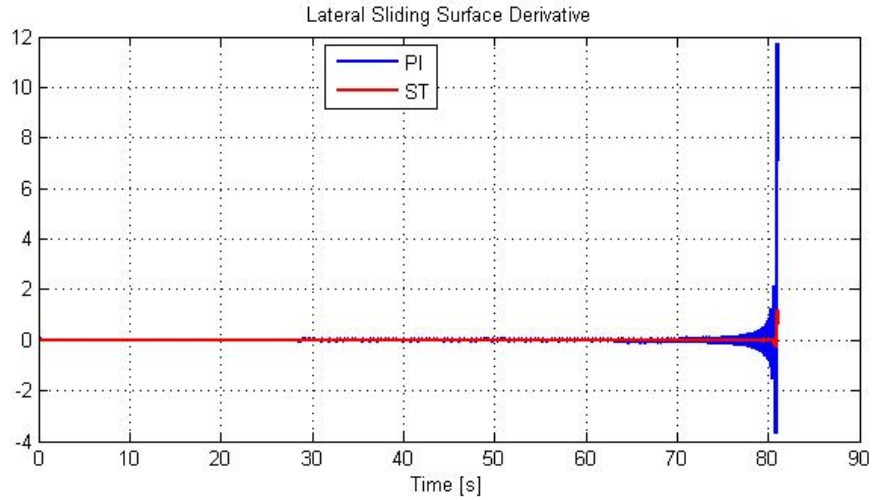

Figure 5.64: Derivative of lateral sliding variable

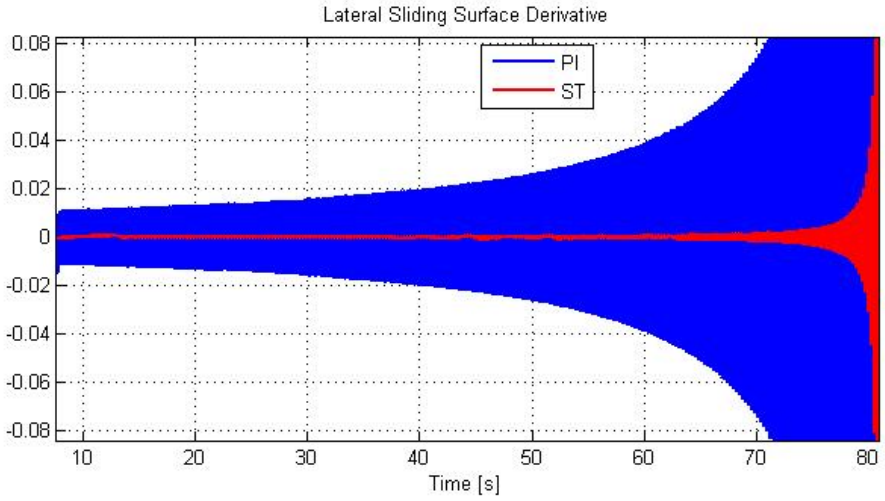

Figure 5.65: Derivative of lateral sliding variable (zoomed)

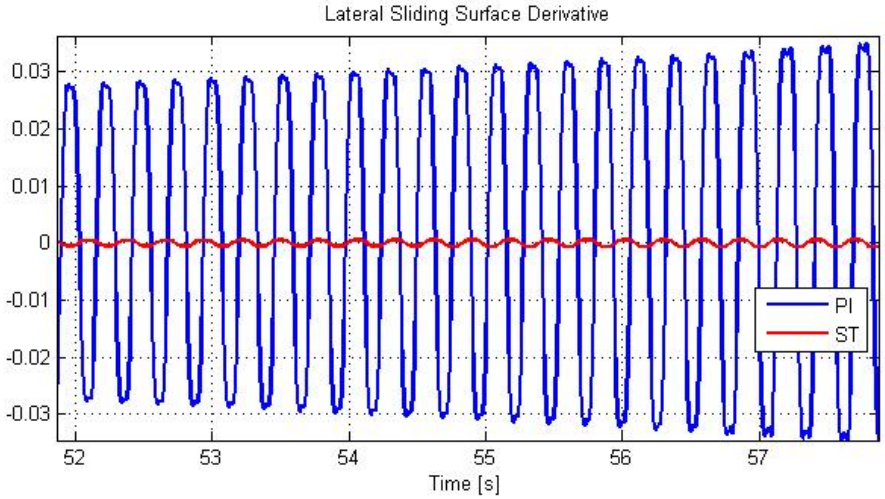

Figure 5.66: Derivative of lateral sliding variable (zoomed)

5.4.2 Scenario - 2

In this scenario, the shooter flies with heading to north and releases the missile at 0.85 Mach when the target flies with 135° heading at 0.85 Mach. At the time of shoot, there is approximately 22.3 km distance between the shooter and target. In this scenario it is assumed that the target makes no evasion maneuver. Initial conditions are stated in Table 5.5 and the results are stated with figures as follows.

Table5.5: Initial conditions of Scenario – 2

Scenario(t_0)	Missile	Target
$X[km]$	0	20
$Y[km]$	0	10
$Altitude[km]$	6	6
$Velocity[Mach]$	0.85	0.85
$Heading\ Angle[deg]$	0	135
$Target\ Maneuver$	0	

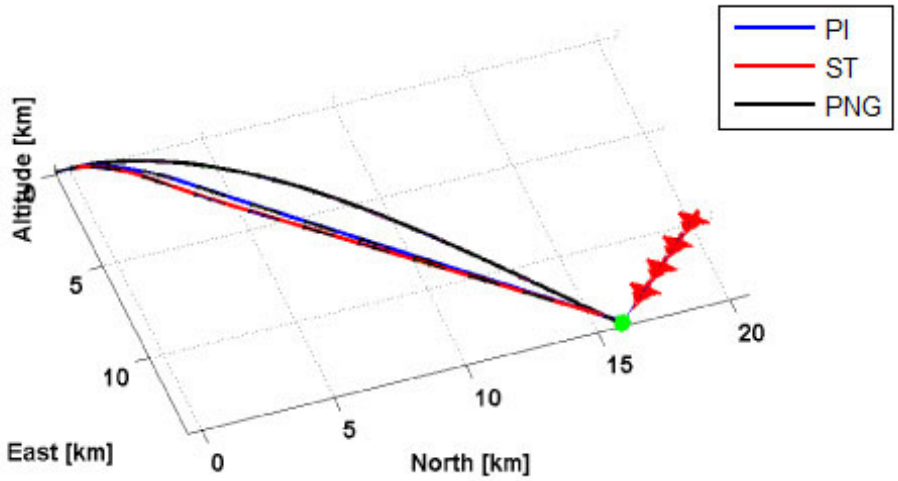

Figure 5.67: Missile and target trajectories

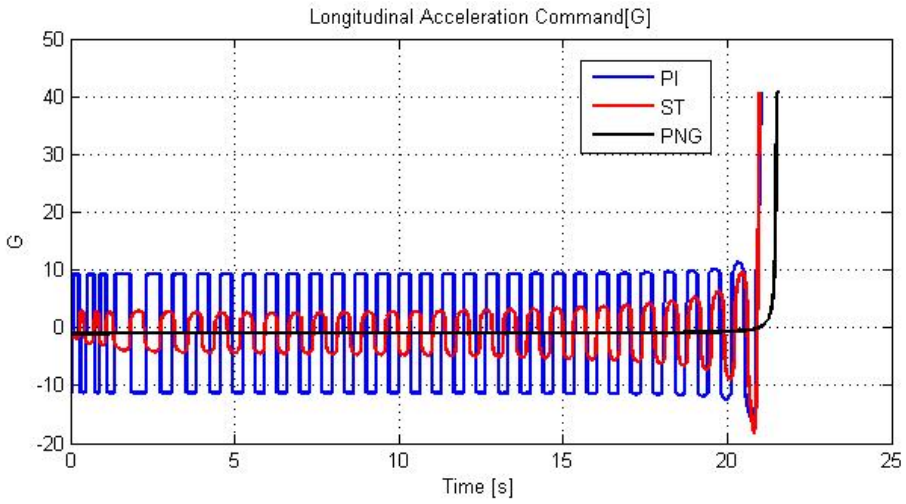

Figure 5.68: Longitudinal acceleration command

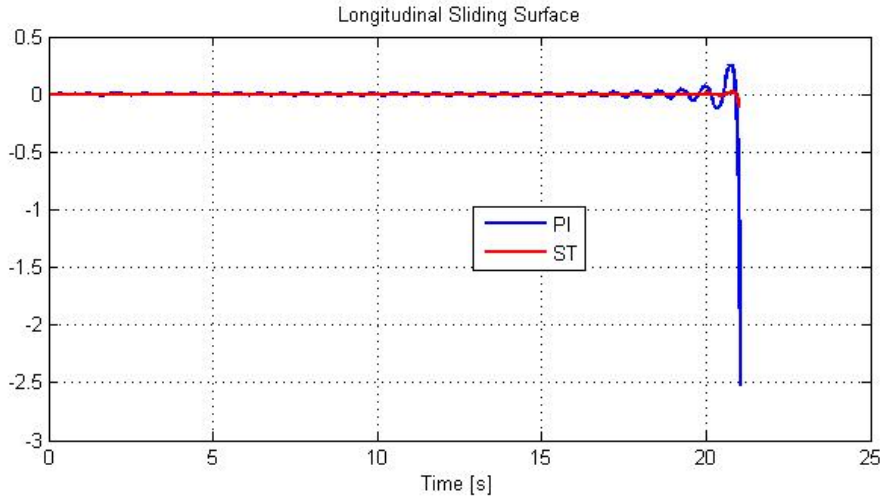

Figure 5.69: Longitudinal sliding surface

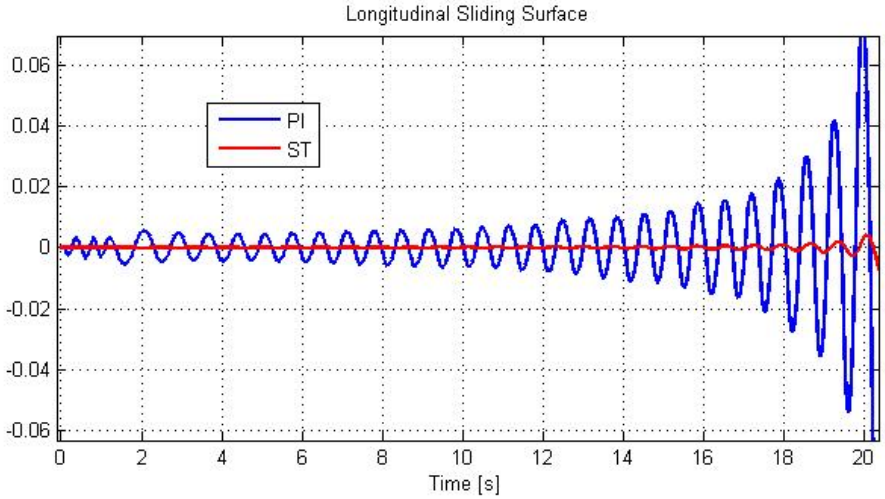

Figure 5.70: Longitudinal sliding surface (zoomed)

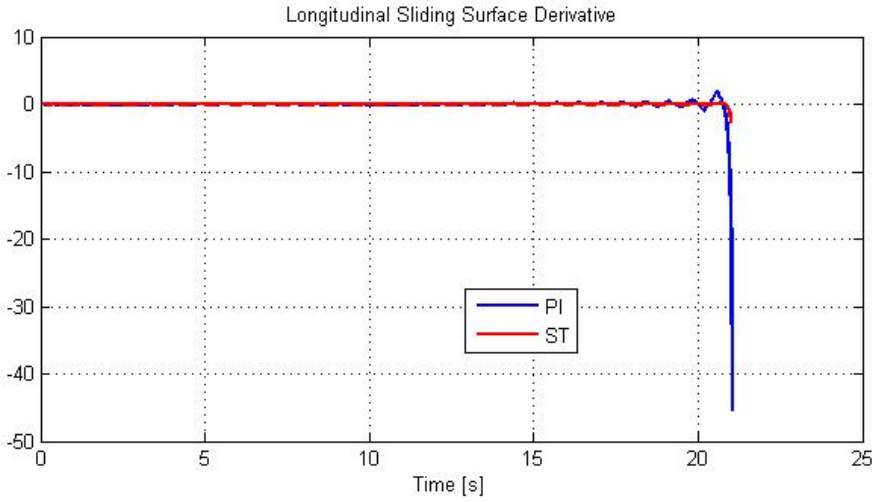

Figure 5.71: Derivative of longitudinal sliding variable

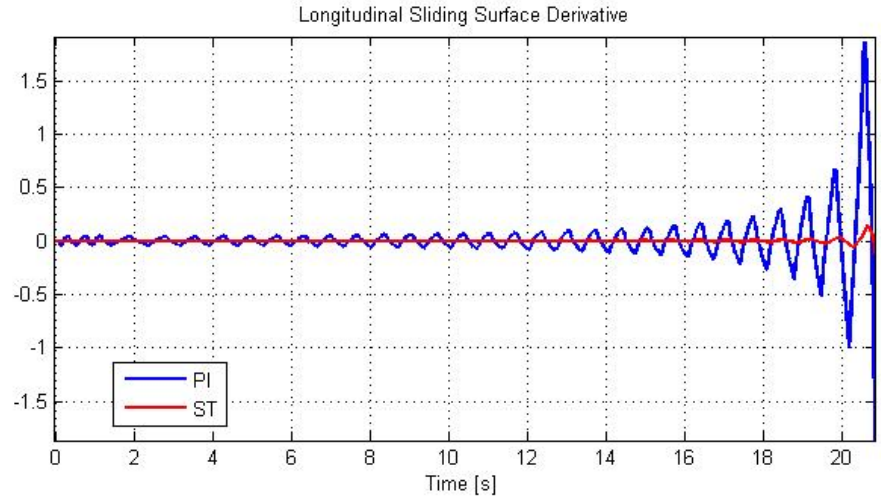

Figure 5.72: Derivative of longitudinal sliding variable (zoomed)

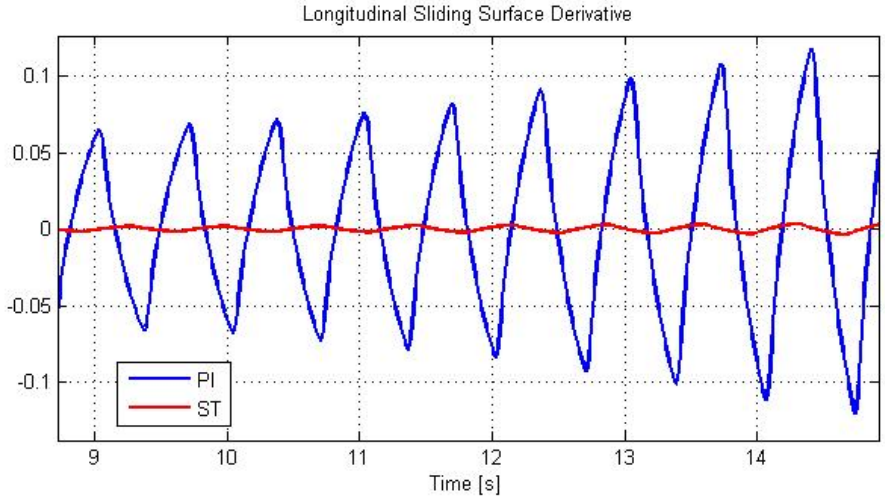

Figure 5.73: Derivative of longitudinal sliding variable (zoomed)

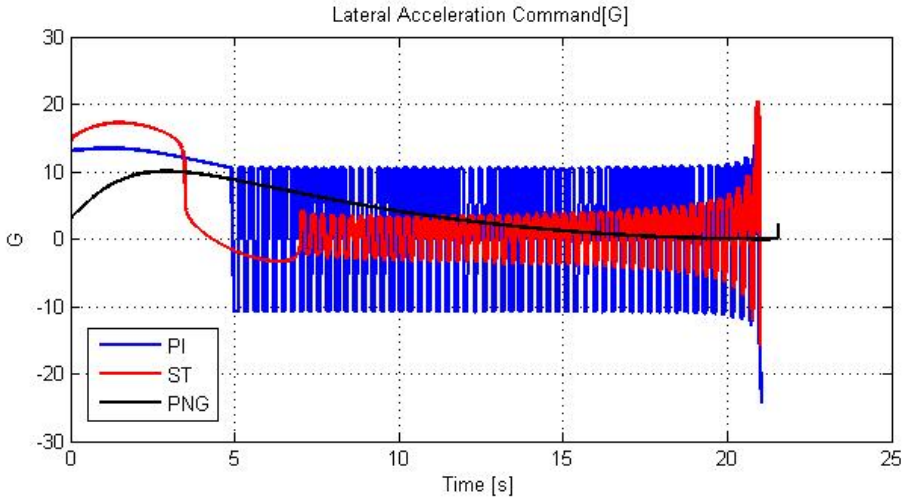

Figure 5.74: Lateral acceleration command

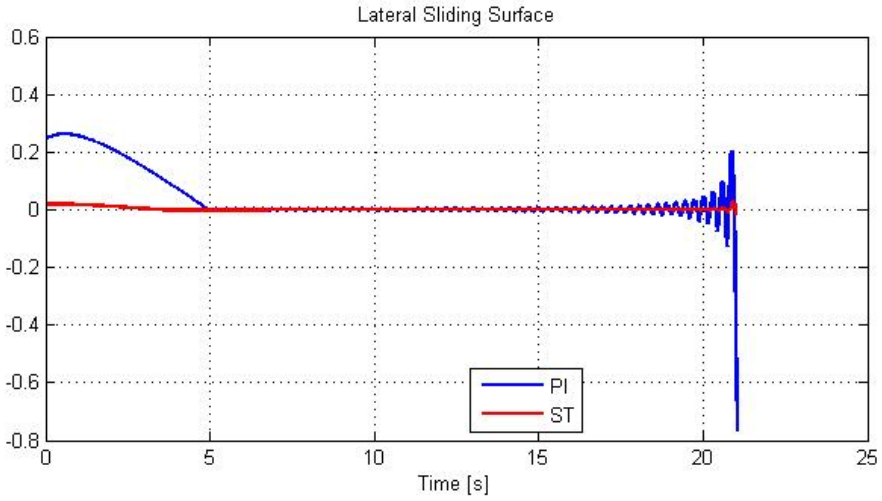

Figure 5.75: Lateral sliding surface

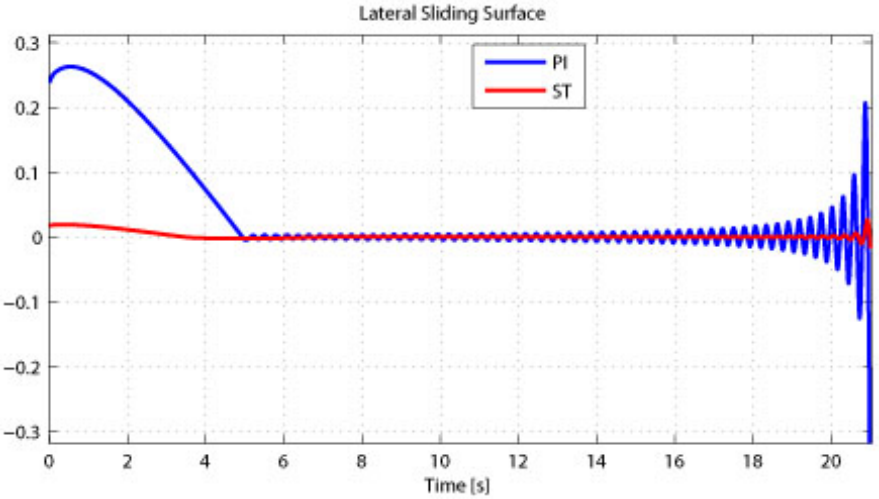

Figure 5.76: Lateral sliding surface (zoomed)

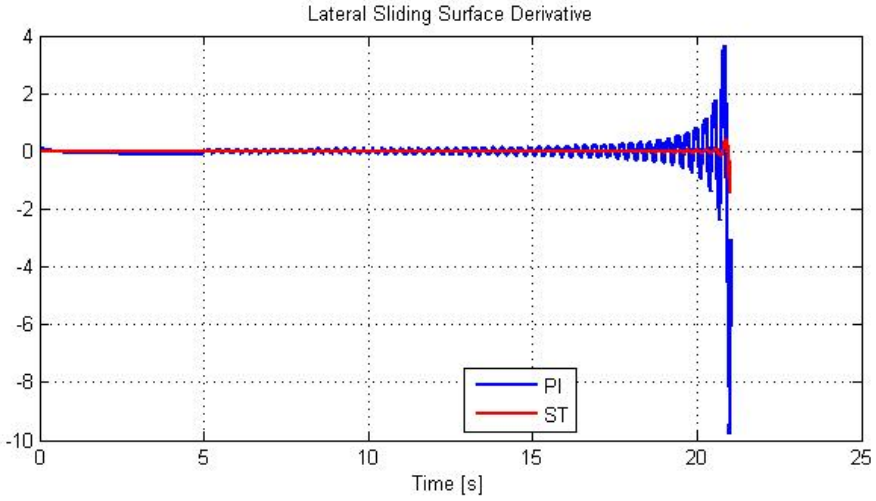

Figure 5.77: Derivative of lateral sliding variable

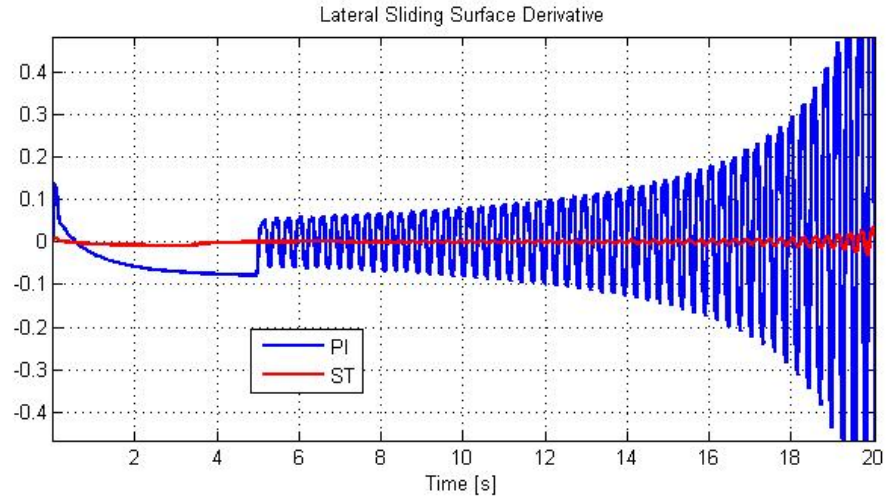

Figure 5.78: Derivative of lateral sliding variable (zoomed)

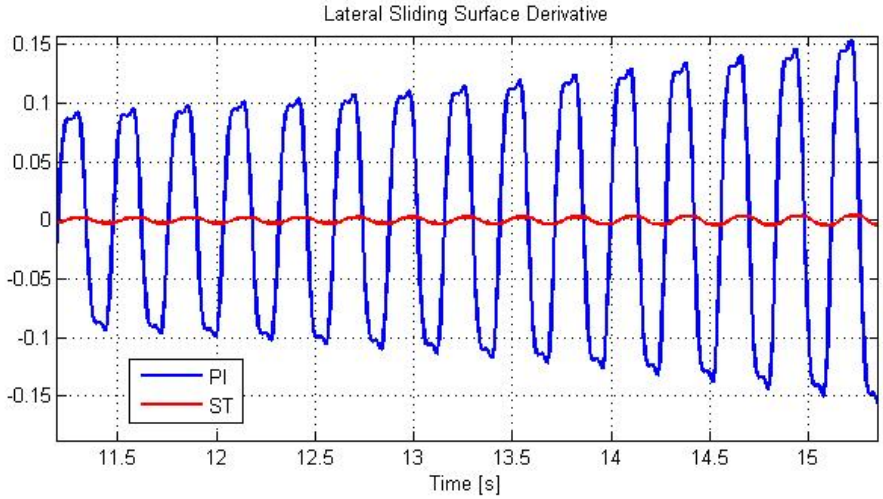

Figure 5.79: Derivative of lateral sliding variable (zoomed)

5.4.3 Scenario - 3

In this scenario, the shooter flies with heading to north and releases the missile at 0.85 Mach when the target flies with 135° heading at 0.85 Mach. At the time of shoot, there is approximately 11.2 km distance between the shooter and target. In this scenario it is assumed that the target makes no evasion maneuver. Initial conditions are stated in Table 5.6 and the results are stated with figures as follows.

Table5.6: Initial conditions of Scenario – 3

Scenario(t_0)	Missile	Target
$X[km]$	0	10
$Y[km]$	0	5
$Altitude[km]$	6	6
$Velocity[Mach]$	0.85	0.85
$Heading\ Angle[deg]$	0	135
$Target\ Maneuver$	0	

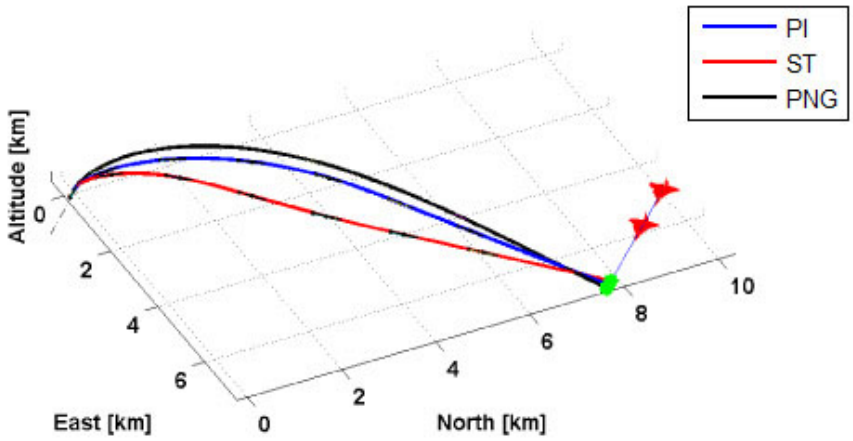

Figure 5.80: Missile and target trajectories

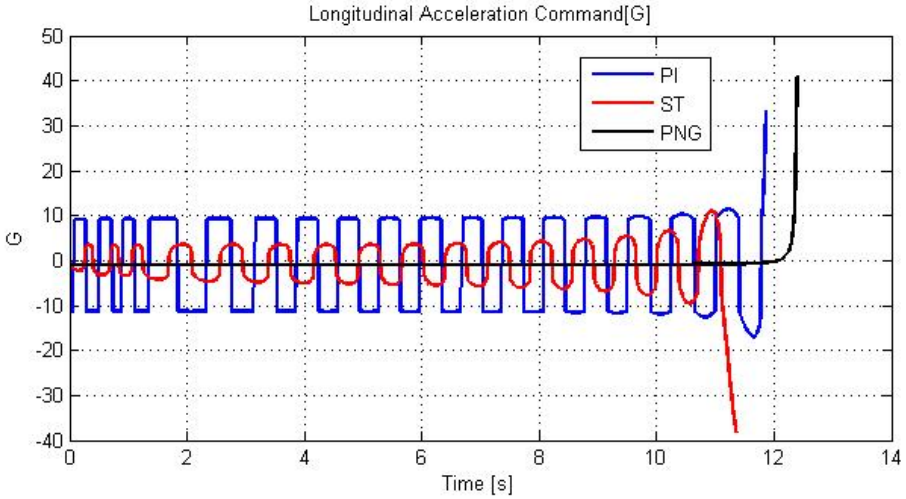

Figure 5.81: Longitudinal acceleration command

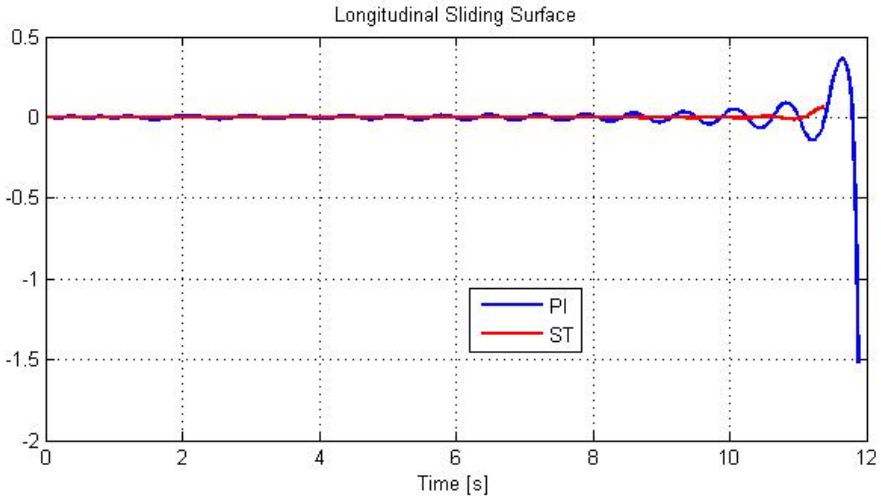

Figure 5.82: Longitudinal sliding surface

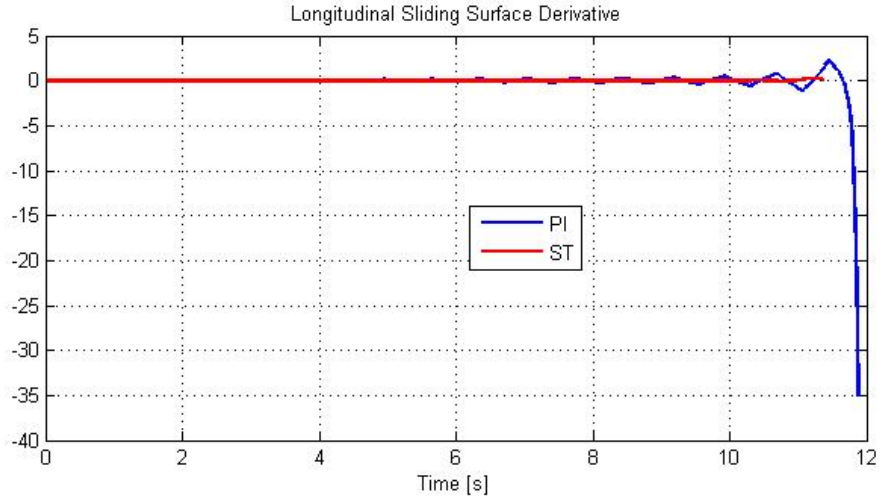

Figure 5.83: Derivative of longitudinal sliding variable

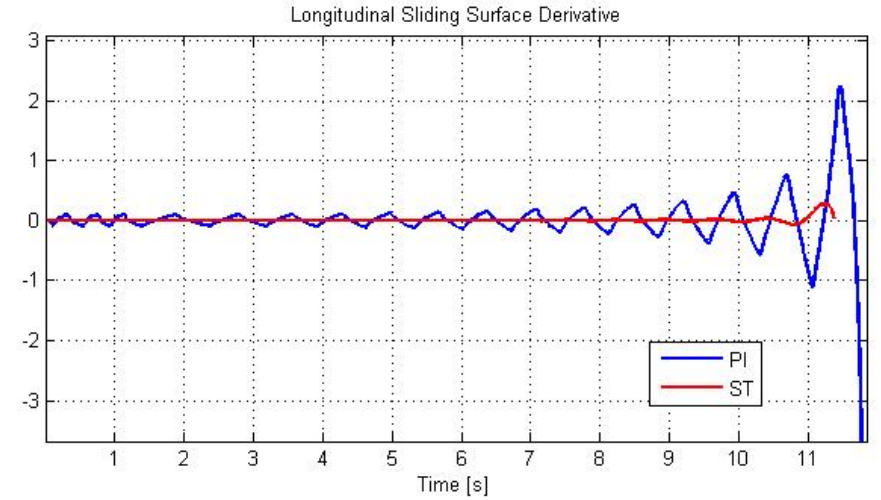

Figure 5.84: Derivative of longitudinal sliding variable (zoomed)

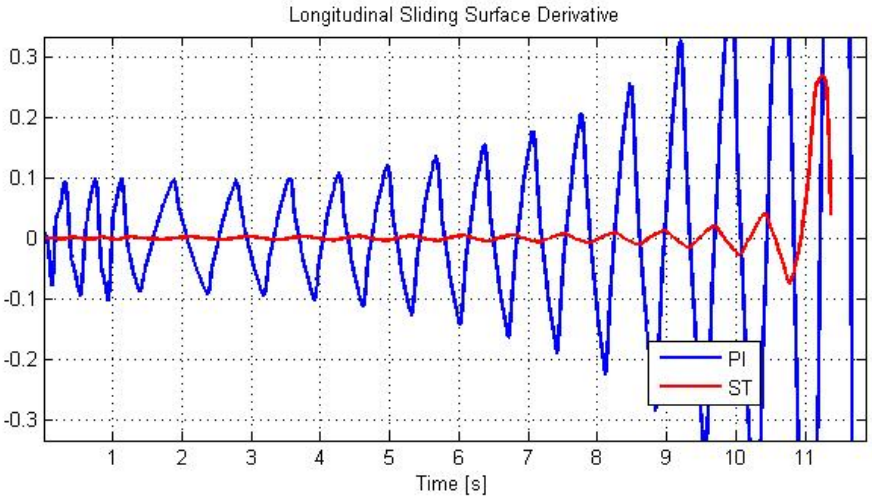

Figure 5.85: Derivative of longitudinal sliding variable (zoomed)

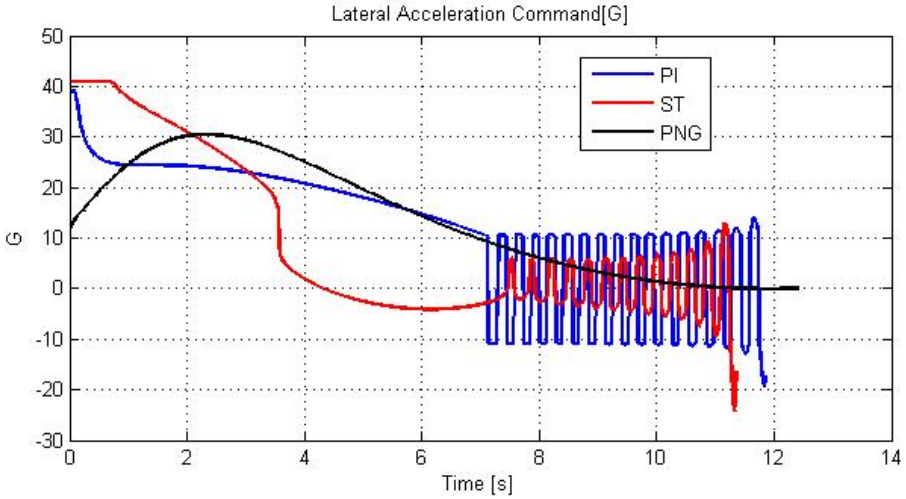

Figure 5.86: Lateral acceleration command

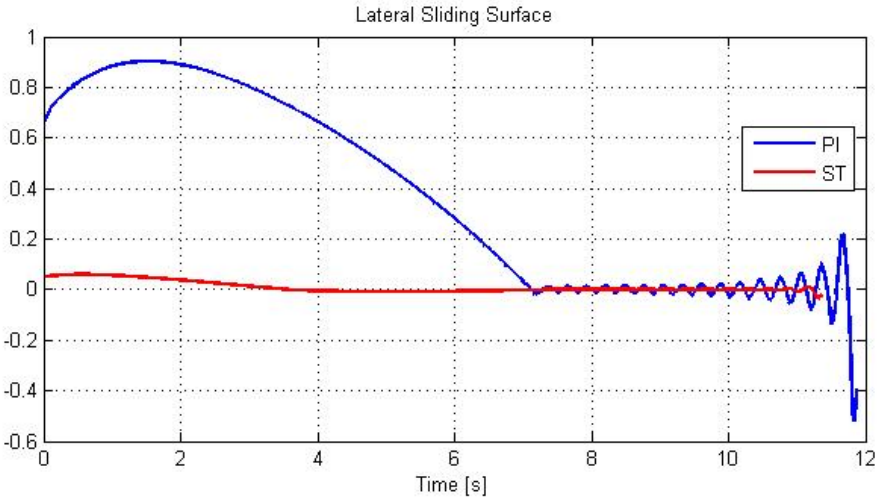

Figure 5.87: Lateral sliding surface

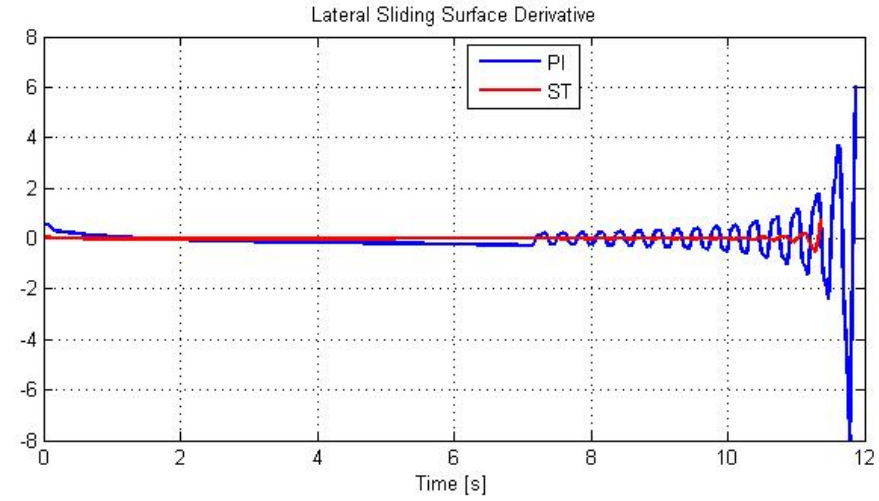

Figure 5.88: Derivative of lateral sliding variable

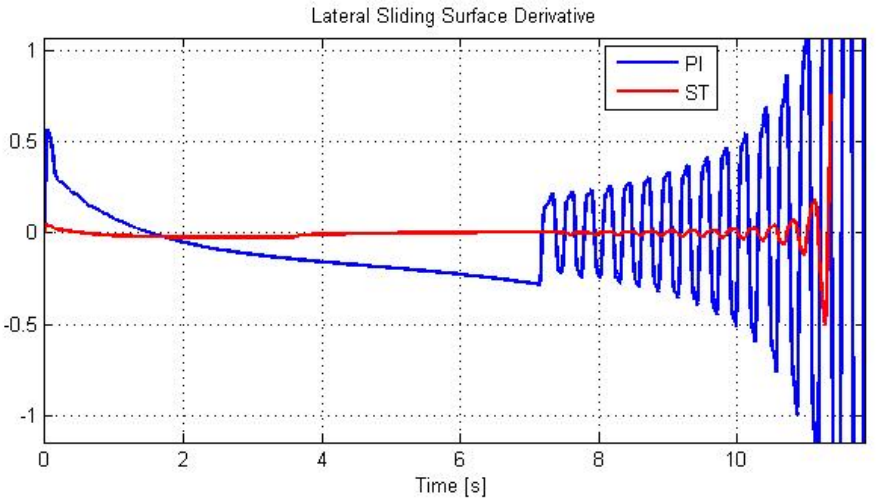

Figure 5.89: Derivative of lateral sliding variable (zoomed)

5.4.4 Scenario - 4

In this scenario, the shooter flies with heading to north and releases the missile at 0.85 Mach when the target flies with 135° heading at 1 Mach. At the time of shoot, there is approximately 4.2 km distance between the shooter and target. In this scenario, the target makes an evasion maneuver with 10g in lateral plane. Initial conditions are stated in Table 5.7 and the results are stated with figures as follows.

Table5.7: Initial conditions of Scenario – 4

Scenario(t_0)	Missile	Target
$X[km]$	0	3
$Y[km]$	0	3
$Altitude[km]$	6	6
$Velocity[Mach]$	0.85	1
$Heading\ Angle[deg]$	0	135
$Target\ Maneuver$	10 g lateral	

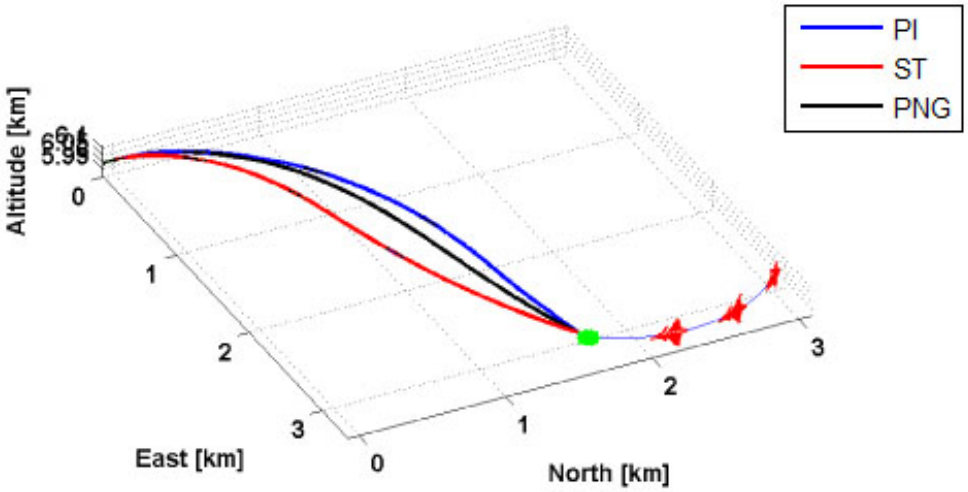

Figure 5.90: Missile and target trajectories

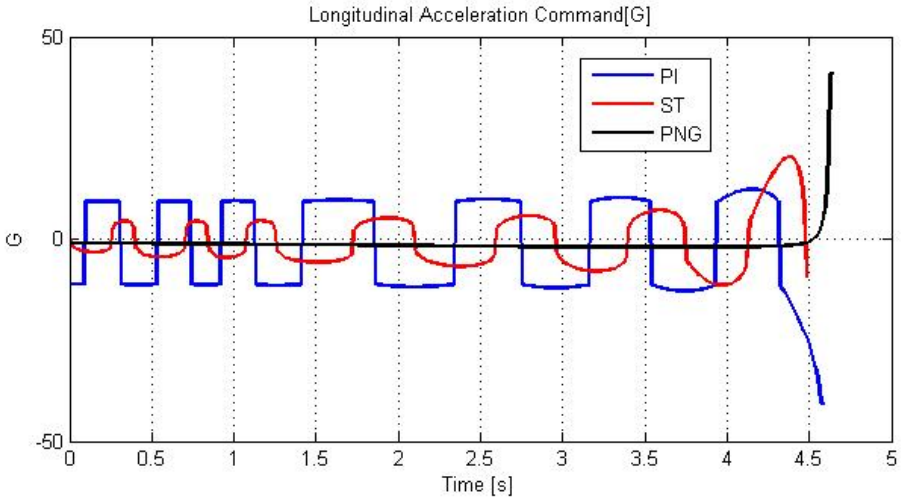

Figure 5.91: Longitudinal acceleration command

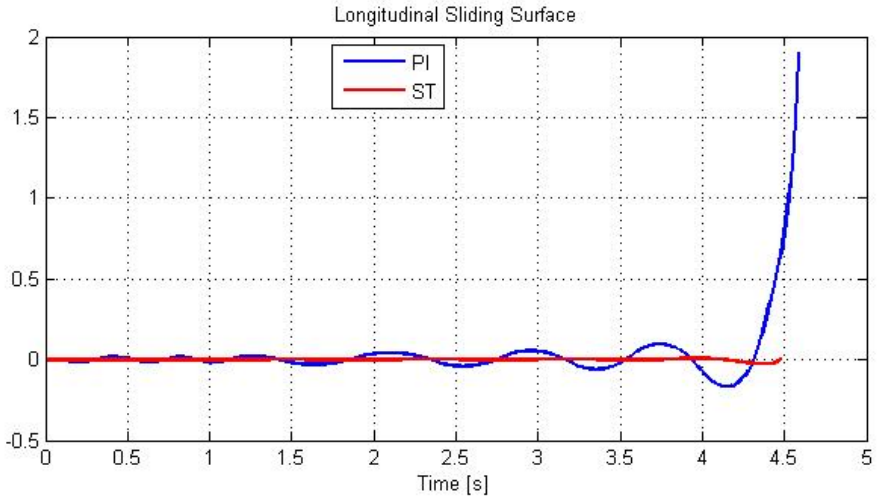

Figure 5.92: Longitudinal sliding surface

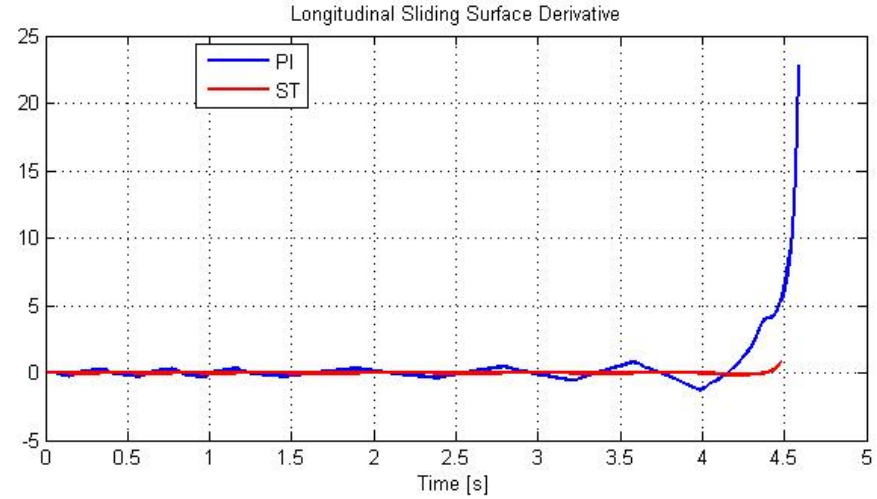

Figure 5.93: Derivative of longitudinal sliding variable

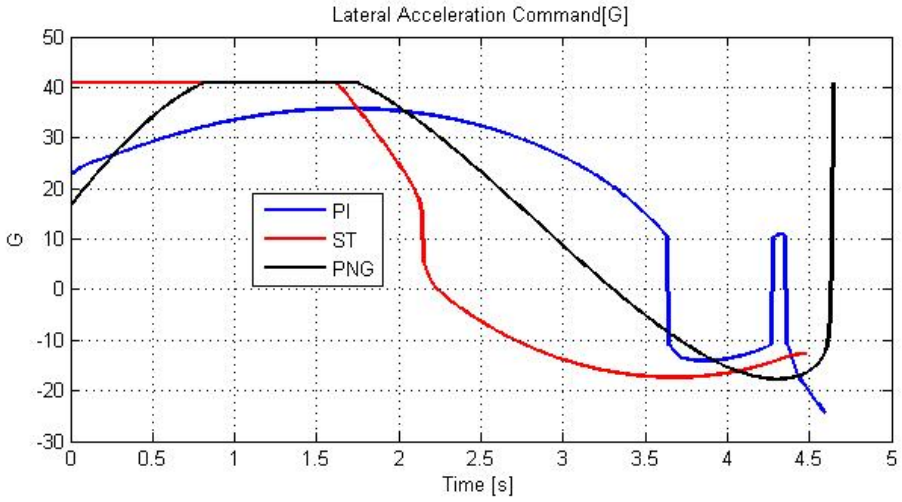

Figure 5.94: Lateral acceleration command

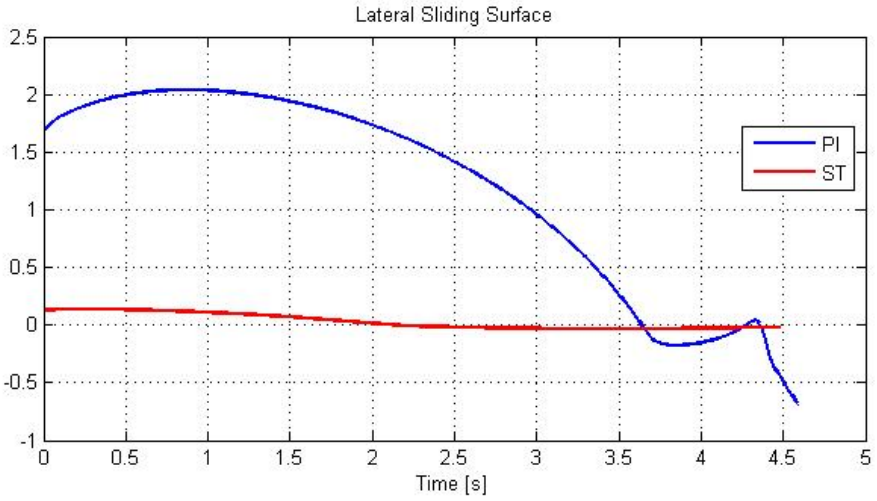

Figure 5.95: Lateral sliding surface

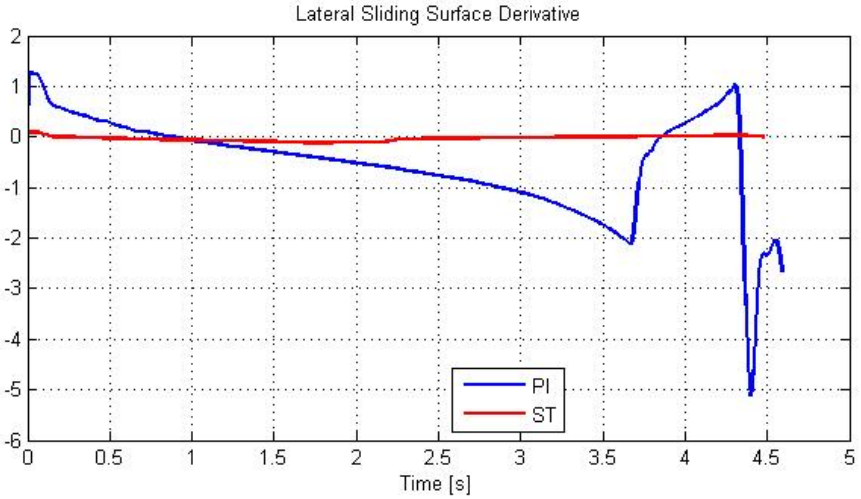

Figure 5.96: Derivative of lateral sliding variable

5.4.5 Scenario - 5

In this scenario, the shooter flies with heading to north and releases the missile at 0.85 Mach when the target flies with 90° heading at 1 Mach. At the time of shoot, there is 3 km distance between the shooter and target. In this scenario, the target makes no evasion maneuver. Initial conditions are stated in Table 5.8 and the results are stated with figures as follows.

Table5.8: Initial conditions of Scenario – 5

Scenario(t_0)	Missile	Target
$X[km]$	0	3
$Y[km]$	0	0
$Altitude[km]$	6	6
$Velocity[Mach]$	0.85	1
$Heading\ Angle[deg]$	0	90
$Target\ Maneuver$	0	

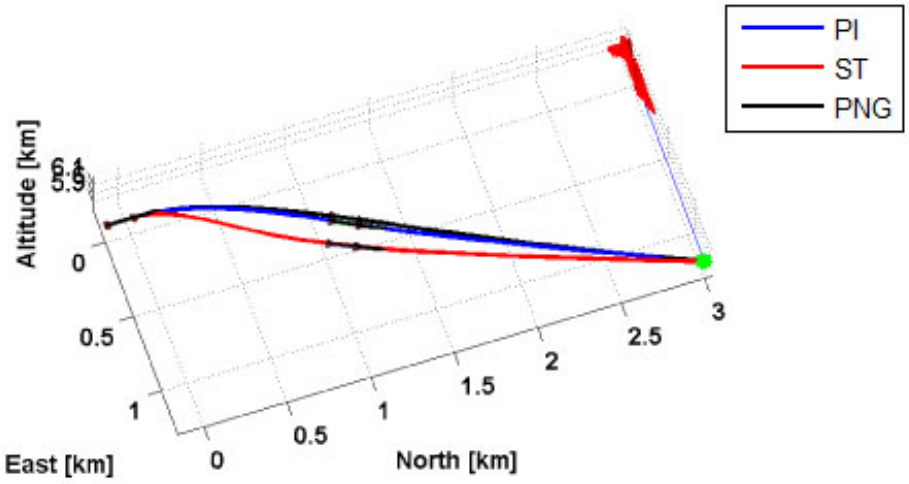

Figure 5.97: Missile and target trajectories

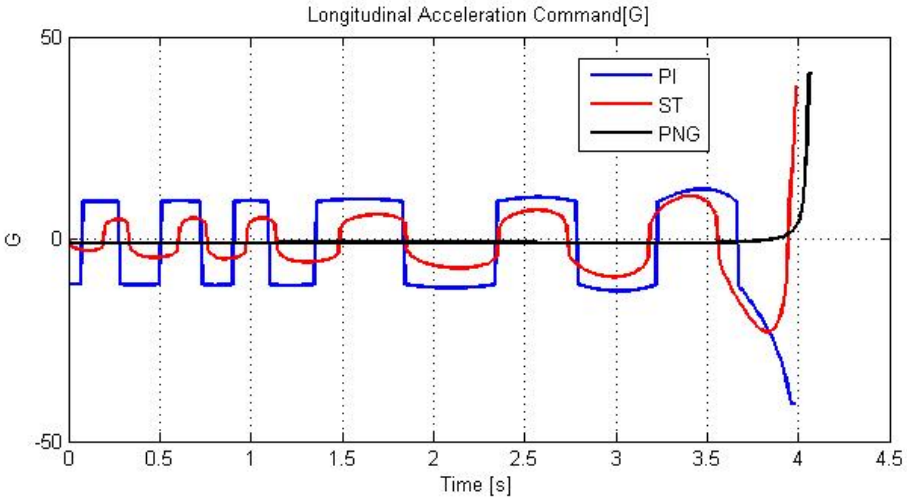

Figure 5.98: Longitudinal acceleration command

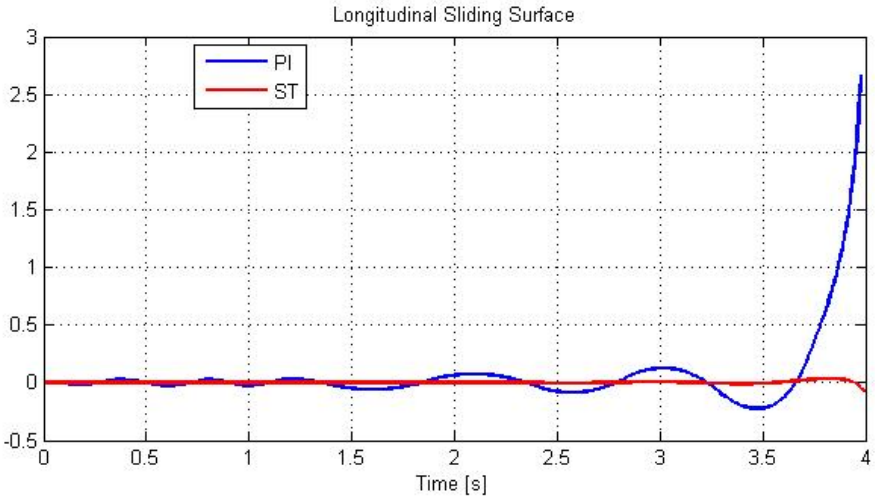

Figure 5.99: Longitudinal sliding surface

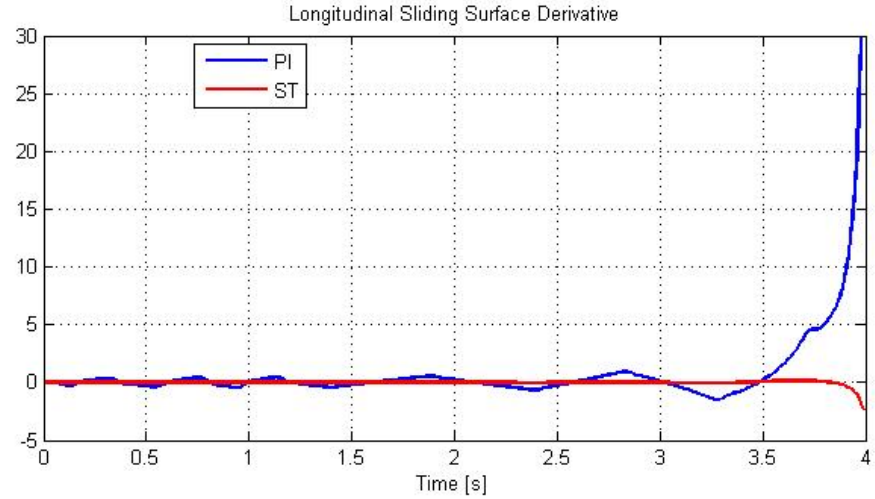

Figure 5.100: Derivative of longitudinal sliding variable

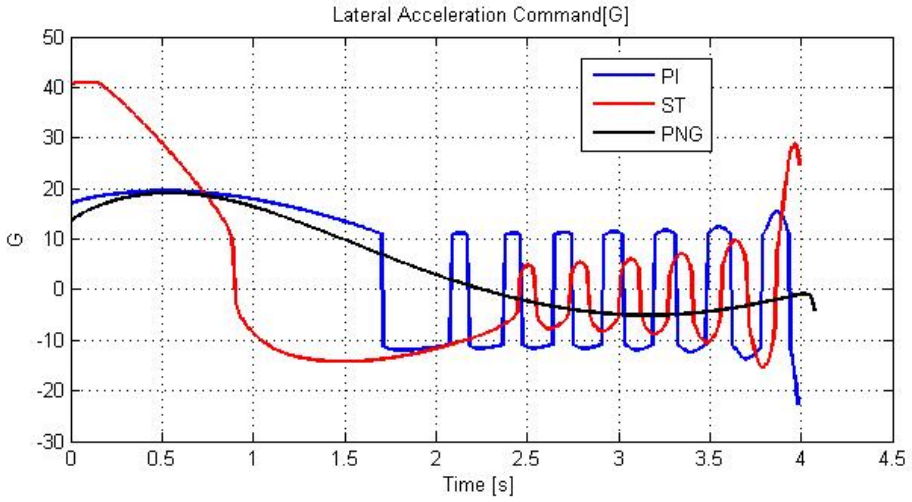

Figure 5.101: Lateral acceleration command

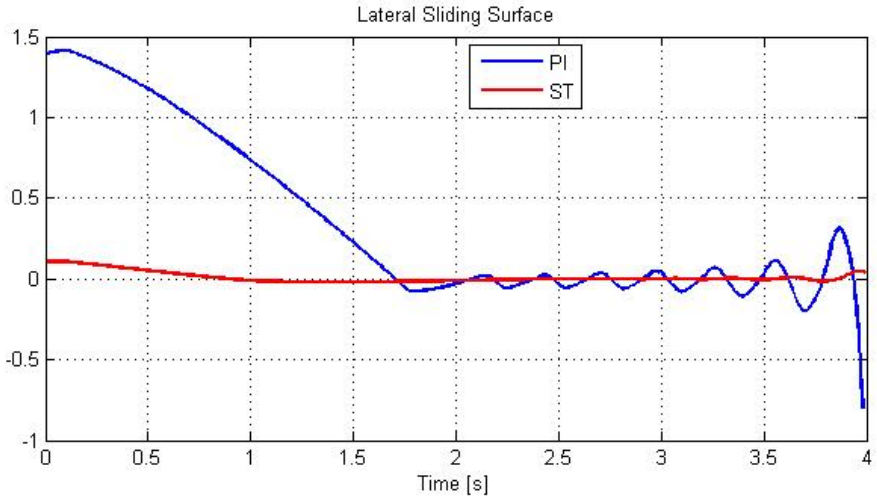

Figure 5.102: Lateral sliding surface

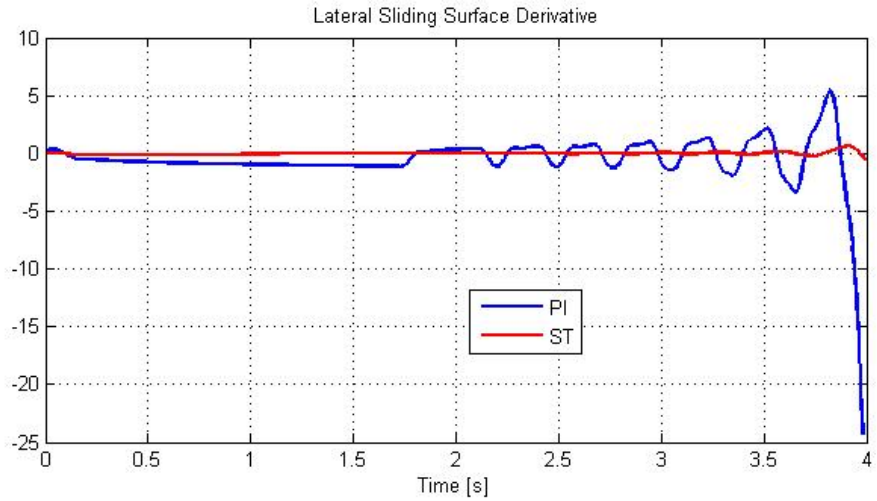

Figure 5.103: Derivative of lateral sliding variable

5.4.6 Scenario - 6

In this scenario, the shooter flies with heading to north and releases the missile at 0.85 Mach when the target flies with 250° heading at 1 Mach. At the time of shoot, there is approximately 7 km distance between the shooter and target. In this scenario, the target makes an evasion maneuver with 8g in lateral plane and 3g in longitudinal plane. Initial conditions are stated in Table 5.9 and the results are stated with figures as follows.

Table5.9: Initial conditions of Scenario – 6

Scenario(t_0)	Missile	Target
$X[km]$	0	5
$Y[km]$	0	-5
$Altitude[km]$	6	6
$Velocity[Mach]$	0.85	1
$Heading\ Angle[deg]$	0	250
$Target\ Maneuver$	8 g lateral 3 g longitudinal	

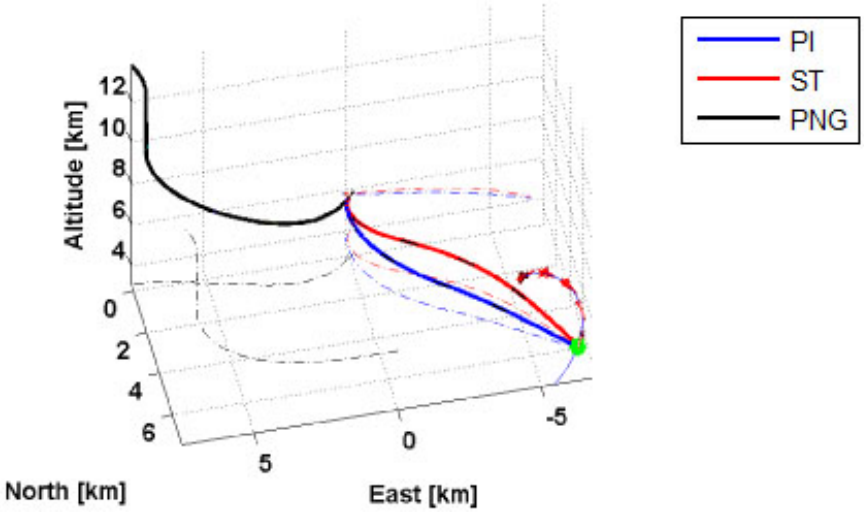

Figure 5.104: Missile and target trajectories

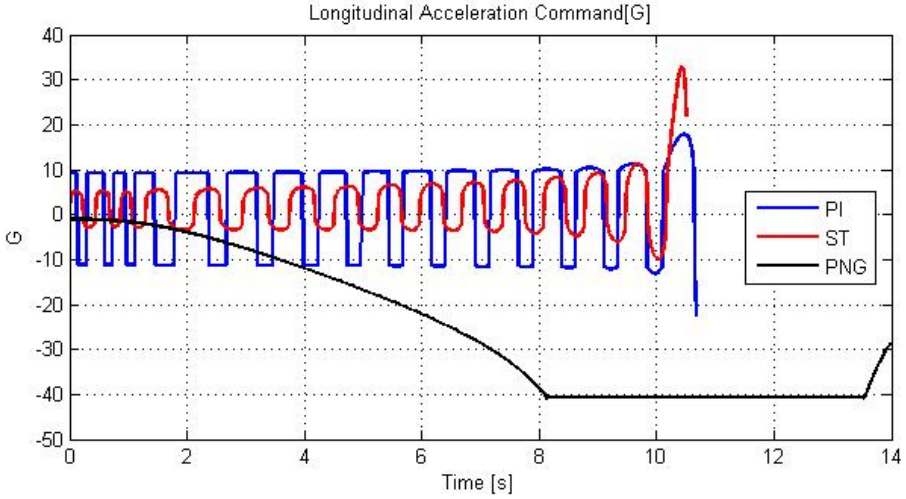

Figure 5.105: Longitudinal acceleration command

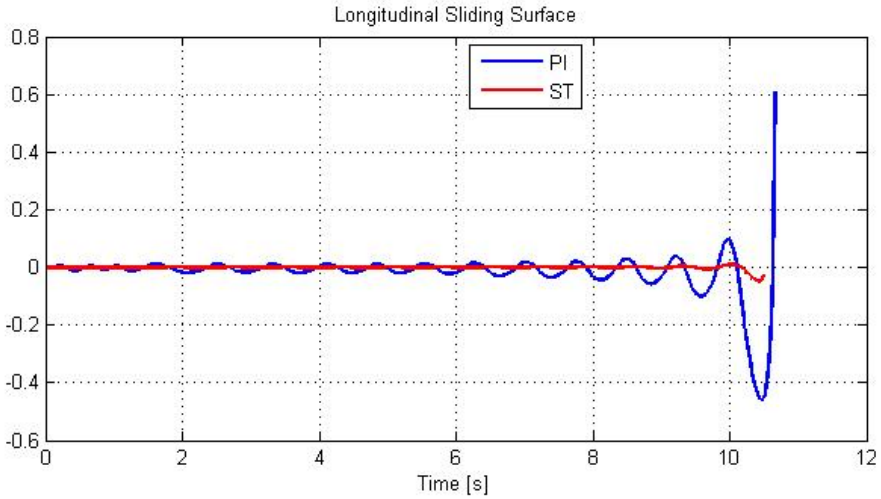

Figure 5.106: Longitudinal sliding surface

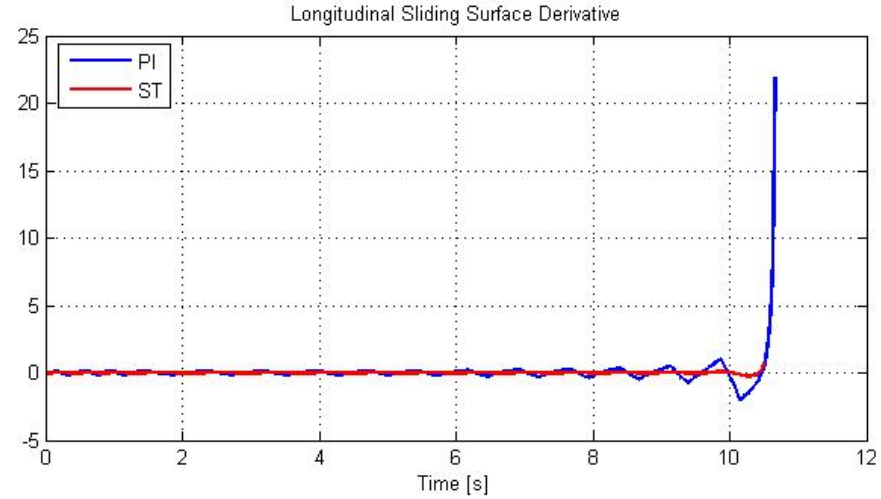

Figure 5.107: Derivative of longitudinal sliding variable

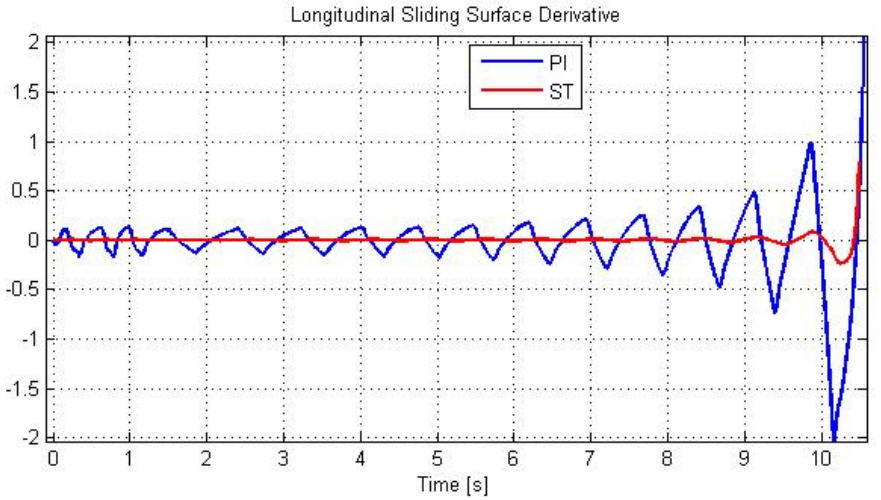

Figure 5.108: Derivative of longitudinal sliding variable (zoomed)

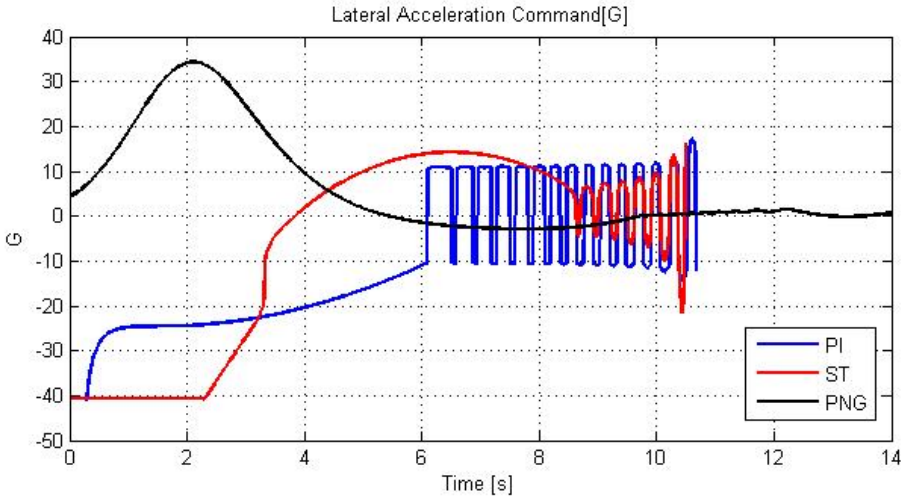

Figure 5.109: Lateral acceleration command

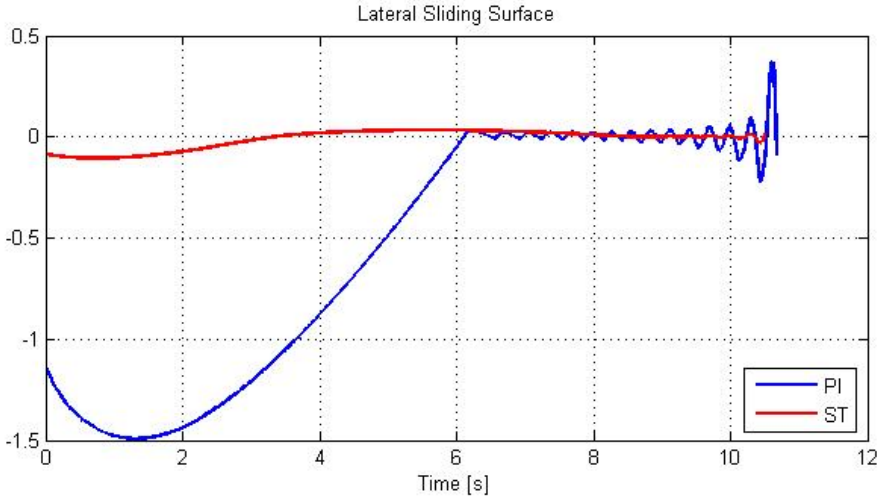

Figure 5.110: Lateral sliding surface

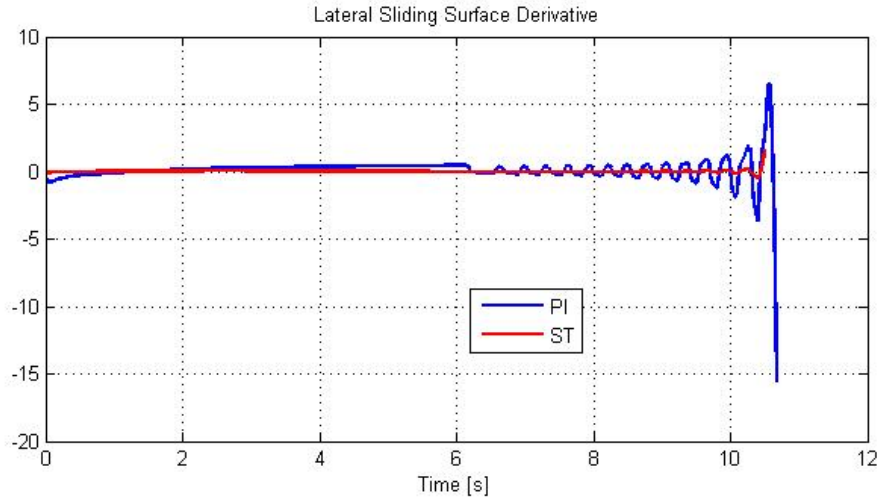

Figure 5.111: Derivative of lateral sliding variable

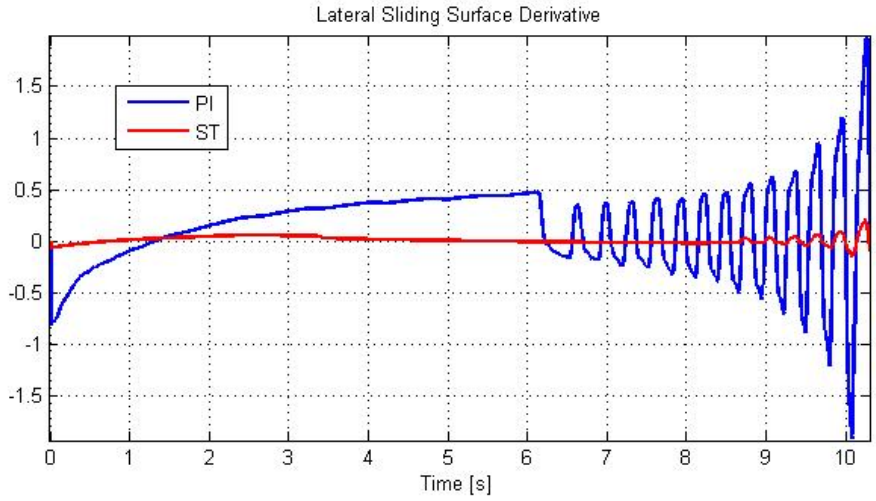

Figure 5.112: Derivative of lateral sliding variable (zoomed)

5.4.7 Scenario - 7

In this scenario, the shooter and target flies with heading to north and at 0.85 Mach and 1.2 Mach, respectively. At the time of shoot, there is approximately 11 km distance between the shooter and target. In this scenario, the target makes an evasion maneuver with 8g in lateral plane and 3g in longitudinal plane. Initial conditions are stated in Table 5.10 and the results are stated with figures as follows.

Table5.10: Initial conditions of Scenario – 7

Scenario(t_0)	Missile	Target
$X[km]$	0	4
$Y[km]$	0	-10
$Altitude[km]$	6	6
$Velocity[Mach]$	0.85	1.2
$Heading\ Angle[deg]$	0	0
$Target\ Maneuver$	8 g lateral 3 g longitudinal	

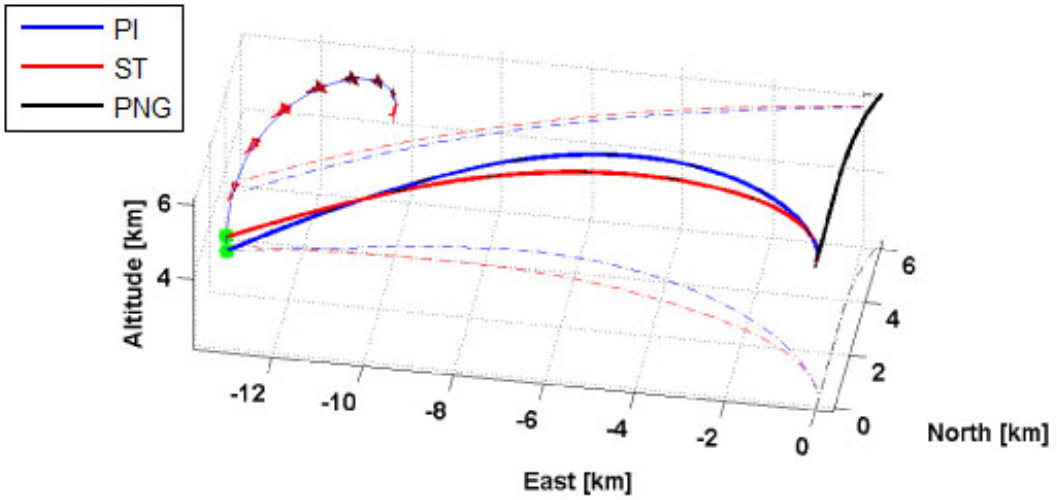

Figure 5.113: Missile and target trajectories

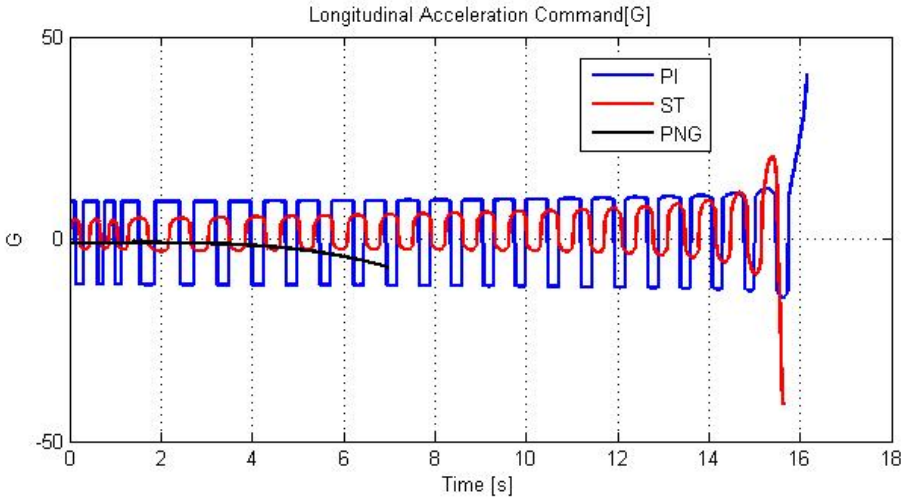

Figure 5.114: Longitudinal acceleration command

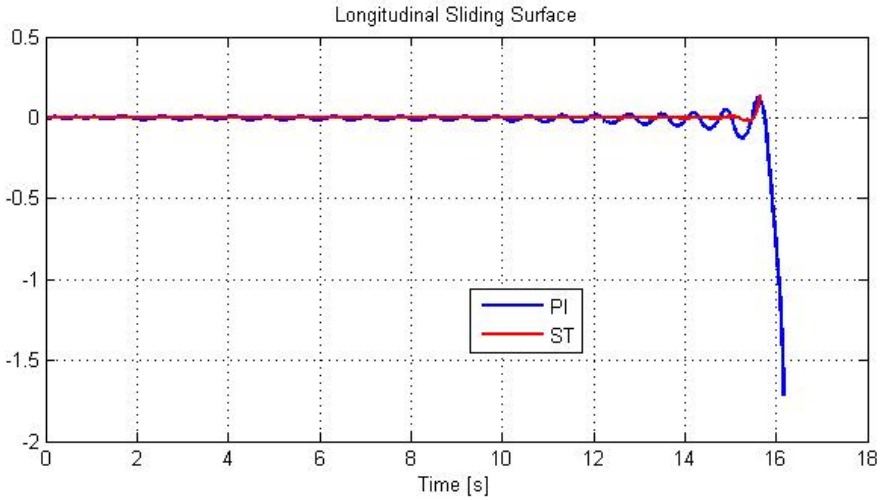

Figure 5.115: Longitudinal sliding surface

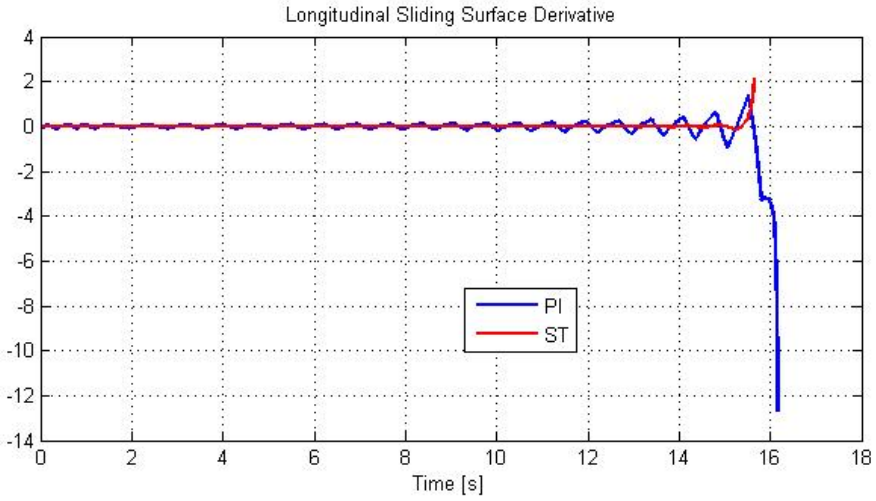

Figure 5.116: Derivative of longitudinal sliding variable

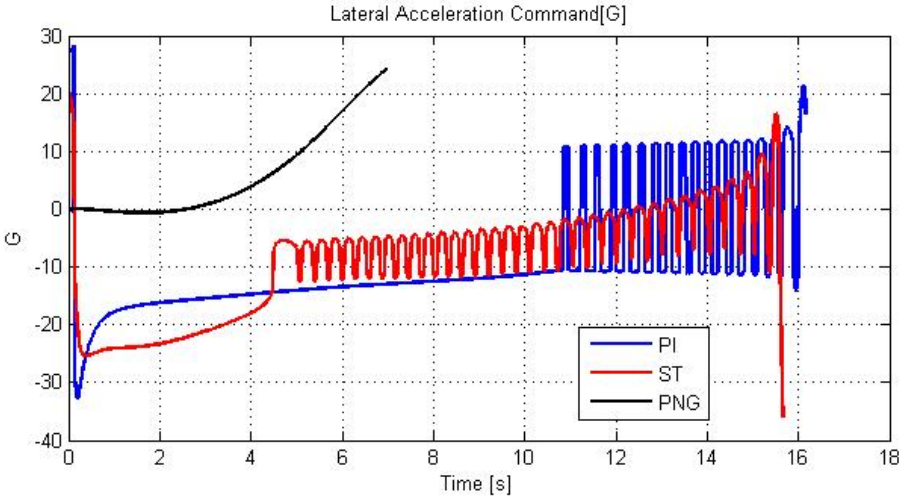

Figure 5.117: Lateral acceleration command

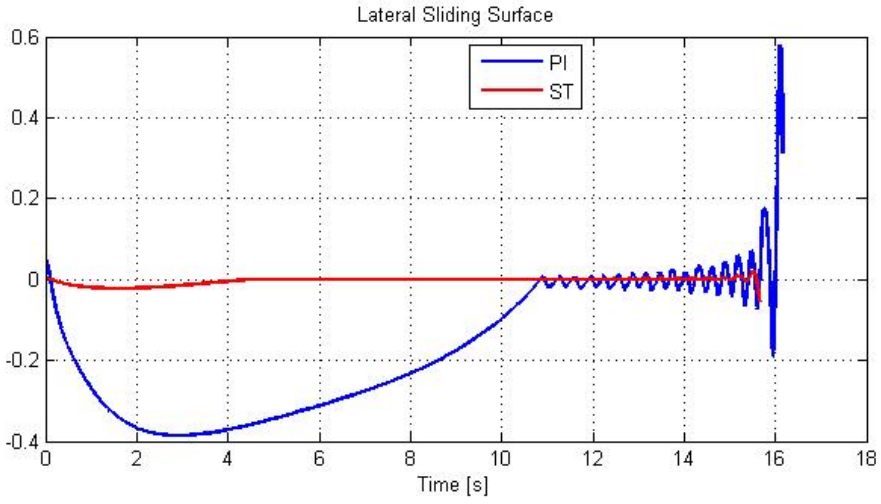

Figure 5.118: Lateral sliding surface

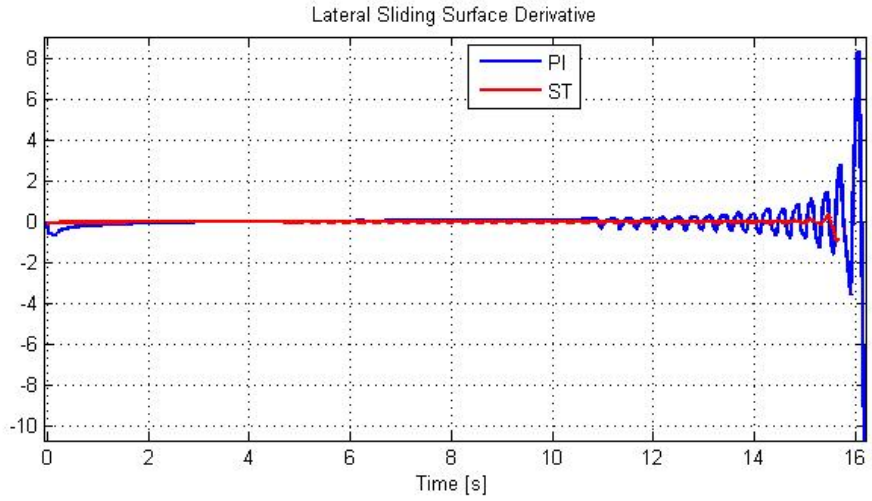

Figure 5.119: Derivative of lateral sliding variable

5.4.8 Scenario - 8

In this scenario, the shooter flies with heading to north and releases the missile at 0.85 Mach when the target flies with 160° heading at 1 Mach. At the time of shoot, there is approximately 18 km distance between the shooter and target. In this scenario, the target makes an evasion maneuver with 6g in lateral plane and 2g in longitudinal plane. Initial conditions are stated in Table 5.11 and the results are stated with figures as follows.

Table5.11: Initial conditions of Scenario – 8

Scenario(t_0)	Missile	Target
$X[km]$	0	15
$Y[km]$	0	-10
$Altitude[km]$	6	6
$Velocity[Mach]$	0.85	1
$Heading\ Angle[deg]$	0	160
$Target\ Maneuver$	6 g lateral 2 g longitudinal	

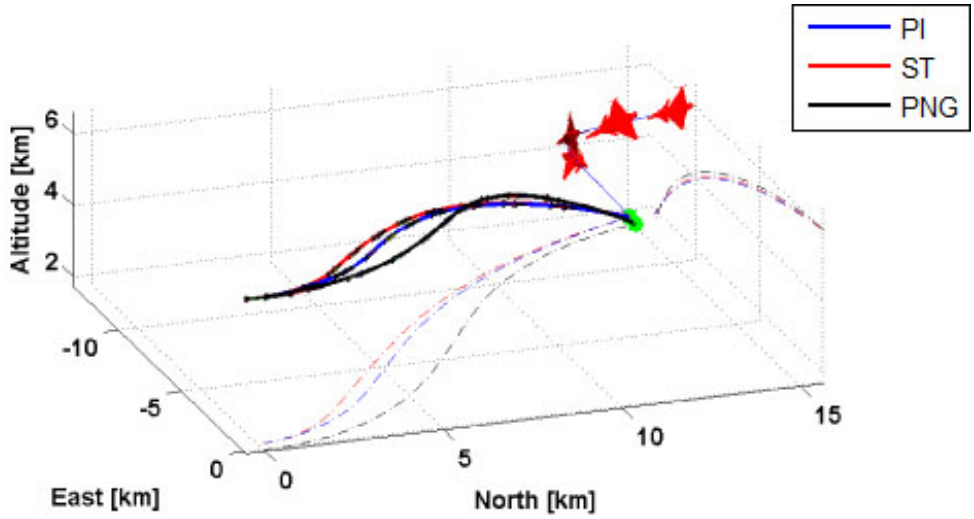

Figure 5.120: Missile and target trajectories

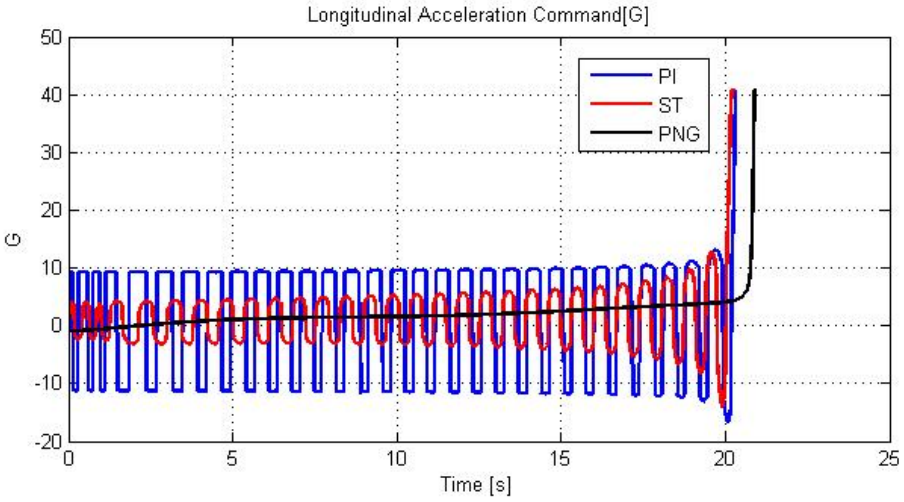

Figure 5.121: Longitudinal acceleration command

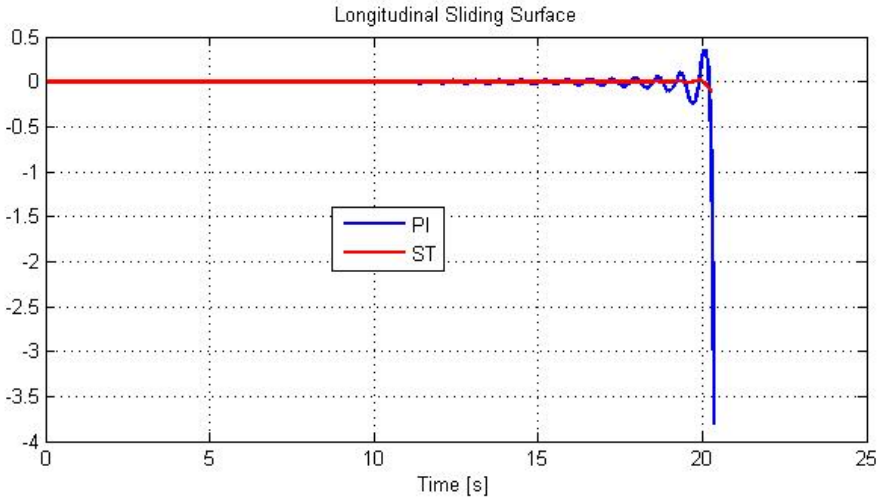

Figure 5.122: Longitudinal sliding surface

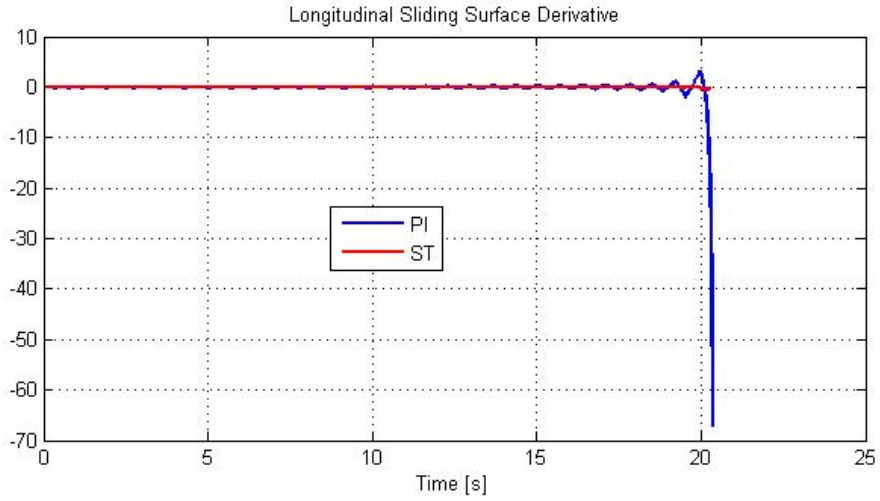

Figure 5.123: Derivative of longitudinal sliding variable

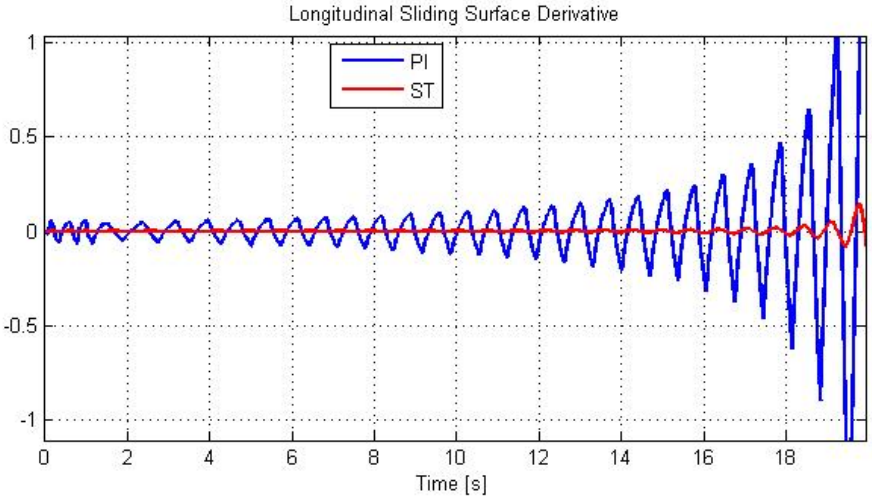

Figure 5.124: Derivative of longitudinal sliding variable (zoomed)

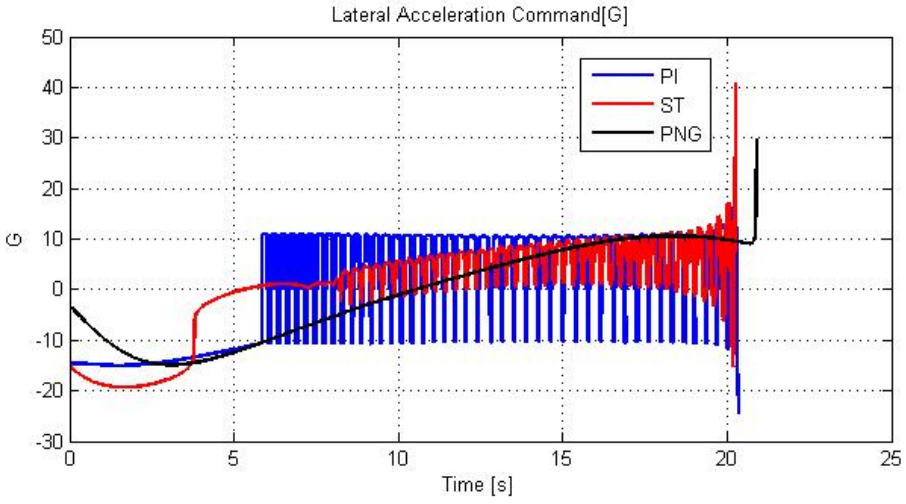

Figure 5.125: Lateral acceleration command

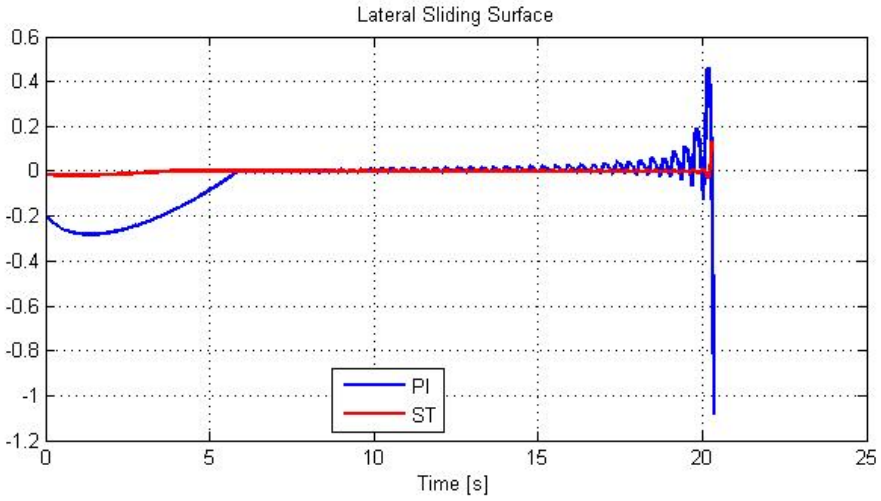

Figure 5.126: Lateral sliding surface

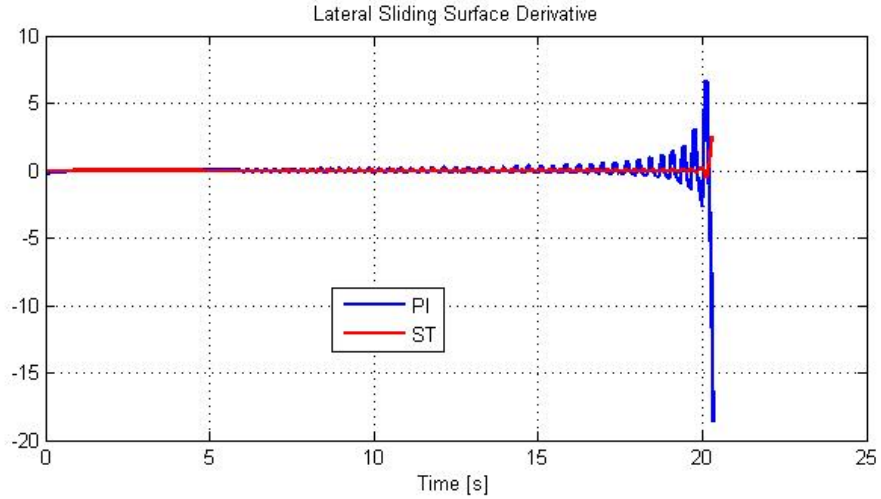

Figure 5.127: Derivative of lateral sliding variable

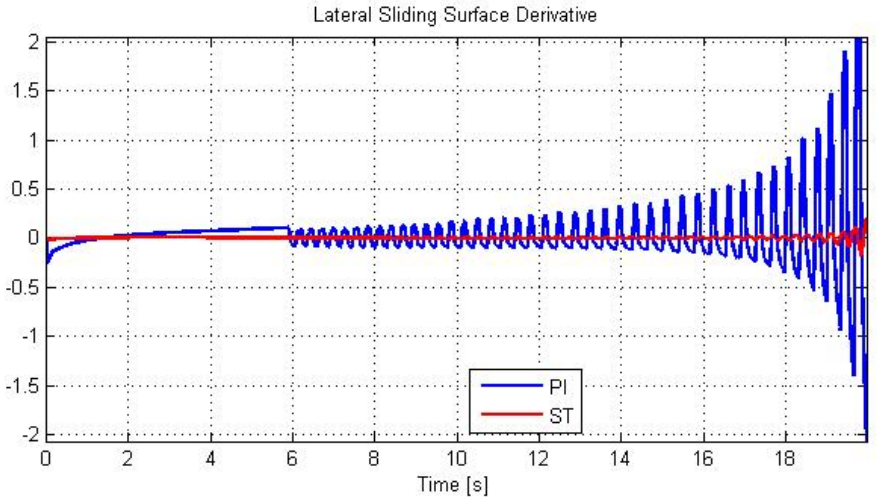

Figure 5.128: Derivative of lateral sliding variable (zoomed)

5.4.9 Scenario - 9

In this scenario, the shooter flies with heading to north and releases the missile at 0.85 Mach when the target flies with 90° heading at 1 Mach. At the time of shoot, there is 3 km distance between the shooter and target. In this scenario, the target makes no evasion maneuver. Initial conditions are stated in Table 5.12 and the results are stated with figures as follows.

Table5.12: Initial conditions of Scenario – 9

Scenario(t_0)	Missile	Target
$X[km]$	0	3
$Y[km]$	0	0
$Altitude[km]$	6	6
$Velocity[Mach]$	0.85	1
$Heading\ Angle[deg]$	0	90
$Target\ Maneuver$	0	

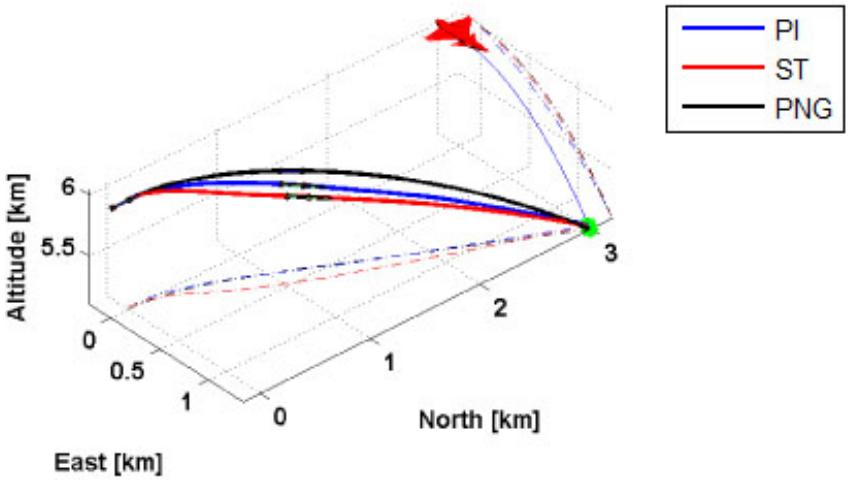

Figure 5.129: Missile and target trajectories

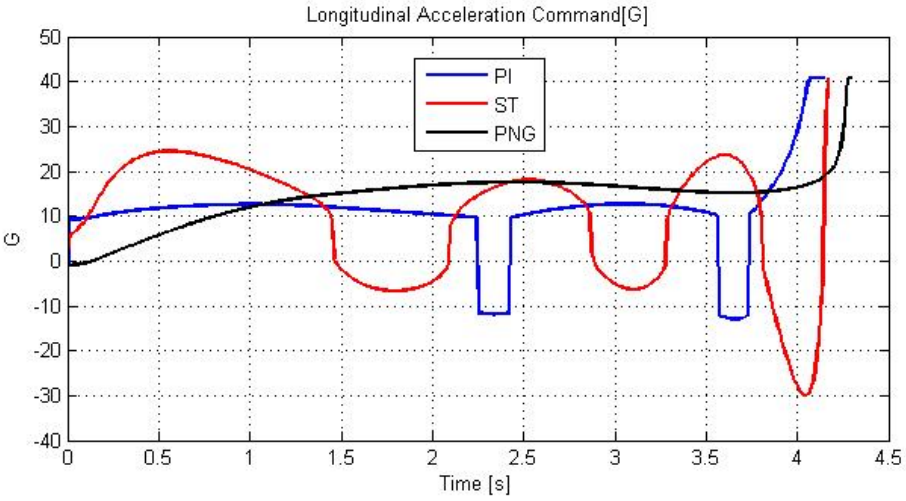

Figure 5.130: Longitudinal acceleration command

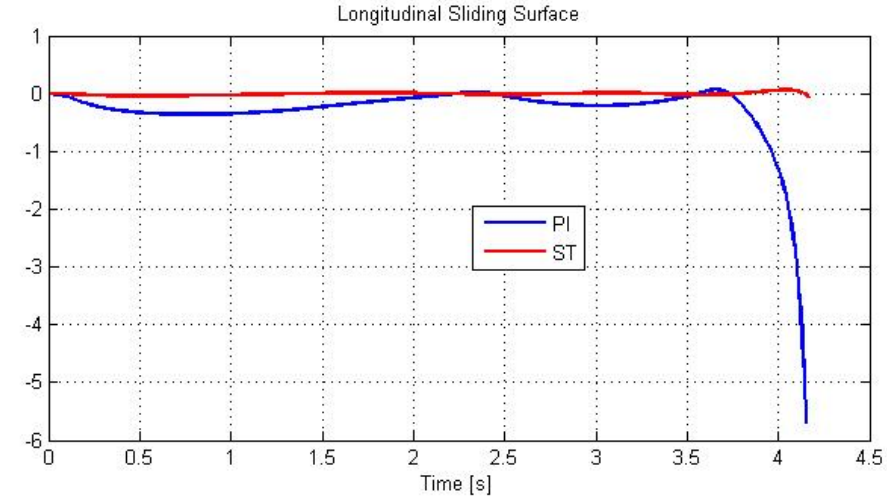

Figure 5.131: Longitudinal sliding surface

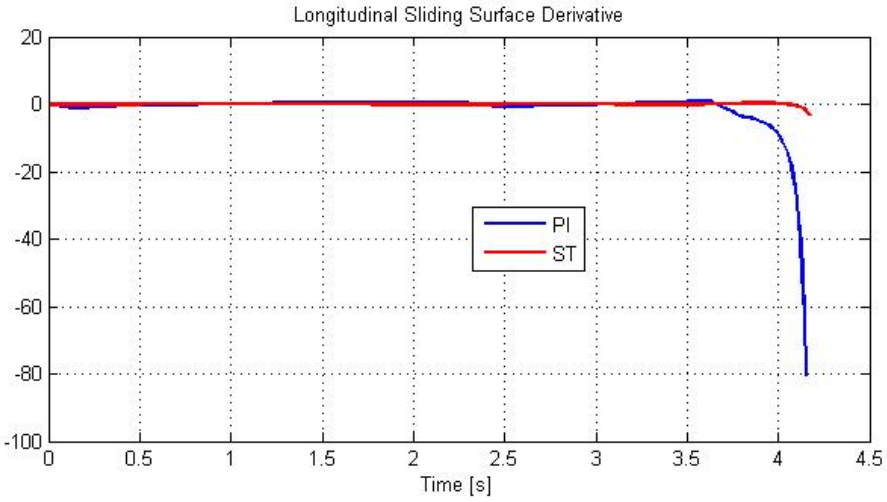

Figure 5.132: Derivative of longitudinal sliding variable

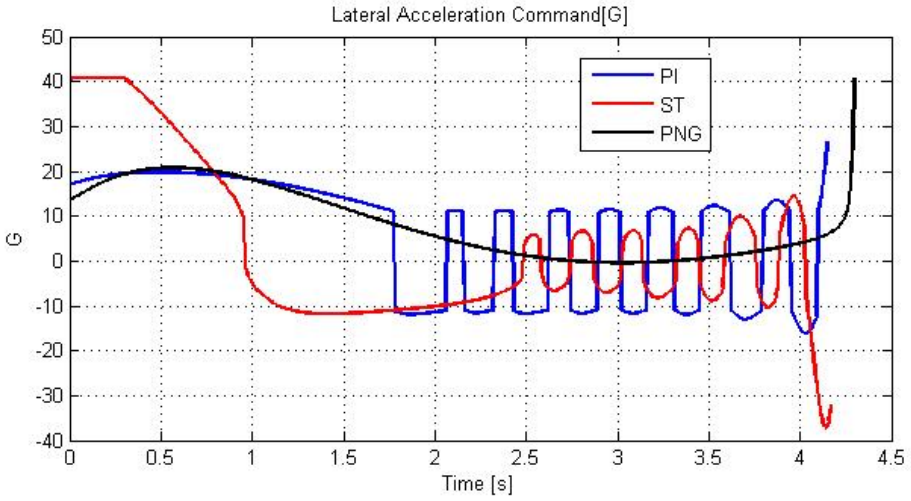

Figure 5.133: Lateral acceleration command

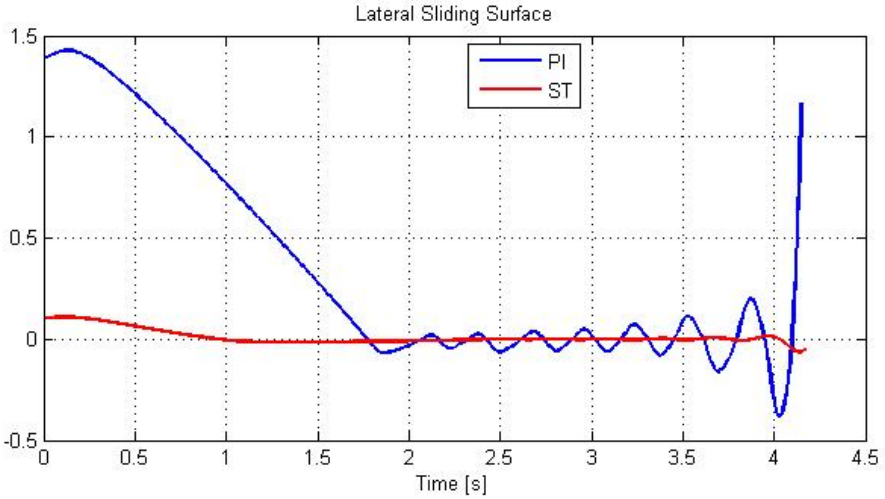

Figure 5.134: Lateral sliding surface

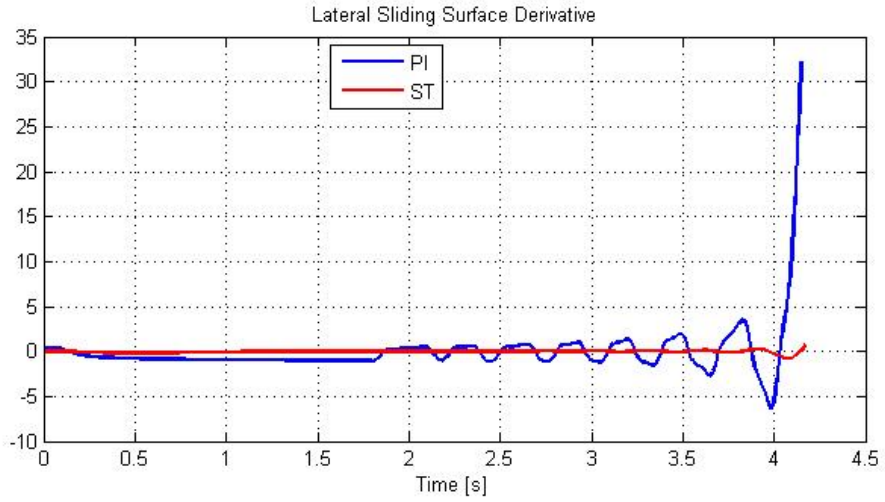

Figure 5.135: Derivative of lateral sliding variable

5.4.10 Scenario - 10

In this scenario, the shooter flies with heading to north and releases the missile at 0.85 Mach when the target flies with 45° heading at 1 Mach. At the time of shoot, there is 15 km distance between the shooter and target. In this scenario, the target makes an evasion maneuver with 3.5g in longitudinal plane. Initial conditions are stated in Table 5.13 and the results are stated with figures as follows.

Table5.13: Initial conditions of Scenario – 10

Scenario(t_0)	Missile	Target
$X[km]$	0	-15
$Y[km]$	0	0
$Altitude[km]$	6	10
$Velocity[Mach]$	0.85	1
$Heading\ Angle[deg]$	0	45
$Target\ Maneuver$	3.5 g longitudinal	

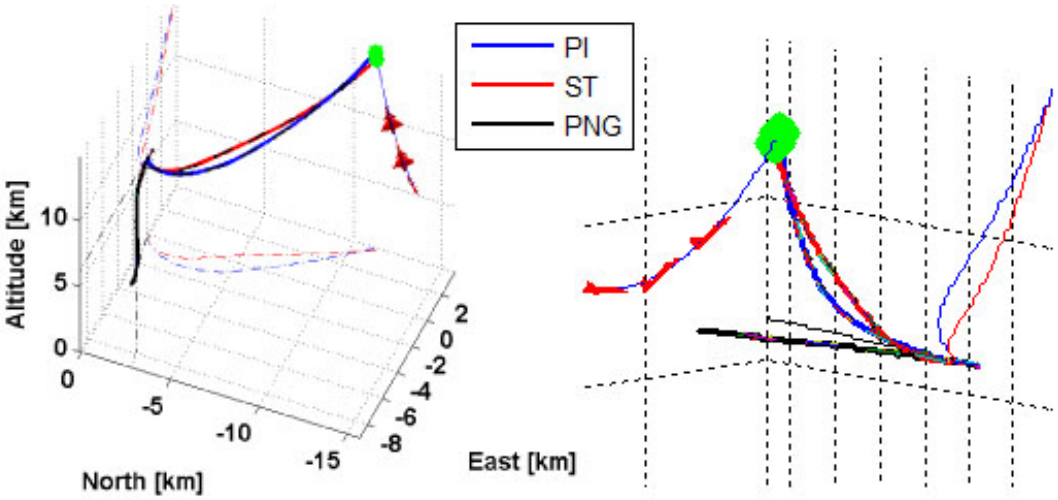

Figure 5.136: Missile and target trajectories

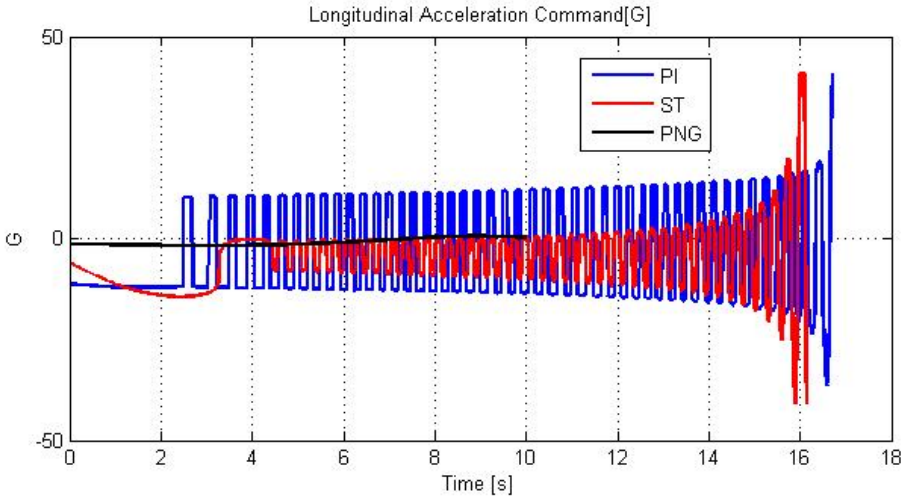

Figure 5.137: Longitudinal acceleration command

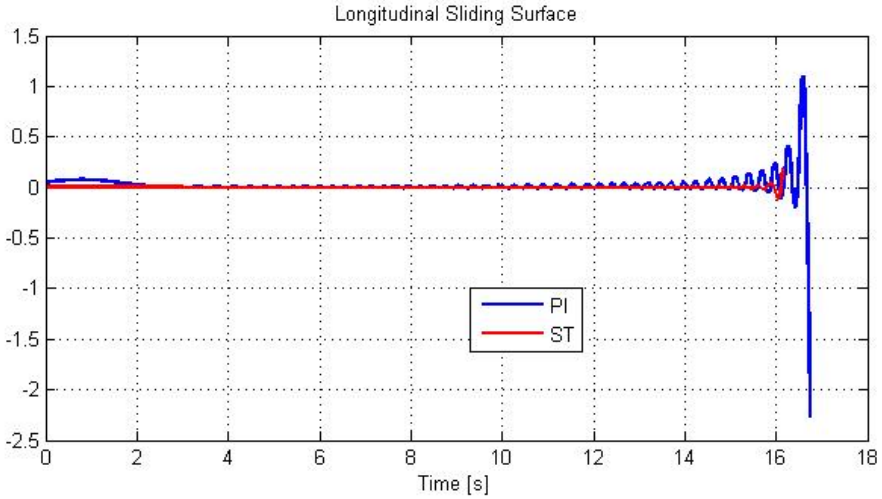

Figure 5.138: Longitudinal sliding surface

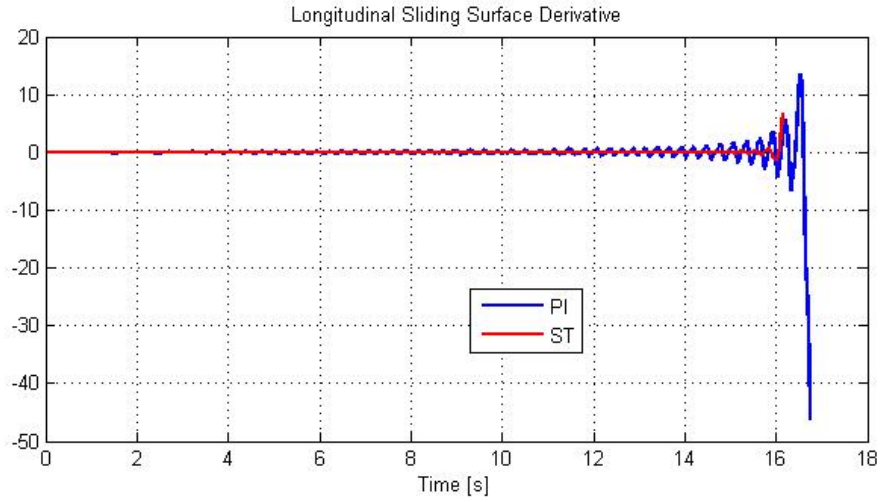

Figure 5.139: Derivative of longitudinal sliding variable

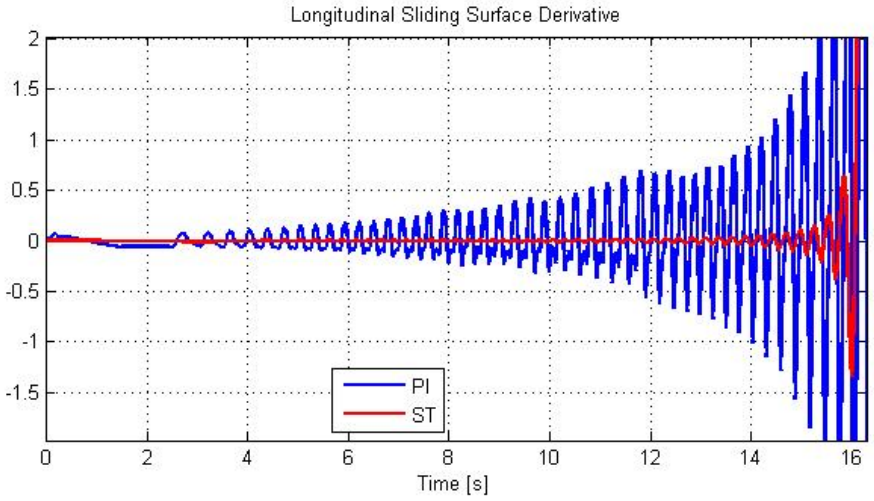

Figure 5.140: Derivative of longitudinal sliding variable (zoomed)

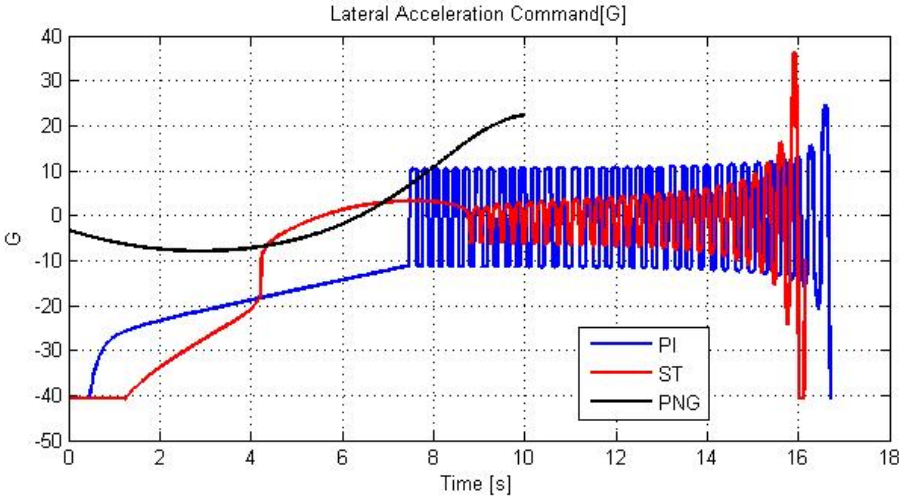

Figure 5.141: Lateral acceleration command

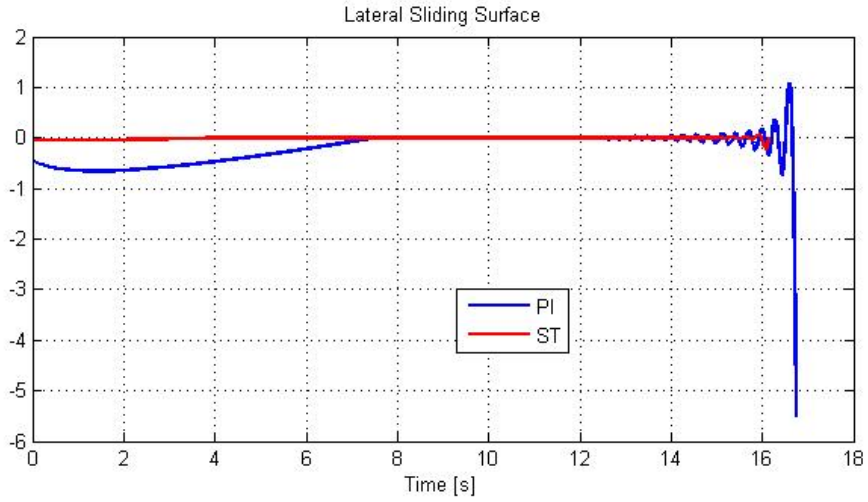

Figure 5.142: Lateral sliding surface

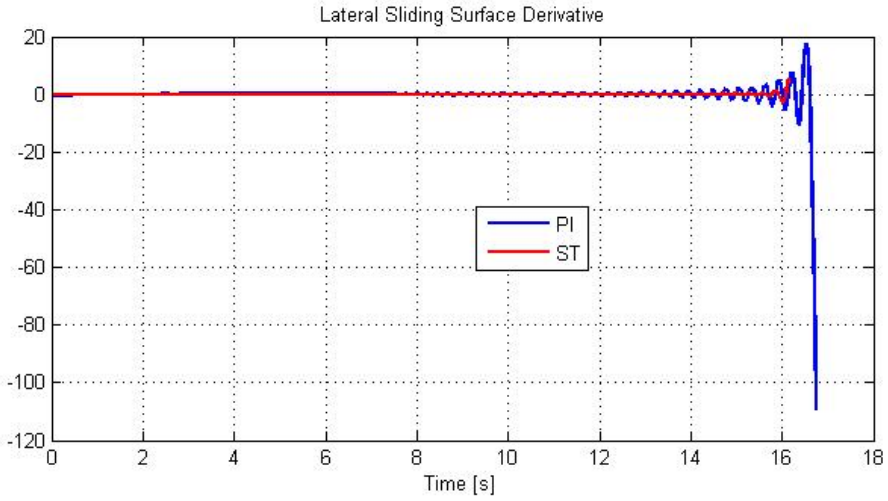

Figure 5.143: Derivative of lateral sliding variable

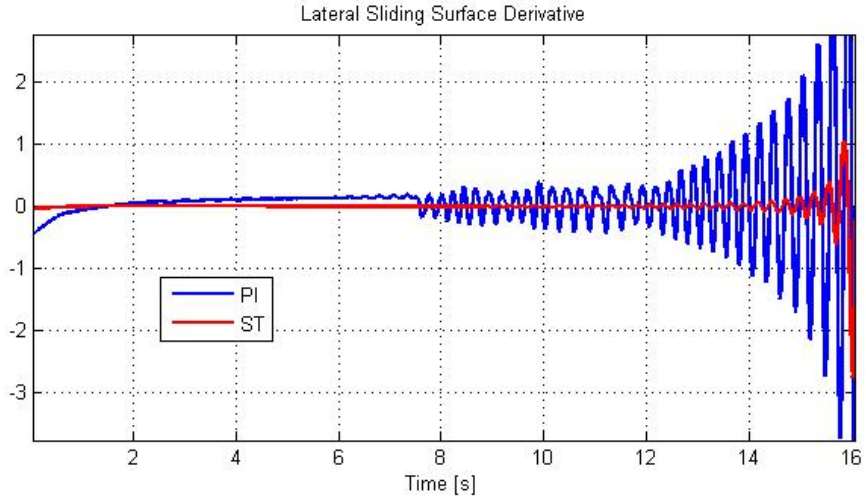

Figure 5.144: Derivative of lateral sliding variable (zoomed)

5.5 Conclusion

In this chapter, firstly, to understand the chattering attenuation of the super twisting guidance law over first order sliding mode guidance method, a first order guidance method that uses LOS rate as a sliding surface is derived. Then with two long range interception scenarios, these two methods that use LOS rate surface are compared. As the result, satisfactory results are obtained with super twisting guidance rule when the derivative of the sliding variable variables are compared for the scenarios.
Then, the proposed PI surface and super twisting guidance rules are compared with 10 different, from long range to short range and also including high off-boresight engagement scenarios to see the chattering attenuation of second order super twisting method over first order PI surface method. Besides, these two methods are compared with PNG law for the same scenarios to understand the interception performance. In

all scenarios, it can be clearly seen from the derivative of sliding variable and also guidance command figures. that super twisting method is better than PI surface method when Super twisting method results in lower chattering magnitudes and related to this, lower guidance command magnitudes during sliding mode occurs.

CHAPTER 6

CONCLUSION AND FUTURE WORK

6.1 Summary

In this study, firstly, an agile missile model is obtained with appropriate inputs to Missile Datcom program. Aerodynamic coefficients are tabled for the inputs of angle of attack, angle of sideslip and Mach number. After construction of aerodynamic force and moments, other equations of motion are modelled and nonlinear 6DOF model of the missile is prepared for the simulation.

Aerodynamic model and equations of motion are linearized around uncoupled flight conditions and state space models of longitudinal and lateral planes are obtained to be able to use in autopilot design.

Autopilot design points are determined by examining the aerodynamic data and LQT design is considered for rate loops with an automatic design program to cope with 1350 design points. This process which is basically a quadratic weight search, ends up with a no steady state error controller gains that are scheduled with respect to AOA, AOS, Mach number and altitude. Pitch and yaw rate loops are closed with acceleration autopilots that track the guidance commands generated by the guidance method. Acceleration autopilots are designed as PI controllers by using classical root locus design logic. Similarly, roll angle autopilot is designed with P controllers since there is an integrator in open loop already. Designed autopilots are implemented to the simulation environment and tracking performance is verified with many different interception simulations.

The missile flies in 'X' configuration and vertical and horizontal planes are decoupled with the roll autopilot that keeps the roll angle zero during flight. Guidance commands are applied to body longitudinal and lateral axis as a result of this decoupling action. Totally 3 sliding mode guidance laws are stated in this study. Firstly, sliding surface is chosen as LOS rate and a first order guidance law is derived primarily to compare with the super twisting method. Secondly, PI surface is proposed to overcome the interception failures caused by the methods that consist of LOS rate surface. PI gains

are found with GA optimization procedure by considering two reference scenarios. The gains are applied to many other scenarios and satisfactory results are obtained.

As a second order sliding control method, super twisting method is applied to missile guidance problem as the third guidance method. It is observed that the rules to choose parameters of this method defined for control applications in literature is not reasonable for guidance problem. As a result, firstly, it is preferred to choose these parameters with GA. According to the same reference scenarios used in PI gain selection procedure, parameters are determined and these static gains are applied to many different scenarios. Although, static gains are applied, these gains has given satisfactory results in many interception cases. Then, an adaptive gain rule is proposed to maneuver proportional to requirements of engagement geometry and avoid using excessive energy.

After PI surface and super twisting guidance rules are derived, by adding PNG law to comparison procedure to understand the performance of sliding mode guidance rules, methods are compared with 10 different interception cases.

6.2 Results and Future Work

For this study, a BVR missile that can fly up to 100 seconds and has maneuverability up to 40g with only aerodynamic capabilities is considered. Conceptually, it is assumed that the missile has a data link capability that receives target data from the aircraft and an active radar seeker. Besides, the target data is assumed to be known perfectly and obtained from the shooter aircraft through data link until the missile goes active. To make the study more realistic, uncertainties can be added to data measured from the target and true measurements can be estimated by applying different filtering techniques. In real world applications, this estimation has a crucial importance since it affects directly the interception success.

Maneuverability capability of the model can be increased with more agile missile geometry definition and also full spherical engagement area capabilities can be increased by adding TVC to the model for the next AAM missile guidance and control applications.

For missile body rate autopilots, LQT method is preferred to consider CAS limitations by adding CAS states to the state space models. In addition to this, LQT method lets to design stable and robust suboptimal autopilots quickly and gives the opportunity to prepare automatic design procedures to handle many conditions. For all design points, the weighting parameter of the quadratic weight matrix Q that coincides with tracking error is searched through an algorithm. This algorithm finds the controller gains that satisfies the design requirements and chose the one that gives the fastest response. As a result of rate autopilot design procedure, satisfactory autopilot responses are obtained and all gains are tabled to use the in outer loop design pro-

cedure. Acceleration autopilots are designed for longitudinal and lateral channels as the outer loop of pitch and yaw rate autopilots with PI controllers. Phi autopilot is designed as the outer loop of roll rate autopilot with P controllers. As in inner loop design, a gain search algorithm that finds the root locus gains that satisfy the design requirements of outer loops. Autopilot design procedure ends up with controllers that have fast transient responses and stability margins. Many autopilot design conditions are considered and 1350 design points are handled. The reason for choosing such a large design space is the variations of aerodynamic parameters though different AOA, AOS and Mach numbers. Increasing AOA and AOS brings agility up to stall angles and this agility shows itself with changes in sign of aerodynamic stability derivatives. Since agility requires large flight parameter space in general, this brings large autopilot design space. Nevertheless, it is all up to aerodynamic coefficients and to design engineer. If the computational complexity and time for the autopilot design process is not a problem, elimination of design conditions may not be necessary if the aim is to use a gain scheduled autopilot. In this study, $\pm 20^\circ$ AOA and AOS are taken as maximal values. However agile missiles may encounter up to 60° with TVC and that may result in a much more larger design space and increasing design conditions can bring the necessity of adaptive autopilot design methods.

It is shown that sliding mode guidance is a preferable choice for the robustness to target acceleration uncertainty and steering the missile to target quickly. As an option of first order sliding mode guidance law, a method that uses PI surface is derived. Proportional and integral gains are obtained with a GA optimization process that use two scenarios to calculate an optimal solution. In this study, the static gains that GA has given are used. These gains are simulated for many different scenarios and satisfactory results are obtained about interception time, keeping target in FOV with an immediate turn.

To attenuate chattering, as a second order sliding mode control method super twisting method is chosen to apply to the guidance problem. It is observed that common parameter selection rules which are stated in literature are not applicable to the guidance problem. As applied for PI surface method, GA and the same two scenarios are used to determine these parameters. Static gains are applied to many scenarios and satisfactory result are obtained. With continuing studies, it is seen that this parameters can be determined according to a rule related to the sliding surface adaptively. The logic behind the adaptive method, how much the LOS rate, then increase the parameters according to a function of the sliding surface and increase the acceleration command. As a result of simulations that compare static gains with adaptive rule, same engagement performance is obtained with smaller magnitude of acceleration commands. Super twisting method is an efficient way to attenuate chattering and different rules to find the parameters of this and PI surface method can be derived or any other optimization methods can be tried for better guidance and chattering attenuation. An adaptive rule may be derived that considers off-boresight angle, range

to the target or LOS rate to determine these parameters. As another option, with the optimization processes for different scenarios for different ranges, off-boresight angles and LOS rates, these parameters can be stored and tabled. Then, appropriate gains can be chosen during flight with gain scheduling. However, this option may require more computational effort and time.

This study has the aim of showing the effectiveness of second order method over first order sliding mode guidance methods and for that aim, super twisting method is chosen, applied and an adaptive rule is developed for guidance problem. Any other second order methods can be applied and better guidance methods can be derived. However, it should be always considered that different first order guidance methods that may help to decrease chattering and also have a better interception capabilities can be derived, too. The key is to chose an appropriate sliding surface and propose a logical reaching law.

REFERENCES

[1] R.L. Shaw. *Fighter Combats: Tactics and Maneuvering*. The United States Naval Institute, 1985.

[2] N.A. Shneydor. *Missile Guidance and Pursuit: Kinematics, Dynamics and Control*. Horwood Publishing, 1988.

[3] P.J. Yuan, J.S. Chern. Ideal Proportional Navigation. *Journal of Guidance, Control, and Dynamics*, 15(5):1161-1166, 1992.

[4] H.J. Pastric, S. Setlzer and M.E. Warren. Guidance Laws for Short Range Homing Missile. *Journal of Guidance, Control, and Dynamics*, 4(2):98-108, 1981.

[5] P. Zarchan and F.W. Nesline. A New Look at Classical vs Modern Homing Missile Guidance. *Journal of Guidance and Control*, 4(1):78-85, 1981.

[6] C. Heller and I. Yaesh. Optimal Setting of the Proportional-Navigation Gain. *Journal of Guidance, Control, and Dynamics*, 36(3):888-891, 2013.

[7] J.R. Cloutier, J.H. Evers and J.J. Feeley. Assessment of Air to Air Missile and Guidance Technology. *IEEE Control Systems Magazine*, 9:27-34, 1989.

[8] R.K. Kiefer and P.L. Vergez. Target Acceleration Modeling for Tactical Missile Guidance. *Journal of Guidance*, 7(3):315-321, 1984.

[9] C. Edwards, E.F. Colet and L. Fridman. *Advances in Variable Structure and Sliding Mode Control*. Springer, 2006.

[10] R.A. DeCarlo, S.H. Zak and S.V. Drakunov. Variable Structure, Sliding Mode Controller Design. *The Control Handbook*. CRC Press, 1:941:951, 1999.

[11] M. Innocenti, F. Pellegrini and F. Nasuti. A VSS Guidance Law for Agile Missiles. Proc. of the AIAA Guidance, Navigation, and Control Conference, AIAA-1997-3473:179-188, 1997.

[12] K.R. Babu, I.G. Sarma and K.N. Swamy. Switched Bias Proportional Navigation for Homing Guidance Against Highly Maneuvering Targets. *AIAA Journal of Guidance, Control*, 17(6):1357-1363, 1994.

[13] D. Zhou, C. Mu, Q. Ling and W. Xu. Optimal Sliding-Mode Guidance of a Homing-Missile. Proc. of the 38th Conference on Decision and Control, pages 5131-5136, 1999.

[14] A. Levant et al. Aircraft Pitch Control Via Second Technique. *AIAA Journal of Guidance, Control, and Dynamics*, 23(4):586-594, 2000.

[15] A. Levant. Sliding Order and Sliding Accuracy in Sliding Mode Control. *International Journal of Control*, 58(6):1247-1263, 1993.

[16] G. Bartolini, A. Ferrara and A. Levant and E. Usai. On Second Order Sliding Mode Controllers. *Variable Structure Systems, Sliding Mode and Nonlinear Control Lecture Notes in Control and Information Sciences*. Springer-Verlag, 247:329-350, 1999.

[17] M.K. Khan, K.B. Goh and S.K. Spurgeon. Second Order Sliding Mode Control of a Diesel Engine. *Asian Journal of Control*, 5(4):614-619, 2003.

[18] H. Imine and T. Madani. Sliding Mode Control for Automated Lane Guidance of Heavy Vehicle. *International Journal of Robust and Nonlinear Control*, 23:67-76, 2013.

[19] M. Chettouh, R. Toumi and M. Hamerlain. High-Order Sliding Modes for a Robot Driven by Pneumatic Artificial Rubber Muscles. *Advanced Robotics*, 22(6-7):689-704, 2008.

[20] Y.B. Shtessel, I.A. Shkolnikov and A. Levant. Guidance and Control of Missile Interceptor using Second-Order Sliding Modes. IEEE Transactions on Aerospace and Electronic Systems, 45(1):110-124, 2009.

[21] G.M. Marks, Y.B. Shtessel, H. Gratt and I.A. Shkolnikov. Effects of High Order Sliding Mode Guidance and Observers on Hit-to-Kill Interceptions. AIAA Guidance, Navigation, and Control Conference and Exhibit, 2005.

[22] G. Bartolini, A. Pisano, E. Punta and E. Usai. A survey of applications of second-order sliding mode control to mechanical systems. *International Journal of Control*, 76:9-10, 2003.

[23] A. Damiano, G.L. Gatto and I. Morangiu. Second-Order Sliding-Mode Control of DC Drives. IEEE Transactions on Industrial Electronics, 51(2):364-373, 2004.

[24] M. Ulu, M.K. Leblebicioğlu. Birinci ve İkinci Dereceden Kayan Kipli Güdüm Yöntemi ile Havadan Havaya Füze Güdümü Uygulaması. 2013.

[25] I. Eker. Second-order sliding mode control with experimental application. ISA Transactions, 49:394-405, 2010.

[26] A. Rhif. A High Order Sliding Mode Control with PID Sliding Surface: Simulation on a Torpedo. *International Journal of Information Technology, Control and Automation*, 2(1):13-18, 2012.

[27] Y. Stepanenko, Y. Cao and C. Su. Variable Structure Control of Robotic Manipulator with PID Sliding Surfaces. *International Journal of Robust and Nonlinear Control*, 8:79-90, 1998.

[28] E.M. Jafarov, M.N.A. Parlakçı and Y. Istefanopulos. A New Variable Structure PID Controller Design for Robot Manipulators. IEEE Transactions on Control Systems Technology, 13(1):122-130, 2005.

[29] P.H. Zipfel. *Modelling and Simulation of Aerospace Vehicle Dynamics*. AIAA Inc., 2007.

[30] W. Blake. *Missile Datcom User's Manual*. 2008.

[31] B.L. Stevens, F.L. Lewis. *Aircraft Control and Simulation.* John Wiley and Sons Inc., 1992.

[32] G.F. Franklin, J.D. Powell and A.E. Naeini. *Feedback Control Of Dynamic Systems.* Prentice Hall, 2009.

[33] Ç. Evcimen. Development and Comparison of Autopilot and Guidance Algorithms for Missiles. M.S. Thesis in METU. M.S. Department of Electrical and Electronics Engineering. August 2007.

[34] K. Ogata. *Modern Control Engineering.* Prentice Hall, 1997.

[35] P. Zarchan. *Tactical and Strategic Missile Guidance.* AIAA Inc, 1994.

[36] D. Kirk. *Optimal Control Theory: An Introduction.* Dover Punblications Inc, 2004.

[37] R. Yanushevsky. *Modern Missile Guidance.* CRC Press, 2008.